UNIVERSITAT POLITÈCNICA DE CATALUNYA BARCELONATECH

Different approaches to improve groundwater resources management: submarine groundwater discharge and managed aquifer recharge

Sònia Jou Claus

UNIVERSITAT POLITÈCNICA DE CATALUNYA

DIFFERENT APPROACHES TO IMPROVE GROUNDWATER RESOURCES MANAGEMENT: SUBMARINE GROUNDWATER DISCHARGE AND MANAGED AQUIFER RECHARGE

by

Sònia Jou Claus

Advised by Dr. Albert Folch Sancho and Dra.Paula Rodríguez Escales

This thesis is submitted in the fulfilment of the requirements for the PhD degree to the doctoral school of the Universitat Politècnica de Catalunya

in the

Department of Civil and Environmental Engineering

Hydrogeology Group (UPC-CSIC)

May 2022

Grup d'**H**idrologia **S**ubterrània
UNIVERSITAT POLITÈCNICA DE CATALUNYA

Sònia Jou Claus

Different approaches to improve groundwater resources management: submarine groundwater discharge and managed aquifer recharge

Ph.D. Thesis, May 2022

Supervisor: Albert Folch Sancho and Paula Rodríguez Escales

This thesis has been financed by FI 2017 and by the Spanish Government, (grant nos. PID2019-110212RB-C22 and PID2019- 110311RB-C21), MONOPOLIOS (RTI2018-101990-B-100, MINECO/FEDER) and Project CEX2018-000794-S, by the Catalan Research Project RESTORA (ACA210/18/00040) and TerraMar (grant no. ACA210/18/00007) and by EU project MARADENTRO (PCI2019-103425 and PCI2019-103603).

Universitat Politècnica de Catalunya

Hydrogeology Group (UPC-CSIC)

Department of Civil and Environmental Engineering

C/Jordi Girona 1-3, Edifici D2, Despatx 004

08034 Barcelona (Catalunya)

“The ant philosophy: Never give up, look ahead, stay positive and do all you can”

(Jim Rohn)

UNIVERSITAT POLITÈCNICA DE CATALUNYA

Abstract

Department of Civil and Environmental Engineering

by Sònia Jou Claus

Global change is expected to affect significantly the global hydrological behavior, changing mean annual precipitation patterns, increasing length of drought periods, rising evaporation and atmospheric water vapor and decreasing ice cover. Therefore, changes in soil moisture, runoff, recharge, groundwater quantity and quality are consequently affected. In addition, the expected population growth increase pollution while at the same time would imply a growth on demand and a competition for water resources and thus an increase in groundwater extraction.

All these changes imply significant challenges to find solutions that could contribute to mitigate the effects of global change in groundwater quality and its effect on the environment. In this context, the application of remote sensing in groundwater studies represent a useful technique to complement the information obtained with the traditional methods in hydrogeological studies used for the characterization and quantification of water resources. In the same way, Managed Aquifer Recharge (MAR) represents a feasible solution to deal with future water management challenges promoting the storage of available water in aquifers and improving the recharged water quality.

The present dissertation is focused on improving groundwater resources management in two different ways. First, by using remote sensing tools for the characterization of coastal areas and second, by using reactive barriers to improve degradation of contaminants of emerging concern in the context of MAR coupled to the outflow of a waste water treatment plant.

Firstly, we evaluate the usefulness of using freely available thermal infrared (TIR) imagery of the Landsat 8 as an exploratory tool for identifying SGD springs worldwide. The use of satellite thermal data as a technique for identifying SGD springs in sea water is based on the identification of thermally anomalous plumes obtained from the thermal contrasts between groundwater and sea surface water. The main goal of this first part of the conducted research is to demonstrate the significant usefulness of Landsat 8 TIR images as an exploratory tool for identifying SGD springs (karts areas) worldwide and discuss the main limiting factors of using this technique in SGD studies. Results show that satellite TIR

remote sensing is a useful method for identifying coastal springs in karst aquifers both locally and regionally. However, there are some limiting factors that need to be considered as, technical limitations, geological and hydrogeological characteristics of the studied area, environmental and marine conditions, and coastal geomorphology.

Secondly, we present the potential use of satellite chlorophyll (Chl-a) data as a low-cost tool for mapping the spatial and temporal evolution of the ecological influence of SGD in coastal habitats. To distinguish high Chl-a concentrations derived from SGD to those derived from other potential sources, a clustered analysis were applied to Landsat 8 satellite Chl-a data. Results show that satellite Chl-a data offers the possibility to identify and constrain areas where SGD inputs have increased primary productivity and calculate the Chl-a concentration gradient along time induced by SGD.

Finally, we investigate the fate of selected UV filters (UVFs) in two MAR systems; one supplemented with a reactive barrier containing clay and vegetable compost, and the other as a reference system. We monitor benzophenone-3 (BP-3) and its transformation products (TPs) (benzophenone-1 (BP-1), 4,4′-dihydroxybenzophenone (4-DHB), 4-hydroxybenzophenone (4-HB) and 2,2'-dihydroxy-4-methoxybenzophenone (DHMB)), benzophenone-4 (BP-4) and avobenzone (AVO) at all involved compartments (water, soil, and biofilm), before and after modifying redox conditions through a pulse of lithium acetate. Results show that the implementation of a reactive barrier in MAR systems improve substantially the degradation extent of UVFs, especially of BP-3 and its TPs.

The present dissertation contributes to improve groundwater resources management throughout new methodological and technical approaches to deal with the new challenges of today's society.

UNIVERSITAT POLITÈCNICA DE CATALUNYA

Resumen

Department of Civil and Environmental Engineering

por Sònia Jou Claus

Se espera que el cambio global afecte significativamente el comportamiento hidrológico global, cambiando los patrones de precipitación media anual, aumentando la duración de los períodos de sequía, aumentando la evaporación y el vapor de agua atmosférico y disminuyendo la capa de hielo. Por lo tanto, los cambios en la humedad del suelo, la escorrentía, la recarga, la cantidad y la calidad del agua subterránea se verán afectados. Además, el crecimiento poblacional esperado incrementará la contaminación al mismo tiempo que implicará un crecimiento de la demanda y una competencia por los recursos hídricos y por ende un aumento en la extracción de aguas subterráneas.

Todos estos cambios implican desafíos importantes para encontrar soluciones que puedan contribuir a mitigar los efectos en la calidad del agua subterránea y su efecto en el medio ambiente. En este contexto, la aplicación de la teledetección en estudios de aguas subterráneas representa una técnica útil para complementar la información obtenida con los métodos tradicionales en estudios hidrogeológicos utilizados para la caracterización y cuantificación de recursos hídricos. Del mismo modo, la Recarga Gestionada de Acuíferos representa una solución factible para hacer frente a los desafíos futuros de la gestión del agua, promoviendo el almacenamiento del agua disponible en los acuíferos y mejorando la calidad del agua recargada.

La presente tesis se centra en mejorar la gestión de los recursos hídricos subterráneos de dos maneras diferentes. En primer lugar, mediante el uso de herramientas de teledetección para la caracterización de las zonas costeras y, en segundo lugar, mediante el uso de barreras reactivas para mejorar la degradación de los contaminantes de preocupación emergente en el contexto de la recarga gestionada de acuíferos acoplada al efluente de una planta de tratamiento de aguas residuales.

En primer lugar, se evalúa la posibilidad de utilizar imágenes infrarrojas térmicas (TIR) disponibles gratuitamente de Landsat 8 como una herramienta exploratoria para identificar manantiales SGD en todo el mundo. El uso de datos térmicos satelitales como técnica para identificar manantiales de SGD en agua de mar se basa en la identificación de penachos térmicamente anómalos obtenidos a partir del contraste térmico existente entre las aguas subterráneas y las aguas superficiales del mar. El objetivo principal de esta

primera parte de la investigación es demostrar la utilidad de las imágenes térmicas de Landsat 8 como una herramienta exploratoria para identificar manantiales SGD (áreas de karts) en todo el mundo y discutir los principales factores limitantes del uso de esta técnica en estudios de SGD. Los resultados muestran que la teledetección satelital TIR es un método útil para identificar manantiales costeros en acuíferos kársticos tanto a nivel local como regional. Sin embargo, existen algunos factores limitantes que deben considerarse, como limitaciones técnicas, características geológicas e hidrogeológicas del área de estudio, condiciones ambientales y marinas y geomorfología costera.

En segundo lugar, se presenta el uso potencial de los datos satelitales de clorofila (Chl-a) como una herramienta de bajo coste para mapear la evolución espacial y temporal de la influencia ecológica de SGD en las zonas costeras. Para distinguir las altas concentraciones de Chl-a derivadas de SGD de las derivadas de otras fuentes potenciales, se aplicó un análisis agrupado a los datos de Chl-a. Los resultados muestran que los datos satelitales de Chl-a ofrecen la posibilidad de identificar y restringir áreas donde las entradas de SGD han aumentado la productividad primaria y calcular el gradiente de concentración de Chl-a a lo largo del tiempo inducido por SGD.

Finalmente, se investiga el destino de los filtros UV seleccionados, en dos sistemas de recarga gestionada de aquíferos (MAR); uno complementado con una barrera reactiva a base de arcilla y compost vegetal, y el otro como sistema de referencia. Se ha monitoreado benzofenona-3 (BP-3) y sus productos de transformación (TP) (benzofenona-1 (BP-1), 4,4′-dihidroxibenzofenona (4-DHB), 4-hidroxibenzofenona (4-HB) y 2, 2'-dihidroxi-4-metoxibenzofenona (DHMB)), benzofenona-4 (BP-4) y avobenzona (AVO) en todos los compartimentos involucrados (agua, suelo y biopelícula), antes y después de modificar las condiciones redox mediante un pulso de acetato de litio. Los resultados muestran que la implementación de una barrera reactiva en los sistemas MAR mejora sustancialmente el grado de degradación de los filtros UV, especialmente de BP-3 y sus TP.

La presente tesis ha contribuido a mejorar la gestión de los recursos hídricos subterráneos a través de nuevos enfoques metodológicos y técnicos para hacer frente a los nuevos retos de la sociedad actual.

UNIVERSITAT POLITÈCNICA DE CATALUNYA

Resum

Department of Civil and Environmental Engineering

per Sònia Jou Claus

El canvi global s'espera que afecti significativament el comportament hidrològic global, canviant els patrons de precipitació mitjana anual, augmentant la durada dels períodes de sequera, augmentant l'evaporació i el vapor d'aigua atmosfèric i disminuint la capa de gel. Per tant, els canvis en la humitat del sòl, l'escorrentia, la recàrrega, la quantitat i la qualitat de l'aigua subterrània es veuran afectats. A més, el creixement poblacional esperat incrementarà la contaminació alhora que implicarà un creixement de la demanda i una competència pels recursos hídrics i, per tant, un augment en l'extracció d'aigües subterrànies.

Tots aquests canvis impliquen reptes importants per trobar solucions que puguin contribuir a mitigar els efectes en la qualitat de l'aigua subterrània i el seu efecte al medi ambient. En aquest context, l'aplicació de la teledetecció en estudis d'aigües subterrànies representa una tècnica útil per complementar la informació obtinguda amb els mètodes tradicionals en estudis hidrogeològics utilitzats per caracteritzar i quantificar recursos hídrics. De la mateixa manera, la Recàrrega Gestionada d'Aqüífers representa una solució factible per fer front als futurs desafiaments en la gestió de l'aigua, promovent l'emmagatzematge de l'aigua disponible als aqüífers i millorant la qualitat de l'aigua recarregada.

Aquesta tesi es centra en millorar la gestió dels recursos hídrics subterranis de dues maneres diferents. En primer lloc, mitjançant l'ús d'eines de teledetecció per a la caracterització de les zones costaneres i, en segon lloc, mitjançant l'ús de barreres reactives per millorar la degradació dels contaminants de preocupació emergent en el context de la recàrrega gestionada d'aqüífers acoblada a l'efluent d'una planta de tractament d'aigües residuals.

En primer lloc, s'avalua la possibilitat d'utilitzar imatges infraroges tèrmiques (TIR) disponibles gratuïtament de Landsat 8 com a eina exploratòria per identificar fonts de SGD a tot el món. L'ús de dades tèrmiques de satèl·lit com a tècnica per identificar fonts de SGD al mar es basa en la identificació de plomalls tèrmicament anòmals obtinguts a partir del contrast tèrmic existent entre les aigües subterrànies i les aigües superficials del mar. L'objectiu principal d'aquesta primera part de la investigació és demostrar la utilitat de les

imatges infraroges tèrmiques (TIR) de Landsat 8 com a eina exploratòria per identificar fonts de SGD (àrees càrstiques) a tot el món i discutir quins són els principals factors limitants d'aquesta tècnica en estudis de SGD. Els resultats mostren que la teledetecció amb imatges de satèl·lit tèrmiques, és un mètode útil per identificar fonts costaneres en aqüífers càrstics tant a nivell local com regional. No obstant això, hi ha alguns factors que cal considerar, com ara, limitacions de la tècnica, característiques geològiques i hidrogeològiques de l'àrea d'estudi, condicions ambientals i marines i la geomorfologia costanera.

En segon lloc, es presenta l'ús potencial de dades de clorofil·la (Chl-a) obtingudes amb satèl·lit, com una eina de baix cost per mapejar l'evolució espacial i temporal de la influència ecològica de la SGD a les zones costaners. Per distingir les altes concentracions de Chl-a derivades de SGD de les derivades d'altres fonts potencials, s'ha aplicat una anàlisi d' agrupament a les dades de Chl-a. Els resultats mostren que les dades de Chl-a obtingudes amb satèl·lit ofereixen la possibilitat d'identificar i restringir àrees on les entrades de SGD han augmentat la productivitat primària i calcular el gradient de concentració de Chl-a al llarg del temps induït per la SGD.

Finalment, s'investiga el destí dels filtres UV seleccionats, en dos sistemes de recàrrega gestionada d'aqüífers; un complementat amb una barrera reactiva a base d'argila i compost vegetal, i l'altre com a sistema de referència. Es monitoritza la benzofenona-3 (BP-3) i els seus productes de transformació (TP) (benzofenona-1 (BP-1), 4,4′-dihidroxibenzofenona (4-DHB), 4-hidroxibenzofenona (4-HB) i 2 , 2'-dihidroxi-4-metoxibenzofenona (DHMB)), benzofenona-4 (BP-4) i avobenzona (AVO) en tots els compartiments involucrats (aigua, sòl i biopel·lícula), abans i després de modificar les condicions redox mitjançant un pols d'acetat de liti. Els resultats mostren que la implementació d'una barrera reactiva als sistemes de recàrrega gestionada d'aqüífers millora substancialment la degradació dels filtres UV, especialment de la BP-3 i els seus TP.

Aquesta tesi ha contribuït a millorar la gestió dels recursos hídrics subterranis a través de nous enfocaments metodològics i tècnics per fer front als nous reptes de la societat actual.

Acknowledgments

Aquests podrien ser uns agraïments molt molt llargs us ho ben asseguro! Ja que ha estat un camí llarg i pedregós que no hagués estat possible sense el suport de molta gent que potser inclús sense saber-ho han fet possible que avui estiguis aquí assegut llegint aquesta tesi.

I com no, començant agraint al meu director i directora de tesi l'Albert Folch i la Paula Rodríguez. A tu Albert primer de tot per enredar-me a demanar una beca i acabar fent una tesi (tinc dubtes de si això hauria d'aparèixer o no als agraïments.... jajajaj). Recordo aquell dia com si fos ahir, on jo propensa a fluir per la vida i a dir que SI a tot vaig pensar en silenci "tranquil·la Sònia aquestes coses no toquen mai". Doncs si que toquen si!! També vull agrair-te per ser el meu terapeuta psicològic durant tot aquest temps i escoltar-me en cada un dels meus alts i baixos de la tesi traient sempre la part positiva de tot i sobretot per deixar-me fer el que m'ha agradat. Tranquils que si seguiu llegint aquesta tesi i us endinseu pels diferents capítols entendreu molt bé perquè ho dic! Per això i per tot el teu suport i confiança en mi, moltes gràcies per aguantar-me durant tots aquests anys!
Ens queda pendent fer una segona tesi junts, però aquest cop perquè m'ensenyis les teves habilitats de venedor i orador professionals!
I a tu Paula per confiar i creure en mi tot i el meu super debut en l'assaig de traçadors on mai es va arribar a injectar el traçador (o si més no, el que volíem) que vam estar mostrejant durant 3 mesos. Sort que tot i semblar impossible hem obtingut resultats xulos! I per la redacció de la tesi, no tindria la mateixa qualitat sense la teva ajuda. Fem un bon tàndem, potser per com dius tu perquè estem una mica taradetes i ens agrada l'organització i les dates! O potser perquè a dins portem l'aire pur de les muntanyes de l'Alta Ribagorça.

A tot el grup de Grup d'Hidrologia Subterrània, a la Tere per tota la gestió amb els tiquets, factures i compres, sort que tens solucions per tot, al Xavi, al Marteen per l'ajuda en tot el "papeleo" inicial i al Dani per la seva contribució en aquesta recerca i pel teu riure contagiós. A tots els coleguis de recerca però també de frustracions, èxits, alegries, congressos, festes, dinars, cafès.... (Daniela, Bella, Rodrigo, Malik, Guido, Arnau, Jose, Bieito, Guillem, Buse i Yufi). A la Vera, per aconseguir que comencéssim els dilluns amb alegria, si ho heu llegit bé... el secret? Uns pastissos deliciosos! I tu Uri, company de TOC de sorollets, de cafès dramàtics i de sentiments en vers la tesi, ho aconseguirem!!!

A tots aquells que ja han marxat del grup i que s'estan obrint el seu propi camí, Guillem (tot un yanke), Carme, a la super professora Gumby, Mireia, al turtelcitoo i als seus bolus i sesions, a la patati de la Miki (i els seus intents fallits de reciclatge de capsules de cafè) i a la Nuri per tot el seu suport, complicitat, ajuda i aventures viscudes.

A tots els participants del projecte de recàrrega de Palamós però en especial a la Lurdes, Cristina i a la Sara per les mil i una aventures viscudes, que no puc evitar recordar amb un somriure, passant des de animals morts en llocs impossibles, nius de vespes, accidents a hores intempestives de la nit, aventuretes amb el cotxe per Cardedeu amb 2km d'autonomia, i com no als magnífics menús del càmping! I per suposat per tota l'ajuda rebuda durant l'assaig. I al Jesús i a la Sílvia per la seva expertesa i coneixements.

Al Jordi i Valentí de l'autònoma, per les llargues discussions i els diferents punts de vista sobre la SGD. Als teus cors i milers de versions del primer article Jordi! Estic segura que aquesta recerca no hagués estat la mateixa sense la vostra contribució.

A la Júlia i a Sílvia pels nombrosos berenars de gordis que heu hagut de suportar durant els meus alts i baixos durant la tesi. Per pensar des de el dia 1 en el modelito que portaré el dia de la meva defensa. Aquesta tesi també és fruit del vostre suport incondicional.

I finalment als meus pares i a la meva família que sempre han confiat en mi i m'han deixat fer tot el que m'agrada, però sobretot per com m'han recolzat al llarg d'aquest llarg viatge que ha estat la tesi. A la iaia que tot i no entendre massa bé encara de que he fet la tesi sempre ha estat molt orgullosa de mi.

I a tu Omar, per empenyem a seguir sempre i per fer-me creure en mi mateixa i en el que faig. Per suposat per les milions de revisions de l'anglès que m'has fet i l'ajuda amb les figures (photoshop pot amb tot i més) això si "amenaçant-me" en que t'hauria de posar a la portada de la tesi! I potser tens raó.... I potser a la portada també hi ha alguna cosa de tu.... Al nostre Samba pels nombrosos passejos inspiradors per Collserola i la nostre pitxi Boira gran apassionada en dormir sobre la funda del portàtil i en passejar-se per sobre del teclat.

DE TOT COR, GRÀCIES!

Per la realització d'aquesta tesi he rebut l'ajuda econòmica d'una beca de la Generalitat de Catalunya FI- 2017. This research was partly funded by the Spanish Government, (grant nos. PID2019-110212RB-C22 and PID2019-110311RB-C21), MONOPOLIOS (RTI2018-101990-B-100, MINECO/FEDER) and Project CEX2018-000794-S, by the Catalan Research Project RESTORA (ACA210/18/00040) and TerraMar (grant no. ACA210/18/00007) and by EU project MARADENTRO (PCI2019-103425 and PCI2019-103603).The authors want to thank the support of the Generalitat de Catalunya to GHS (grant no. 2017 SGR 1485) and MERS(grantno.2018SGR-1588)for additional funding.

-A vosaltres, pare i mare, que m'ho heu donat tot-

Contents

List of Figures

List of Tables

Abbreviations

AVO: avobenzone

BP-3: benzophenone-3

BP-1: benzophenone-1

BP-4: benzophenone-4

BTCs: Breakthrough curves

CECs: Contaminants of emerging concern

Chl-a: Chlorophyll-a

CT: Compost-treatment

DHMB: 2,2'-dihydroxy-4-methoxybenzophenone

DN: Digital number

DOC: Dissolved organic carbon

DZ: Dinamic zones

EC: Electrical conductivity

Eh: Redox potential

EPS: Extracellular polymeric substances

MAR: Managed aquifer recharge

SAT: Soil aquifer treatment

SD: Standard deviation

SGD: Submarine groundwater discharge

SST: Sea surface temperature

ST: Sand-treatment

TIR-RS: Thermal infrared remote sensing

TPs: Transformation products

UVFs: Ultraviolet filters

WWTP: Waste water treatment plant

4-DHB: 4,4′-dihydroxybenzophenone

4-HB: 4-hydroxybenzophenone

Chapter 1

Introduction and objectives

1.1. Introduction

Only less than 1% of freshwater in the Earth surface is available for human uses and groundwater accounts for nearly all its useable part (UNESCO, 1999). Groundwater is an essential part of the hydrological cycle being a valuable natural resource providing a primary source of water for agriculture, domestic, and industrial uses. It is vital also for sustaining streams, lakes, wetlands, and other dependent ecosystems (Kløve et al. 2014). Therefore, its proper management and protection is needed to guarantee both human life and ecosystem services.

Nevertheless, global change threats the good status of groundwater bodies, significantly affecting the global hydrological behavior (Hansen et al. 2016), in the space, time and frequency domains (Milly et al. 2005; Holman 2006). Global change is modifying annual precipitation patterns, increasing length of droughts, evaporation and atmospheric water vapor, and, decreasing ice cover (Easterling et al. 2000; Barnett et al. 2005; Allan and Soden 2008). Consequently, changes in soil moisture, runoff, aquifer recharge, groundwater discharge, and storage are induced. All of them have an impact on the hydrological cycle, including both groundwater quantity and quality.

Regarding groundwater quality, global change also affects it in many ways. As a result of the decrease in groundwater resources amount, dilution mechanisms are less effective and contaminant concentration becomes higher. For instance, there is an increase of salt concentration and total-dissolved solids during dry periods (Grimm et al. 2008). Besides this, groundwater quality is highly affected by the increase of population, especially in the coastal areas, where around of 50-70% of the world population live (Benoit et al. 2007). In these areas, an important quality problem is seawater intrusion. This process is defined as the salt water flow inland, which is higher during lower groundwater discharge and recedes towards the sea when the recharge is greater (López and Gómez, 2007). In high populated coastal areas, groundwater quality is also affected by human activities (agriculture, industry, waste water, etc.), which in turn, may affect coastal ecosystems when polluted groundwater discharges in to the sea.

Other quality problems are related to the management of waste water treatment plants (WWTP). The fact that population are concentrated in big areas (cities) promotes high loads of pollutants in the WWTP influents. For traditional pollutants (e.g. organic matter, suspended soils, pathogens), it does not represent a big problem since there is enough knowledge and enough technology to treat them until non-risky concentration. Indeed,

most of the current WWTPs have been designed to treat these pollutants. Nevertheless, the current WWTPs do not have enough capacity to remove the new pollutants, like Contaminants of Emerging Concern (CECs). These compounds are at much lower concentration than the traditional ones - at least three orders of magnitude, between nano- and micrograms per liter. Besides this, they comprise a wide range of compounds with different physical and chemical properties: pharmaceuticals, micro and nanoplastics, antibiotic resistance genes… As they are not treated, they are present in the outflow of the WWTP appearing in several environmental systems (surface water, groundwater, seawater, etc.).

Therefore, there are several threats that affect groundwater resources availability at global scale due to pollution. However, there is not a unique solution to solve all different groundwater quality problems. Oppositely, each issue needs to be specifically addressed, using the best tool that allows to manage and minimize the impact of each water quality problem.

1.1 The impact of submarine groundwater discharge and the use of remote sensing

Groundwater salinization in coastal areas results in a decline in the quality and quantity of existing groundwater resources. At the same time, groundwater from coastal aquifer discharge in to the coastal areas as part of the submarine groundwater discharge (SGD).
SGD is an important component of water cycle and is defined as the flow of water through continental and insular margins from the seabed to the coastal ocean, regardless of fluid composition or driving force, and thus includes meteoric fresh groundwater but also seawater circulating through the coastal aquifer or permeable sediments (Burnett et al. 2003; Taniguchi et al. 2019a; Garcia-Orellana et al. 2021).

According to Garcia-Orellana et al. (2021), groundwater discharge can be grouped into the following five different pathways: (1) terrestrial groundwater discharge, (2) density-driven seawater circulation, (3) seasonal exchange of seawater, (4) shore face circulation of seawater and, (5) centimeter-scale porewater exchange (PEX). The discharge of fresh groundwater (pathway 1) and, to a lesser extent, density-driven seawater circulation (pathway 2) are the only mechanisms representing a net source of freshwater, to the coastal ocean, usually mixed with seawater. The SGD discharge process occurs mainly through three different ways: coastal onshore springs, which discharge on the coastline via surface sinkholes (Garcia-Solsona et al., 2010; Mejías et al., 2012); submarine springs, where the discharge occurs via deep sinkholes (Bakalowicz, 2015; Fleury et al., 2007); and, diffuse

discharge, non-concentrated discharge that occurs throughout sediments (Rodellas et al., 2014).

Several studies have demonstrated that SGD is also an important process delivering nutrients and other solutes to marine ecosystems (Paytan et al. 2006; Rodellas et al. 2015; Cho et al. 2018). Indeed, this nutrient discharge impacts significantly on coastal marine ecosystems, modifying biogeochemical cycles (Valiela et al. 1992; Boehm et al. 2004) and altering the ecological status of the coastal water bodies (Lecher and Mackey 2018; Alorda-Kleinglass et al. 2021). A proxy to determine the status of coastal ecosystem is the study of phytoplankton abundance and dynamics (Hays 2005; Paerl 2006). The simplest method for measuring primary productivity is by analyzing chlorophyll-a (Chl-a). Traditionally, it has been measured *in-situ* or by discrete water samples. These methods are time-consuming, expensive and laborious, especially, when the goal is to cover large areas and to obtain periodic information of remote areas with difficult access (Glasgow et al. 2004; Bierman et al. 2011).

Understanding and, therefore, mapping SGD is a challenge even when it is relied on the application of multitude of traditional *in situ* methods. These methods include different procedures such as traditional local knowledge, visual observation, changes in vegetation or changes in water temperature and salinity, seepage meters or radioactive isotope tracers (Mejías et al., 2012; Schubert et al., 2014). Nevertheless, they are not good enough to characterize SGD at large scale, the application of most of them has an economical cost relatively high and its efficiency to evaluate the impact of SGD on coastal ecosystems is limited.

In this context, the application of remote sensing in SGD studies could be an alternative methodology for identifying SGD locations. Furthermore, it may help to assess the areas influenced by SGD as well as the impact of SGD on coastal biogeochemical cycles, thus contributing to better constrain the effects of SGD on coastal ecosystems.

Remote sensing is a technique that allows extracting information of the environment from images at different wavelengths, improving and complementing the information obtained from traditional methods. Remote sensors installed in satellites, airplanes and drones, collect data by detecting the electromagnetic radiation that is reflected from Earth. There is a significant number of satellite platforms and programs that can be grouped according to their temporal and spatial resolution: low spatial resolution 1km - 250m (NOAA-AVHRR, TERRA, AQUA, etc.), mean spatial resolution 100m - 15m (Landsat, TERRA-ASTER, IRS-WIFS, etc.), high spatial resolution 10m - 2m (QUICKBIRD, IKONOS, etc.) and very high spatial resolution <2 (LIDAR…). Remote sensing data can be used indirectly or directly to

detect different water quality indicators (Gholizadeh, 2016). The most commonly measured qualitative parameters of water by means of remote sensing are: chlorophyll-a, secchi disk depth, colored dissolved organic matters, total organic carbon, total suspended matters and turbidity, obtained using a combination of multispectral bands and temperature obtained using thermal infrared (TIR) images. Furthermore, satellite remote sensing is a cost-effective method of global coverage allowing the study of inaccessible zones and/or areas with data scarcity (Wilson and Rocha, 2012). However, the suitability and the potential of satellite images to perform SGD research has been only evaluated in a few studies at local scale and its applicability as a SGD characterization tool need to be evaluated in more detail.

1.2 The impact of Contaminant of Emerging Concern and the use of Managed Aquifer Recharge

As stated above, the current WWTPs do not allow to remove CECs until non risky concentrations for human and for ecosystem are reached. Indeed, most of these compounds are non-legislated and they are released to the environment within the WWTP outflows.
In this context, it is needed to develop technologies capable to treat a wide range of CECs that at the same time can be easily coupled to WWTP. One example of a type of CECs is Ultraviolet filters (UVF) which are constituents of a large number of personal care and hygiene products and other consumer goods (Tran et al., 2013) and may have toxic effects on aquatic and terrestrial organisms. This compounds, as other CECS are released to the environment within the WWTP outflows.

In this context, Managed Aquifer Recharge (MAR) is a technology that increases the availability of water in aquifers through enhancing the infiltration and the subsequent transit travel along the aquifer. In addition, MAR can act as a biogeochemical reactor improving recharged water quality during its passage through the soil (Greskowiak et al. 2006) by decreasing the concentration of suspended solids, pathogens, nitrogen, phosphates, metals, dissolved organic carbon (Bouwer 2002) and CECs. If MAR is coupled to a WWTP, it contributes to increase water resources and to stimulate circular economy. Nevertheless, this combination must ensure that source water quality (the outflow of the WWTP) meets the standards. For that, Valhondo et al. (2014) suggested the installation of a reactive barrier at the bottom of an infiltration basin to enhance the removal of CECs. The reactive barriers consist of different materials providing a range of sorption sites (neutral, cationic, and anionic) and enhancing biodegradation by the release of labile organic carbon, which promotes a wide range of redox states enlarging degradation pathways and, therefore removal of CECs (Valhondo et al. 2015).

Biodegradation and sorption are essential processes for organic contaminants attenuation during subsurface flow (Maeng et al 2011; Shaffer et al.2012). CECs are biodegraded in groundwater under aerobic and anaerobic conditions, but mainly by co-metabolism (Tran et al., 2013) forming different transformation products (TPs) depending on the degradation pathway. Sorption of CECs is governed by their affinity to the solid organic phases and by the electrostatic and similar interactions among the ionized molecule and the charged solid surfaces (Torresi et al., 2017). These sorption mechanisms are affected by numerous chemical parameters of the solution (ionic strength, pH, concentrations of competing ions) and solid surfaces (its composition, surface charge and the age of organic matter) (Schaffer et al., 2012). Recent studies (Rodríguez-Escales and Sanchez-Vila 2020) have demonstrated that, besides traditional sedimentary organic surfaces, biofilms can act as active sorbents to organic compounds in porous media. Biofilms are an assemblage of microorganism comprising microbial species attached to a surface and encased in a self-synthesized matrix with water and extracellular polymeric substances (EPS). Therefore, biofilms are the site for biotransformation of organic compounds and can retain them through several mechanisms.

In this context, although there is some experimental evidence of organic compounds retention in wastewater treatment plants biofilms (Torresi et al. 2017), there is no experimental evidence about retention of organic compounds in the porous media biofilms. More importantly, there are no works about the resilience of biotransformation and retention mechanisms with respect to changes in redox conditions, which is expected in a MAR facility.

1.2. Motivation and objectives

In this context it is necessary to find solutions that could contribute to mitigate the effects of global change in groundwater; increasing the amount of water resources, improving their management and enhancing their quality.

For that, the main objective of this dissertation is to improve groundwater resources management in two different ways. The first one, by using remote sensing tools for the characterization of groundwater in coastal areas; and, the second one, by using reactive barriers to improve degradation of contaminants of emerging concern in the context of managed aquifer recharge coupled to the outflow of a waste water treatment plant. With this, this dissertation will contribute to improve two important problems related with groundwater quality: characterizing SGD discharge and its ecological impact and improving the removal of CECs in the outflow of WWTPs.

To accomplish this broad objective, specific goals are identified:

- To study the usefulness of satellite TIR images at different sites, covering a large scale and in different seasons to assess whether Landsat 8 TIR-RS can be used as an exploratory tool for identifying SGD springs worldwide for long-term analysis.
- To discuss the influencing factors to be considered in the identification of SGD at the local and regional level.
- To evaluate the potential use of Landsat 8 satellite Chl-a data for identifying SGD-impacted coastal areas.
- To map the spatial extension and temporal evolution of SGD-influenced areas using Landsat 8 satellite Chl-a data for different selected sites.
- To evaluate the role of reactive barriers made up of compost in the degradation of UVFs and its transformation products.
- To evaluate the impact of varying redox conditions on both sorption and degradation processes of UV filters in MAR systems.
- To evaluate the impact of biofilm in the fate of UV filters.

1.3. Thesis outline

The resulting document is structured in five chapters. The introduction to the problem is presented in Chapter 1. Chapter 2 thoroughly compares reported SGD locations with satellite-data-derived thermal anomalies in order to assess the suitability of satellite TIR-data for conducting SGD research. The goal of this chapter is to study the usefulness of satellite TIR images at different sites, covering a large scale and in different seasons to

assess whether Landsat 8 TIR remote sensing can be used as an exploratory tool for identifying SGD springs worldwide, from local to regional scales, for long-term analysis. Chapter 2 also provides a discussion about the influencing factors to be considered in the identification of SGD at the local and regional level.

Chapter 3, focuses on understanding the impact of SGD on coastal biogeochemical cycles and on the extension of areas influenced by SGD, contributing thus to better constrain the poorly assessed effects of SGD on coastal ecosystems. The goal of this chapter is evaluate the potential use of Landsat 8 satellite Chl-a data for identifying and constraining SGD-impacted coastal areas and mapping the spatial extension and temporal evolution of SGD-influenced areas.

Chapter 4 is focused on the effect of compost reactive barriers in the fate of UVFs and their transformation products in a MAR facility. As a side objective, it is also evaluated the role of biofilm and organic mineral surfaces in the fate of UVFs as well as the effect of varying redox conditions in both sorption and degradation.

Finally, Chapter 5 presents the conclusions obtained during the performed research.

The Appendix includes supplementary information of the previous chapters. Appendix A, the supplementary information of chapter 2; Appendix B, the supplementary information f chapter 3 and Appendix C, the supplementary information of chapter 4. At the end of the appendix, two scientific published papers were included, one with being the base of chapter 2 and the other one I co-authored during the PhD development period. That paper explore how irrigated agriculture, mining and tourism dependent on a multi-layered groundwater system could affect the groundwater system by analysing the sustainability of the new abstraction regimes before, during and after La Niña event 2016/17 in Kwale, Kenya. As part of the approach, induced changes in seawater intrusion are also studied. Geochemical models to understand the geochemical processes occurring in the area affected by seawater intrusion dynamics are developed using PHREEQC software.

Chapter 2

Applicability of Landsat 8 Thermal Infrared Sensor for Identifying Submarine Groundwater Discharge Springs in the Mediterranean Sea Basin

Jou-Claus, S., Folch, A., Garcia-Orellana, J., 2021. Applicability of Landsat 8 Thermal Infrered Sensor for Identifying Submarine Groundwater Discharge Springs in the Mediterranean Sea Basin. Hydrology and Earth System Sciences, 25,9,9.

2.1. Introduction

Submarine groundwater discharge (SGD) is an important component of the hydrological cycle and has been commonly defined as any flow of water across the continental margin in the ocean-aquifer interface, regardless of fluid composition or driving force, with spatial scale lengths of meters to kilometers (Burnett and Dulaiova 2003; Moore 2010; Taniguchi et al. 2019a). This definition includes meteoric fresh groundwater resulting from inland recharge, but also seawater circulated through the sediments of coastal aquifers (Burnett & Dulaiova, 2003). Both water flows mix in coastal aquifers, where biogeochemical reactions may occur when this groundwater interacts with the geological matrix (Moore, 1999; Moosdorf et al., 2021; Rocha et al., 2021; Ruiz-González et al., 2021). This dynamic mixing zone influences the transfer of chemical compounds such as nutrients, trace metals and other contaminants to coastal waters (Boehm et al. 2004a; Rodellas et al. 2015; Trezzi et al. 2016; Alorda-Kleinglass et al. 2019).

SGD-derived inputs from chemical compounds can highly impact coastal ecosystems by influencing productivity, biomass, species composition and sonification (Krest et al. 2000; Garcés et al. 2011; Garcia-Orellana et al. 2016; Andrisoa et al. 2019). According to Garcia-Orellana et al., (2021) groundwater discharge pathways of SGD can be grouped into five different SGD pathways according to the characteristics of the processes: 1) Terrestrial groundwater discharge; 2) Density-driven seawater circulation; 3) Seasonal exchange of seawater; 4) Shoreface circulation of seawater and 5) cm-scale porewater exchange (PEX). The discharge of fresh groundwater (Pathway 1) and, to a lesser extent, density-driven seawater circulation (Pathway 2), are the only mechanisms that represents a net source of freshwater, usually mixed with seawater, to the coastal ocean. The SGD discharge process related to this fresher fraction of SGD occurs mainly through three different ways: coastal onshore springs, which discharge on the coastline via surface sinkholes (Garcia-Solsona et al., 2010; Mejías et al., 2012); submarine springs, where the discharge occurs via deep sinkholes (Bakalowicz, 2015; Fleury et al., 2007); and diffuse discharge, a type of discharge which is not concentrated and occurs throughout sediments (Rodellas et al. 2012).

Identifying and mapping groundwater discharge areas is challenging, despite the number of traditional methods available for locating the main groundwater discharge locations and quantifying their flow rates. These methods include simple procedures such as deploying traditional local knowledge, conducting visual observation, monitoring changes in vegetation as well as in water temperature and salinity, and using seepage meters or radioactive isotope tracers (Mejías et al. 2012; Schubert et al. 2014; Rosenberry et al. 2020; Garcia-Orellana et al. 2021). Apart from these methods, several authors have suggested

Thermal Infrared Remote Sensing (TIR-RS) as an alternative methodology for identifying potential SGD spring sites, since it enables the screening and study of inaccessible zones and/or areas with a scarcity of hydrogeological information (Wilson & Rocha, 2012). Temperature has been used successfully to study SGD by comparing the relatively constant temperature of groundwater with that of surface seawaters, which fluctuates seasonally (Dale & Miller, 2007). In general, groundwater maintains a relatively constant temperature between depths of 5 m and 100 m, approximately 1 - 2 ºC higher than the mean annual air temperature (Anderson 2005). The detection of SGD springs via TIR-RS is possible in any environment where there is thermal contrast between the discharging fluid and the receiving surface water body (Kelly et al. 2013). TIR images have the potential to identify the location of major SGD springs, as well as to study their spatial and temporal variability, by exploring the temperature difference between coastal seawater and brackish groundwater discharges at different times.

There are two types of platforms for obtaining thermal infrared information: airborne TIR-RS (airplane, helicopter and drone), and satellite TIR-RS (Modis, Aster, Landsat). Airborne TIR has been used for different applications; for example Shaban et al. (2005) and Akawwi et al. (2008) conducting aerial TIR surveys along the Mediterranean and Dead Sea coastlines to identify potential SGD sites. Kelly et al. (2013) used TIRS images from localized point-source SGD to demonstrate that groundwater plume areas are linearly and highly correlated to in-situ groundwater fluxes. Airborne TIR-RS has also been applied in combination with other methods, not only for qualitative SGD recognition, but also for quantifying groundwater flows from freshwater springs (Danielescu et al., 2009; Mejías et al., 2012). In the coastal carbonate aquifer of El Maestrazgo (Iberian Peninsula), a combination of complementary techniques was used to locate submarine springs via airborne high-resolution thermal infrared, radon measurements and physical-chemical anomalies, and to quantify the groundwater discharge by direct quantification with flowmeters and Ra isotopes (Mejías et al., 2012). Tamborski et al. (2015) combined airborne TIR overflights with coastal radionuclide surveys to investigate the significance of SGD along the north shore of Long Island (NY, US) to provide quantitative evidence for TIR-RS, as a tool to remotely identify and measure SGD. Finally, Danilescu et al. (2009) assessed total freshwater discharge in two small nutrient-sensitive estuaries in Prince Edward Island (Canada), using a combination of TIR images, direct discharge measurements and numerical simulations.

Compared to airplane, helicopter and drone platforms, satellite TIR-RS has some characteristics that limit its use for coastal water observation. The temporal resolution is fixed and varies depending on the satellite, with a minimum daily revisit frequency and a

maximum frequency of every 16 days for a specific area. Furthermore, the spatial resolution, which varies between 30 and 1000 meters, is lower than airborne resolution. This results in the fact that small thermal anomalies, induced by small flows of SGD, are likely not to be detected. Additionally, satellite TIR-RS images are affected by atmospheric conditions (i.e., clouds and shadows). However, satellite TIR-RS imagery has the great advantage of being free of charge (Landsat), easily accessible, globally available, multi-temporal, and covering a regional scale instantaneously. These advantages turn satellite TIR-based approaches into a viable and promising option for detecting SGD worldwide.

There are several satellite missions capable of measuring sea surface temperatures (SST) with a moderate spatial resolution and acquisition: Advanced Spaceborne Thermal Emission and Reflection Radiometer (ASTER), and the Landsat satellite among others, which provide appropriate spatial and temporal resolution for large-scale SGD monitoring. For those sensors suitable for SGD research, Landsat is the one with the longest TIR data provision (from 1982 until today and already planned to go beyond 2030 (Wulder et al. 2019) and the one most widely applied for the purposes of SGD research (Wilson & Rocha, 2012, among others).

The use of satellite imagery in SGD studies has evolved in parallel with the launch of new sensors that feature spatial resolution improvements over previous sensors. However, the application of satellite TIR images is neither extensive nor widespread compared to airborne TIR images. Several SGD studies used Landsat 7 to locate groundwater discharge areas (e.g. Wang et al., 2008); to detect known but previously unmapped SGD locations (Varma et al. 2010); to determine the spatial extent and scale of SGD-derived temperature anomalies (Wilson & Rocha, 2012); and to infer SGD temporal variation using long-term thermal anomaly size variations (Mallast et al., 2014). More recent studies used data obtained by Landsat 8 TIRS to identify and characterize SGD sites using the sensors technical improvements. For example, McCaul et al. (2016) proposed a multiapproach methodology for understanding submarine and intertidal groundwater discharge patterns. Xing et al. (2016) evaluated the ability of satellite remote sensing methods (Landsat 7 and 8) to detect thermal anomalies related to SGD as a possible index of the presence of offshore low-salinity groundwater storage at local scale. To the best of our knowledge, there is no study that thoroughly compares SGD locations with satellite-data-derived thermal anomalies over large spatial scales in order to assess the suitability of satellite TIR-RS data in conducting SGD research.

The aim of this chapter is to study the usefulness of satellite TIR images at different sites, covering a large scale and in different seasons to assess whether Landsat 8 TIR-RS can be

used as an exploratory tool for identifying SGD springs worldwide, from local to regional scales, for long-term analysis. The second aim is to discuss the influencing factors to be considered in the identification of SGD at the local and regional level.

The study was carried out on the coastal karstic aquifers of the Mediterranean Sea basin, where there are many local studies that describe the discharge processes thanks to the significant connectivity between this coastal aquifer type and the sea (e.g., Bakalowicz, 2005; Barberá & Andreo, 2015; Worthington, 1999). In this hydrogeological context, SGD takes place mainly through submarine or aerial springs (point source). Although groundwater discharge from submarine springs represents a negligible fraction of the global SGD (Luijendijk et al. 2020), in some areas, such as the Mediterranean Sea, this fraction can be locally important, strongly influencing marine ecosystems and serving as a freshwater resource for the population (Rodellas et al., 2015; Alorda-Kleinglass et al., 2021). To validate the temporal effectiveness of this technique, Landsat-8 images from 2017 and 2018 on the coasts of the Mediterranean Sea basin were used to locate SGD springs previously described in the scientific literature, showing in which period of the year these SGD springs are observable via satellite. In addition, we will hypothesize and discuss those factors that may condition the identification of SGD springs in order that future studies might take them into account when using satellite remote sensing TIR techniques.

2.2. Methods

2.2.1. Study area

The Mediterranean basin has been selected for this study because it is one of the areas of the world where numerous SGD studies have been carried out and where dozens of coastal springs have been described dating back to ancient times in countries such as Spain, France, Italy, Croatia, Greece, Turkey, Syria, Lebanon and Libya (Figure 2.1). In this study, we focus on a set of 54 springs mentioned in the scientific peer review literature published in English (Basterretxea et al., 2010; Bakalowicz, 2018; Fleury et al., 2007; Mejías et al., 2012 and Garcia-Solsona et al., 2010) where groundwater discharge is known to occur and there is a description of the hydrogeological context of each spring (Table 1, Appendix A). The number of springs included in the study represents at least 88% of the submarine karst springs described in the English peer review literature concerning Mediterranean basin.

The SGD contribution to the Mediterranean, ranges from 3 to $50 \cdot 10^{11}$ $m^3 \cdot yr^{-1}$, where fresh groundwater inputs represent 1 – 25% of the total SGD inputs (Rodellas et al. 2015). SGD has been described and studied in several locations along the Mediterranean coast (e.g., Bakalowicz, 2015; Mejías et al., 2012; Tulipano et al., 2005; Bejannin et al., 2017). The

Mediterranean basin is characterized by 46% of its coastline being formed by karstic aquifers (Bakalowicz, 2015; Fleury et al., 2007; Trezzi et al., 2016). Its narrow continental shelves prevent large tidal amplification along the coast; tidal amplitude is usually less than 0.2 m (Werner et al. 2013). The Mediterranean climate is seasonal, characterized by windy, mild, wet winters and by relatively calm, warm and dry summers. Strong local winds, such as the cold and dry Tramontana, Mistral and Bora, from the north, and the hot and dry Sirocco, from the south, are typical of the region. These strong regional and seasonal wind regimes provide a substantial amount of vertical mixing in the seawater column. In general, the main rainfall season is during fall and spring, with an average annual precipitation of 500 mm y^{-1} (Andreo & Carrasco, 1993). The sea temperature is approximately between 26 - 30 and 14 - 19 ºC in the summer and winter, respectively.

The available information for each of the 54 studied springs (Table 1, Appendix A) shows that the mean flow rates range between 0.009 and 50 $m^3 \cdot s^{-1}$, the distances from the shore range from the coastline to 1 km offshore, and that discharge depths vary between 7 m.a.s.l and 150 m.b.s.l. In accordance with these characteristics, we might classify the studied springs in 5 groups. The first group of springs discharge inland near the seashore and reach the sea through small streams; these karstic springs are located between 300 and 500 m inland and at elevations of 2, 3 and 15 m.a.s.l for Patan in Croatia, Almyros of Iraklio in Greece and Maro in Spain, respectively. The second group of springs discharges in coastal lagoons at a distance of 100 m from the sea shore and a depth of 4 m.b.s.l (Font Dame and Font Estramar in Salses-Laucate lagoon in France), and at an unknown shore distance and 30 m.b.s.l (Vise in Thau lagoon respectively). The third group of springs is located between 0 and 10 m from the shoreline and in shallow sea waters of between 0 and 7 m.b.s.l (Torre Badum, Las Fuentes, Font de Dins in Spain, Ain Zayana in Libya, Agios Nikolaos, Cephalonia and Anavalos Kiveri in Greece and Ovacik and Gokova in Turkey). The fourth group of springs is also located close to the shoreline, but at a water column depth of 12 m.b.s.l. The two springs of this group are Moraig in Spain and Port Miou and Bestouan in France. The fifth and last group consists of Mortola in Italy and Chekka in Lebanon, in which discharges occurs offshore between 100 m and 1 km and with a water column depth of between 35 and 150 m.b.s.l.

The type of coastal karst aquifer studied has been defined using the same classification as in Tulipano et al. (2005) for Mediterranean coastal karst aquifers. The first type are systems with poorly-developed, but highly-fractured karstification. This karst type included 3 different subsystems in which 1) faults dissect the aquifer such as in the Gokova (4 springs) (Bayari & Kurttaş, 2002) and Ovacik spring, where the faults are located in the underlying beds that extend towards the sea (Elhatip, 2003); 2) groundwater flows along the zones of

cracks, fractures and karst hollows, such as in the Donnalucata spring (Povinec et al., 2006); and 3) groundwater flows through stratification joints, such as in the Mortola spring (Fleury et al., 2007). The second type are systems with well-developed karstification connected to the sea (e.g., Moraig, Port Miou, Bestouan, Almyros of Iraklio, Almiros of Agios Nikolaos, Cephalonia, Ain Zayana and Chekka). The last type of defined karst system is a well-developed karstification but with low connectivity with the sea. This group is represented by only two springs: Kiveri Anavalos in Greece and Vise in France.

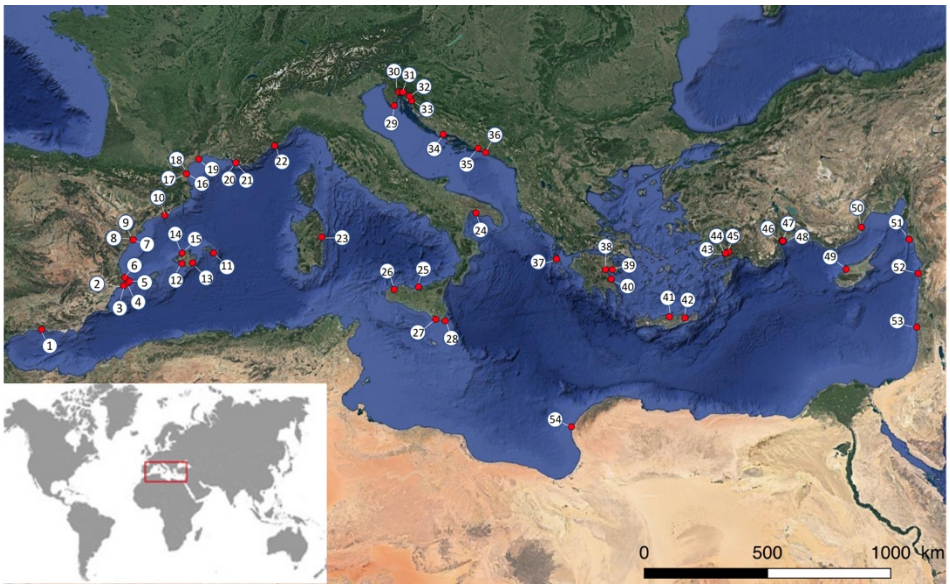

Figure 2.1. Location of the 54 SGD springs used for this study. SGD spring shown in the figure are described in Bakalowicz, 2018; Basterretxea et al., 2010; Fleury et al., 2007; Garcia-Solsona et al ., 2010 and Mejías et al., 2012. © Google Earth 2021.

2.2.2. Landsat 8 TIRS data acquisition

To determine the optimal time period for SGD detection using remote sensing, the SST of a series of images covering all seasons was compared. The TIRS instrument of Landsat 8 is a thermal imager with two thermal infrared bands centered at 10.8 μm and 12.0 μm and a ground sampling distance (GSD) of 100 m. However, all thermal images are resampled using a cubic convolution to 30 m (Roy et al., 2014). To carry out this study, only the thermal band 10 TIRS 1 (10.6 - 11.2 μm) of the 11 Landsat 8 bands was used to study the SGD sites. The other Landsat 8 thermal band, 11 TIRS 2 (11.50 - 12.51 μm), was not used because the data collected in this band had some large calibration uncertainties (U.S. Geological Survey, 2014b).

A total of 27 path/row combinations were analyzed with the Landsat 8 TIR images of the Mediterranean coast between January 2017 and December 2018 to cover all 54 known SGD sites. To that end, a total of 1296 images (2 images per month for the two years of study) were acquired from the U.S. Geological Survey (USGS) with cloud coverage between 0% and 90% in each image. A manual inspection of all images resulted in finer selection of 413 images with cloud-free conditions above the areas of interest (Table 2, Appendix A). The finer selection of cloud-free images was used for subsequent steps.

2.2.3. Deriving SST values from Landsat 8 TIRS data

Data processing included the conversion of digital numbers to SST, including an atmospheric correction of each image following the methodology presented by Chander et al. (2009). Image processing began with radiometric correction, which was performed by converting the digital number (DN) to sensor spectral radiance through band-specific rescaling gain and bias factors according to Equation (1).

$$L\lambda = G_{rescale} * Q_{cal} + B_{rescale} \quad (1)$$

where L_λ is the sensor spectral radiance [$W \cdot m^{-2} \cdot sr^{-1} \cdot \mu m^{-1}$]; $G_{rescale}$ is the band-specific rescaling gain factor [$W \cdot m^{-2} \cdot sr^{-1} \cdot \mu m^{-1} \cdot DN^{-1}$]; Q_{cal} is the quantized and calibrated standard product pixel values (DN) and $B_{rescale}$ is the band-specific rescaling bias factor [$W \cdot m^{-2} \cdot sr^{-1} \cdot \mu m^{-1}$].

The next step was an atmospheric correction to remove the atmospheric component of the recorded thermal signal which strongly depends on atmospheric conditions (aerosol content, humidity, temperature etc.) at a specific recording time and place. To atmospherically correct images at sensor spectral radiance, it was necessary to transform them into surface radiance of an ideal 'black body', considering the scene-specific up- and down- welling radiance and transmission values and the emissivity of the water surface, according to Equation (2) (Barsi et al. 2003).

$$L_t = \frac{L_\lambda - L_U - \tau * (1 - \varepsilon) * L_D}{\tau * \varepsilon} \quad (2)$$

where L_t is the radiance of an ideal 'black body' [$W \cdot m^{-2} \cdot sr^{-1} \cdot \mu m^{-1}$]; L_λ is the sensor spectral radiance [$W \cdot m^{-2} \cdot sr^{-1} \cdot \mu m^{-1}$]; L_U is the upwelling radiance [$W \cdot m^{-2} \cdot sr^{-1} \cdot \mu m^{-1}$]; L_D is the downwelling radiance [$W \cdot m^{-2} \cdot sr^{-1} \cdot \mu m^{-1}$]; ε is the emissivity of the surface [-] and τ is the atmospheric transmission [-].

A web-based atmospheric correction tool (Atmospheric Correction Parameter Calculator) developed by Barsi et al. (2003) based on MODTRAN was used to obtain values for atmospheric transmissivity and the upwelling and downwelling radiances of the atmosphere. The emissivity of water in the Landsat 8 TIR bands ranges from 0.98 (band 11) to 0.99 (band 10) and in this study, we assume a constant emissivity of 0.99 (Wen-Yao et al. 1987).

Finally, to obtain the sea surface temperature (SST), the corrected radiances were introduced into Equation (3).

$$T = \frac{K_2}{\ln\left(\frac{K_1}{L_t} + 1\right)} \qquad (3)$$

where T is the effective sensor brightness temperature [K]; L_t is the radiance of an ideal 'black body' [W·m^{-2}·sr^{-1}·μm^{-1}]; K_1 is prelaunch calibration constant 1 [W·m^{-2}·sr^{-1}·μm^{-1}]; and K_2 is prelaunch calibration constant 2 [ºK].

The resulting atmospherically-corrected SST data represent temperature with an error of less than 1.3 ºK for the temperature range 270 - 330 ºK. This temperature represents the skin temperature of the water (<1 mm of the upper most water layer), which differs from the bulk temperature below it by about 0.1 ºK due to sensible heat fluxes, evaporative heat loss, and long wave radiation (Donlon et al. 2002; Wloczyk et al. 2006).

2.2.4. Site inter-comparison between single image and multiple images

Temperature maps of coastal waters were created from temperature data to assess the significance of the SST anomalies. The identification of SGD spring sites was based on the assumption that temperatures of discharging groundwater may be different than seawater and less variable than seawater temperatures throughout the year. SGD spring sites were analyzed using two different procedures. First, single images were used to identify SGD springs by means of the water temperature anomalies. As a second step of the single image approach, the change between images along the study period was also evaluated. This qualitative analysis allows us to observe variations in the morphology and temperature range of the known discharge plume between images. As a second approach, called multiple imaging, SGD spring sites were detected by evaluating the pixel-by-pixel standard deviation (SD) across all image sets. Lower values of SD were used as indicators for groundwater discharge using sea surface temperature (SST) data series. This statistical parameter has been previously applied in semi-arid areas to study groundwater and surface water

interactions and identify spring discharge into lakes or enclosed seas (Mallast et al., 2014; Tcherepanov et al., 2005). It was assumed that groundwater tends to be less variable than surface water, which varies seasonally and daily. The applied multi-temporal thermal remote sensing approach was based on a variable number of Landsat 8 TIRS images. The images used to calculate the standard deviation varied between 5 and 17 images, depending on the number of images without clouds available for each studied site. The resulting thermal maps were combined with satellite imagery from Google Earth (only the land part) using GIS (QGIS Las Palmas) to show the location the SGD springs at the identified sites.

2.3. Results and discussion

2.3.1. Overall identifications

As an example of the Landsat 8 TIR images analyzed in the Mediterranean Sea basin, the thermal images of the Almyros SGD spring in Agios Nikolaos (Crete, Greece) throughout the year 2017 are shown in Figure 2. In general, a thermal anomaly plume is observed in several of the 23 images (one of the July images is missing) occurring near and perpendicular to the coastline, reflecting the continuous discharge of groundwater. Since a satellite image provides the sea surface temperature (SST) of the first millimeter of seawater (Donlon et al., 2002; Wloczyk et al., 2006), the thermal contrast due to SGD can be observed as the fresh groundwater flows over seawater due to its lower density (i.e., lower salinity) (Wilson & Rocha, 2012). The images series of Almyros Agios Nikolaos (Figure 2.2) shows how thermal contrast caused by the groundwater discharge cannot be observed throughout the whole year. The thermal contrast is more identifiable from the second half of April until the end of October, but the best thermal plume observations were from June to October (Figure 2). Conversely, this spring cannot be identified from November to March. The groundwater discharge was not identified in February and December due to the absence of thermal contrast, and in the other months (January, March and November) because clouds made identification difficult. Thus, the overall percentage of time for optimal SGD spring identification was 37% in 2017.

If the same approach is applied for the total of 54 SGD springs studied, only 23 springs were identified in individual images, representing a 44% success rate for the technique over the entire study period (2017 and 2018). The success percentage for identifying the 23 SGD springs, according to the period of the year, is shown in Supplementary Material 3. The highest success percentage for SGD identification was during the summer, specifically from June to September (Figure 3), which corresponds to an average of 21% of the images analyzed. Conversely, the SGD springs were not identified in the remaining 79% of the

images. The winter period, from December to February (Figure 2.3), had the lowest percentage of SGD spring identifications.

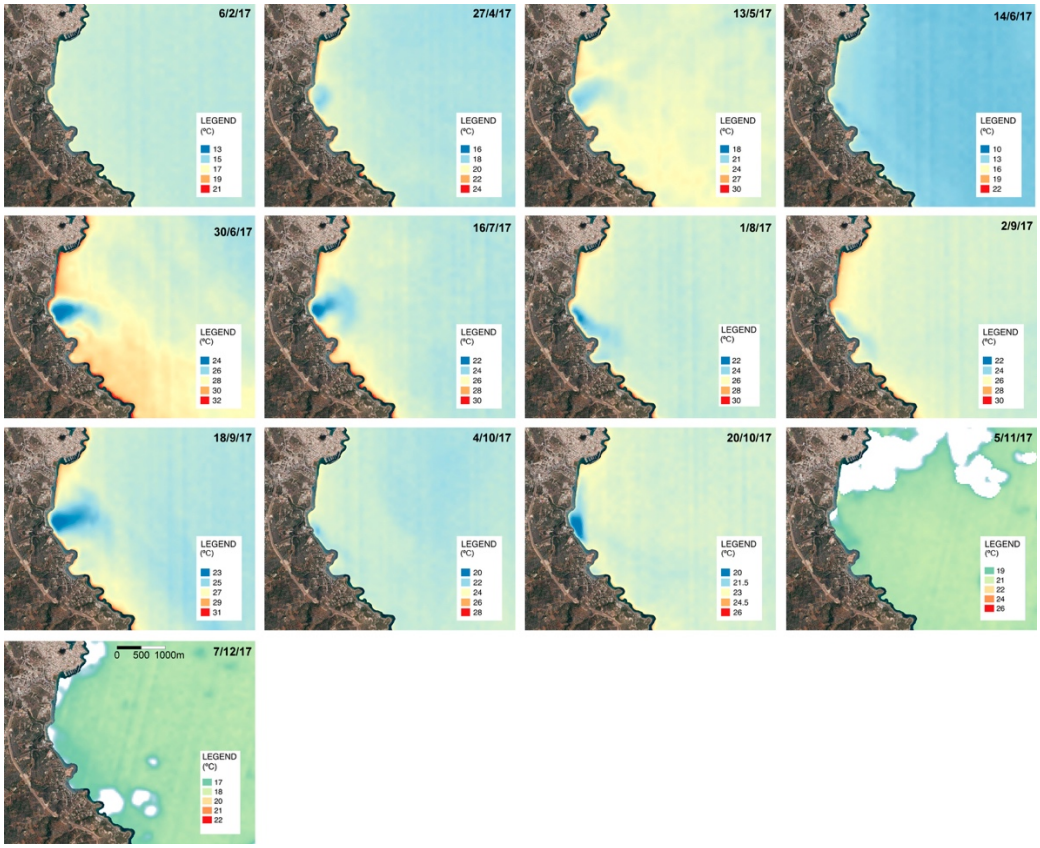

Figure 2.2. SST images (degrees Celsius) obtained via band 10 of Landsat 8 OLI/TIRS of the region of Almyros of Agios Nikolaos (Crete, Greece) throughout 2017. Of the 23 images analyzed, the presence of an SGD spring was clearly visible in nine images that represent a 37 % ratio of success. In January, March and November 2017, it was not possible to obtain an SST image due to the presence of clouds. © Google Earth 2021.

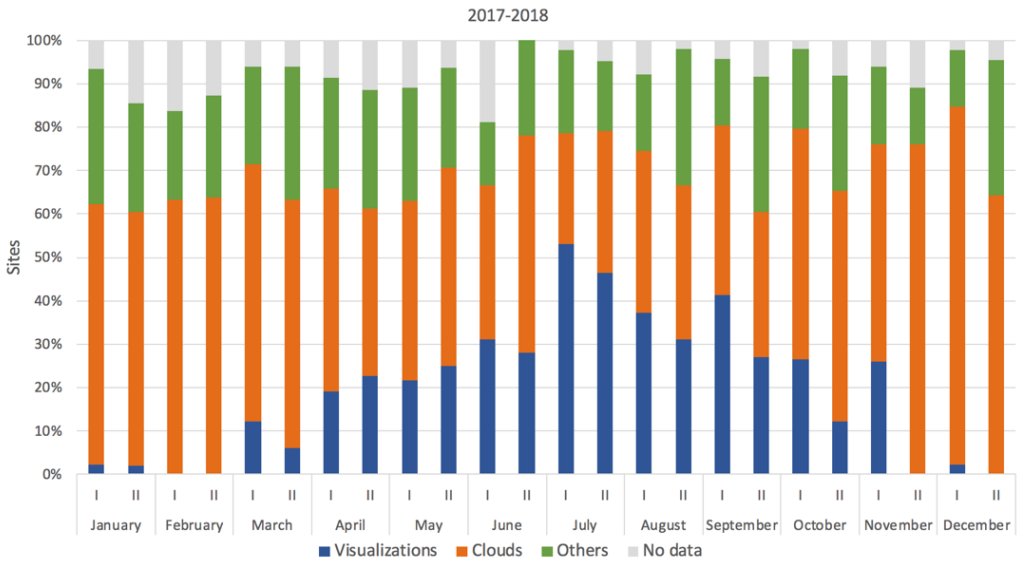

Figure 2.3. Percentage of successful and unsuccessful SGD identifications for all SGD springs that were identified at least once (23 springs representing 44%) throughout the year 2017 and during the year 2018 (based on the selection of 720 images), are shown individually in the Figure 1, Appendix A. The X-axis shows the months of the year. Roman numerals (I and II) represent the two satellite passes per month that cover every area. No image available is represented in grey, color while the presence of clouds is in orange and blue for successful SGD identifications. Those in which images were not covered by clouds, but SGD springs were not identified, are shown in the figure as "others" in green color.

2.3.2. Influencing factors to consider in the identification of SGD springs

The analysis of the images of the Mediterranean coast obtained by Landsat 8 TIRS during 2017 and 2018 was successful for several studied springs but did not identify SGD springs in all the images analyzed. Thus, identifying SGD springs using Landsat 8 TIRS presents some limitations, as the success rate was slightly less than 50%. The following potential limitations were previously reported in the literature in some local studied areas: only information for the first millimeters of seawater is available (Donlon et al., 2002; Wloczyk et al., 2006); spatial resolution (Wilson & Rocha, 2012); period of the year (Bayari & Kurttas 2002; Wilson & Rocha 2012; Xing et al., 2016); the results are highly dependent on atmospheric temperature, seawater currents, wind speed and direction, sea surface effects (Kelly et al., 2013) and cloud cover; and the need for specialist knowledge to convert the data into accessible (visualized) information (McCaul, 2016).

Given the above-mentioned limitations, we propose a conceptual framework of factors representing technical limitations in order to asses those issues that should be considered when applying TIR-RS to the study of SGD. These technical limitation factors can be grouped as follows: (1) technical limitations, (2) geological/hydrogeological characteristics, (3)

environmental and marine conditions, (4) coastal geomorphology and (5) anthropogenic sources (Figure 2.4).

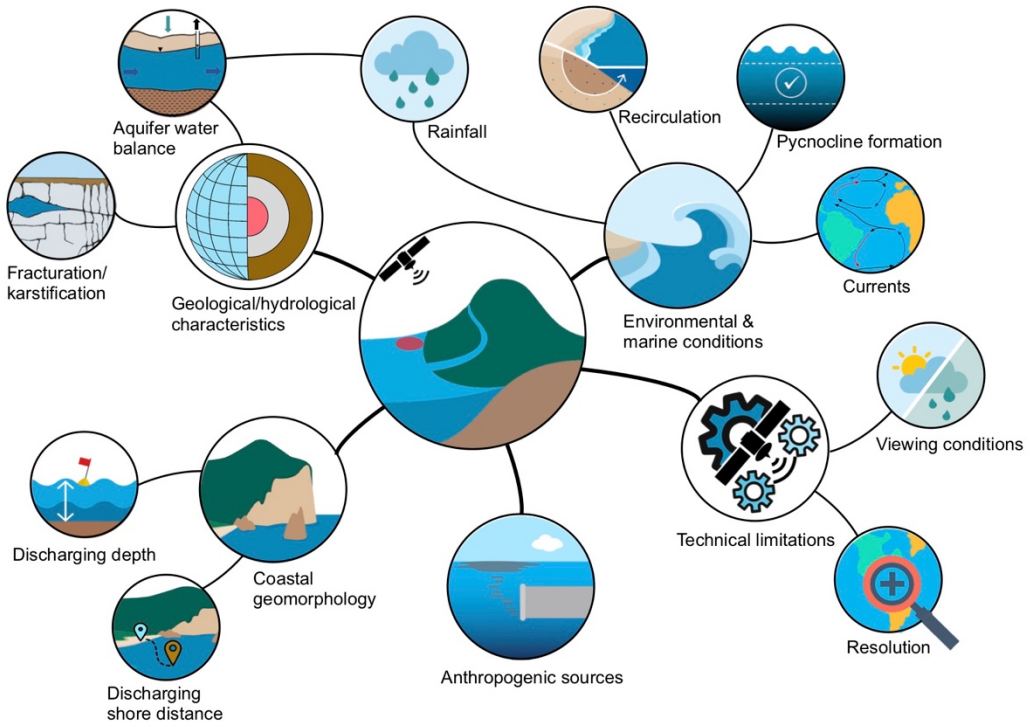

Figure 2.4. Conceptual framework of technical limitation factors that can limit the identification of SGD springs by using Landsat 8 TIRS images.

2.3.2.1. Technical limitation factors

Some of the main limitations of the technique are related to the temporality of obtaining images; the spatial resolution, the availability of images in the desired period and the atmospheric conditions during the image capture. Each satellite has an image acquisition spatial and temporal resolution, and therefore the results are subject to these pre-established conditions. For Landsat 8 TIRS, the temporal resolution is two weeks, and the spatial resolution is 100 m resampled to 30 m, so a smaller thermal anomaly plume than this produced by an SGD spring will not be identified. For example, in the 20 m wide semi-enclosed cove of Alcalfar (Menorca, western Mediterranean) there are several described springs (García-Solsona et al., 2010) that were not identified by satellite due to the small dimensions of the cove (García-Solsona et al., 2010). The availability of satellite images depends, in some cases, on technical problems that the satellite experiences during image collection, which implies that there are annual series of images with some missing images.

In the example used in Figure 2, where the Almyros of Agios Nikolaos (Greece) SGD spring is identified, only 23 of the 24 images that should have been produced during 2017 were obtained. The striping noise that it can be seen in the images (Figure 2.2), and which affect TIR bands especially, is another technical limitation. Sometimes the difference is so large that it would hinder a proper SGD detection (Gerace & Montanaro, 2017).

Other important limitations related to the technique include the atmospheric conditions at the time of the image capture. Clouds and clouds shadows change radiometric information leaving the sea surface and prevent a correct analysis of the images. For the Mediterranean Sea basin, of 80% of the images in which SGD springs were not identified, 60% were due to the high presence of clouds. Thus, clouds are the main factor limiting the identification of SGD springs. The presence of clouds is higher in winter than in summer; therefore, warmer months are much better for identifying SGD springs in the Mediterranean Sea. However, in at least 20% of the cloudless images, it was not possible to observe and locate SGD springs described in the literature. Therefore, a detailed analysis of the cloudless imagery is necessary to confirm the optimal conditions for locating SGD springs in the area of interest (Anderson 2005).

2.3.2.2. Geology and hydrogeology limitation factors

The characteristics of coastal aquifers and the different driving forces that allow groundwater discharge into the sea are other factors that can limit the identification of SGD springs. According to Garcia-Orellana (2021), SGD is the combination of fresh terrestrial groundwater discharge driven by hydraulic gradient between land and sea and saline groundwater discharge from the seawater recirculation through the coastal and continental margin. Thus, the thermal signal of both types of groundwater will define the intensity and shape of the plume that can be observed in the sea.

For coastal aquifer SGD springs, geological factors such as the lithology (e.g., type of rock, degree of karstification, presence of faults and/or fractures, etc.) determine the hydraulic properties that greatly influence the groundwater flow that discharges into the sea (Brunner et al., 2007; Edet et al., 1998). Another aspect to consider is the connectivity of the aquifer with the sea. Coastal aquifers may be totally or partially hydraulically connected to the sea, depending on several factors, such as the geological structure of the aquifer and the seabed, as well as the hydraulic properties of both onshore and offshore geological formations. In addition, the amount of SGD depends on the aquifer water budget, which produces variations in groundwater discharge flow. The main factors that influence this budget are the natural variations in recharge at different temporal scales (rainfall events, seasonality, inter-annual changes) and the abstraction of groundwater, which can reduce

the discharge of the fresh groundwater component of the SGD, or even induce seawater intrusion into the coastal aquifer. Unfortunately, these factors are linked, since in most cases when recharge is low, abstractions tend to be higher.

In the presented research, from the 54 karstic SGD studied springs, information on the type of coastal karst aquifer is only available for 37% of the springs (Figure 2, Appendix A). From those, the first karst type system, characterized by poorly-developed but highly-fractured karstification, represents 11% of the springs and 7% of the total where successfully identified. The second type of karst system, characterized by well-developed karstification connected to the sea, represents 22% of the springs, and half of those were identified (11% of the total). Finally, the third karst type system with well-developed karstification but low connectivity with the sea, represent only 4% of the springs, and half of those were identified (1.8% of the total). Therefore, the best geological and hydrogeological settings for identifying SGD springs are karst systems with well-developed karstification and that are well-connected to the sea, as well as those systems with poorly-developed but highly-fractured karstification. This is because these systems have high transmissivities that can induce high local SGD rates, making it easy to detect their thermal plumes. However, it depends on the recharge area and its rate.

Conversely, low groundwater discharge water volumes may limit the identification of thermal anomalies because they could attenuate the thermal anomaly produced by the SGD. Therefore, low discharge water volumes are unlikely to be identified using this technique. Of the 54 karstic SGD studied springs, the flow rate information was only available for 59% of the springs (Figure 2, Appendix A). Springs with a flow rate lower than 10 $m^3 \cdot s^{-1}$ represent 40% of the springs. From those, only 50% were identified. The springs with a flow rate higher than 10 $m^3 \cdot s^{-1}$ represent 15% of the springs, and from those 60% were identified. This indicates that apart from flow rate, other factors affect the failure to identify these SGD springs on the coastline.

Inter-annual and annual changes, such as humid-dry periods, overexploitation, and extreme events such as strong rainfall storms, etc., can also modify SGD flows. Thus, the research period in which the images were collected is also important because seasonal variations (Lee et al. 2016) can lead to SGD thermal plume variations, not only due to the temperature difference between groundwater and seawater (Lee et al., 2016), but also annual SGD flow rate variations (Michael et al., 2010) that allow their identification.

Regarding hydrogeological conditions in the Mediterranean Sea basin, it was expected that the best seasons for identifying SGD springs using satellite TIR-RS would be spring and autumn, when rainfall is higher and therefore a higher discharge flow rate is expected.

However, results showed that late spring and summer were the best seasons for identifying SGD springs, indicating that other factors influence the identification of SGD springs using this technique.

2.3.2.3. Environmental and marine conditions

Other aspects that could affect the thermal contrast between the groundwater plume and seawater include environmental and marine conditions. Both factors can make the identification of SGD difficult, because they cause seawater mixing with the discharging groundwater, reducing the thermal contrast between them and modifying the sea surface temperature. The main environmental condition that can affect SGD identification is the action of wind, which can mix the first millimeters of the sea surface water, limiting the identification of SGD springs using remote sensing techniques. Similarly, marine conditions can affect SGD identification if they reduce the thermal contrast between the groundwater plume and the seawater. These marine conditions are basically reduced to the coastal water hydrodynamic conditions that can be affected by processes such as the influence of tides or coastal currents, the formation of a pycnocline in surface seawater, or the fetch due to wind action. Tides, coastal currents and fetch generate seawater movement and mix groundwater with seawater, causing a thermal contrast attenuation. Similarly, the presence of a pycnocline can result in less vertical mixing of the water column. In subtropical areas with cold winters and hot summers, such as the Mediterranean Sea, coastal waters often develop a pycnocline during the summer months, as high temperatures increase the evaporation of seawater, generating an increase in salinity and therefore water density. This effect causes cold, fresh groundwater to flow over salty and dense seawater, generating an SGD layer on the sea surface.

The temperature of the Mediterranean Sea oscillates seasonally between 26 - 30 ºC in summer and 14 - 19 ºC in winter, while the groundwater temperature remains relatively constant over time, implying a greater contrast between summer and winter. However, SGD spring visualizations in cloud-free images decrease significantly in winter months compared to warmer months (Figure 2.4). 35% of the springs were identified in summer and only 4% were identified in winter (Figure 2, Appendix A). Consequently, the number of SGD spring visualizations is much higher in summer than in winter. In winter months, wind, water column mixing, currents, etc., are more intense and reduce the thermal contrast. Therefore, environmental and marine conditions during the winter months are unfavorable for the identification of coastal springs.

For this reason, areas where the influence of various marine factors such as tides, coastal currents or fetch is small are ideal for identifying SGD springs, because such factors induce

mixing attenuating the thermal contrast needed to identify SGD springs. Similarly, in subtropical areas such as the Mediterranean Sea, it is easier to identify SGD springs because coastal waters often develop a pycnocline during the summer months, resulting in less vertical mixing of the water column and therefore better identification of SGD springs. Therefore, in the Mediterranean basin, environmental and marine conditions in summer months are much more favorable for the identification of coastal springs than in winter months.

2.3.2.4. Coastal morphology limitation factors

Another aspect that influences SGD thermal plume visualization is the coastal morphology; depending on its characteristics, the seawater residence time in the study zone may allow the formation of a thermal plume. In semi-enclosed areas, such as bays or coves, where the residence time of discharging water in the sea is in the range of one to several days (Tamborski et al., 2020), the formation of thermal plumes from SGD can easily be detected by satellite, in comparison with open sea areas, where the seawater residence time is shorter (less than a day), due to the effect of marine or weather factors such as waves, coastal currents or fetch. Groundwater discharge can occur below sea level, either at shallow (< 10 m) or at greater depths, right on the shoreline or a few meters from it (Zektser & Dzhamalov, 2006). The morphology of the coastal seabed combined with the geological characteristics of the aquifer (e.g., karstification degree and coastal hydraulic gradient) determine both the depth and offshore distance of the groundwater discharge. These two characteristics are very significant, since the location of the SGD spring on the coast is critical for the correct identification of the thermal contrast between groundwater and seawater using satellite thermal images. While groundwater discharges produced at coastal level or several meters inland usually generate thermal contrasts easily detectable by satellite (Mejías et al., 2012), submarine springs located several meters deep often represent a challenge for satellite detection. This is because when groundwater discharges below sea level, it rises to the sea surface generating a buoyant thermal layer of several millimeters, due to its lower density that arises from its temperature and salinity characteristics. Therefore, a greater discharge depth requires more time to reach the sea surface, adapting the SGD's thermal signal at the sea surface to the surrounding water temperature. Thus, marine factors may have a greater influence in balancing the seawater and groundwater temperatures, preventing the recognition of thermal anomalies on the sea surface, as stated by Mallast et al. (2013)

However, the time required for groundwater to reach the sea surface depends not only on the depth of the discharge below sea level, but also on hydrogeological factors, such as the

discharge flow. Thus, SGD springs characterized by shallow depths and large flow rates will favor the detection of SGD-induced thermal plumes on the sea surface, while deep areas with small flows may be undetectable. Intermediate situations, such as shallow areas with small flows or deep areas with large flows, may be detected depending on the relative importance of the environmental and/or marine limiting factors.

For studied springs in the Mediterranean Sea basin, 52% of the springs were located in semi-enclosed coastal areas (Figure 2, Appendix A). Of these, 31% of the studied springs were identified (Port Miou and Bestouan in France; Cephalonia, Anavalos Kiveri and Almyros of Agios Nikolaos in Greece; Martinscica, Perilo, Novijanska, Jurjevska and Patan in Croatia; and Gokova (three springs), Ovacik and Antalya (three springs) in Turkey). These results show that when discharge occurs in semi-enclosed areas, where the seawater residence time is large, the springs can be identified until late autumn, even though the flow of groundwater is relatively small (0.75 $m^3 \cdot s^{-1}$ was reported for the Ovacik spring in Turkey). Therefore, the success in identifying SGD springs in semi-enclosed areas also is higher throughout the year.

Of the 54 SGD studied springs, the distance and depth information are available for 41% of the springs (Figure 2, Appendix A). The first group of springs, which discharge near the seashore and reach the sea through small streams, represents 6% of the springs (Patan in Croatia, Almyros of Iraklio in Greece and Maro in Spain) and from those, 66% were identified (Patan and Almyros of Iraklio). The second group of springs, which represent 6% (Font Dame, Font Estramar and Vise) characterized by discharge in coastal lagoons, was not identified. The third group of springs, which discharge close to the shoreline and in shallow water, represents 20% of the springs (Torre Badum, Las Fuentes, Font de Dins in Spain, Ain Zayana in Libya, Agios Nikolaos, Cephalonia and Anavalos Kiveri in Greece and Ovacik (3 springs) and Gokova in Turkey) and we were able to identify 91% (all of them except Ain Zayana spring). No springs were identified from the fourth group, which represents 6% of the springs (Moraig in Spain and Port Miou and Bestouan in France), and is characterized by discharge close to the shoreline but at a water column depth of 12 m.b.s.l. None of the springs of the fifth group (Mortola in Italy and Chekka in Lebanon), which represent 4% of the springs, characterized by discharge offshore with a water column depth between 35 and 150 m.b.s.l, were identified.

From the analysis of the images obtained by Landsat 8 TIRS and considering the hydrogeological data of the various coastal springs, we conclude that groundwater discharges that occur at significant depths (> 12 m.b.s.l) are unlikely be identified by this technique, probably because the thermal anomaly generated between groundwater and

seawater does not reach the sea surface. This is the probable reason for the failure to identify the springs of Vise in France, Mortola in Italy and Chekka in Lebanon. For the Vise spring, which discharges at 30 m.b.s.l, the hydrogeological information indicates that it is a mixture of karstic water, thermal water and seawater (Aquilina et al. 2002); most likely the discharging groundwater does not produce enough thermal contrast to be detected with a satellite sensor. On the other hand, SGD springs located in very shallow areas, such as the Salses-Laucate lagoon, which has an average maximum depth of 2 m.b.s.l (Bejannin et al. 2017), and where there are two well-known springs (Font Dame and Font Estramar) were not identified. A possible reason is that these types of shallow coastal lagoons are highly influenced by atmospheric temperature, since the small water column has little capacity to buffer temperature fluctuations (Lee et al., 2016). However, Anavalos Kiveri and Torre Badum, identified during winter months, are shallow (0 and to 10 m.b.s.l) SGD springs. Therefore, although initially these types of springs should be easily detectable by satellite, atmospheric factors can greatly influence the formation of the thermal contrast needed to identify them.

The shore distance at which groundwater discharge occurs is another factor that affects the identification of groundwater discharge in coastal areas. SGD springs discharging further than 500 m from the seashore were not recognized, such as the Mortola spring with a distance of 800 m. This may be related to the fact that as the distance to the coast increases, the depth of the water column increases, and the travel time of the fresher groundwater also increases, allowing a complete temperature equilibrium. Furthermore, these zones are more affected by ocean currents that increase water mixing, attenuating the thermal signal.

In some cases, there is not one single factor affecting SGD spring identification, but rather a combination of several factors (flow rate, season, coastal morphology, etc.) which makes it difficult to explain why an SGD spring was not identified.

2.3.2.5. Thermal anomalies from streams and anthropogenic sources

When looking for coastal thermal anomalies by using satellite TIR images, some anomalies can be detected that are not necessarily related to SGD. These anomalies can be from natural sources, such as rivers or streams, or civilian facilities such as ports, thermal power plants, fish farms or wastewater treatment plants. These thermal anomalies may misidentify or mask some SGD springs when discharge occurs in shallow areas with high seawater residence times.

For example, natural water sources, such as small rivers or streams, also produce a thermal signal at sea. As SGD, they may have a different temperature than seawater. This is the case

for the small river near Split in Croatia (Figure 3, Appendix A), which produces a thermal anomaly that could be misinterpreted as an SGD spring. Furthermore, when SGD and rivers discharge at the same location, the thermal signal of SGD will be masked and/or modified by surface water discharge. In the case of civil facilities, the most common facilities that could be confused with SGD springs would be the discharges from wastewater treatment plants as they usually discharge water with a different thermal signal than the sea. For example, in the Hyperion Treatment Plant (HTP) and the Orange County Sanitation District (OCSD) wastewater diversion events in Southern California, where treated water discharge takes place at depth, it is possible to detect its thermal effect on the coastal waters (DiGiacomo et al. 2004) with SST differences of at least 0.5 ºC identifiable with TIR-RS (Gierach et al. 2017). Other examples of civilian facilities that can generate thermal signals and induce non-identification or masking of SGD springs, are power plants or ports. In the case of the Mediterranean Sea basin, it was observed that facilities located along NE of the Iberian Peninsula, such as the Vandellós II nuclear power plant, the port of Barcelona, and the port of Benicarló, showed thermal anomalies similar to those produced by the SGD springs (Figure 3, Appendix A). These outflows can also mask and modify the SGD thermal signal of the plume when both outflows take place at the same location, such as the case of Peñíscola in Spain, where the SGD discharge takes place at the same location as the port (Figure 3, Appendix A).

2.3.3. Application of the multi-temporal SST series method

In some studied areas, there may be low thermal contrast that can prevent the identification of SGD springs. In these cases, it is possible to deepen the analysis of the images by using the multi-temporal SST series proposed by Mallast et al. (2014) in the Dead Sea, which minimizes the effect of the previously-indicated limiting factors. Unlike single images, the multi-temporal SST series method allows several images and thus several points in time to be integrated, accentuating the small thermal anomalies for easy identification. An example of the usefulness of the multi-temporal SST series method is in the Serra d'Irta (Eastern Iberian Peninsula) (Mejías et al., 2012; Garcia-Solsona et al., 2010; Trezzi et al., 2016). At this site, Mejías et al. (2012) identified four large thermal anomalies (Torre Badum, Punta del Pebret and Les Fonts springs) by using airborne thermal remote sensing that were not identified using Landsat 7, by using airborne thermal remote sensing. Using single images with Landsat 8 TIRS, only the Torre Badum spring was identified, compared with the four thermal anomalies identified by aerial thermal infrared images in 2012. The multi-temporal SST series method, which integrates 10 cloud free images from 2017 to 2018, enables the identification of Torre Badum and Les Fonts, 2 of the 4 springs identified in 2012 by Mejías et al. (2012) (Figure 2.5).

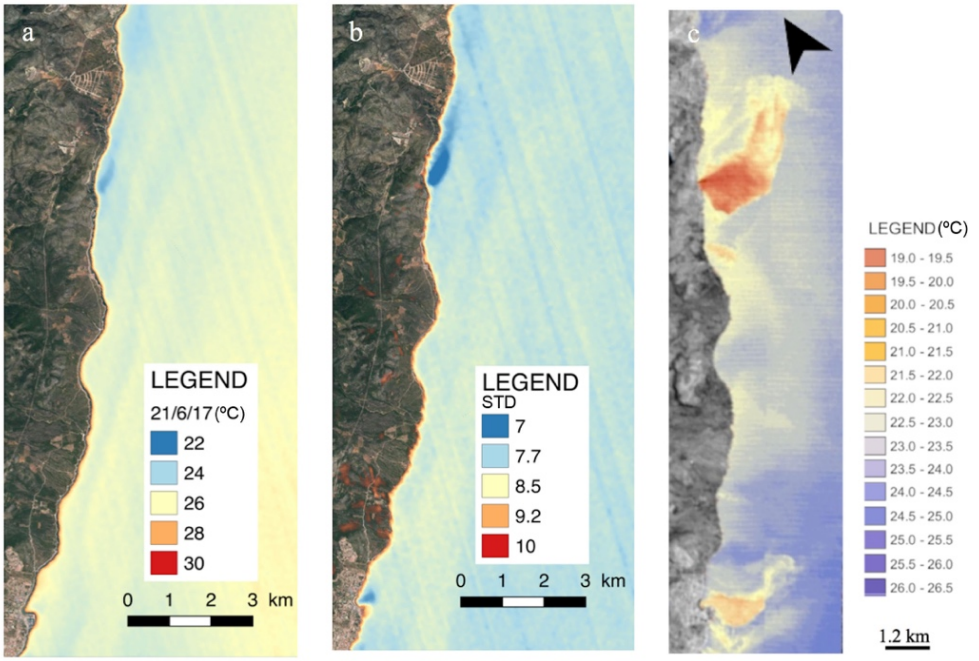

Figure 2.5. a) Serra d'Irta single image map using an image taken on 21/6/17. One spring in the middle of the Torre Badum spring was identified. b) Serra d'Irta Standard Deviation (STD) map using 10 cloud free images acquired between 2017-2018. Two springs in Serra d'Irta, in the south the Les Fonts beach in Alcossebre spring, and in the middle the Torre Badum spring, were identified. c) Image modified from Mejías et al. (2012) where SGD springs were identified using aerial thermal infrared images. © Google Earth 2021.

Although the multi-temporal SST series method is better for identifying SGD springs because thermal contrast is enhanced, this method did not enable SGD spring identification in other places where the single image method did not identify them. Furthermore, with multi-temporal SST series, the temporal morphological information, such as the shape and size of the discharge plume, is lost (Mallast et al., 2013). Conversely, single images allow the identification of morphological variations in the discharge plume and the temperature variations along that plume. Therefore, if the study objective is to identify SGD springs, the multi-temporal SST series method is the best option, but if the objective is to study the SGD plume variation, single images are better.

2.3.4. Identification of new SGD springs: challenges and recommendations for future SGD studies

One of the main objectives of this study is to demonstrate the great usefulness of satellite TIR imagery at local and regional scales, identifying SGD springs not previously described in the scientific literature. An example of this usefulness is the identification of 21 SGD

springs undescribed in the bibliography along the Croatian coast using single images (Figure 2.6). This demonstrates that the analysis of single images obtained from Landsat 8 TIRS allows the identification of new SGD springs. Therefore, this economical technique is very useful in inaccessible areas (Gumma & Pavelic, 2013; Edet et al., 1998). For this reason, in the design of SGD studies at both local and regional levels, it is recommended that the coastal water temperatures for thermal anomalies first be screened using the presented satellite based TIR-RS approach, as this will help narrow the sampling surveys. Although the study of the thermal images during a single year should be sufficient to identify potential coastal springs, it is highly advisable to analyze thermal images over several years, since there may be one or several factors (technical, marine, environmental, hydrogeological, etc.) that may alter the SGD thermal signal.

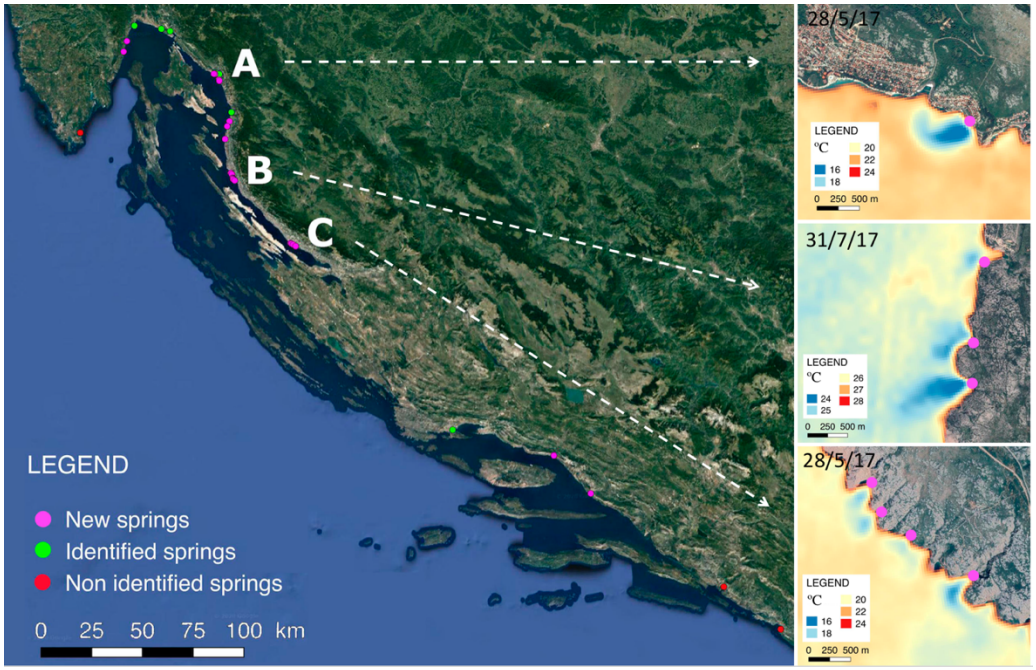

Figure 2.6. Springs reported in the literature (described SGD spring) vs new SGD spring identified with Landsat 8 TIRS. New SGD springs, not reported in the literature are represented in pink. Springs reported in the literature are represented in white. © Google Earth 2021

Although this study focused on the discharge of groundwater from springs located in karst aquifers, the study of satellite TIR-RS images could be extrapolated to other types of aquifers where the discharge is more diffused and where the proportion of meteoric water is lower. To identify thermal plumes, water discharging into the sea, whether of meteoric origin or marine circulation, must have acquired sufficient thermal contrast in the coastal

aquifer before discharge. This thermal contrast can also occur in places where coastal aquifers are volcanic rocks or fractured granites, and even in sedimentary formations. However, in each case, the specific geological context (aquifer matrix, hydraulic parameter distribution, etc.) should be considered in the analysis.

Several studies have shown the possibility of quantifying SGD through the study of thermal plumes obtained by aircrafts (Tamborski et al., 2015; Danielescu et al., 2009; Mejías et al.,2012). By determining the thermal plume area, which is often directly related to the discharge volume, SGD may be quantitatively identified. However, there are several factors that can alter the thermal plume shape that could result in error. Furthermore, because the TIR-RS image only allows us to observe less than 1 mm of the sea surface, and thus prevents a determination of the volume beneath the thermal plume, the required information is missing. Moreover, quantification by means of images represents a major challenge, because satellite images (e.g., Landsat 8 TIRS) can only be obtained once every 16 days, and many factors can alter the shape of the plume independent of the actual discharge. Therefore, unless the discharge occurs in locations where the environmental and marine conditions are well-known, quantification by satellite images represents a major challenge that should be further investigated.

Although this study focused regionally on the Mediterranean Sea basin, it can be extrapolated to other parts of the world, in places where the SGD has sufficient thermal contrast when discharging into the sea. This technique has been successfully used in regional areas such as Ireland (Wilson & Rocha, 2012; McCaul et al., 2016) or the Laizhou Bay in China (Xing et al., 2016). However, in areas where the thermal contrast between the sea and the aquifer is low and/or temperature does not fluctuate during the year, such as in tropical zones, the use of satellite images represents a challenge that must be explored in detail. Furthermore, it is important to perform an initial study to attempt to identify the previously-described main factors that can limit SGD spring identification in the study area, to try to control/avoid these effects.

2.4. Conclusions

This study demonstrates that satellite remote sensing is a useful tool for the identification of coastal SGD springs in karst aquifers, both locally and regionally, by performing an initial screening of the coastal water temperature images to identify possible thermal anomalies that can help narrow SGD study sampling surveys. However, this study highlights limiting factors that should be considered: (1) technical limitations, (2) geological/hydrogeological characteristics, (3) environmental and marine conditions and (4) coastal geomorphology.

In the karstic coastal aquifer of the Mediterranean Sea basin, the highest success percentage of SGD visualizations was during June, July, August and September. The main factor limiting the identification of SGD springs were clouds, which are far more abundant in winter months. The best geological and hydrogeological settings for identifying SGD springs were karst systems with well-developed karstification that are well-connected to the sea, as well as those systems with poorly-developed, but highly-fractured karstification. Environmental and marine conditions (such as pycnocline formation, light winds etc.) in the summer months were much more favorable for the identification of coastal springs than in the winter months. Semi-enclosed areas, where the seawater residence time is large, favor the identification of SGD springs throughout the year. Groundwater discharges that occurred at a depth of more than 12 m.b.s.l or in very shallow waters were not identified. Also, SGD springs that discharged further than 500 m from the seashore were not recognized.

Multi-temporal SST series are better for identifying SGD springs in coastal zones, but the information for changes in the discharge plume changes is lost, while single images are more suited to studying the morphological variations in the discharge plume and temperature variations along the plume.

Although this study focused regionally on the Mediterranean Sea basin, it can be extrapolated to other parts of the world and other aquifer types, in places where the SGD has sufficient thermal contrast when discharging into the sea and where the specific geological contexts (e.g., aquifer matrix and hydraulic parameters distribution) are considered. Long time series are better for identifying SGD spring areas, since there may be one or several factors (technical, marine, environmental, hydrogeological, etc.) that can alter the SGD's thermal signal. It is recommended to first screen the coastal water temperature images obtained by satellite to identify possible thermal anomalies that will help narrow the sampling surveys. This technique allows the identification and quantification of SGD springs in zones without hydrogeological information.

The author gratefully acknowledge Francisco Carreño Conde, from the Universidad Rey Juan Carlos, for the initial discussions on the topic and Ulf Mallast, from the Helmholtz Centre for Environmental Research – UFZ, for the constructive comments. This research was partly funded by the Spanish Government (grant nos. PID2019-110212RB-C22 and PID2019- 110311RB-C21) the "Maria de Maeztu" program for Units of Ex- cellence (grant no. CEX2019-000940-M) of the Spanish Government and the project TerraMar (grant no. ACA210/18/00007) of the Catalan Water Agency. The authors want to thank the support of the Generalitat de Catalunya to GHS (grant no. 2017 SGR 1485) and MERS(grantno.2018SGR-1588)for additional funding.

Chapter 3

SGD ecological influence in coastal areas delimited with satellite remote sensing

Jou-Claus, S., Folch, A., Garcia-Orellana, J., Rodellas, V., Fernàndez-Garcia, D. 2022. SGD ecological influence in coastal areas delimited with satellite remote sensing. Manuscript submitted to Limnology and Oceanography Letters.

3.1. Introduction

Productivity in coastal areas responds largely to land-ocean interaction processes in which nutrients are supplied to seawater (Cloern and Jassby 2010). Although riverine inputs have traditionally been considered the main source of nutrients to the coast, it is well-known that other processes such as, atmospheric deposition, anthropogenic inputs (effluents of wastewater treatment plants or spills) or submarine groundwater discharge (SGD) also contribute to coastal biogeochemical cycles (Jickells et al. 2017). SGD is defined as "the flow of water through continental and insular margins from the seabed to the coastal ocean, regardless of fluid composition or "driving force" and thus includes meteoric fresh groundwater but also seawater circulating through the coastal aquifer or permeable sediments (Burnett et al. 2003; Taniguchi et al. 2019a; Garcia-Orellana et al. 2021).

Several studies have demonstrated that SGD is also an important pathway delivering nutrients and other chemical solutes to marine ecosystems (Paytan et al. 2006; Rodellas et al. 2015; Cho et al. 2018). As the concentration of nutrients in SGD is often much higher than concentrations in receiving water bodies, even relatively small SGD flows can constitute significant nutrient inputs and impact coastal biogeochemical budgets (Moore 2010; Santos et al. 2021). Thus, several studies have shown that SGD-driven nutrients inputs have a significant impact on coastal marine ecosystems since these fluxes may modify biogeochemical cycles (Valiela et al. 1992; Mayfield et al. 2021) and could alter the ecological status of the coastal water bodies and services these ecosystems provide (Lecher and Mackey 2018; Alorda-Kleinglass et al. 2021).

Several studies have shown increases of phytoplankton biomass linked to SGD-derived nutrient inputs (Rodellas et al. 2014; Tovar-Sánchez et al. 2014; Wang et al. 2018) and some investigations have documented the uptake of SGD-driven nutrients to primary producers (Lapointe et al. 2004; Honda et al. 2018; Andrisoa et al. 2019). Furthermore, short-term changes in the composition of coastal microalgal communities have been also reported, leading, in some cases, to adverse effects such as coastal eutrophication or harmful algae blooms (e.g., Adolf et al. 2019). The abundance, biomass and dynamics of phytoplankton in coastal areas reflect the prevailing environmental conditions and represent key parameters for assessing information on the ecological status, as well as on the coastal water quality (Hays 2005; Paerl 2006).

Despite the evident significance of SGD to coastal marine ecosystems, there are still limited number of studies that quantify the biological impacts of SGD, particularly when compared to studies estimating SGD rates and SGD-driven solutes fluxes (Lecher and Mackey 2018). The traditional and simplest method used as a proxy for measuring primary productivity is

through the photosynthetic pigment, Chl-*a*. This parameter (Chl-a) is widely used in oceanography for environmental monitoring of harmful algal blooms, critical coastal habitats (e.g., seagrasses), eutrophication processes and a variety of hazards in the coastal and estuarine zones (Kratzer and Tett 2009; Cui et al. 2010, Klemas 2011; Kratzer et al. 2014, Ryan et al. 2008; Wei et al. 2008; Shen et al. 2012; Frolov et al. 2013). The traditional method for measuring primary productivity is through in situ or discrete water samples analysis of Chl-*a*, which can be time-consuming, expensive and laborious when interested in covering large areas, obtaining periodic information or studying remote areas with difficult access (Glasgow et al. 2004; Bierman et al. 2011). However, the use of remote sensing to obtain Chl-a information is now a widely used tool in oceanography to study the seasonal and interannual variability in algal biomass and primary production (Bricaud et al. 2002; Bosc et al. 2004), the algal blooming patterns and anomalies (Barale et al. 2008) or determining the biophysical impact of discharged wastewater in nearshore environment (Trinh et al. 2017). However, the use of remote sensing-derived Chl-a data has not been used in SGD studies, although this technique is widely used in other environmental disciplines due to its low-cost and long-range. Thus, remote sensing could provide instrumental information on the impact of SGD on coastal biogeochemical cycles and on the extension of areas influenced by SGD, contributing thus to better constrain the poorly assessed effects of SGD on coastal ecosystems. In addition, the use of remote sensing could help determine the impact of SGD in remote or inaccessible areas or in areas without previous information, which usually require difficult and costly campaigns over long periods to cover in detail the area of influence of SGD both spatially and temporally. In this context, remote sensing could provide a cost-effective method to obtain preliminary information of Chl-a concentration in SGD-influenced sites from ocean color multispectral data. This method could thus allow characterizing the ecological influence of SGD in large study areas with high temporal coverage, reasonable accuracy and global coverage, in a similar manner as done with thermal data to localize freshwater springs in coastal areas (Wilson and Rocha 2012; Mallast et al. 2013; Jou-Claus et al. 2021).

This work aims to evaluate the potential use of Landsat 8 satellite Chl-a data for identifying and constraining SGD-impacted coastal areas and mapping the spatial extension and temporal evolution of SGD-influenced areas.

3.2. Methodology

3.2.1. Chlorophyll data acquisition with Landsat 8

Ocean color multispectral data are measured from space by the Operational Land Imager (OLI) radiometer aboard Landsat 8. These sensors have the spatial resolution (30 m for

multi spectral visible data) and signal-to-noise ratio necessary to provide useful products derived from ocean color along the coastal zone (Vanhellemont and Ruddick 2014). Ocean color remote sensing measurements define the relationship between the inherent optical properties of the ocean, or the absorption and scattering properties of the constituents, and water-leaving radiance. This data can be used to describe components of water quality, such as cyanobacterial pigments (CYP), total suspended mater (TSM), Colored dissolved organic matter (CDOM), attenuation coefficient of diffuse light (Kd), turbidity/secchi disk depth (Turb/SD) and chlorophyll-a (Chl-a) concentration (Gholizadeh et al. 2016). Algorithms are available to estimate the Chl-a concentrations by 1) retrieving the radiant flux from the target surface, 2) correcting the signal from the atmosphere, 3) transforming the radiant energy collected by the satellite sensor into the remotely sensing reflectance (R_{rs}), and 4) converting the R_{rs} values into products. In order to derive the biomass product associated with Chl-a, the reflectance in the blue and green wavelengths is often used (Franz et al. 2014; Mobley et al. 2016).

Landsat 8 raw data for this study sites were downloaded from the USGS Earth Explorer website for the period 2014 and 2019 (USGS, 2021). We used Data Analysis System (SeaDAS), which is an open-source software package distributed by NASA, for processing and analyzing chlorophyll data. Chl-*a* was calculated using the standard OC2 algorithm (O'Reilly et al. 1998) from the NASA Ocean Biology Processing Group, using the above-calculated R_{rs}:

$$log_{10}(chl_a) = a_0 + \sum_{i=1}^{4} a_i log_{10}\left(\frac{R_{rs}(\lambda_{blue})}{R_{rs}(\lambda_{green})}\right)^i \quad (1)$$

where a_0 and a_i are sensor specific coefficients, and R_{rs} (λ_{blue}) and R_{rs} (λ_{green}) are the instrument-specific wavelengths 482 and 561 nm, respectively, on the OLI sensor aboard Landsat 8 (NASA, 2021).

3.2.2. Delimitation of areas influenced by SGD

3.2.2.1. Study sites

The main challenge in identifying and constraining the extent of the SGD-influenced zone is to distinguish high SGD-derived Chl-a concentrations from those derived from other potential sources. To this aim, we selected five coastal areas distributed all over the world where significant inputs of terrestrial SGD to the coastal zone have been identified (Figure 2). Furthermore, this study sites are characterized by no perennial streams and therefore SGD dominates water inputs to the ocean. SGD study sites are Aimakapä fishpond in Hawai

(Johnson et al. 2008), Pantai Baron in Indonesia (Oehler et al. 2018), Bangdu Bay in Jeju Island (Lee et al. 2016), La Paz Bay in México (Urquidi-Gaume et al. 2016) and Serra d'Irta in the east of the Iberian Peninsula (Mejías et al. 2012). These areas represent different hydrogeologic and climatic conditions. The climate is warm and dry in the Aimakapä fishpond, Hawaii (mean rainfall of 600 $mm \cdot y^{-1}$ and temperature of 24ºC (Johnson et al. 2008)), tropical in Pantai Baron (mean rainfall of up to 2000 $mm \cdot y^{-1}$ and temperature of 27 ºC (Oehler et al. 2018)), maritime in Bangdu Bay (mean rainfall of 1634 $mm \cdot y^{-1}$ and temperature of 16ºC) (Lee et al. 2016), arid in La Paz (mean rainfall of 200 $mm \cdot y^{1}$, evapotranspiration rate is of 2000–2200 mm and mean temperature 27ºC) (Urquidi-Gaume et al. 2016) and Mediterranean in Serra d'Irta (mean rainfall 500 $mm \cdot y^{-1}$ and temperature 21ºC) (Mejías et al. 2012).

3.2.2.2. Clustering chlorophyll zones

Chl-a concentration was used to delineate areas ecologically-influenced by SGD. A k-means unsupervised clustering algorithm (Odeh et al. 1992) was used to classify similar Chl-a concentrations into temporally dynamic zones (DZ) (Figure 1b). The Grouping Analysis tool in ArcMap 10.4.1 (ESRI, Redlands, CA) was used for the DZ delineation. The Calinski-Harabasz criterion (CHC) (Harabasz et al., 1974), was used to rank clusters, delineate DZ and select the optimum number of DZs (Eq. 2). The CHC, also known as a pseudo F-statistic, measures the ratio of between DZ differences and within DZ similarity.

$$CHC = \frac{BMZSS/(DZ_n - 1)}{WMZSS/(N - DZ_n)} \quad (2)$$

where BMZSS is the between-zones sum of squares, DZn is the number of considered zones, WMZSS is the within-zone sum of squares, and N is the number of pixels. High CHC values indicate high homogeneity within DZ and heterogeneity between DZ.
The Chl-a averages and maximum and minimum values within each DZ were calculated for further comparison between different DZs.

3.2.2.3. Box plots and background concentration

Differences in Chl-a concentrations across the DZs were assessed using box plots (SPSS Statistics) (Figure 1c). Results show that small DZs of high Chl-a concentration and high standard deviations are characteristic of the areas influenced by SGD. In contrast, large DZs associated with low Chl-a concentration and low standard deviations are characteristic of the background. We are interested in differentiating Chl-a concentration values from the background values because in some areas or specific periods of the year the Chl-a

background concentrations could be higher and also due to the influence of other sources of nutrients.

Chl-a background concentration was obtained from three transects offshore (polygons of 4.0 x 0.5 km perpendicular to the shoreline) in areas apparently not influenced by SGD (according to remote images and previous literature). The highest Chl-a concentration in these polygons (represented with a dashed line in Figure 1c) was used to determine the threshold between DZs from areas influenced by SGD (Chl-a concentrations above the limit) and Chl-a background (Chl-a concentrations below the limit) (Figure1d).

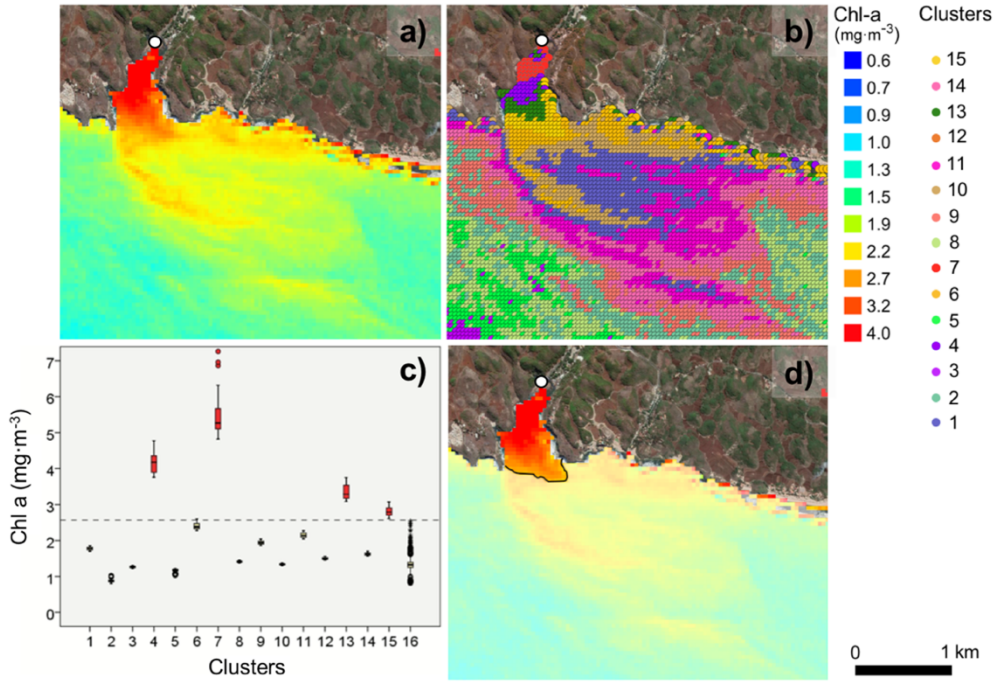

Figure 3.1. Example of the methodological approach followed to obtain the area influenced by SGD. Example of Pantai Baron (Indonesia). a) Chl-a data processed using SeaDAS, b) similar Chl-a concentrations divided in clusters, c) box plots of Chl-a concentration vs clusters and d) derived SGD-ecological influence area. Black line represents the SGD ecological influence boundary. The white dot is the location of the SGD source according to Oehler et al. (2018).

3.3. Results and discussion

3.3.1. Ecological influence of SGD

Chl-a concentrations derived from satellite data for all selected locations are shown in Figure 2. At each location, high Chl-a concentrations can be visually defined in areas close to the previously identified SGD spots (according to the literature). In addition, a clear

offshore Chl-a concentration gradient is observed from the location of the SGD coastal springs, with relatively high concentrations, that slowly decrease with distance from the source. The detection of a high Chl-a concentration at those locations close to SGD sources reveals the existence of areas with increased primary productivity, most likely as a consequence of nutrient inputs supplied by SGD (there are no other significant and point-like nutrient sources in the area). Chl-a data from remote sensing allows thus to identify and constrain a zone where SGD has driven an increase on phytoplankton biomass, i.e. an area with ecological impacts derived from SGD.

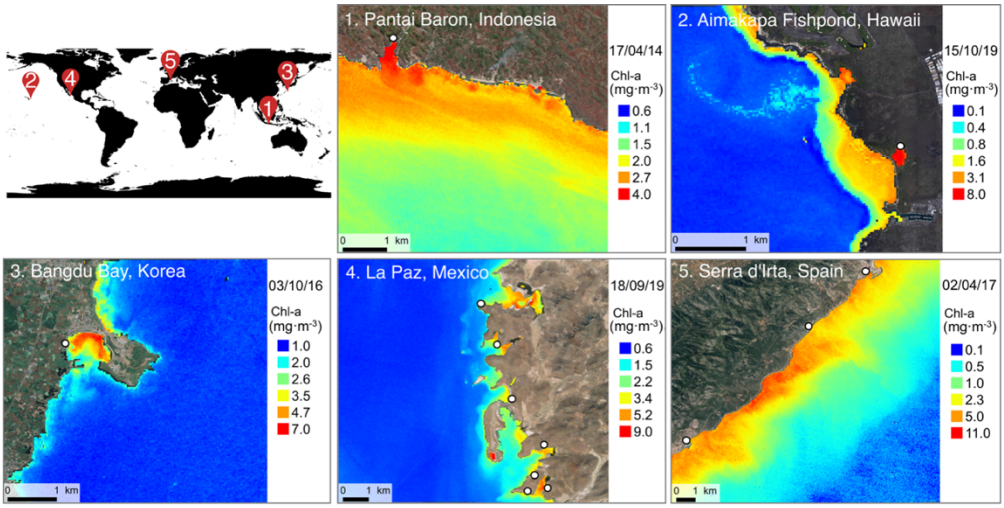

Figure 3.2. Chl-a data of the SGD springs used for this study. The SGD point-source springs are described in: 1. Oehler et al. (2018), 2: Johnson et al. (2008), 3: Lee et al. (2016), 4: Urquidi-Gaume et al. (2016) and 5: Mejías et al. (2016). White dots are the location of SGD sources.

3.3.2. Constraining the SGD ecological influence

Although the influence of SGD on coastal ecology can be identified directly from satellite Chl-a imagery, we also set out to constrain the area of Chl-a plumes and thus the area influenced by SGD.

The area ecologically influenced by the SGD (Figure 3 and supplementary material S.1, S.2, S.3 and S.4) has been constrained using the conservative methodological approach described in section 2.2 where a high Chl-a concentration considered as background and thus results obtained that probably exclude some areas also affected by the SGD.

The extent of the Chl-a plumes allows identifying and constraining areas with direct ecological influence of SGD, since they present Chl-a concentrations above background levels that can only be ascribed to SGD.

This approach allows thus identifying areas where SGD inputs have produced increases on primary productivity, providing data on Chl-a concentrations variations with a relatively good spatial resolution (30x30 m). To illustrate the potential of this approach, the monthly temporal evolution of the area ecologically impacted by SGD in Pantai Baron (Yogyakarta, Indonesia) for 2014 is shown in Figure 3. The temporal evolutions of the other study sites are included in the supplementary material S.1, S.2, S.3 and S.4. In all the study sites, the ecological area impacted by SGD near the described spring can be identified throughout the year. However, neither the extension of the area of influence nor the Chl-a concentrations were constant throughout the studied time period. In Pantai Baron, the area of influence of SGD varied between 0.02 and 0.20 km^2, with a large and intense Chl-a plume observed during January, April and May and a smaller and less intense plume in February or August. The mean Chl-a concentration of this areas of ecological influence varied between 2 and 4 $mg \cdot m^{-3}$, with higher Chl-a concentrations observed in April and lower in August. In Aimakapä fishpond, the area of SGD influence varied between 0.08 and 0.60 km^2, with a large and intense Chl-a plume observed during August and September and smaller plume between November and December. The mean Chl-a concentration of this area varies between 3 and 20 $mg \cdot m^{-3}$ with higher Chl-a concentration in February and November. In Bangdu Bay, most of the images are covered by clouds, but in which the study area is free the area of SGD influence varied between 0.46 and 0.88 km^2, with a large and intense Chl-a plume observed during May and July and smaller plume in December. The mean Chl-a concentration of this area varies between 3 and 6 $mg \cdot m^{-3}$, with higher Chl-a concentration in May and December. For the areas of La Paz and Serra d'Irta it was difficult to assign an area of ecological influence and an average concentration of Chl-a due to the SGD, since the discharge occurs at several points along the entire coast.

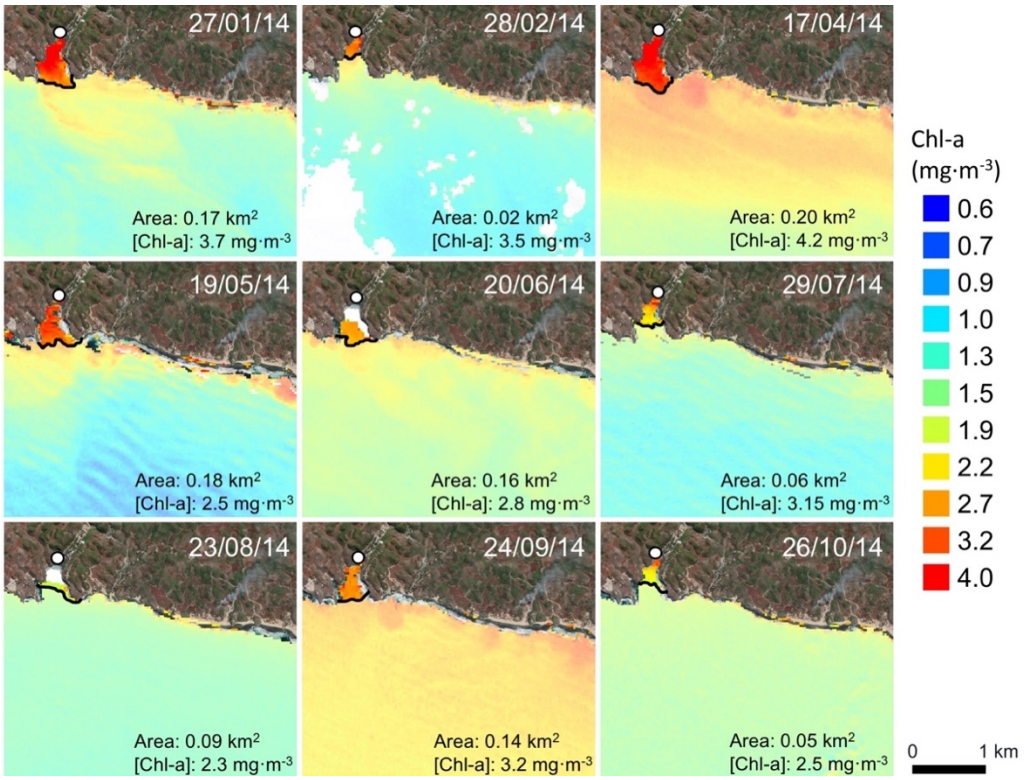

Figure 3.3. Chl-a data of the region of Pantai Baron (Yogiakarta, Indonesia) throughout 2014. In November and December 2014, it was not possible to obtain Chl-a data due to the presence of clouds. Black line represents the SGD ecological influence boundary. White dots are the location of SGD sources.

Temporal analysis of the extent and distribution of Chl-a concentrations can provide instrumental information on the seasonal variability of SGD-nutrient inputs and their ecological implications.

However, it is important to highlight that the temporal variability of the SGD ecological influence is not only produced by changes in nutrient fluxes supplied by SGD (i.e., temporal variations in SGD-nutrient fluxes), but also depends on the characteristics of the coastal ocean, including water properties (i.e. temperature, salinity, light penetration into the water column, turbulence, pH, stratification), retention and dispersion of solutes (i.e. residence time of solutes) and the characteristics of marine communities (e.g. types of phytoplankton, competition between species (Gobler and Boneillo 2003; Blanco et al. 2008; Troccoli-Ghinaglia et al. 2010; Lecher and Mackey 2018; Taniguchi et al. 2019b), but also the limiting factors of the Landsat 8 acquisition technique (Jou et al., 2021). For a detailed assessment of the ecological implications of SGD and their temporal variations, Chl-a remote sensing data should thus be combined with other information and measurements.

The analysis of the areas of ecological influence of the SGD would allow comparison of the degrees of influence between the different study areas. This type of comparison would allow the use of Landsat 8 Chl-a data to obtain large-scale SGD ecological influence maps. However, it is important to keep in mind that the coastal waters of each study area may be characterized by various constituents with different optical behaviors that influence the color of the water and thus the remote sensing data. Therefore, the inherent optical properties of each study area will be determined not only by phytoplankton, but also by absorption and scattering by total suspended material (TSM) and colored dissolved organic matter (CDOM) (Tilstone et al. 2011), as well as by the reflectance of bottom substrates in shallow coastal waters.

3.4. Conclusions and potential applications

Many studies (Sugimoto et al., 2017; Lecher and Mackey 2018, among others) suggest that there is a need of more extensive studies coupled with kinetic and quantitative indices of phytoplankton production and SGD to confirm the influence of nutrient transport via SGD on primary production. In this context, Landsat 8 satellite data has the spatial resolution and the necessary signal to noise ratio to provide useful data derived products along coastlines, being a powerful tool to study the potential ecological impacts of SGD in different areas worldwide. The approach proposed in this study offers the possibility to identify areas where SGD inputs have increased primary productivity and calculate the temporal and spatial variability of Chl-a concentrations in an area influence by SGD. This approach represents and economic and effective method to introduce an ecological dimension on SGD studies, which are often only based on the evaluation of chemical fluxes. If data on vertical Chl-a profiles in SGD-impacted areas can be collected, it would allow characterizing the total inventory of Chl-a, which can be used to estimate the total primary productivity in the area produced by SGD inputs (Cloern et al. 1995). Importantly, it also allows recovering ecological information related to past studies and samplings, which is not available by other means and document the temporal variations on the ecological impacts of SGD. Furthermore, this methodology is also particularly appropriate to obtain preliminary information on inaccessible or remote study sites, at a reduced time and economical costs compared with in situ field measurements.

The authors acknowledge the financial support of Spanish Ministry of Science, Innovation and Universities Through the project MEDISTRAES (grant nos. PID2019-110212RB-C22 and PID2019-110311RB-C21) the "Maria de Maeztu" programme for Units of Excellence (grant no. CEX2019-000940-M) and the Project TerraMar (grant no. ACA210/18/00007) of the Catalan Water Agency. The authors want to thank the support of the Generalitat de Catalunya to GHS (grant no. 2017 SGR 1485) and MERS (grant no. 2018 SGR-1588) for additional funding.

Chapter 4

Evaluating the fate of benzophenone-UV filters and transformation products during Soil Aquifer Treatment: role of reactive barriers, biofilm and fluctuating redox state

Jou-Claus, S., Rodríguex-Esacles, P., Martínez-Landa, L., Diaz-Cruz, M.S., Carrera, J., Sunyer-Caldú, A., Quintana, G., Valhondo, C., 2022. Evaluating the fate of benzophenne-UV filters and tranformation products during Soil Aquifer Treatment: role of recative barriers, biofilm and fluctuating redox state. Manuscript submitted to Water Research.

4.1. Introduction

Ultraviolet filters (UVFs) are contaminants of emerging concern (CECs) produced and used in large quantities worldwide. They are constituents of a large number of personal care and hygiene products and other consumer goods (Tran et al. 2013). UVFs can be organic (absorb UV radiation) or inorganic (reflect and scatter UV radiation, such as TiO_2 or ZnO). Organic UVFs comprise a broad group of compounds with quite different chemical properties. Benzophenones, such as benzophenone-3 (BP-3), benzophenone-4 (BP-4) and avobenzone (AVO), are among the most used. These compounds, as other UVFs, are characterized by being photo-stable and lipophilic (Rodil et al. 2009), so they can be bioaccumulated and biomagnified along the trophic web (Gago-Ferrero et al., 2013; Molins-Delgado et al., 2017). Benzophenones and their derivatives have been reported as endocrine disruptors (Calafat et al., 2008). They cause adverse effects in fish and rodents fecundity (Kunz and Fent, 2009), neurotoxicity, cytotoxicity, and Hirschsprung disease (Wang et al. 2021). In humans, they have been associated to estrogen-dependent diseases such as endometriosis (Kunisue et al. 2012). Despite the lipophilic nature of most UVFs, they have been detected in all types of water: surface, seawater (Kawaguchi et al., 2006), wastewater (Li et al., 2007), tap water (Díaz-Cruz et al. 2012), and groundwater (Jurado et al. 2014). Furthermore, UVFs have been found in solid environmental matrices such sewage sludge (Gago-Ferrero et al., 2011b), sediments (Barón et al., 2013), and biota (fish, marine mammals, birds, and invertebrates) (Alonso et al., 2015).

Managed aquifer recharge (MAR) is considered a potential source of UVFs into groundwater bodies (Park and Lee, 2018), especially if the origin of the recharged water is the effluent of a waste water treatment plant (WWTP). Although MAR would contribute to increase water resources and to stimulate circular economy, this combination must ensure that source water quality meets the standards. Consequently, Valhondo et al. (2014) suggested the installation of a reactive barrier at the bottom of an infiltration basin to enhance degradation and sorption processes of recalcitrant contaminants. At this point, MAR acts as a tertiary treatment, named Soil Aquifer Treatment (SAT). The reactive barriers consist of different materials providing a range of sorption sites (neutral, cationic, and anionic) and enhancing biodegradation by the release of labile organic carbon, which promotes a wide range of redox states enlarging degradation pathways and, therefore removal of CECs (Valhondo et al. 2015).

UVFs biodegrade in groundwater under aerobic and anaerobic conditions, but mainly by co-metabolism (Tran et al., 2013). Liu et al. (2012) studied the biodegradation of BP-3 in batch experiments under different reduction oxidation conditions and found that half- life

was between 4 and 10 days. They also observed the formation of different transformation products (TPs) depending on the degradation pathway.

Sorption of UVFs is governed by their affinity to the solid organic phases (as characterized by octanol-water partition coefficient, K_{ow} or organic carbon-water partition coefficient, K_{oc}) and by the electrostatic and similar interactions among the ionized molecule and the charged solid surfaces (Torresi et al., 2017). These sorption mechanisms are affected by numerous chemical parameters of the solution (ionic strength, pH, concentrations of competing ions) and solid surfaces (its composition, surface charge and the age of organic matter) (Schaffer et al., 2012). Ionizable organic molecules with pK_a within the experimental pH range mat change their ionic state and therefore their sorption tendency. In groundwater and, particularly, in SAT applications, pH oscillates between 7 and 8. This is quite relevant for some UVFs, such benzophenones, since pK_a's are within this range. Consequently, to understand the fate of these compounds is also relevant to understand the pH evolution of the geochemical system.

Recent studies (Rodríguez-Escales and Sanchez-Vila 2020) have demonstrated that, besides traditional sedimentary organic surfaces, biofilms can act as active sorbents to organic compounds in porous media. Biofilms are an assemblage of microorganism comprising microbial species attached to a surface and encased in a self-synthesized matrix with water and extracellular polymeric substances (EPS). Therefore, biofilms are the site for biotransformation of organic compounds and can retain them through several mechanisms. Inside the biofilm, there are both positive and negative charges, which favor the retention of anionic and cationic species, as well as lipids, which favor the retention of lipophilic compounds. Although there is some experimental evidence of organic compounds retention in wastewater treatment plants biofilms (Torresi et al. 2017), there is no experimental evidence about retention of organic compounds in the porous media biofilms. More importantly, there is no work about the resilience of biotransformation and retention mechanisms with respect to changes in redox conditions, which is expected in a SAT facility.

This study is aimed at evaluating the role of biofilms and organic mineral surfaces in the fate of benzophenone-type UVFs and the impact of varying redox conditions on both sorption and degradation. The selected UVFs were BP-3 and its TPs (benzophenone-1 (BP-1), 4,4′-dihydroxybenzophenone (4-DHB), 4-hydroxybenzophenone (4-HB) and 2,2'-dihydroxy-4-methoxybenzophenone (DHMB)), BP-4 and AVO. Analyzed samples comprise water, soil and biofilm, the compartments involved in SAT operations implemented with a reactive barrier. With this goal, the temporal and spatial evolution of the UVFs was compared after a slug injection of acetate, which enhanced redox processes, in two SAT

replicates, one containing a reactive barrier at the infiltration basin and the other without reactive barrier.

4.2. Materials and methods

4.2.1. Site description and pilot aquifer recharge system

The pilot SAT system is located in the WWTP of Palamós, (Catalonia, Spain) (Figure 4.1). The site consists of 6 replicates (15 m long, 2.38 m wide, and 1.5 m depth) emulating MAR-SAT systems with an aquifer made up of fine sand (0.1- 0.2 mm grain size) coupled with an infiltration basin of 1.15 m high, 2.38 m wide, and 1.5 m long. The systems are fed with the WWTP secondary effluent, previously homogenized in a reservoir with 24 h retention time. A detailed description of the pilot can be found elsewhere (Valhondo et al. 2020b).

Two of the six systems were used in this study; one without reactive barrier, made up of sand (sand-treatment, ST), and the other with a 1 m thick reactive barrier made up of sand (49% in volume), vegetal compost (49%) and clay (2%) (compost-treatment, CT) installed at the bottom of the infiltration basin. The systems are equipped with monitoring points distributed along the flow path (10 piezometers and the inflow and the outflow points of the systems) (Figure 4.1). Nine piezometers were installed in three sections, at 1.3 m (Section A), 6.3 m (section B), and 12.3 m (Section C) from the infiltration basin. Every section contains three PVC piezometers of 53 mm diameter, each open (10 cm screened interval) at a different height from the aquifer base: 0.1-0.2 m (piezometer 1), 0.6-0.7 m (piezometer 2) and 1.2-1.3 m (piezometer 3). Additionally, a fully screened inclined piezometer at the base of the reactive barrier can collect water exiting the barrier. Finally, outflow is integrated and collected by means of a discharge pipe installed at the base of the aquifer end. Head, electrical conductivity (EC), and temperature were measured regularly with CTD/CD-Divers (Schlumberger water services, Delf, The Netherlands).

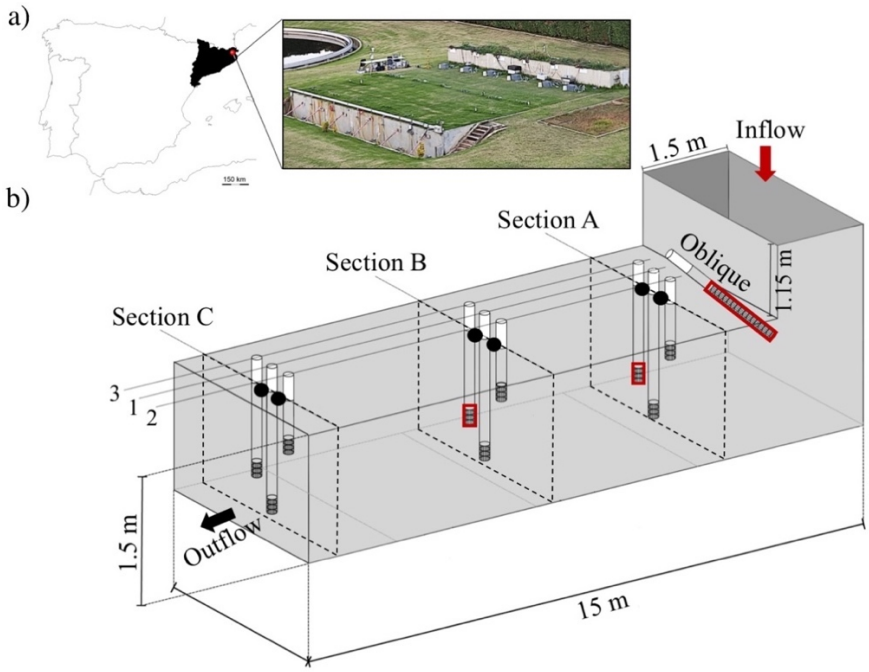

Figure 4.1. The Soil Aquifer Treatment (SAT) pilot system at Palamós (Girona, Spain). a) Location and picture of the facility with the six systems. b) Detailed scheme of the monitoring points at each system. Black dots represent the sand sampling points whereas the red squares represent the biofilm and water sampling points.

4.2.2. Experimental design

The experiment consisted of injecting 57 L of water from the WWTP spiked with lithium acetate (LiAc) at 17.8 mg/L in the infiltration basins of the two selected systems -ST, and CT- and the subsequent monitoring of the hydrochemical parameters and UVFs concentrations. Water, soil, and biofilm samples were collected during 86 d at scheduled times after the test started.

Electrical conductivity of the WWTP effluent displayed variability and occasional peaks that can be used to obtain the breakthrough curves (BTCs) of a conservative tracer. Figure 1, Appendix C shows the BTCs at different monitoring points. Sampling periods were selected to capture the BTCs at each piezometer (Figure 1, Appendix C). The average recharge inflow was set to 1 L/min and the head of the outlet was set at 135 cm for both systems.

LiAc was selected because Li^+ is as a sorptive tracer and Ac^- acts as the source of easily degradable organic carbon. Li^+ was an adequate tracer in this case because 1) it does not interact with UVFs determinations as colorimetric tracers or bromide (Abdallah et al.

2015); 2) it is absent in Palamós wastewater; 3) it is non-degradable, and 4) it allows us to characterize adsorption (Anghel et al. 2002).

4.2.3. Sampling

4.2.3.1. Groundwater: hydrochemistry and UV Filters

Water samples were collected from the inlet (recharge water), piezometers and outlet of the two SAT systems (in total, 50 samples per system). Samples were collected after purging the piezometers using drive pumps. Physicochemical field parameters (EC, pH, redox potential (Eh), and temperature) were measured *in situ* with a multiparameter probe (YSI Inc. Yellow Springs, OH, USA). Alkalinity was measured in the field with an alkalinity test kit (Merck Millipore). Water hydrochemistry characterization consisted in the analysis of dissolved organic carbon (DOC), NH_4^+, major cations and anions.

The water samples for DOC and ions determinations were filtered in the field through 0.22 µm nylon membrane filters. Aliquots for DOC were collected in muffled glass bottles of 20 mL, whereas for major cations and anions were collected in polypropylene bottles of 20 and 40 mL, respectively. Samples for DOC analysis were acidified with HCl and those for cation determination with HNO_3. The samples were shipped to laboratory under cool conditions and stored under 4 °C. Samples for UVFs analysis were collected in amber glass bottles of 150 ml, immediately frozen, and kept in the dark to prevent from photo- and bio-degradation.

4.2.3.2. Soil: Total organic carbon and sorbed UV

UVFs sorption was characterized by soil monitoring before, during, and after LiAc injection (detailed times in Figure 1, Appendix C). Solid samples were taken in the three sections of the two systems: near piezometers A2, B2, and C2 (see Figure 1) using a 110 cm long and 1 cm wide drill. Eight soil samples were collected for each system to determine the UVFs concentrations as well as the fraction of organic carbon. Samples were extracted near the open interval of the piezometer and they were completely water saturated. Samples to analyze organic carbon were stored in 13 mL polypropylene bottles (5 g per sample) and kept under 4ºC until analysis. Samples to analyze UVFs were stored in muffled amber glass bottles (20 g per sample) and kept in the dark at -20ºC until analysis.

4.2.3.3. Biofilm: Total bacteria, EPS and sorbed UV Filters

To characterize UVFs sorption into the biofilm, we constructed biotraps that were installed in 3 piezometers (O, A2 and B2) of each SAT system (Figure 4.1). Biotraps were made up of

siliceous fine sand present in the aquifer, which was previously muffled during 5 h at 600 ºC to eliminate the organic carbon fraction. The sand (127.23 g) was placed in a cylindrical sand bag (12 cm long, 3 cm diameter) made of nylon with a mesh size of 0.3x0.3 mm. Sand bags were packed into a protective plastic mesh (5 × 5 mm). Biotraps were installed one month before the test to promote bacterial growth and biofilm formation under normal operation conditions. Sampling was performed before, during, and after the LiAc peak at the monitoring points (Figure 4.1 and Figure 1, Appendix C). For sampling, the bags were opened, and the sand was collected with a spatula. Afterwards, bags were reinstalled in the piezometers for later sampling.

Samples for UVFs analyses (200-400 g per sample) were collected in 200 mL muffled amber glass bottles. Samples for EPS analyses were collected in 13 mL polypropylene bottles (7g per sample) and were stored frozen until analysis. Samples for bacterial analyses were collected in muffled glass bottles (2.3 g per sample) where 10 mL of filtered water (0.2 μm filter pore) from the site and 100 μL of formaldehyde (37%) were added. They were stored under 4 °C until analyses.

The parameters to be determined were: the UVFs concentrations in the biofilm (7 samples per system) and the amount of biofilm and bacterial density (9 samples per system). Since no interaction between silica sand and organic compounds is expected, sorbed UVFs detected in biotraps are associated to the biofilm presence.

4.2.4. Chemicals

All the UVFs standards used were of >98% of purity. BP-3, BP-4, AVO, BP-1 and 4-DHB were purchased from Sigma Aldrich (Darmstadt, Germany). DHMB was obtained from Merck (Darmstadt, Germany). The isotopically labelled internal standards, as 2-hydroxy-4-methoxy- 2′,3′,4′,5′,6′-d5 (BP3-d5), (±)-3-(4-methylbenzylidene-d4) camphor (4MBC-d4), and 5-(2,5-dimethylphenoxy)-2,2-bis(tri-deuteriomethyl) pentanoic acid (GMF-d6) were from CDN isotopes (Quebec, Canada). Table 4.1 lists physicochemical properties of monitored compounds.
LiAc was 99% of purity and was purchased from Thermo Fisher Scientific (Waltham, MA, USA). HCl, HNO_3 and CH_2O analytical grade were provided by Merck (Darmstadt, Germany).

Table 1. Physicochemical properties of UVFs ("ChemSpider | Search and share chemistry," n.d.).

Abbrevation	Other names	CAS	MW (g/mol)	$logK_{ow}$	$logK_{oc}$	pK_a	Solubility (g/l,H_2O,25ºC)
BP-3	Oxybenzone; 2-hydroxy-4-methoxybenzophenone	131-57-7	228.24	3.79	3.10	7.56	0.21
BP-4	5-benzoyl-4-hydroxy-2-methoxybenzene sulfonic acid; HMBS; Sulisobenzone	4065-45-6	308.31	0.37	1.96	-2.42	0.65
AVO	1-(4-tert-butylphenyl)-3-(4-methoxyphenyl)propane-1,3-dione	70356-09-1	310.39	4.51	3.23	6.55	0.0015
Analyzed transformation products of BP-3:							
BP-1	2,4-dihydroxybenzophenone	131-56-6	214.22	2.96	3.46	7.09	0.39
DHMB/ (BP-8)	2,2'-dihydroxy-4-methoxybenzophenone; benzophenone-8; dioxybenzone	131-53-3	224.24	3.82	3.32	6.78	0.052
4HB	4-hydroxybenzophenone	1137-42-4	198.22	3.02	3.24	7.85	0.41
4DHB	4,4'-dihydroxybenzophenone	611-99-4	214.22	2.19	3.45	7.55	0.60

4.2.5. Analytical methods

4.2.5.1. Hydrochemistry of water

DOC was measured with a TOC-VCSH analyzer Shimadzu (Kyoto, Japan) in the filtered water samples. Cationic species were analyzed by inductively-coupled plasma optical emission spectroscopy (ICP- OES) using an iCAP 6500 instrument (Thermo Fisher Scientific). NH_4^+ was analyzed using an Ion Selective Electrode (Thermo Fisher Scientific, Massachusetts, USA). Major anions (F^-, Cl^-, NO_3^-, Br^-, NO_2^-, PO_4^{3-} and SO_4^{-2}) were determined by ion chromatography (Dionex, Sunnyvale, CA, USA) using an Ionpack AS9 2x250 mm column and Na_2CO_3 9 mM solution as mobile phase.

4.2.5.2. Total Organic Carbon in solid samples

TOC was determined by organic elemental analysis (Thermo Scientific, Milan, Italy). Before the analysis the samples were dried in an oven at 50ºC for 24 h and then were ground with a ball mill. Mineral carbonate from the samples was removed with 6M HCl to isolate organic carbon. Subsequently, 20 mg of each sample were weighed and V_2O_5 was added to facilitate combustion. The samples were analyzed at 120 mL/min flow, combustion oven at 1000 ºC, chromatographic column at 60ºC, and oxygen loop of 10 mL at 100 kPa.

4.2.5.3. Bacterial density and content of polysaccharides in EPS

Bacterial density and EPS determinations are described in Perujo et al. (2017). Bacterial density was measured by flow cytometry and results are reported as bacterial cells·10^7/g sediment dry weight (dw). EPS were extracted by a cation exchange resin and the content of polysaccharides was measured spectrophotometrically.

4.2.5.4. UVFs analysis in water, soil and biofilm

Water samples for UVFs analysis were vacuum filtered twice, first using 1 mm glass fiber filters (Whatman, Fairfield, CT, USA) and then through 0.45 μm nylon membrane filters and stored at -20 °C in the dark until analysis. Analytical determinations were performed using on-line solid phase extraction coupled to high performance liquid chromatography-tandem mass spectrometry (on-line-SPE-HPLC-MS/MS), as described in Gago-Ferrero et al. (2013). Briefly, 5 ml of the water samples were extracted and purified in an automated on-line SPE-LC Sym- biosis™ Pico (Spark Holland. Emmen, The Netherlands) instrument using PLRPs on-line SPE cartridges. The trapped analytes were eluted from the SPE cartridge with the chromatographic mobile phase and introduced into an LC analytical column Hibar Purosher® STAR® HR R-18 (50 mm × 2.0 mm, 5 μm). The mobile phase consisted of HPLC-grade water and acetonitrile (ACN) with 0.1% formic acid as a modifier to analyze in positive ionization mode, and 5 mM of NH_4Ac as modifier to when analyzing in negative ionization mode. MS/MS detection was performed in a 4000 QTRAP™ MS/MS mass spectrometer (Applied Biosystems-Sciex. Foster City, USA) under selected reaction monitoring mode (SRM) for improved selectivity and sensitivity. Analyses were run in both positive and negative modes using an electrospray ionization source (ESI+, ESI). Quantification was performed by isotopic dilution using isotopically labelled internal standards specified in the chemicals section. Method limits of detection (LODs) ranged from 0.2 to 3.0 ng/L.

Soil and biofilm samples were analyzed using a QuEChERS-based methodology originally developed for the determination of UVFs in vegetables (Sunyer-Caldú and Diaz-Cruz 2021). In the case of the biofilms, the development and further validation of the analytical method was performed. Briefly, samples were freeze-dried and 5 g-dw of soil and 1 g-dw of biofilm were used for the analysis. QuEChERS kits from BEKOlut® (citrate and PSA-Kit-02 kits) were used for extraction and purification. Finally, an aliquot of 5 mL was evaporated and reconstituted to 1 mL with MeOH. This extract was analyzed in the same conditions as the water samples without the online-SPE process (HPLC-MS/MS). The quantification of the analytes was carried out using 10 matrix matched standard solutions ranging from 1 to 700

ng/mL to build the calibration curves. LODs ranged from 0.04 to 0.17 ng/g dw for soils and from 0.18 to 0.87 ng/g dw for biofilm. For the analysis of biofilm, the performance of the validated method is presented in section Appendix C.

4.3. Results and discussion

4.3.1. Transport in the SAT systems

The first step to understand the fate of UVFs is to understand transport in the SAT systems. We assess transport using electrical conductivity (EC) and Li^+, along with species affected by biochemical processes at O, A2 and B2 observation points in both CT and ST (Figure 4.2). Sampling was performed along the whole system, but only the most relevant observations are displayed. The BTC of salinity (EC) displays a very fast response at point O of the ST (it was not recorded in the CT), below the barrier and a long tail (some 4 days). This observation is consistent with the BTC of Li^+, whose peak arrival was similar to that salinity but whose tail was much heavier and lasted a lot longer. This type of response is attributed to heterogeneity (e.g., Brusseau and Srivastava, 1999). A portion of the flux takes place along preferential flow paths, but a significant portion flows through much slower paths or exchanges with immobile zones, with an aggregate residence time of up to 4 days. The preferential flow paths display little adsorption surface for Li^+, which explains why it is only slightly retarded. Adsorption surfaces concentrate in the slow flowing portion, hence the long tail of the Li^+ BTC. Flow in the CT is slightly more uniformly distributed than in the ST, as deduced from the Li^+ BTC, which is slightly more delayed, and displays a lower peak concentration and steeper tail.

BTCs at point A2 were similar to those at point O, only delayed and also a bit faster in the ST. The EC tail is similar to that of the point O, which, together with the small drop in maximum EC, indicates a very small dispersion. That is transport from O to A2 is virtually plug flow (slightly slower for CT than for ST). Salinity BTCs at B2 are similar for both systems. Both are markedly diluted and with a slightly longer tail for CT than for ST. Note that Li^+ and EC display similar peak arrival times but different tails, confirming that some preferential flow still occurs. To summarize, transport through the reactive barrier was largely driven by preferential flow, with a broad range of residence times. On the other hand, transport in the aquifer was what might be expected from a relatively homogeneous aquifer with relatively small dispersion for short transport length (up to A2), but more significant dispersion up to B2.

4.3.2. Degradation of labile organic carbon and redox zonation

Redox zonation is largely controlled by the oxidation of dissolved organic carbon (DOC) and ammonium. The BTCs of DOC (Figure 4.2e and 4.2f) were similar to those of Li^+ in that they displayed a fast peak and a much lower concentration for the CT than for the ST. The main difference is that the tails of the fast degrading acetate were steep, which we attribute to strong biochemical activity in the slow flow and immobile portions (possibly biofilms), especially in the CT. In fact, DOC was mostly degraded by the time the plume reached the B2 point (fully degraded in CT). That is, the presence of the reactive barrier enhanced the biological activity and the organic carbon oxidation, which is consistent with observations of Valhondo et al. (2020a and b). It should be pointed out that the reactive barrier was installed two years before the slug injection with the goal of releasing of DOC to favor reducing conditions. DOC release was expected to be exhausted after these two years (Canelles et al. 2021). The fact that degradation is higher in the CT system may be caused its richer bacterial activity, which is in agreement with observations obtained from column experiments using the same materials (Modrzyński et al. 2021).

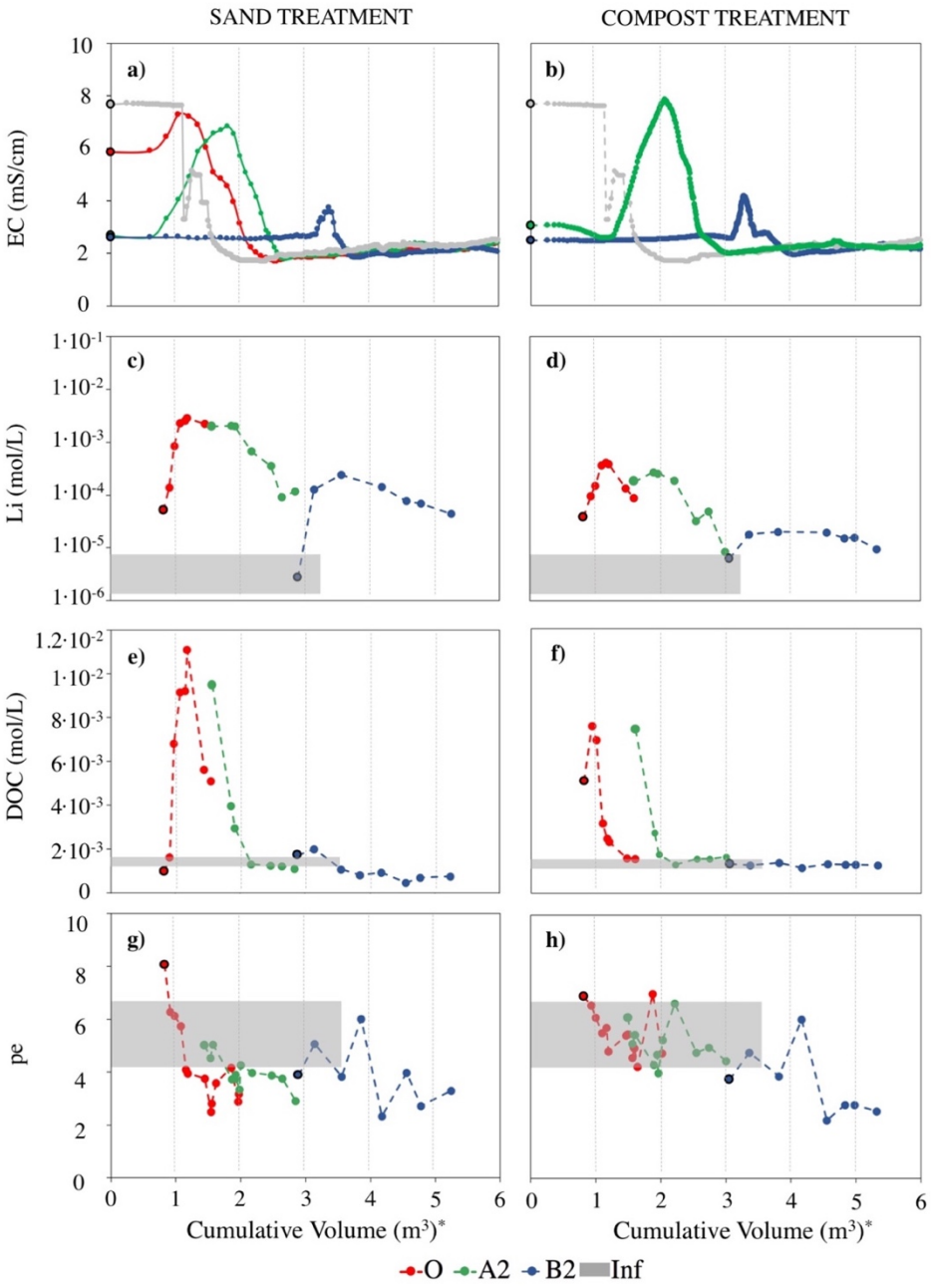

Figure 4.2: Breakthrough curves (BTCs) of electrical conductivity (EC) (a and b), redox potential (g and h), concentrations of lithium (c and d), dissolved organic carbon (DOC) (e and f)), and *pe* versus cumulative volume (square root scale) at observation points O (red, EC not acquired in the CT), A2 (green), and B2 (blue) in the ST (left) and CT (right) systems. The shadow rectangles represent the range of inflow values. Black points represent the conditions prior to tracer injection.

The redox potential (Figure 4.2f and 4.2g) was quantified as *pe* (computed as $pe = EhF/2.3RT$, where Eh is the measured redox potential, F the Faraday constant, R the gas constant, and T temperature). Redox potential was measured during sampling, thus representing the mixture of captured waters, which explain the observed fluctuations. The injection of easily degradable DOC leads to reducing conditions (i.e., a fast drop in *pe*). A lower *pe* was reached in the ST, where *pe* values decreased fast, from 8 to 3 - 4 (associated to Mn reducing conditions) than in the CT, where *pe* dropped to the range of 4-7. This latter range is usually associated to denitrification processes, but nitrate was virtually absent in the inflow which is ammonium rich. These differences in the redox potential may be explained by higher denitrification rates in the CT (Figure 4.3). Under normal operation (first point in the graphs of all observation points), ammonium depletion occurred in both systems, but much more in the CT, whose NH_4^+ dropped some 4 mmol/L, than in the ST. The fact that NO_3^- only increased 0.1 mmol/L implies that denitrification was also marked in the CT. The injection of acetate leads to reducing conditions, which might explain the slight decrease in ammonium (nitrification is hindered) in the ST and the drop in nitrate (denitrification is also hindered), but not the drop of ammonium in the CT. At this point, we conjecture the potential existence of other ammonium oxidation processes leaded by the presence of other electron acceptors such as manganese (Luther et al., 1997), iron (Yang et al., 2012), or even the presence of annamox (Hu et al., 2011). Nevertheless, we do not have the enough experimental evidence to confirm any of these processes. Note that, downstream of the CT barrier, NH_4^+ builds up. This can be explained by the potential desorption of sorbed ammonia until reach equilibrium conditions.

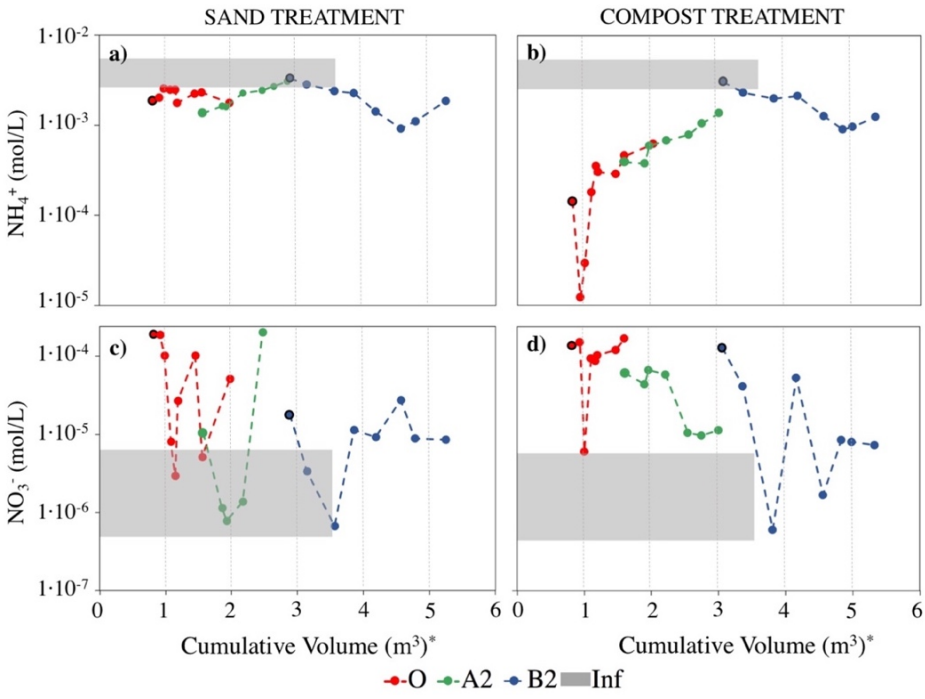

Figure 4.3. Breakthrough curves (BTCs) of ammonium (a, b) and nitrate (c, d) versus cumulative volume (square root scale) along the two SAT systems. The shadow rectangle represents the variability of concentrations in the influent. The black points represent the prior conditions before the injection of lithium acetate.

Mn (II) concentration in solution (Mn^{+2}), as a product of the reduction of Mn (IV) oxides (MnO_2), was comparable in the two systems. Mn reduction occurred prior to the test, a small increase was observed as the reducing front reached the observation points and slowly returned to pre-test conditions (Figure 4.5). Note that manganese reduction was observed in the same samples where denitrification was occurring. This is explained by 1) the potential coexistence of these two processes at similar redox potentials (Stumm and Morgan 1996) or 2) the fact that water sampling was done by pumping, which implied flow average concentrations and a potential induced mixing of waters with different hydrochemistry.

Initial Fe concentrations in solution (assumed Fe^{+2}, given the neutral pH) were low and comparable to those of the inflow, suggesting that little, if any, iron reduction occurred during normal operation prior to the test. Fe concentration grew at all observation points as the reducing front reached them, which indicates Fe (III) reduction, similar to the Mn reduction discussed above. Nevertheless, whereas Mn^{+2} concentration was stable in time, a decrease of Fe^{+2} concentration is observed in B2, with a tendency to the inflow

concentration. This decrease of Fe^{+2} could be associated with potential precipitations of secondary iron minerals. Indeed, this is geochemical plausible since the saturation index of some sulfur minerals (e.g. pyrite and mackinawite) are higher than 0 (results not shown) and a similar behavior has been previously observed in similar environments (Rodríguez-Escales et al. 2020).

Sulfate concentrations dropped after the reducing front reached every observation point (see Figure 4.4), but did not differ significantly from the inflow concentration. Thus, it might be conjectured that some sulfate reduction has occurred after the acetate injection, which would be consistent with the slight drop in Fe concentrations.

Overall, the initial redox state, as characterized by changes in DOC, pe, Fe, Mn and sulfate, was similar in the two systems. This suggests that the DOC release capacity of the reactive layer had been exhausted after two years of operation. However, the response to acetate injection was significantly different. The CT system displayed to a much larger capacity for DOC degradation and ammonium oxidation. This suggests a rich and diverse bacterial population, which is consistent with less fingering during infiltration (biofilms increase water retention and reduce permeability) and with the findings of Valhondo et al. 2020a, who showed that the presence of a reactive barrier enhanced the CECs removal in our SAT system.

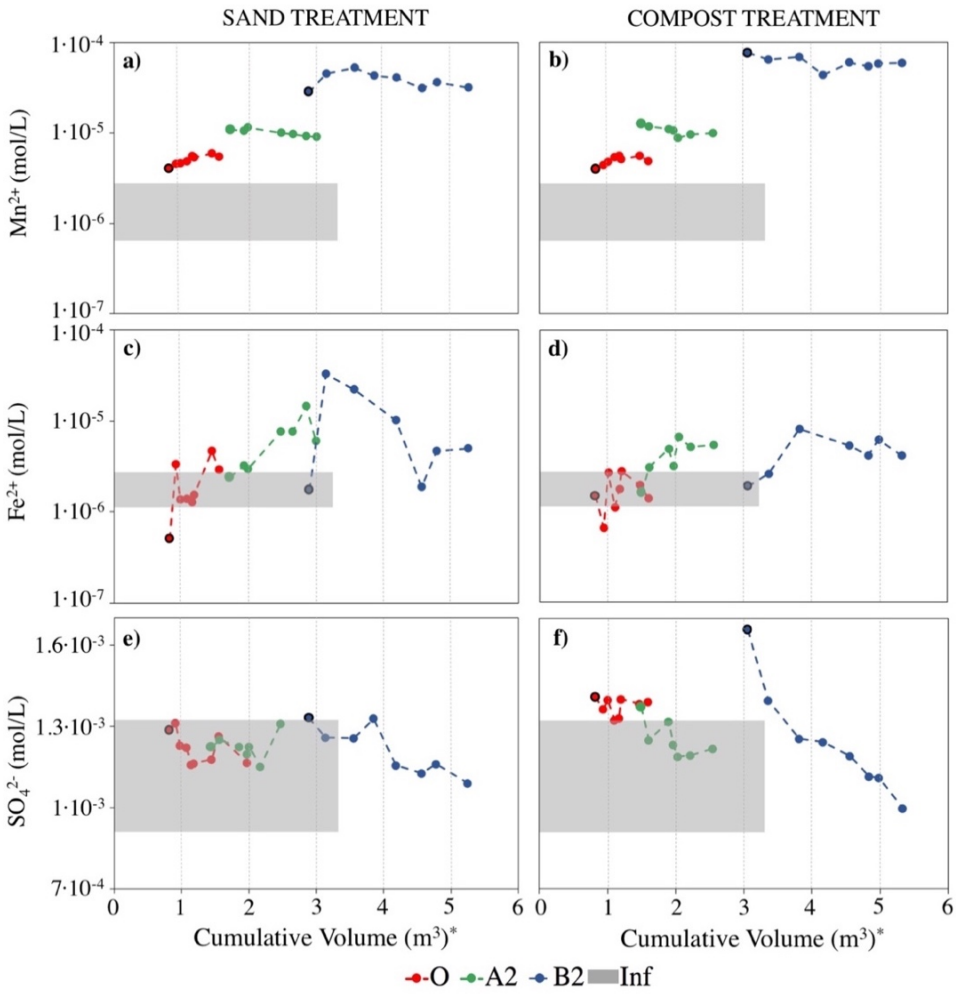

Figure 4.4. Breakthrough curves (BTCs) of manganese (a,b), iron (b,c), and sulfate (d,e) versus cumulative volume (square root scale) along the two SAT systems. The shadow rectangle represents the variability of concentration in the influent. The black points represent the prior conditions before the injection of lithium acetate.

4.3.3. UV filters occurrence in water, soil and biofilm

Figure 5 displays the concentration profiles of the BP-3 and its TPs that were found only in water (all but 4-HB). BP-3 displayed a sizeable concentration in the influent, as indicated by the shadowed rectangles in Figure 4.5a and b. Under normal operation, prior to the acetate injection (indicated by black symbols in Figure 4.5), BP-3 concentration remained comparable to inflow values at all monitored points in the ST, but fell below detection limits after point O in the CT. This behavior was similar for all TPs (Figure 4.5).

After the acetate injection, BP-3 initially dropped in both systems, concurring with the tracer peaks, but then rebounded back to levels comparable to the inflow concentration (Figures 4.2 e and f). The BP-3 decrease suggests an enhanced biodegradation because of the acetate presence, as reported by Liu et al. (2012). The rebound is explained because: 1) after the acetate peak, the system tended to the prior conditions, especially in ST; and 2) we conjecture a potential competitive sorption of BP-3. The acetate injection induced changes, which could favor the decay of some microbial communities and their detachment from the solid structure, thus favoring the dragging of EPS and all sorbed substances by the fluid flow- as BP-3.

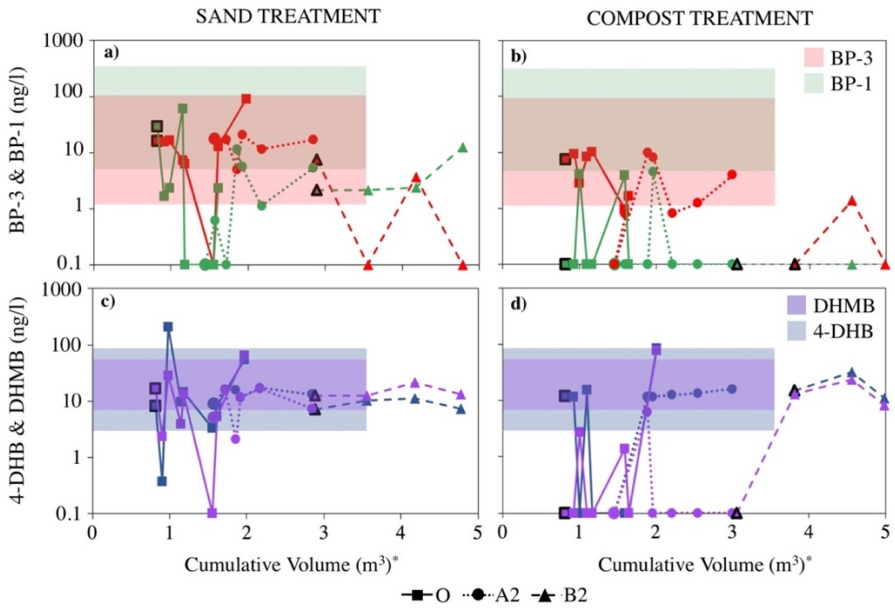

Figure 4.5. Concentration profiles of BP-3 and BP-1 (a, b), 4-DHB and DHMB (c, d) versus cumulative volume (square root scale) along the SAT pilot systems. The shadow rectangle represents the variability of concentration in the influent. The black points represent the prior conditions before the injection of lithium acetate.

BP-3 is biotransformed in some TPs (Figure 4.6). First, it can be biotransformed into BP-1 via demethylation of the methoxy substituent (Mao et al., 2019). This transformation pathway can occur both in oxic and anoxic conditions (Liu et al., 2012). Note that BP-1 was also present in the influent water (Figure 5a and 5b), meaning it was already present in the inlet water of the WWTP or it was formed there, as observed in Mao et al. (2019). After the injection of LiAc, BP-1 dropped in the ST and remained below detection at the CT. As BP-3, it rebounded.

BP-1 biodegradation can lead to the formation of 4-DHB (Liu et al. 2012). Similarly and under oxic conditions, BP-3 can form DHMB (Kim and Choi, 2014) (Figure 4.6a). Both were identified in pore waters and followed a similar behavior as BP-3 and BP-1. Prior to the

injection, their concentrations were comparable to the inflow along the ST and were below detection limit in CT. Also, the concentrations of both dropped as the acetate peak reached every observation point, and rebounded back to normal operation concentrations after the peak in the ST, but remained comparable to inflow concentrations in A2 and B2 points of the CT.

Finally, 4-HB, can be formed from 4-DHB or, directly, from BP-1 by a hydroxyl group loss (Mao et al., 2019) (Figure 4.6a). Interestingly, this compound was not present in the inflow water. Thus, it was formed in the SAT systems, demonstrating that our systems enhanced the biodegradation of BP-3 regardless the reactive barrier. Similarly to the other TPs, its concentration was lower in CT (Figure 4.7b).

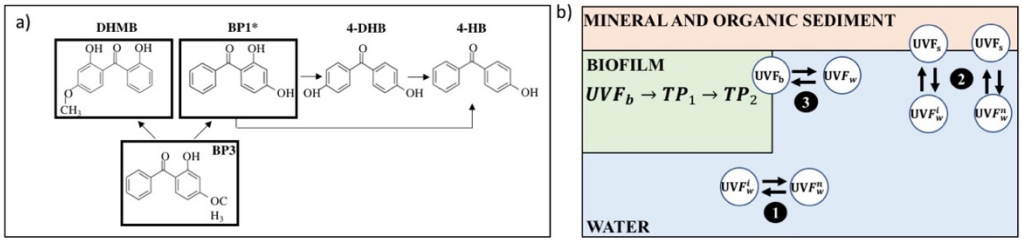

Figure 4.6. Summary of a) biodegradation pathways of BP-3 and b) main partitioning processes, where 1) is the pH dependent ionization of UVF, controlled by pK_a ; 2) retention in the sediment (adsorption onto mineral surfaces of ionic forms or absorption into organic sediment fractions); 3) absorption into biofilm. UVF refers to ultra-violet filter in water (w), biofilm (b) or sediment (s) in neutral (n) or ionic (i) form. *Compounds also formed in anoxic conditions.

Overall, CT showed lower concentrations for BP-3 and its TPs in water. We attribute this to a higher degradation capacity of this system induced by the reactive barrier in a similar way as reported for acetate degradation (see Section 3.1). The differences between the two systems can be associated to: 1) the geochemical conditions promoted by the reactive barrier facilitated the degradation of UVFs; 2) the compost reactive barrier induced a different microbial population capable to degrade these compounds; and 3) a higher sorption capacity of the system induced by the compost reactive barrier. Although the number of bacteria detected in the different sections of the systems were similar (Table 1, Appendix C), the processes discussed so far imply that microbial communities were different.

Regarding the occurrence of BP-3 and TPs in solid phases, the only compound detected was 4-HB (Figure 4.7). Its accumulation was especially important in biofilm. Since diffusion in the biofilm is comparable to that in water (Horn and Morgenroth 2006), partitioning of BP-3 and its TPs between the biofilm and bulk solution is largely governed their affinity to

organic matter, which is significant and comparable for all of them (values of K_{ow} and K_{oc} are listed in Table 1). Also, pK_a values are similar. This implies that retention 4-HB in the biofilm cannot be attributed to preferential partitioning. Therefore, we attribute the accumulation of 4-HB in the biofilm to an unbalance between its formation and degradation. Since degrading bacteria concentrate in the biofilm, its presence in the soil organic matter was low.

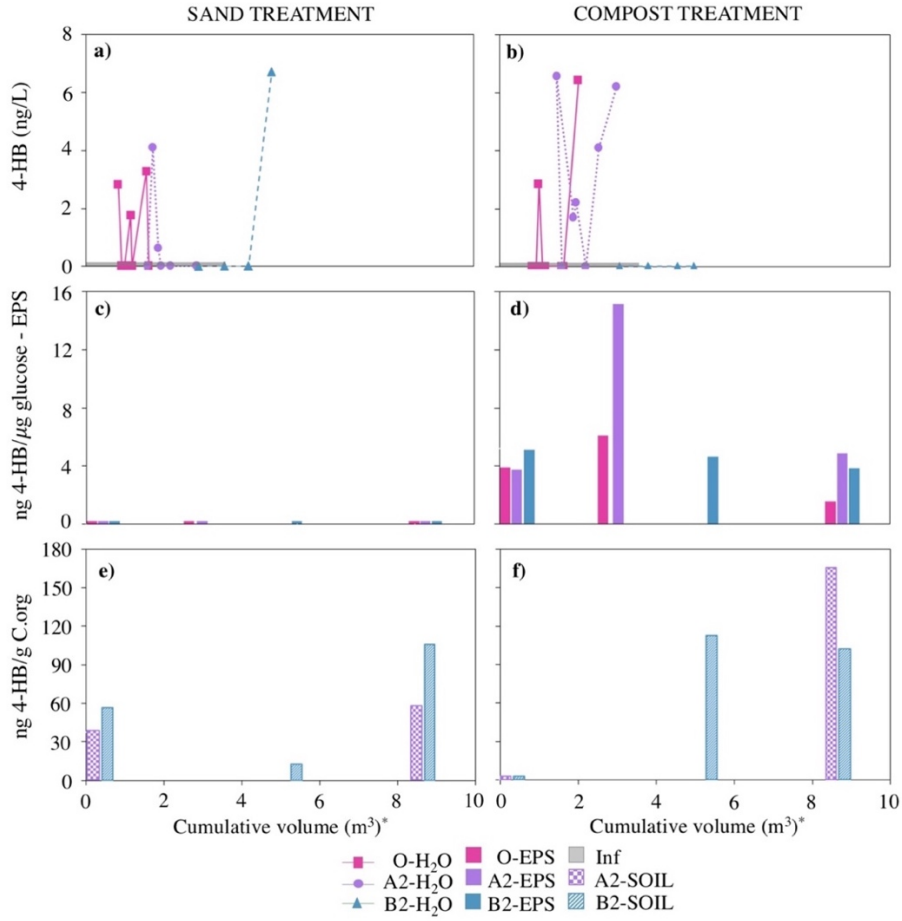

Figure 4.7. Concentration profiles of 4-HB in water (a, b), biofilm (c, d), and sediment (e, f) *versus* cumulative volume (square root scale) along the SAT pilot systems.

Regarding the other monitored UVFs, BP-4 was detected in water samples at concentrations between one and two orders of magnitude higher than the other UVFs, which is consistent with its low degradability both in the WWTP (inflow concentrations were high) and in the SAT systems. BP-4 was found in soil samples, more often than in biofilm (Figure 4.8). This agrees with the low affinity of BP-4 to the organic phase in the biofilm ($logK_{ow} = 0.37$). On

the other hand, BP-4 was mainly in its ionic form ($pk_a = -2.42$), which could enhance the ionic interaction with positive surfaces, like Fe and Mn oxides, as observed by Chang et al. (2018).

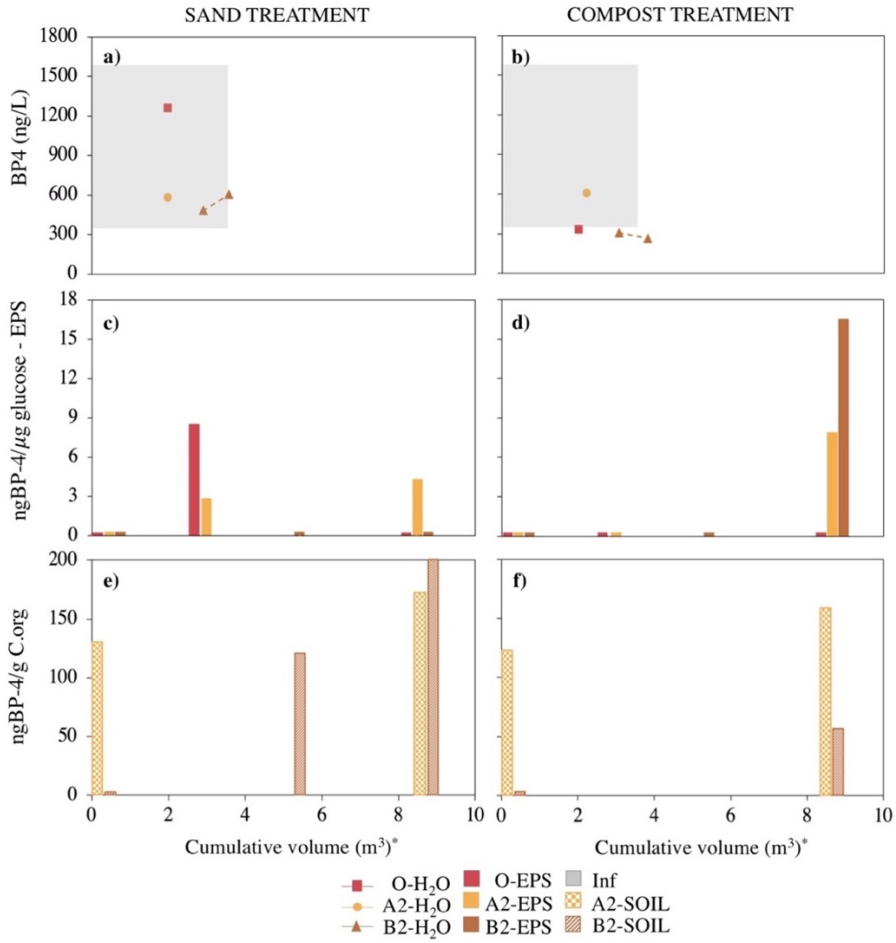

Figure 4.8. Concentration profiles of BP-4 in water (a, b), biofilm (c, d), and sediment (e, f) *versus* cumulative volume (square root scale) along the SAT pilot systems.

AVO has a structure similar to that of BP-3. Interestingly, this compound was not present in the influent water but it was detected in water samples from the SAT systems. As far as we know, there is no literature about the potential formation of AVO as a derivative product of other UVFs. Therefore, we conjecture 1) that AVO reverts-back from a conjugate (as a glucuronide conjugate typical from Phase II metabolism); or 2) a potential desorption from the biofilm and sediment, which is not likely due to the high log*Kow*. AVO was detected in most of the biofilm samples from both systems and at similar concentrations (Figure 4.9).

This could be related to its high affinity to the organic phase in the biofilm ($logK_{ow}$ = 4.51) and slow degradability.

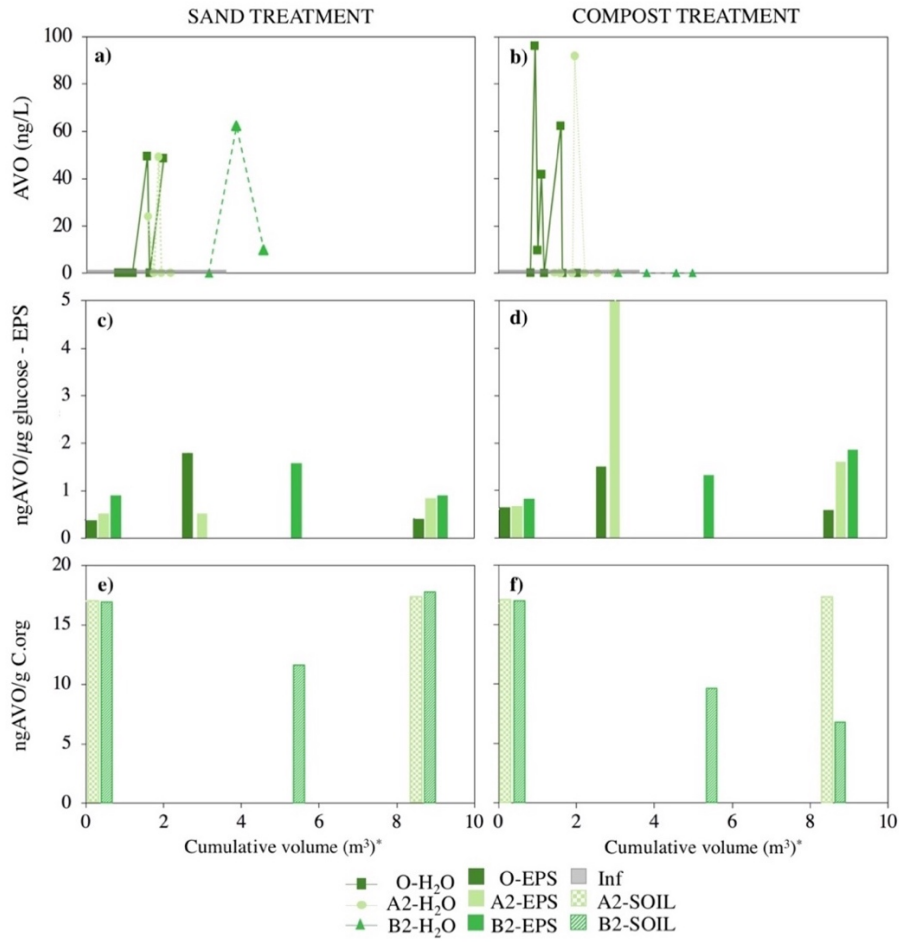

Figure 4.9. Concentration profiles of AVO in water (a, b), biofilm (c, d), and sediment (e, f) *versus* cumulative volume (square root scale) along the SAT pilot systems.

Summarizing, we have detected two UVFs and one TP in the biofilm and the sediment compartments: BP-4, AVO and 4-HB. This study documents for the first time that UVFs are accumulated in biofilms formed in the porous media and in a SAT context. Hence, this work opens a new paradigm in the understanding of organic pollutants fate in aquifers, adding biofilm as a new environmental compartment for their retention and degradation.

4.3. Conclusions

The fate of selected benzophenone-type organic UVFs and its sensitivity to varying redox conditions was investigated in two soil aquifer treatment (SAT) pilot systems. Overall, the SAT systems studied were found to contribute to the elimination of the UVFs present in urban WWTP effluents. The installation of a compost-based reactive barrier enhances their degradation rates.

The reactive barrier was successful at providing diverse redox conditions and hydrochemistry of SAT systems after acetate injection. Fe reducing condition was achieved in both SATs, despite CT displayed more variability. In particular, ammonia oxidation processes were more important in CT than in ST, especially in the vicinity of the infiltration zone.

Three TPs of BP-3 (BP-1, 4-DHB, and DHMB) were detected. Similar to BP-3, the degradation of these TPs was highest in the CT. This could be associated with a higher variability of the redox conditions and, consequently, to a higher diversity of microbial communities. Besides, the microbiome of the CT appeared to be more adapted to the degradation of recalcitrant organic compounds. Interestingly, 4-HB was the only TP of BP-3 found in the biofilm and in the sediment, which not only reflects its affinity to organic matter, similar to the other TPs, but also suggests a much slower degradation kinetics, than its parents. Regarding the other UVFs, BP-4 and AVO were found in the solid matrices. BP-4 concentration in water was quite high due to its a low degradability. Consequently, this compound was sorbed into both the sediment and the biofilm. On the other hand, AVO was not found in the water but it was detected in the biofilm and in the sediment. This was explained by its high affinity to the organic phase in the biofilm ($logK_{ow}$ = 4.51).

This study demonstrates that implementing a reactive barrier in an infiltration basin improves the degradation of benzophenone-type UVFs and, specially, of BP-3 and its TPs, and that biofilm can act as an additional environmental compartment favoring the retention and degradation of UVFs in porous media. Indeed, to the author's knowledge, this is the first work reporting the occurrence of benzophenone-type UVFs in biofilms formed in aquifers, contributing to a better understanding of their fate in porous media and, especially, in SAT systems. Beyond aquifers, the role of biofilms as an additional environmental compartment would imply that aquatic ecosystems would be exposed to a higher dose of UVFs and likely to many other organic pollutants than those calculated through the measured concentrations in water, suspended particulate matter, sediments and biota.

The authors gratefully acknowledge the Consorci d'Aigües de la Costa Brava Girona (CACBG) for the access to the WWTP, and to BEKOlut® for the provision of the QuEChERS used and Pedro Chamorro for his help in the UVFs analysis. This research was funded by the Catalan Research Project RESTORA (ACA210/18/00040), by the Spanish government, MONOPOLIOS (RTI2018-101990-B-100, MINECO/FEDER) and Project CEX2018-000794-S) and by EU project MARADENTRO (PCI2019-103425 and PCI2019-103603).

Chapter 5

General conclusions and future work

All the investigations carried out as data acquisition, data post-processing , data analysis and field work, have been aimed at improving the current knowledge of SGD behavior and its ecological implications and the fate of UV filters in a MAR facility.

The study of SGD detection using satellite TIR remote sensing demonstrates that this technique is a useful tool for the identification of coastal SGD springs in karst aquifers and can be applied from local to regional scale. Comparing the two tested approaches, single image and multitemporal thermal analyses, we conclude that the second one is better for identifying SGD springs in coastal zones. Nevertheless, this method does not allow to characterize the changes in the discharge plume, which can be done it more precisely using single images. Therefore, they are more suited to studying the morphological variations in the discharge plume and temperature variations along the plume. In this chapter, the following limiting factors have been identified when applying TIR remote sensing to the study of SGD: (1) technical limitations, (2) geological /hydrogeological characteristics, (3) environmental and marine conditions and (4) coastal geomorphology. In this context, long time series are better for identifying SGD springs areas, since there may be one or several limiting factors that can alter the SGD's thermal signal.

Satellite chlorophyll (Chl-a) data has been used as a tool to identify and map the impact of SGD on coastal biogeochemical cycles, the extension of areas influenced by SGD and its spatio-temporal variations. Its use has contributed to better constrain the limited assessed effects of SGD on coastal ecosystems. The presented methodological approach allows identifying Chl-a concentrations above background levels, which are directly associated to the ecological influence of SGD. By knowing the temporal changes of Chl-a concentration and Chl-a background concentration in a specific zone, it is possible to identify the areas where primary productivity has increased and associate it to SGD inputs.

This research highlights the significance of using satellite remote sensing as a complement to observations collected from field surveys. Using satellite remote sensing allows to estimate different environmental parameters at global scale with resolution from meters to kilometers. These satellite observations could be used as a complementary methodology to identify and characterize SGD since it allows screening inaccessible areas and zones without hydrogeological information.

In this dissertation only temperature and chlorophyll-a have been used separately to study SGD. However, remote sensing allows to measure other useful parameters as colored dissolved organic matters, total suspended matter, and turbidity among others. Therefore, evaluating the importance of all these parameters when studying SGD and its combination

(for instance combining temperature, Chlorophyll-a and others in an specific area) will provide additional information to SGD studies as well as useful information for environmental monitoring and ecosystem management in coastal areas. Furthermore, when remote sensing data is combined with specific in situ data can allow a detailed characterization of SGD influenced areas helping to quantify SGD related processes as flow and nutrients discharge, biogeochemical processes, environmental impact, etc. Lastly, despite sea water intrusion not being evaluated as part of this dissertation, remote sensing data obtained to characterize SGD flow can be used as an indicator of sea water intrusion, as higher (fresh) SGD flows should be linked with a reduction of the sea water intrusion. However, further research is needed to evaluate this hypothesis.

Focusing on managed artificial recharge, the implementation of compost reactive barrier in an infiltration basin increased the removal of benzophenone-type UVFs and, specially, of BP-3 and its transformation products. This improvement was directly related to the compost barrier, which, enhanced the reduction-oxidation processes providing a wider range of reactions and, consequently, of microbial diversity. In this sense, it is still needed a deeper understanding of all geochemical changes induced by the reactive barriers, specially, on the secondary processes related to the formation of new surfaces. Besides this, this dissertation has experimentally demonstrated that biofilm can retain organic compounds and it acts as an additional environmental compartment. Understanding the compounds' dynamic in biofilm is complex. It depends on several processes that occur simultaneously: portioning, diffusion or degradation. Although this complexity, its inclusion in environmental analysis would be relevant for those compounds with high $logK_{ow}$ (higher than 3).

This dissertation has contributed to improve groundwater resources management throughout new methodological and technical approaches to deal with the new challenges of today's society. It is expected that the results will help to use satellite remote sensing data in SGD studies to support research and monitoring, providing a cost-effective complement to traditional monitoring efforts. It is also expected that the results will help to improve the management of MAR systems according to the different targets of quantity and quality.

.

References

Abdallah, P., Deborde, M., Dossier Berne, F., Karpel Vel Leitner, N., 2015. Kinetics of Chlorination of Benzophenone-3 in the Presence of Bromide and Ammonia. Environ. Sci. Technol. 49, 14359–14367. https://doi.org/10.1021/acs.est.5b03559

Adolf, J. E., J. Burns, J. K. Walker, and S. Gamiao. 2019. Near shore distributions of phytoplankton and bacteria in relation to submarine groundwater discharge-fed fishponds, Kona coast, Hawai'i, USA. Estuar. Coast. Shelf Sci. **219**: 341–353. doi:10.1016/j.ecss.2019.01.021

Akawwi, E., Al-Zouabi, A., Kakish, M., Koehn, F., Sauter, M., 2008. Using thermal infrared imagery (TIR) for illustrating the submarine groundwater discharge into the eastern shoreline of the Dead Sea-Jordan. Am. J. Environ. Sci. 4, 693–700. https://doi.org/10.3844/ajessp.2008.693.700

Allan, R.P., Soden, B.J., 2008. Atmospheric warming and the amplification of precipitation extremes. Science (80). 321, 1481–1484. https://doi.org/10.1126/SCIENCE.1160787/SUPPL_FILE/ALLAN.SOM.PDF

Alonso, M., Feo, M.L., Corcellas, C., Gago-Ferrero, P., Bertozzi, C., Marigo, J., Flach, L., Meirelles, A.C., Carvalho, V., Azevedo, A., Torres, J.P., Lailson-Brito, J., Malm, O., Diaz-Cruz, M.S., Eljarrat, E., Barceló, D., 2015. Toxic heritage: Maternal transfer of pyrethroid insecticides and sunscreen agents in dolphins from Brazil. Environ. Pollut. 207, 391–402. https://doi.org/10.1016/J.ENVPOL.2015.09.039

Alorda-Kleinglass, A., Garcia-Orellana, J., Rodellas, V., Cerdà-Domènech, M., Tovar-Sánchez, A., Diego-Feliu, M., Trezzi, G., Sánchez-Quilez, D., Sanchez-Vidal, A., Canals, M., 2019. Remobilization of dissolved metals from a coastal mine tailing deposit driven by groundwater discharge and porewater exchange. Sci. Total Environ. 688, 1359–1372. https://doi.org/10.1016/j.scitotenv.2019.06.224

Alorda-Kleinglass, A., Ruiz-Mallén, I., Diego-Feliu, M., Rodellas, V., Bruach-Menchén, J.M., Garcia-Orellana, J., 2021. The social implications of Submarine Groundwater Discharge from an Ecosystem Services perspective: A systematic review. Earth-Science Rev. 221. https://doi.org/10.1016/J.EARSCIREV.2021.103742

Anderson, M.P., 2005. Heat as a ground water tracer. Ground Water 43, 951–968. https://doi.org/10.1111/j.1745-6584.2005.00052.x

Andreo, B., Carrasco, F., 1993. Estudio hidrogeológico del entorno de la Cueva de Nerja.

Andrisoa, A., Stieglitz, T.C., Rodellas, V., Raimbault, P., 2019. Primary production in coastal lagoons supported by groundwater discharge and porewater fluxes inferred from

nitrogen and carbon isotope signatures. Mar. Chem. 210, 48–60. https://doi.org/10.1016/j.marchem.2019.03.003

Anghel, I., Turin, H.J., Reimus, P.W., 2002. Lithium sorption to Yucca Mountain tuffs. Appl. Geochemistry 17, 819–824. https://doi.org/10.1016/S0883-2927(02)00041-0

Aquilina, L., Ladouche, B., Doerfliger, N., Seidel, J.L., Dupuy, C., Le Strat, P., 2002. Origin, evolution and residence-time of saline thermal fluids (Balaruc springs, S-France): Implications for large-scale fluid transfer across the continental shelf. Chem. Geol. 192(1), 1–21.

Arnell, N.W., 1999. Climate change and global water resources. Glob. Environ. Chang. 9, 31–49. https://doi.org/10.1016/S0959-3780(99)00017-5

Bakalowicz, M., 2018. Coastal Karst groundwater in the mediterranean: A resource to be preferably exploited onshore, not from Karst Submarine springs. Geosci. 8. https://doi.org/10.3390/geosciences8070258

Bakalowicz, M., 2015. Karst and karst groundwater resources in the Mediterranean. Environ. Earth Sci. 74, 5–14. https://doi.org/10.1007/s12665-015-4239-4

Bakalowicz, M., 2005. Karst groundwater: A challenge for new resources. Hydrogeol. J. 13, 148–160. https://doi.org/10.1007/s10040-004-0402-9

Barale, V., Jaquet, J.M., Ndiaye, M., 2008. Algal blooming patterns and anomalies in the Mediterranean Sea as derived from the SeaWiFS data set (1998-2003). Remote Sens. Environ. 112, 3300–3313. https://doi.org/10.1016/J.RSE.2007.10.014

Barberá, J.A., Andreo, B., 2015. Hydrogeological processes in a fluviokarstic area inferred from the analysis of natural hydrogeochemical tracers. The case study of eastern Serranía de Ronda (S Spain). J. Hydrol. 523, 500–514. https://doi.org/10.1016/j.jhydrol.2015.01.080

Barnett, T.P., Adam, J.C., Lettenmaier, D.P., 2005. Potential impacts of a warming climate on water availability in snow-dominated regions. Nature 438, 303–309. https://doi.org/10.1038/nature04141

Barón, E., Gago-Ferrero, P., Gorga, M., Rudolph, I., Mendoza, G., Zapata, A.M., Díaz-Cruz, S., Barra, R., Ocampo-Duque, W., Páez, M., Darbra, R.M., Eljarrat, E., Barceló, D., 2013. Occurrence of hydrophobic organic pollutants (BFRs and UV-filters) in sediments from South America. Chemosphere 92, 309–316. https://doi.org/10.1016/j.chemosphere.2013.03.032

Barsi, J.A., Barker, J.L., Schott, J.R., 2003. An Atmospheric Correction Parameter Calculator for a Single Thermal Band Earth-Sensing Instrument. Int. Geosci. Remote Sens. Symp. 5, 3014–3016. https://doi.org/10.1109/igarss.2003.1294665

Basterretxea, G., Tovar-Sanchez, A., Beck, A.J., Masqué, P., Bokuniewicz, H.J., Coffey, R., Duarte, C.M., Garcia-Orellana, J., Garcia-Solsona, E., Martinez-Ribes, L., Vaquer-Sunyer, R., 2010. Submarine groundwater discharge to the coastal environment of a Mediterranean island (Majorca, Spain): Ecosystem and biogeochemical significance.

Ecosystems 13, 629–643. https://doi.org/10.1007/s10021-010-9334-5

Bayari, C.S., Kurttaş, T., 2002. Coastal and submarine karstic discharges in the Gökova Bay, SW Turkey. Q. J. Eng. Geol. Hydrogeol. 35, 381–390. https://doi.org/10.1144/1470-9236/01034

Bejannin, S., van Beek, P., Stieglitz, T., Souhaut, M., Tamborski, J., 2017. Combining airborne thermal infrared images and radium isotopes to study submarine groundwater discharge along the French Mediterranean coastline. J. Hydrol. Reg. Stud. 13, 72–90. https://doi.org/10.1016/j.ejrh.2017.08.001

Bierman, P., Lewis, M., Ostendorf, B., Tanner, J., 2011. A review of methods for analysing spatial and temporal patterns in coastal Water quality. Ecol. Indic. 11, 103–114. https://doi.org/10.1016/j.ecolind.2009.11.001

Blanco, A.C., Nadaoka, K., Yamamoto, T., 2008. Planktonic and benthic microalgal community composition as indicators of terrestrial influence on a fringing reef in Ishigaki Island, Southwest Japan. Mar. Environ. Res. 66, 520–535. https://doi.org/10.1016/j.marenvres.2008.08.005

Boehm, A.B., Shellenbarger, G.G., Paytan, A., 2004a. Groundwater discharge: Potential association with fecal indicator bacteria in the surf zone. Environ. Sci. Technol. 38, 3558–3566. https://doi.org/10.1021/es035385a

Boehm, A.B., Shellenbarger, G.G., Paytan, A., 2004b. Groundwater discharge: Potential association with fecal indicator bacteria in the surf zone. Environ. Sci. Technol. 38, 3558–3566. https://doi.org/10.1021/es035385a

Bosc, E., Bricaud, A., Antoine, D., 2004. Seasonal and interannual variability in algal biomass and primary production in the Mediterranean Sea, as derived from 4 years of SeaWiFS observations. Global Biogeochem. Cycles 18. https://doi.org/10.1029/2003GB002034

Bricaud, A., Bosc, E., Antoine, D., 2002. Algal biomass and sea surface temperature in the Mediterranean Basin Intercomparison of data from various satellite sensors, and implications for primary production estimates. Remote Sens. Environ. 81, 163–178. https://doi.org/10.1016/S0034-4257(01)00335-2

Brunner, P., Hendricks Franssen, H.J., Kgotlhang, L., Bauer-Gottwein, P., Kinzelbach, W., 2007. How can remote sensing contribute in groundwater modeling? Hydrogeol. J. 15, 5–18. https://doi.org/10.1007/s10040-006-0127-z

Brusseau, M.L., Srivastava, R., 1999. Nonideal transport of reactive solutes in heterogeneous porous media: 4. Analysis of the Cape Cod Natural-Gradient Field Experiment. WATER Resour. Res. 35, 1113–1125. https://doi.org/10.1029/1998WR900019

Burnett, W.C., Bokuniewicz, H., Huettel, M., Moore, W.S., Taniguchi, M., 2003. Groundwater and pore water inputs to the coastal zone. Biogeochemistry 66, 3–33. https://doi.org/10.1023/B:BIOG.0000006066.21240.53

Burnett, W.C., Dulaiova, H., 2003. Estimating the dynamics of groundwater input into the

coastal zone via continuous radon-222 measurements. J. Environ. Radioact. 69, 21–35. https://doi.org/10.1016/S0265-931X(03)00084-5

Calafat, A.M., Wong, L.Y., Ye, X., Reidy, J.A., Needham, L.L., 2008. Concentrations of the sunscreen agent benzophenone-3 in residents of the United States: National Health and Nutrition Examination Survey 2003-2004. Environ. Health Perspect. 116, 893–897. https://doi.org/10.1289/ehp.11269

Canelles, A., Rodríguez-Escales, P., Modrzyński, J.J., Albers, C., Sanchez-Vila, X., 2021. Impact of compost reactive layer on hydraulic transport and C & N cycles: Biogeochemical modeling of infiltration column experiments. Sci. Total Environ. 770, 145490. https://doi.org/10.1016/j.scitotenv.2021.145490

Chander, G., Markham, B.L., Helder, D.L., 2009. Summary of current radiometric calibration coefficients for Landsat MSS, TM, ETM+, and EO-1 ALI sensors. Remote Sens. Environ. 113, 893–903. https://doi.org/10.1016/j.rse.2009.01.007

Chang, Y., Bai, Y., Huo, Y., Qu, J., 2018. Benzophenone-4 Promotes the Growth of a Pseudomonas sp. and Biogenic Oxidation of Mn(II). Environ. Sci. Technol. 52, 1262–1269. https://doi.org/10.1021/ACS.EST.7B05014

Cho, H.M., Kim, G., Kwon, E.Y., Moosdorf, N., Garcia-Orellana, J., Santos, I.R., 2018. Radium tracing nutrient inputs through submarine groundwater discharge in the global ocean. Sci. Reports 2018 81 8, 1–7. https://doi.org/10.1038/s41598-018-20806-2

Cloern, J. E., C. Grenz, and L. Vidergar-Lucas. 1995. An empirical model of the phytoplankton chlorophyll : carbon ratio-the conversion factor between productivity and growth rate. Limnol. Oceanogr. **40**: 1313–1321. doi:10.4319/LO.1995.40.7.1313

Cloern, J.E., Jassby, A.D., 2010. Patterns and scales of phytoplankton variability in estuarine-coastal ecosystems. Estuaries and Coasts 33, 230–241. https://doi.org/10.1007/S12237-009-9195-3/FIGURES/5

Cui, T., Zhang, J., Groom, S., Sun, L., Smyth, T., Sathyendranath, S., 2010. Validation of MERIS ocean-color products in the Bohai Sea: A case study for turbid coastal waters. Remote Sens. Environ. 114, 2326–2336. https://doi.org/10.1016/j.rse.2010.05.009

Dale, R.K., Miller, D.C., 2007. Spatial and temporal patterns of salinity and temperature at an intertidal groundwater seep. Estuar. Coast. Shelf Sci. 72, 283–298. https://doi.org/10.1016/j.ecss.2006.10.024

Danielescu, S., MacQuarrie, K., Faux, R., 2009. The integration of thermal infrared imaging, discharge measurements and numerical simulation to quantify the relative contributions of freshwater inflows to small estuaries in Atlantic Canadae. Hidrol. Process. 23, 2847–2859.

Díaz-Cruz, M.S., Gago-Ferrero, P., Llorca, M., Barceló, D., 2012. Analysis of UV filters in tap water and other clean waters in Spain. Anal. Bioanal. Chem. 402, 2325–2333. https://doi.org/10.1007/s00216-011-5560-8

DiGiacomo, P.M., Washburn, L., Holt, B., Jones, B.H., 2004. Coastal pollution hazards in

southern California observed by SAR imagery: Stormwater plumes, wastewater plumes, and natural hydrocarbon seeps. Mar. Pollut. Bull. 49, 1013–1024. https://doi.org/10.1016/j.marpolbul.2004.07.016

Donlon, C.J., Minnett, P.J., Gentemann, C., Nightingale, T.J., Barton, I.J., Ward, B., Murray, M.J., 2002. Toward Improved Validation of Satellite Sea Surface Skin Temperature Measurements for Climate Research. J. Clim. 15, 353–369. https://doi.org/10.1175/1520-0442(2002)015<0353:TIVOSS>2.0.CO;2

Easterling, D.R., Meehl, G.A., Parmesan, C., Changnon, S.A., Karl, T.R., Mearns, L.O., 2000. Climate extremes: observations, modeling, and impacts. Science 289, 2068–2074. https://doi.org/10.1126/SCIENCE.289.5487.2068

Edet, A.E., Okereke, C.S., Teme, S.C., Esu, E.O., 1998. Application of remote-sensing data to groundwater exploration: A case study of the Cross River State, southeastern Nigeria. Hydrogeol. J. 6, 394–404. https://doi.org/10.1007/s100400050162

Fent, K., Weston, A.A., Caminada, D., 2006. Ecotoxicology of human pharmaceuticals. Aquat. Toxicol. 76, 122–159. https://doi.org/10.1016/j.aquatox.2005.09.009

Fent, K., Zenker, A., Rapp, M., 2010. Widespread occurrence of estrogenic UV-filters in aquatic ecosystems in Switzerland. Environ. Pollut. 158, 1817–1824. https://doi.org/10.1016/j.envpol.2009.11.005

Fleury, P., Bakalowicz, M., de Marsily, G., 2007. Submarine springs and coastal karst aquifers: A review. J. Hydrol. 339, 79–92. https://doi.org/10.1016/j.jhydrol.2007.03.009

Franco, A., Fu, W., Trapp, S., 2009. Erratum: Influence of soil pH on the sorption of ionizable chemicals: Modeling advances (Environmental Toxicology and Chemistry (2009) 28 (458-464). Environ. Toxicol. Chem. 28, 2018. https://doi.org/10.1897/1552-8618-28.9.2018

Franz, B.A., Bailey, S.W., Kuring, N., Werdell, P.J., 2014. Ocean Color Measurements from Landsat-8 OLI using SeaDAS. Proc. Ocean Opt. 26–31.

Frolov, S., Kudela, R.M., Bellingham, J.G., 2013. Monitoring of harmful algal blooms in the era of diminishing resources: A case study of the U.S. West Coast. Harmful Algae 21–22, 1–12. https://doi.org/10.1016/j.hal.2012.11.001

Gago-Ferrero, P., Alonso, M.B., Bertozzi, C.P., Marigo, J., Barbosa, L., Cremer, M., Secchi, E.R., Azevedo, A., Lailson-Brito, J., Torres, J.P.M., Malm, O., Eljarrat, E., Díaz-Cruz, M.S., Barceló, D., 2013. First determination of UV filters in marine mammals. octocrylene levels in Franciscana dolphins. Environ. Sci. Technol. 47, 5619–5625. https://doi.org/10.1021/es400675y

Gago-Ferrero, P., Díaz-Cruz, M.S., Barceló, D., 2011a. Occurrence of multiclass UV filters in treated sewage sludge from wastewater treatment plants. Chemosphere 84, 1158–1165. https://doi.org/10.1016/j.chemosphere.2011.04.003

Gago-Ferrero, P., Díaz-Cruz, M.S., Barceló, D., 2011b. Fast pressurized liquid extraction with

in-cell purification and analysis by liquid chromatography tandem mass spectrometry for the determination of UV filters and their degradation products in sediments. Anal. Bioanal. Chem. 400, 2195–2204. https://doi.org/10.1007/s00216-011-4951-1

Garcés, E., Basterretxea, G., Tovar-Sánchez, A., 2011. Changes in microbial communities in response to submarine groundwater input. Mar. Ecol. Prog. Ser. 438, 47–58. https://doi.org/10.3354/meps09311

Garcia-Orellana, J., López-Castillo, E., Casacuberta, N., Rodellas, V., Masqué, P., Carmona-Catot, G., Vilarrasa, M., García-Berthou, E., 2016. Influence of submarine groundwater discharge on 210Po and 210Pb bioaccumulation in fish tissues. J. Environ. Radioact. 155–156, 46–54. https://doi.org/10.1016/j.jenvrad.2016.02.005

Garcia-Orellana, J., Rodellas, V., Tamborski, J., Diego-Feliu, M., van Beek, P., Weinstein, Y., Charette, M., Alorda-Kleinglass, A., Michael, H.A., Stieglitz, T., Scholten, J., 2021. Radium isotopes as submarine groundwater discharge (SGD) tracers: Review and recommendations. Earth-Science Rev. 103681. https://doi.org/10.1016/j.earscirev.2021.103681

Garcia-Solsona, E., Garcia-Orellana, J., Masqué, P., Garcés, E., Radakovitch, O., Mayer, A., Estradé, S., Basterretxea, G., 2010. An assessment of karstic submarine groundwater and associated nutrient discharge to a Mediterranean coastal area (Balearic Islands, Spain) using radium isotopes. Biogeochemistry 97, 211–229. https://doi.org/10.1007/s10533-009-9368-y

Gerace, A., Montanaro, M., 2017. Remote Sensing of Environment Derivation and validation of the stray light correction algorithm for the thermal infrared sensor onboard Landsat 8. Remote Sens. Environ. 191, 246–257. https://doi.org/10.1016/j.rse.2017.01.029

Gholizadeh, M. H., A. M. Melesse, and L. Reddi. 2016. A Comprehensive Review on Water Quality Parameters Estimation Using Remote Sensing Techniques. Sensors **16**. doi:10.3390/s16081298

Gierach, M.M., Holt, B., Trinh, R., Jack Pan, B., Rains, C., 2017. Satellite detection of wastewater diversion plumes in Southern California. Estuar. Coast. Shelf Sci. 186, 171–182. https://doi.org/10.1016/j.ecss.2016.10.012

Giokas, D.L., Sakkas, V.A., Albanis, T.A., 2004. Determination of residues of UV filters in natural waters by solid-phase extraction coupled to liquid chromatography-photodiode array detection and gas chromatography-mass spectrometry. J. Chromatogr. A 1026, 289–293. https://doi.org/10.1016/j.chroma.2003.10.114

Glasgow, H.B., Burkholder, J.A.M., Reed, R.E., Lewitus, A.J., Kleinman, J.E., 2004. Real-time remote monitoring of water quality: A review of current applications, and advancements in sensor, telemetry, and computing technologies. J. Exp. Mar. Bio. Ecol. 300, 409–448. https://doi.org/10.1016/j.jembe.2004.02.022

Gobler, C.J., Boneillo, G.E., 2003. Impacts of anthropogenically influenced groundwater seepage on water chemistry and phytoplankton dynamics within a coastal marine system. Mar. Ecol. Prog. Ser. 255, 101–114. https://doi.org/10.3354/MEPS255101

Grimm, N. B., S. H. Faeth, N. E. Golubiewski, C. L. Redman, J. Wu, X. Bai, and J. M. Briggs. 2008. Global change and the ecology of cities. Science (80-.). **319**: 756–760. doi:10.1126/SCIENCE.1150195/SUPPL_FILE/GRIMM.SOM.REV.PDF

Gumma, M.K., Pavelic, P., 2013. Mapping of groundwater potential zones across Ghana using remote sensing, geographic information systems, and spatial modeling. Environ. Monit. Assess. 185, 3561–3579. https://doi.org/10.1007/s10661-012-2810-y

Hansen, J., Sato, M., Hearty, P., Ruedy, R., Kelley, M., Masson-Delmotte, V., Russell, G., Tselioudis, G., Cao, J., Rignot, E., Velicogna, I., Tormey, B., Donovan, B., Kandiano, E., Von Schuckmann, K., Kharecha, P., Legrande, A.N., Bauer, M., 2016. Ice melt, sea level rise and superstorms: Evidence from paleoclimate data, climate modeling, and modern observations that 2 °c global warming could be dangerous. Atmos. Chem. Phys. 16, 3761–3812. https://doi.org/10.5194/ACP-16-3761-2016

Hays, C.G., 2005. Effect of nutrient availability, grazer assemblage and seagrass source population on the interaction between Thalassia testudinum (turtle grass) and its algal epiphytes. J. Exp. Mar. Bio. Ecol. 314, 53–68. https://doi.org/10.1016/j.jembe.2004.08.017

Holman, I.P., 2006. Climate change impacts on groundwater recharge-uncertainty, shortcomings, and the way forward? Hydrogeol. J. 14, 637–647. https://doi.org/10.1007/S10040-005-0467-0/FIGURES/7

Honda, H., R. Sugimoto, and S. Kobayashi. 2018. Submarine Groundwater Discharge and its Influence on Primary Production in Japanese Coasts: Case Study in Obama Bay. 101–115. doi:10.1007/978-981-10-7383-0_8

Horn, H., Morgenroth, E., 2006. Transport of oxygen, sodium chloride, and sodium nitrate in biofilms. Chem. Eng. Sci. 61, 1347–1356. https://doi.org/10.1016/j.ces.2005.08.027

Hu, B.L., Shen, L.D., Xu, X.Y., Zheng, P., 2011. Anaerobic ammonium oxidation (anammox) in different natural ecosystems. Biochem. Soc. Trans. 39, 1811–1816. https://doi.org/10.1042/BST20110711

Jickells, T. D., E. Buitenhuis, K. Altieri, and others. 2017. A reevaluation of the magnitude and impacts of anthropogenic atmospheric nitrogen inputs on the ocean. Global Biogeochem. Cycles **31**: 289–305. doi:10.1002/2016GB005586

Johnson, A.G., Glenn, C.R., Burnett, W.C., Peterson, R.N., Lucey, P.G., 2008. Aerial infrared imaging reveals large nutrient-rich groundwater inputs to the ocean. Geophys. Res. Lett. 35, 1–6. https://doi.org/10.1029/2008GL034574

Jou-Claus, S., Folch, A., Garcia-Orellana, J., 2021. Applicability of Landsat 8 thermal infrared sensor for identifying submarine groundwater discharge springs in the Mediterranean Sea basin. Hydrol. Earth Syst. Sci. 25, 4789–4805. https://doi.org/10.5194/HESS-25-4789-2021

Jurado, A., Gago-Ferrero, P., Vàzquez-Suñé, E., Carrera, J., Pujades, E., Díaz-Cruz, M.S., Barceló, D., 2014. Urban groundwater contamination by residues of UV filters. J.

Hazard. Mater. 271, 141–149. https://doi.org/10.1016/j.jhazmat.2014.01.036

Kawaguchi, M., Ito, R., Endo, N., Sakui, N., Okanouchi, N., Saito, K., Sato, N., Shiozaki, T., Nakazawa, H., 2006. Stir bar sorptive extraction and thermal desorption-gas chromatography-mass spectrometry for trace analysis of benzophenone and its derivatives in water sample. Anal. Chim. Acta 557, 272–277. https://doi.org/10.1016/j.aca.2005.08.087

Kelly, J.L., Glenn, C.R., Lucey, P.G., 2013. High-resolution aerial infrared mapping of groundwater discharge to the coastal ocean. Limnol. Oceanogr. Methods 11, 262–277. https://doi.org/10.4319/lom.2013.11.262

Kim, G., 2003. Large submarine groundwater discharge (SGD) from a volcanic island. Geophys. Res. Lett. 30, 1–4. https://doi.org/10.1029/2003gl018378

Kim, S., Choi, K., 2014. Occurrences, toxicities, and ecological risks of benzophenone-3, a common component of organic sunscreen products: A mini-review. Environ. Int. 70, 143–157. https://doi.org/10.1016/j.envint.2014.05.015

Klemas, V., 2011. Remote sensing techniques for studying coastal ecosystems: An overview. J. Coast. Res. 27, 2–17. https://doi.org/10.2112/JCOASTRES-D-10-00103.1

Kløve, B., Ala-Aho, P., Bertrand, G., Gurdak, J.J., Kupfersberger, H., Kværner, J., Muotka, T., Mykrä, H., Preda, E., Rossi, P., Uvo, C.B., Velasco, E., Pulido-Velazquez, M., 2014. Climate change impacts on groundwater and dependent ecosystems. J. Hydrol. 518, 250–266. https://doi.org/10.1016/J.JHYDROL.2013.06.037

Kratzer, S., Tett, P., 2009. Using bio-optics to investigate the extent of coastal waters: A Swedish case study. Hydrobiologia 629, 169–186. https://doi.org/10.1007/s10750-009-9769-x

Kratzer, S., Therese Harvey, E., Philipson, P., 2014. The use of ocean color remote sensing in integrated coastal zone management-A case study from Himmerfjärden, Sweden. Mar. Policy 43, 29–39. https://doi.org/10.1016/j.marpol.2013.03.023

Krest, J.M., Moore, W.S., Gardner, L.R., Morris, J.T., 2000. Marsh nutrient export supplied by groundwater discharge: Evidence from radium measurements. Global Biogeochem. Cycles 14, 167–176. https://doi.org/10.1029/1999GB001197

Kunisue, T., Chen, Z., Buck Louis, G.M., Sundaram, R., Hediger, M.L., Sun, L., Kannan, K., 2012. Urinary concentrations of benzophenone-type UV filters in U.S. women and their association with endometriosis. Environ. Sci. Technol. 46, 4624–4632. https://doi.org/10.1021/es204415a

Kunz, P.Y., Fent, K., 2009. Estrogenic activity of ternary UV filter mixtures in fish (Pimephales promelas) - An analysis with nonlinear isobolograms. Toxicol. Appl. Pharmacol. 234, 77–88. https://doi.org/10.1016/j.taap.2008.09.032

Laws, B. V., Dickenson, E.R.V., Johnson, T.A., Snyder, S.A., Drewes, J.E., 2011. Attenuation of contaminants of emerging concern during surface-spreading aquifer recharge. Sci. Total Environ. 409, 1087–1094. https://doi.org/10.1016/j.scitotenv.2010.11.021

Lecher, A., Mackey, K., 2018. Synthesizing the Effects of Submarine Groundwater Discharge on Marine Biota. Hydrology 5, 60. https://doi.org/10.3390/hydrology5040060

Lecher, A.L., Mackey, K.R.M., Paytan, A., 2017. River and Submarine Groundwater Discharge Effects on Diatom Phytoplankton Abundance in the Gulf of Alaska. Hydrology. https://doi.org/10.3390/hydrology4040061

Lee, E., Kang, K.M., Hyun, S.P., Lee, K.Y., Yoon, H., Kim, S.H., Kim, Y., Xu, Z., Kim, D.J., Koh, D.C., Ha, K., 2016. Submarine groundwater discharge revealed by aerial thermal infrared imagery: a case study on Jeju Island, Korea. Hydrol. Process. 30, 3494–3506. https://doi.org/10.1002/hyp.10868

Li, W., Ma, Y., Guo, C., Hu, W., Liu, K., Wang, Y., Zhu, T., 2007. Occurrence and behavior of four of the most used sunscreen UV filters in a wastewater reclamation plant. Water Res. 41, 3506–3512. https://doi.org/10.1016/j.watres.2007.05.039

Liu, Y.S., Ying, G.G., Shareef, A., Kookana, R.S., 2012. Biodegradation of the ultraviolet filter benzophenone-3 under different redox conditions. Environ. Toxicol. Chem. 31, 289–295. https://doi.org/10.1002/etc.749

Loaiciga, H.A., Valdes, J.B., Vogel, R., Garvey, J., Schwarz, H., 1996. Global warming and the hydrologic cycle. J. Hydrol. 174, 83–127. https://doi.org/10.1016/0022-1694(95)02753-X

Luijendijk, E., Gleeson, T., Moosdorf, N., 2020. Fresh groundwater discharge insignificant for the world's oceans but important for coastal ecosystems. Nat. Commun. 11, 1260. https://doi.org/10.1038/s41467-020-15064-8

Luther, G.W., Sundby, B., Lewis, B.L., Brendel, P.J., Silverberg, N., 1997. Interactions of manganese with the nitrogen cycle: Alternative pathways to dinitrogen. Geochim. Cosmochim. Acta 61, 4043–4052. https://doi.org/10.1016/S0016-7037(97)00239-1

Mallast, U., Gloaguen, R., Friesen, J., Rödiger, T., Geyer, S., Merz, R., Siebert, C., 2014. How to identify groundwater-caused thermal anomalies in lakes based on multi-temporal satellite data in semi-arid regions. Hydrol. Earth Syst. Sci. 18, 2773–2787. https://doi.org/10.5194/hess-18-2773-2014

Mallast, U., Siebert, C., Wagner, B., Sauter, M., Gloaguen, R., Geyer, S., Merz, R., 2013. Localisation and temporal variability of groundwater discharge into the Dead Sea using thermal satellite data. Environ. Earth Sci. 69, 587–603. https://doi.org/10.1007/s12665-013-2371-6

Mao, F., He, Y., Gin, K.Y.H., 2019. Occurrence and fate of benzophenone-type UV filters in aquatic environments: A review. Environ. Sci. Water Res. Technol. 5, 209–223. https://doi.org/10.1039/c8ew00539g

Mayfield, K. K., A. Eisenhauer, D. P. Santiago Ramos, and others. 2021. Groundwater discharge impacts marine isotope budgets of Li, Mg, Ca, Sr, and Ba. Nat. Commun. 2021 121 **12**: 1–9. doi:10.1038/s41467-020-20248-3

McCaul, M., Barland, J., Cleary, J., Cahalane, C., McCarthy, T., Diamond, D., 2016. Combining

remote temperature sensing with in-situ sensing to track marine/freshwater mixing dynamics. Sensors (Switzerland) 16. https://doi.org/10.3390/s16091402

Mejías, M., B. J. Ballesteros, C. Antón-Pacheco, and others. 2014. Remote sensing and GIS for mapping groundwater recharge and discharge areas in salinity prone catchments, southeastern Australia. J. Hydrol. **74**: 149–156. doi:10.1016/j.chemosphere.2019.124826

Mejías, M., Ballesteros, B.J., Antón-Pacheco, C., Domínguez, J.A., Garcia-Orellana, J., Garcia-Solsona, E., Masqué, P., 2012. Methodological study of submarine groundwater discharge from a karstic aquifer in the Western Mediterranean Sea. J. Hydrol. 464–465, 27–40. https://doi.org/10.1016/j.jhydrol.2012.06.020

Michael, H.A., Mulligan, A.E., Harvey, C.F., 2005. Seasonal oscillations in water exchange between aquifers and the coastal ocean. Nature 436, 1145–1148. https://doi.org/10.1038/nature03935

Milly, P.C.D., Dunne, K.A., Vecchia, A. V., 2005. Global pattern of trends in streamflow and water availability in a changing climate. Nat. 2005 4387066 438, 347–350. https://doi.org/10.1038/NATURE04312

Mobley, C.D., Werdell, J., Franz, B., Ahmad, Z., Bailey, S., 2016. Atmospheric correction for satellite ocean color radiometry. A Tutor. Doc. NASA Ocean Biol. Process. Gr. 1–73.

Modrzyński, J.J., Aamand, J., Wittorf, L., Badawi, N., Hubalek, V., Canelles, A., Hallin, S., Albers, C.N., 2021. Combined removal of organic micropollutants and ammonium in reactive barriers developed for managed aquifer recharge. Water Res. 190, 116669. https://doi.org/10.1016/j.watres.2020.116669

Molins-Delgado, D., Mánez, M., Andreu, A., Hiraldo, F., Eljarrat, E., Barceló, D., Díaz-Cruz, M.S., 2017. A Potential New Threat to Wild Life: Presence of UV Filters in Bird Eggs from a Preserved Area. Environ. Sci. Technol. 51, 10983–10990. https://doi.org/10.1021/ACS.EST.7B03300

Moore, W.S., 2010. The Effect of Submarine Groundwater Discharge on the Ocean. Ann. Rev. Mar. Sci. 2, 59–88. https://doi.org/10.1146/annurev-marine-120308-081019

Moore, W.S., 1999. The subterranean estuary: A reaction zone of ground water and sea water. Mar. Chem. 65, 111–125. https://doi.org/10.1016/S0304-4203(99)00014-6

Moosdorf, N., Böttcher, M.E., Adyasari, D., Erkul, E., Gilfedder, B.S., Greskowiak, J., Jenner, A.-K., Kotwicki, L., Massmann, G., Müller-Petke, M., Oehler, T., Post, V., Prien, R., Scholten, J., Siemon, B., Ehlert von Ahn, C.M., Walther, M., Waska, H., Wunderlich, T., Mallast, U., 2021. A State-Of-The-Art Perspective on the Characterization of Subterranean Estuaries at the Regional Scale. Front. Earth Sci. 9, 95. https://doi.org/10.3389/feart.2021.601293

Nieto, A., Borrull, F., Marcé, R.M., Pocurull, E., 2009. Determination of personal care products in sewage sludge by pressurized liquid extraction and ultra high performance liquid chromatography-tandem mass spectrometry. J. Chromatogr. A 1216, 5619–5625. https://doi.org/10.1016/j.chroma.2009.05.061

O'Reilly, J.E., Maritorena, S., Mitchell, B.G., Siegel, D.A., Carder, K.L., Garver, S.A., Kahru, M., McClain, C., 1998. Ocean color chlorophyll algorithms for SeaWiFS. J. Geophys. Res. Ocean. 103, 24937–24953. https://doi.org/10.1029/98JC02160/FORMAT/PDF

Odeh, I.O.A., McBratney, A.B., Chittleborough, D.J., 1992. Soil Pattern Recognition with Fuzzy-c-means: Application to Classification and Soil-Landform Interrelationships. Soil Sci. Soc. Am. J. 56, NP-NP. https://doi.org/10.2136/SSSAJ1992.03615995005600020050X

Oehler, T., Eiche, E., Putra, D., Adyasari, D., Hennig, H., Mallast, U., Moosdorf, N., 2018. Seasonal variability of land-ocean groundwater nutrient fluxes from a tropical karstic region (southern Java, Indonesia). J. Hydrol. 565, 662–671. https://doi.org/10.1016/j.jhydrol.2018.08.077

Paerl, H.W., 2006. Assessing and managing nutrient-enhanced eutrophication in estuarine and coastal waters: Interactive effects of human and climatic perturbations, in: Ecological Engineering. pp. 40–54. https://doi.org/10.1016/j.ecoleng.2005.09.006

Park, S., Lee, W., 2018. Removal of selected pharmaceuticals and personal care products in reclaimed water during simulated managed aquifer recharge. Sci. Total Environ. 640–641, 671–677. https://doi.org/10.1016/j.scitotenv.2018.05.221

Paytan, A., Shellenbarger, G.G., Street, J.H., Gonneea, M.E., Davis, K., Young, M.B., Moore, W.S., 2006. Submarine groundwater discharge: An important source of new inorganic nitrogen to coral reef ecosystems. Limnol. Oceanogr. 51, 343–348. https://doi.org/10.4319/lo.2006.51.1.0343

Perujo, N., Sanchez-Vila, X., Proia, L., Romaní, A.M., 2017. Interaction between Physical Heterogeneity and Microbial Processes in Subsurface Sediments: A Laboratory-Scale Column Experiment. https://doi.org/10.1021/acs.est.6b06506

Rocha, C., Robinson, C.E., Santos, I.R., Waska, H., Michael, H.A., Bokuniewicz, H.J., 2021. A place for subterranean estuaries in the coastal zone. Estuar. Coast. Shelf Sci. 250, 107167. https://doi.org/10.1016/j.ecss.2021.107167

Rodellas, V., Garcia-Orellana, J., Garcia-Solsona, E., Masqué, P., Domínguez, J.A., Ballesteros, B.J., Mejías, M., Zarroca, M., 2012. Quantifying groundwater discharge from different sources into a Mediterranean wetland by using 222Rn and Ra isotopes. J. Hydrol. 466–467, 11–22. https://doi.org/10.1016/j.jhydrol.2012.07.005

Rodellas, V., Garcia-Orellana, J., Masqué, P., Feldman, M., Weinstein, Y., Boyle, E.A., 2015. Submarine groundwater discharge as a major source of nutrients to the Mediterranean Sea. Proc. Natl. Acad. Sci. U. S. A. 112, 3926–3930. https://doi.org/10.1073/pnas.1419049112

Rodellas, V., Garcia-Orellana, J., Tovar-Sánchez, A., Basterretxea, G., López-Garcia, J.M., Sánchez-Quiles, D., Garcia-Solsona, E., Masqué, P., 2014. Submarine groundwater discharge as a source of nutrients and trace metals in a Mediterranean bay (Palma Beach, Balearic Islands). Mar. Chem. 160, 56–66. https://doi.org/10.1016/j.marchem.2014.01.007

Rodil, R., Moeder, M., Altenburger, R., Schmitt-Jansen, M., 2009. Photostability and phytotoxicity of selected sunscreen agents and their degradation mixtures in water. Anal. Bioanal. Chem. 395, 1513–1524. https://doi.org/10.1007/s00216-009-3113-1

Rodríguez-Escales, P., Barba, C., Sanchez-Vila, X., Jacques, D., Folch, A., 2020. Coupling Flow, Heat, and Reactive Transport Modeling to Reproduce In Situ Redox Potential Evolution: Application to an Infiltration Pond. Environ. Sci. Technol. 54, 12092–12101. https://doi.org/10.1021/ACS.EST.0C03056

Rodríguez-Escales, P., Sanchez-Vila, X., 2020. Modeling the fate of UV filters in subsurface: Co-metabolic degradation and the role of biomass in sorption processes. Water Res. 168, 115192. https://doi.org/10.1016/j.watres.2019.115192

Rosenberry, D.O., Duque, C., Lee, D.R., 2020. History and evolution of seepage meters for quantifying flow between groundwater and surface water: Part 1 – Freshwater settings. Earth-Science Rev. https://doi.org/10.1016/j.earscirev.2020.103167

Rufí-Salís, M., Garcia-Orellana, J., Cantero, G., Castillo, J., Hierro, A., Rieradevall, J., Bach, J., 2019. Influence of land use changes on submarine groundwater discharge. Environ. Res. Commun. 1, 031005. https://doi.org/10.1088/2515-7620/ab1695

Ruiz-González, C., Rodellas, V., Garcia-Orellana, J., 2021. The microbial dimension of submarine groundwater discharge: current challenges and future directions. FEMS Microbiol. Rev. https://doi.org/10.1093/femsre/fuab010

Ryan, J.P., Gower, J.F.R., King, S.A., Bissett, W.P., Fischer, A.M., Kudela, R.M., Kolber, Z., Mazzillo, F., Rienecker, E. V., Chavez, F.P., 2008. A coastal ocean extreme bloom incubator. Geophys. Res. Lett. 35, 4–8. https://doi.org/10.1029/2008GL034081

Santos, I.R., Chen, X., Lecher, A.L., Sawyer, A.H., Moosdorf, N., Rodellas, V., Tamborski, J., Cho, H.M., Dimova, N., Sugimoto, R., Bonaglia, S., Li, H., Hajati, M.C., Li, L., 2021. Submarine groundwater discharge impacts on coastal nutrient biogeochemistry. Nat. Rev. Earth Environ. 2, 307–323. https://doi.org/10.1038/S43017-021-00152-0

Schaffer, M., Boxberger, N., Börnick, H., Licha, T., Worch, E., 2012. Sorption influenced transport of ionizable pharmaceuticals onto a natural sandy aquifer sediment at different pH. Chemosphere 87, 513–520. https://doi.org/10.1016/j.chemosphere.2011.12.053

Schlumpf, M., Schmid, P., Durrer, S., Conscience, M., Maerkel, K., Henseler, M., Gruetter, M., Herzog, I., Reolon, S., Ceccatelli, R., Faass, O., Stutz, E., Jarry, H., Wuttke, W., Lichtensteiger, W., 2004. Endocrine activity and developmental toxicity of cosmetic UV filters - An update. Toxicology 205, 113–122. https://doi.org/10.1016/j.tox.2004.06.043

Schubert, M., Scholten, J., Schmidt, A., Comanducci, J.F., Pham, M.K., Mallast, U., Knoeller, K., 2014. Submarine groundwater discharge at a single spot location: Evaluation of different detection approaches. Water (Switzerland) 6, 584–601. https://doi.org/10.3390/w6030584

Shaban, A., Khawlie, M., Abdallah, C., Faour, G., 2005. Geologic controls of submarine

groundwater discharge: Application of remote sensing to north Lebanon. Environ. Geol. 47, 512–522. https://doi.org/10.1007/s00254-004-1172-3

Shen, L., Xu, H., Guo, X., 2012. Satellite remote sensing of harmful algal blooms (HABs) and a potential synthesized framework. Sensors (Switzerland). https://doi.org/10.3390/s120607778

Stumm, W., Morgan, J.J., 1996. Aquatic chemistry: Chemical Equilibria and Rates in Natural Waters, Wiley. https://doi.org/10.5860/choice.33-6312

Sunyer-Caldú, A., Diaz-Cruz, M.S., 2021. Development of a QuEChERS-based method for the analysis of pharmaceuticals and personal care products in lettuces grown in field-scale agricultural plots irrigated with reclaimed water. Talanta 230, 122302. https://doi.org/10.1016/J.TALANTA.2021.122302

Tamborski, J., van Beek, P., Conan, P., Pujo-Pay, M., Odobel, C., Ghiglione, J.F., Seidel, J.L., Arfib, B., Diego-Feliu, M., Garcia-Orellana, J., Szafran, A., Souhaut, M., 2020. Submarine karstic springs as a source of nutrients and bioactive trace metals for the oligotrophic Northwest Mediterranean Sea. Sci. Total Environ. 732, 1–14. https://doi.org/10.1016/j.scitotenv.2020.139106

Tamborski, J.J., Rogers, A.D., Bokuniewicz, H.J., Cochran, J.K., Young, C.R., 2015. Identification and quantification of diffuse fresh submarine groundwater discharge via airborne thermal infrared remote sensing. Remote Sens. Environ. 171, 202–217. https://doi.org/10.1016/j.rse.2015.10.010

Taniguchi, M., Dulai, H., Burnett, K.M., Santos, I.R., Sugimoto, R., Stieglitz, T., Kim, G., Moosdorf, N., Burnett, W.C., 2019a. Submarine Groundwater Discharge: Updates on Its Measurement Techniques, Geophysical Drivers, Magnitudes, and Effects. Front. Environ. Sci. 7, 1–26. https://doi.org/10.3389/fenvs.2019.00141

Taniguchi, M., Dulai, H., Burnett, K.M., Santos, I.R., Sugimoto, R., Stieglitz, T., Kim, G., Moosdorf, N., Burnett, W.C., 2019b. Submarine Groundwater Discharge: Updates on Its Measurement Techniques, Geophysical Drivers, Magnitudes, and Effects. Front. Environ. Sci. https://doi.org/10.3389/fenvs.2019.00141

Tcherepanov, E.N., Zlotnik, V.A., Henebry, G.M., 2005. Using Landsat thermal imagery and GIS for identification of groundwater discharge into shallow groundwater-dominated lakes. Int. J. Remote Sens. 26, 3649–3661. https://doi.org/10.1080/01431160500177315

Torresi, E., Polesel, F., Bester, K., Christensson, M., Smets, B.F., Trapp, S., Andersen, H.R., Plósz, B.G., 2017. Diffusion and sorption of organic micropollutants in biofilms with varying thicknesses. Water Res. 123, 388–400. https://doi.org/10.1016/j.watres.2017.06.027

Tovar-Sánchez, A., G. Basterretxea, V. Rodellas, and others. 2014. Contribution of groundwater discharge to the coastal dissolved nutrients and trace metal concentrations in Majorca Island: Karstic vs detrital systems. Environ. Sci. Technol. **48**: 11819–11827. doi:10.1021/es502958t

Tran, N.H., Urase, T., Ngo, H.H., Hu, J., Ong, S.L., 2013. Insight into metabolic and cometabolic activities of autotrophic and heterotrophic microorganisms in the biodegradation of emerging trace organic contaminants. Bioresour. Technol. 146, 721–731. https://doi.org/10.1016/j.biortech.2013.07.083

Trezzi, G., Garcia-Orellana, J., Rodellas, V., Masqué, P., Garcia-Solsona, E., Andersson, P.S., 2017. Assessing the role of submarine groundwater discharge as a source of Sr to the Mediterranean Sea. Geochim. Cosmochim. Acta 200, 42–54. https://doi.org/10.1016/j.gca.2016.12.005

Trezzi, G., Garcia-Orellana, J., Rodellas, V., Santos-Echeandia, J., Tovar-Sánchez, A., Garcia-Solsona, E., Maqué, P., 2016. Submarine groundwater discharge: a significant source of dissolved trace metals to the North Western Mediterranean Sea. Marine Chemistry. Mar. Chem. 186, 90–100. https://doi.org/10.1016/j.marchem.2016.08.004

Trinh, R.C., Fichot, C.G., Gierach, M.M., Holt, B., Malakar, N.K., Hulley, G., Smith, J., 2017. Application of Landsat 8 for monitoring impacts of wastewater discharge on coastal water quality. Front. Mar. Sci. 4, 329. https://doi.org/10.3389/FMARS.2017.00329/BIBTEX

Troccoli-Ghinaglia, L., Herrera-Silveira, J.A., Comín, F.A., Díaz-Ramos, J.R., 2010. Phytoplankton community variations in tropical coastal area affected where submarine groundwater occurs. Cont. Shelf Res. 30, 2082–2091. https://doi.org/10.1016/J.CSR.2010.10.009

Tulipano, L., Panagopoulus, A., Fidelibus, M.D., 2005. COST ACTION 621"Groundwater management of coastal karstic aquifers",Final Report.

Urquidi-Gaume, M., Santos, I.R., Lechuga-Deveze, C., 2016. Submarine groundwater discharge as a source of dissolved nutrients to an arid coastal embayment (La Paz, Mexico). Environ. Earth Sci. 75, 1–13. https://doi.org/10.1007/s12665-015-4891-8

Valhondo, C., Carrera, J., Ayora, C., Barbieri, M., Nödler, K., Licha, T., Huerta, M., 2014. Behavior of nine selected emerging trace organic contaminants in an artificial recharge system supplemented with a reactive barrier. Environ. Sci. Pollut. Res. 21, 11832–11843. https://doi.org/10.1007/s11356-014-2834-7

Valhondo, C., Carrera, J., Ayora, C., Tubau, I., Martinez-Landa, L., Nödler, K., Licha, T., 2015. Characterizing redox conditions and monitoring attenuation of selected pharmaceuticals during artificial recharge through a reactive layer. Sci. Total Environ. 512–513, 240–250. https://doi.org/10.1016/j.scitotenv.2015.01.030

Valhondo, C., Carrera, J., Martínez-Landa, L., Wang, J., Amalfitano, S., Levantesi, C., Diaz-Cruz, M.S., 2020a. Reactive Barriers for Renaturalization of Reclaimed Water during Soil Aquifer Treatment. Water 2020, Vol. 12, Page 1012 12, 1012. https://doi.org/10.3390/W12041012

Valhondo, C., Martínez-Landa, L., Carrera, J., Díaz-Cruz, S.M., Amalfitano, S., Levantesi, C., 2020b. Six artificial recharge pilot replicates to gain insight into water quality enhancement processes. Chemosphere 240. https://doi.org/10.1016/j.chemosphere.2019.124826

Valiela, I., Foreman, K., LaMontagne, M., Hersh, D., Costa, J., Peckol, P., DeMeo-Andreson, B., D'Avanzo, C., Babione, M., Sham, C.H., Brawley, J., Lajtha, K., 1992. Couplings of watersheds and coastal waters: Sources and consequences of nutrient enrichment in Waquoit Bay, Massachusetts. Estuaries 1992 154 15, 443–457. https://doi.org/10.2307/1352389

Vanhellemont, Q., Ruddick, K., 2014. Turbid wakes associated with offshore wind turbines observed with Landsat 8. Remote Sens. Environ. 145, 105–115. https://doi.org/10.1016/J.RSE.2014.01.009

Varma, S., Turner, J., Underschultz, J., 2010. Estimation of submarine groundwater discharge into Geographe Bay, Bunbury, Western Australia. J. Geochemical Explor. 106, 197–210. https://doi.org/10.1016/j.gexplo.2010.02.003

Wang, J., Meng, X., Feng, C., Xiao, J., Zhao, X., Xiong, B., Feng, J., 2021. Benzophenone-3 induced abnormal development of enteric nervous system in zebrafish through MAPK/ERK signaling pathway. Chemosphere 280. https://doi.org/10.1016/J.CHEMOSPHERE.2021.130670

Wang, L.T., McKenna, T.E., Deliberty, T.L., 2008. Locating Ground-Water Discharge Areas In Rehoboth And Indian River Bays And Indian River, Delaware Using Landsat 7 Imagery. https://doi.org/DOI: 10.13140/RG.2.1.2934.6166

Wei, G.F., Tang, D.L., Wang, S., 2008. Distribution of chlorophyll and harmful algal blooms (HABs): A review on space based studies in the coastal environments of Chinese marginal seas. Adv. Sp. Res. 41, 12–19. https://doi.org/10.1016/j.asr.2007.01.037

Wen-Yao, L., Field, R.T., Gantt, R.G., Klemas, V., 1987. Measurement of the Surface Emissivity. Remote Sens. Environ. 5, 97–109. https://doi.org/10.1016/0034-4257(87)90009-5

Werner, A.D., Bakker, M., Post, V.E.A., Vandenbohede, A., Lu, C., Ataie-Ashtiani, B., Simmons, C.T., Barry, D.A., 2013. Seawater intrusion processes, investigation and management: Recent advances and future challenges. Adv. Water Resour. 51, 3–26. https://doi.org/10.1016/j.advwatres.2012.03.004

Wilson, J., Rocha, C., 2012. Regional scale assessment of Submarine Groundwater Discharge in Ireland combining medium resolution satellite imagery and geochemical tracing techniques. Remote Sens. Environ. 119, 21–34. https://doi.org/10.1016/j.rse.2011.11.018

Wloczyk, C., Richter, R., Borg, E., Nueberts, W., 2006. Sea and lake surface temperature retrieval from Landsat thermal data in Northern Germany. Int. J. Remote Sens. 27 (12), 2489–2502. https://doi.org/10.1080/01431160500300206

Worthington, S.R.H., 1999. A comprehensive strategy for understanding flow in carbonate aquifers. Karst Model. 30–37.

Wulder, M.A., Loveland, T.R., Roy, D.P., Crawford, C.J., Masek, J.G., Woodcock, C.E., Allen, R.G., Anderson, M.C., Belward, A.S., Cohen, W.B., Dwyer, J., Erb, A., Gao, F., Griffiths, P., Helder, D., Hermosilla, T., Hipple, J.D., Hostert, P., Hughes, M.J., Huntington, J., Johnson, D.M., Kennedy, R., Kilic, A., Li, Z., Lymburner, L., McCorkel, J., Pahlevan, N., Scambos,

T.A., Schaaf, C., Schott, J.R., Sheng, Y., Storey, J., Vermote, E., Vogelmann, J., White, J.C., Wynne, R.H., Zhu, Z., 2019. Current status of Landsat program, science, and applications. Remote Sens. Environ. 225, 127–147. https://doi.org/10.1016/j.rse.2019.02.015

Xing, Q., Braga, F., Tosi, L., Lou, M., Zaggia, L., Teatini, P., Gao, X., Yu, L., Wen, X., Shi, P., 2016. Detection of Low Salinity Groundwater Seeping into the Eastern Laizhou Bay (China) with the Aid of Landsat Thermal Data. J. Coast. Res. 74, 149–156. https://doi.org/10.2112/si74-014.1

Yang, W.H., Weber, K.A., Silver, W.L., 2012. Nitrogen loss from soil through anaerobic ammonium oxidation coupled to iron reduction. Nat. Geosci. 5, 538–541. https://doi.org/10.1038/NGEO1530

Zektser, I.S., Everett, L.G., Dzhamalov, R.G., 2006. Submarine Groundwater, CRC Press. https://doi.org/10.1201/9781420005257

.

Supporting information

This section comprises supporting information for Chapters 2, 3 and 4.

Appendix A. Supplementary information of Chapter 2

Appendix B. Supplementary information of Chapter 3

Appendix C. Supplementary information of Chapter 4

Appendix A. Supplementary information of Chapter 2

Table 1, Appendix A: Overview of known SGD sites along the Mediterranean coast.

Country	ID/Name		Flow rate ($m^3 \cdot s^{-1}$)	Depth (m)	Distance (m)	Type	Literature
Spain	1	Maro-Cerro Gordo	0.031	15-20	0 (on the cliff side)	ND	Backalowicz, 2018
	2	Moraig	0.3-9.0	-12	0 (on the cliff side)	2	Fleury et al., 2007
	3	Toix	ND	-8	Seashore	2	Fleury et al., 2007
	4	Agua dulce	ND	Coastal and submarine	ND	ND	Backalowicz, 2018
	5	Almirante Gallinera	ND	ND	ND	ND	Backalowicz, 2018
	6	Alfaro-Mediodia	65 and 84 hm3/y	ND	ND	ND	Backalowicz, 2018
	7	Torre Badum	2	0	<10	ND	Mejías et al., 2012
	8	La Fuentes	0.03-0.17	ND	<10	ND	Mejías et al., 2012
	9	Font de Dins	1.1-0.4	ND	<10	ND	Mejías et al., 2012
	10	La Falconera	0.1	ND	0	ND	Backalowicz, 2018
	11	Alcaufar	ND	ND	ND	ND	Garcia-Solsona et al., 2010
	12	Migjorn-El Pla	1	ND	ND	ND	Basterretxea et al., 2010
	13	Llevant	0.009	ND	ND	ND	Basterretxea et al., 2010
	14	Font des Verger	0.01-1	ND	ND	ND	Basterretxea et al., 2010
	15	Ses Ufanes	20-30	ND	ND	ND	Basterretxea et al., 2010
France	16	Fitou	0.1	ND	ND	2	Bejannin et al., 2017
	17	Laucate	ND	ND	ND	2	Bejannin et al., 2017
	18	Fontdame-Fontestramar	1-15	4	100	2	Fleury et al., 2007
	19	Vise	>0.1	-30	ND	3	Bejannin et al., 2017
	20	Port-Miou	0.5-0.7	-12	ND	2	Fleury et al., 2007
	21	Bestoua	ND	ND	ND	2	Fleury et al., 2007
Italy	22	Mortola	0.2	-36	800	1	Fleury et al., 2007

	23	Bue Marino Cave (Sardinia)	ND	ND	ND	ND	Backalowicz, 2018
	24	Taranto	ND	-19	ND	ND	Fleury et al., 2007
	25	Cefalú	ND	ND	ND	ND	Backalowicz, 2018
	26	Castellamare	ND	ND	ND	ND	Backalowicz, 2018
	27	Donnalucata	0.004-0.012	ND	Onshore and offshore	1	Burnett&Dulaiova 2006
	28	Pozzalo	ND	ND	ND	ND	Backalowicz, 2018
Croatia	29	South Istria	0.024	ND	ND	ND	Backalowicz, 2018
	30	Martinscica	0.4	ND	ND	ND	Backalowicz, 2018
	31	Perilo	ND	ND	ND	ND	Backalowicz, 2018
	32	Novijanska	>0.4	ND	ND	ND	Backalowicz, 2018
	33	Jurjevska	50-0.6	ND	ND	ND	Backalowicz, 2018
	34	Patan	0.5-10	2.7	500	ND	Backalowicz, 2018
	35	Slano	ND	ND	ND	ND	Backalowicz, 2018
	36	Robinzon	2	ND	ND	ND	Backalowicz, 2018
Grece	37	Cephalonia	1-10	0	Seashore	2	Fleury et al., 2007
	38	Kiveri-Anavalos	9-11	0 to -7	0 to few m	3	Fleury et al., 2007
	39	E.argolis	ND	ND	ND	ND	Backalowicz, 2018
	40	Parnon	ND	ND	ND	ND	Backalowicz, 2018
	41	Almiros of Iraklio	2-30	3	1000	2	Fleury et al., 2007
	42	Agios Nikolaos	>2.3	4-7	0.5	2	Fleury et al., 2007
Turkey	43	Gokova-1	0.02-0.10	0	Seashore	1	Bayari&Kurttas., 2015
	44	Gokova-2	ND	0	Seashore	1	Bayari&Kurttas., 2015
	45	Gokova-3	ND	0	Seashore	1	Bayari&Kurttas., 2015
	46	Antalya-1	ND	ND	ND	ND	Backalowicz, 2018
	47	Antalya-2	ND	ND	ND	ND	Backalowicz, 2018
	48	Antalya-3	ND	ND	ND	ND	Backalowicz, 2018

	49	Lefke (Chipre)	ND	ND	ND	ND	Backalowicz, 2018
	50	Ovacik	0.74	-1.5 to -3	2 m	1	Elhatip, 2003
Syria	51	Latakia					Backalowicz, 2018
Lebanon	52	Chekka	60	-10 to -150	100m-1km	2	Fleury et al., 2007
Israel	53	Dor	$4.05*10^{-11}$	ND	ND	ND	Weinstein et al., 2011
Libya	54	Ain Zayanah	1-5	0-1	Seashore	2	Fleury et al., 2007

Table 2, Appendix A: Landsat 8 auxiliary data.

Site	ID	Date	Time	Path	Row	Scene cloud %
1	LC08_L1TP_200035_20181231_20190130_01_T1	31/12/18	10:50	200	35	4.91
	LC08_L1TP_200035_20181215_20181227_01_T1	15/12/18	10:50	200	35	0.23
	LC08_L1TP_200035_20181012_20181030_01_T1	12/10/18	10:50	200	35	0.02
	LC08_L1TP_200035_20180926_20181009_01_T1	26/9/18	10:50	200	35	10.02
	LC08_L1TP_200035_20180825_20180829_01_T1	25/8/18	10:50	200	35	9.44
	LC08_L1TP_200035_20180809_20180815_01_T1	9/8/18	10:50	200	35	0.54
	LC08_L1TP_200035_20180708_20180717_01_T1	8/7/18	10:50	200	35	14.06
	LC08_L1TP_200035_20180622_20180703_01_T1	22/6/18	10:50	200	35	23.21
	LC08_L1TP_200035_20180419_20180501_01_T1	19/4/18	10:50	200	35	14.13
	LC08_L1TP_200035_20180403_20180417_01_T1	3/4/18	10:50	200	35	5.02
	LC08_L1TP_200035_20171212_20171223_01_T1	12/12/17	10:50	200	35	4.01
	LC08_L1TP_200035_20171110_20171121_01_T1	10/11/17	10:50	200	35	14.10
	LC08_L1TP_200035_20171025_20171107_01_T1	25/10/17	10:50	200	35	10.81
	LC08_L1TP_200035_20170923_20171013_01_T1	23/9/17	10:50	200	35	42.87
	LC08_L1TP_200035_20170822_20170911_01_T1	22/8/17	10:50	200	35	3.56
	LC08_L1TP_200035_20170721_20170728_01_T1	21/7/17	10:50	200	35	0.07
	LC08_L1TP_200035_20170518_20170525_01_T1	18/5/17	10:50	200	35	1.92
	LC08_L1TP_200035_20170331_20170414_01_T1	31/3/17	10:50	200	35	11.58
	LC08_L1TP_200035_20170315_20170328_01_T1	15/3/17	10:50	200	35	57.47
2,3,4,5, 6	LC08_L1TP_198033_20181217_20181227_01_T1	17/12/18	10:37	198	33	11,03
	LC08_L1TP_198033_20181201_20181211_01_T1	1/12/18	10:37	198	33	34,05
	LC08_L1TP_198033_20180928_20181009_01_T1	28/10/18	10:37	198	33	6,42

	LC08_L1TP_198033_20180827_20180911_01_T1	27/9/18	10:37	198	33	6,18
	LC08_L1TP_198033_20180726_20180731_01_T1	26/7/18	10:37	198	33	1,52
	LC08_L1TP_198033_20180710_20180717_01_T1	10/7/18	10:37	198	33	1,15
	LC08_L1TP_198033_20180624_20180704_01_T1	24/6/18	10:37	198	33	6,18
	LC08_L1TP_198033_20180405_20180417_01_T1	5/4/18	10:37	198	33	0,2
	LC08_L1TP_198033_20180131_20180207_01_T1	31/1/18	10:37	198	33	5,35
	LC08_L1TP_198033_20171230_20180103_01_T1	30/12/17	10:37	198	33	0,7
	LC08_L1TP_198033_20171112_20171121_01_T1	12/11/17	10:37	198	33	0,14
	LC08_L1TP_198033_20171027_20171107_01_T1	27/10/17	10:37	198	33	0,07
	LC08_L1TP_198033_20171011_20171024_01_T1	11/10/17	10:37	198	33	6,68
	LC08_L1TP_198033_20170925_20171013_01_T1	25/9/17	10:37	198	33	0,31
	LC08_L1TP_198033_20170824_20170913_01_T1	24/8/17	10:37	198	33	3,99
	LC08_L1TP_198033_20170621_20170630_01_T1	21/6/17	10:37	198	33	5,76
	LC08_L1TP_198033_20170520_20170525_01_T1	20/5/17	10:37	198	33	0,28
	LC08_L1TP_198033_20170504_20170515_01_T1	4/5/17	10:37	198	33	8,82
	LC08_L1TP_198033_20170402_20170414_01_T1	2/4/17	10:37	198	33	0,09
	LC08_L1TP_198033_20170301_20170316_01_T1	1/3/17	10:37	198	33	2,78
	LC08_L1TP_198033_20170112_20170311_01_T1	12/1/17	10:37	198	33	1,13
7,8,9	LC08_L1TP_198032_20180928_20181009_01_T1	28/9/18	10:36	198	32	0,42
	LC08_L1TP_198032_20180726_20180731_01_T1	26/7/18	10:36	198	32	0,28
	LC08_L1TP_198032_20180710_20180717_01_T1	10/7/18	10:36	198	32	2,36
	LC08_L1TP_198032_20180624_20180704_01_T1	24/6/18	10:36	198	32	19,94
	LC08_L1TP_198032_20180421_20180502_01_T1	21/4/18	10:36	198	32	16,3
	LC08_L1TP_198032_20180405_20180417_01_T1	5/4/18	10:36	198	32	0,07
	LC08_L1TP_198032_20180131_20180207_01_T1	31/1/18	10:36	198	32	8,41
	LC08_L1TP_198032_20180115_20180120_01_T1	15/1/18	10:36	198	32	10,19
	LC08_L1TP_198032_20171230_20180103_01_T1	30/12/17	10:36	198	32	14,49
	LC08_L1TP_198032_20171128_20171207_01_T1	28/11/17	10:36	198	32	0,81
	LC08_L1TP_198032_20171112_20171121_01_T1	12/11/17	10:36	198	32	0,75
	LC08_L1TP_198032_20171027_20171107_01_T1	27/10/17	10:36	198	32	0,27
	LC08_L1TP_198032_20170925_20171013_01_T1	25/9/17	10:36	198	32	11,41
	LC08_L1TP_198032_20170824_20170913_01_T1	24/8/17	10:36	198	32	3,36
	LC08_L1TP_198032_20170808_20170823_01_T1	8/8/17	10:36	198	32	24,18
	LC08_L1TP_198032_20170621_20170630_01_T1	21/6/17	10:36	198	32	0,27

	LC08_L1TP_198032_20170520_20170525_01_T1	20/5/17	10:36	198	32	3,16
	LC08_L1TP_198032_20170504_20170515_01_T1	4/5/17	10:36	198	32	9,31
	LC08_L1TP_198032_20170418_20170501_01_T1	18/4/17	10:36	198	32	4,92
	LC08_L1TP_198032_20170402_20170414_01_T1	2/4/17	10:36	198	32	7,42
	LC08_L1TP_198032_20170317_20170328_01_T1	17/3/17	10:36	198	32	0,13
	LC08_L1TP_198032_20170301_20170316_01_T1	1/3/17	10:36	198	32	0,03
	LC08_L1TP_198032_20170112_20170311_01_T1	12/1/17	10:36	198	32	4,83
10	LC08_L1TP_197031_20181124_20181210_01_T1	24/11/18	10:30	197	31	8,24
	LC08_L1TP_197031_20181023_20181031_01_T1	23/10/18	10:30	197	31	2,27
	LC08_L1TP_197031_20180921_20180928_01_T1	21/9/18	10:30	197	31	5,19
	LC08_L1TP_197031_20180820_20180829_01_T1	20/8/18	10:30	197	31	0,4
	LC08_L1TP_197031_20180804_20180814_01_T1	4/8/18	10:30	197	31	11,54
	LC08_L1TP_197031_20180719_20180731_01_T1	19/7/18	10:30	197	31	1,32
	LC08_L1TP_197031_20180703_20180717_01_T1	3/7/18	10:30	197	31	10,04
	LC08_L1TP_197031_20180601_20180614_01_T1	1/6/18	10:30	197	31	17,96
	LC08_L1TP_197031_20180430_20180516_01_T1	30/4/18	10:30	197	31	21,24
	LC08_L1TP_197031_20180209_20180222_01_T1	9/2/18	10:30	197	31	2,4
	LC08_L1TP_197031_20180124_20180206_01_T1	24/1/18	10:30	197	31	0,91
	LC08_L1TP_197031_20171223_20180103_01_T1	23/12/17	10:30	197	31	6,88
	LC08_L1TP_197031_20171121_20171206_01_T1	21/11/17	10:30	197	31	0,54
	LC08_L1TP_197031_20170902_20170916_01_T1	2/9/17	10:30	197	31	11,32
	LC08_L1TP_197031_20170817_20170826_01_T1	17/8/17	10:30	197	31	0,22
	LC08_L1TP_197031_20170716_20170727_01_T1	16/7/17	10:30	197	31	4,06
	LC08_L1TP_197031_20170630_20170715_01_T1	30/6/17	10:30	197	31	16,01
	LC08_L1TP_197031_20170614_20170628_01_T1	14/6/17	10:30	197	31	0,66
	LC08_L1TP_197031_20170411_20170415_01_T1	11/4/17	10:30	197	31	1,23
	LC08_L1TP_197031_20170326_20170329_01_T1	26/3/17	10:30	197	31	10,26
	LC08_L1TP_197031_20170310_20170317_01_T1	10/3/17	10:30	197	31	0,36
	LC08_L1TP_197031_20170222_20170301_01_T1	22/2/17	10:30	197	31	0,45
	LC08_L1TP_197031_20170206_20170216_01_T1	6/2/17	10:30	197	31	6,31
	LC08_L1TP_197031_20170105_20170312_01_T1	5/1/17	10:30	197	31	6,15
11	LC08_L1TP_196032_20180930_20181010_01_T1	30/9/18	10:24	196	32	1.85
	LC08_L1TP_196032_20180626_20180704_01_T1	26/6/18	10:24	196	32	10.86
	LC08_L1TP_196032_20180423_20180502_01_T1	23/4/18	10:24	196	32	15.19

	LC08_L1TP_196032_20171029_20171109_01_T1	29/10/17	10:24	196	32	1.12
	LC08_L1TP_196032_20170911_20170927_01_T1	11/9/17	10:24	196	32	0.75
	LC08_L1TP_196032_20170404_20170414_01_T1	4/4/17	10:24	196	32	0.27
	LC08_L1TP_196032_20170319_20170328_01_T1	19/3/17	10:24	196	32	0.17
16,17, 18,19	LC08_L1TP_197030_20181124_20181210_01_T1	24/11/18	10:29	197	30	7,9
	LC08_L1TP_197030_20181023_20181031_01_T1	23/10/18	10:29	197	30	0,03
	LC08_L1TP_197030_20180820_20180829_01_T1	20/8/18	10:29	197	30	0,88
	LC08_L1TP_197030_20180719_20180731_01_T1	19/7/18	10:29	197	30	0,31
	LC08_L1TP_197030_20171121_20171206_01_T1	21/11/17	10:29	197	30	1
	LC08_L1TP_197030_20171004_20171014_01_T1	4/10/17	10:29	197	30	2,83
	LC08_L1TP_197030_20170817_20170826_01_T1	17/8/17	10:29	197	30	0,66
	LC08_L1TP_197030_20170310_20170317_01_T1	10/3/17	10:29	197	30	0,17
20,21, 22	LC08_L1TP_196030_20180914_20180928_01_T1	14/9/18	10:23	196	30	0,73
	LC08_L1TP_195030_20180907_20180912_01_T1	7/9/18	10:17	195	30	3,99
	LC08_L1TP_195030_20180806_20180815_01_T1	6/8/18	10:17	195	30	2,12
	LC08_L1TP_195030_20180721_20180731_01_T1	21/7/18	10:17	195	30	4,06
	LC08_L1TP_195030_20180619_20180703_01_T1	19/6/18	10:17	195	30	2,16
	LC08_L1TP_196030_20180525_20180605_01_T1	25/5/18	10:23	196	30	3,52
	LC08_L1TP_195030_20180211_20180222_01_T1	11/2/18	10:17	195	30	3,96
	LC08_L1TP_196030_20171114_20171122_01_T1	14/11/17	10:23	196	30	1,19
	LC08_L1TP_195030_20171022_20171107_01_T1	22/10/17	10:17	195	30	1,05
	LC08_L1TP_196030_20170927_20171013_01_T1	27/9/17	10:23	196	30	0,78
	LC08_L1TP_195030_20170920_20170930_01_T1	20/9/17	10:17	195	30	0,04
	LC08_L1TP_195030_20170904_20170916_01_T1	4/9/17	10:17	195	30	4,12
	LC08_L1TP_195030_20170718_20170727_01_T1	18/7/17	10:17	195	30	3,18
	LC08_L1TP_195030_20170702_20170715_01_T1	2/7/17	10:17	195	30	0,39
	LC08_L1TP_196030_20170607_20170616_01_T1	7/6/17	10:23	196	30	0,34
	LC08_L1TP_195030_20170429_20170515_01_T1	29/4/17	10:17	195	30	2,45
	LC08_L1TP_196030_20170420_20170501_01_T1	20/4/17	10:23	196	30	0,08
	LC08_L1TP_195030_20170413_20170501_01_T1	13/4/17	10:17	195	30	1,81
	LC08_L1TP_196030_20170404_20170414_01_T1	4/4/17	10:23	196	30	0,41
	LC08_L1TP_195030_20170328_20170414_01_T1	28/3/17	10:17	195	30	0,76
23	LC08_L1TP_192032_20181223_20190129_01_T1	23/12/18	9:59	192	32	6.47
	LC08_L1TP_192032_20181121_20181129_01_T2	21/11/18	9:59	192	32	29.83

	LC08_L1TP_192032_20180817_20180829_01_T1	17/8/18	9:59	192	32	2.46
	LC08_L1TP_192032_20180630_20180716_01_T1	30/6/18	9:59	192	32	0.7
	LC08_L1TP_192032_20180105_20180118_01_T1	5/1/18	9:59	192	32	14.46
	LC08_L1TP_192032_20171017_20171024_01_T1	17/10/17	9:59	192	32	0.79
	LC08_L1TP_192032_20170830_20170914_01_T1	30/8/17	9:59	192	32	0.01
	LC08_L1TP_192032_20170729_20170811_01_T1	29/7/17	9:59	192	32	0.40
	LC08_L1TP_192032_20170627_20170714_01_T1	27/6/17	9:59	192	32	0.03
	LC08_L1TP_192032_20170408_20180523_01_T1	8/4/17	9:59	192	32	0
	LC08_L1TP_192032_20170219_20180527_01_T1	19/2/17	9:59	192	32	6.49
24	LC08_L1TP_188032_20181227_20190129_01_T1	27/12/18	9.34	188	32	0.59
	LC08_L1TP_188032_20181109_20181116_01_T1	9/11/18	9.34	188	32	1.02
	LC08_L1TP_188032_20180906_20180912_01_T1	6/9/18	9.34	188	32	0
	LC08_L1TP_188032_20180805_20180814_01_T1	5/8/18	9.34	188	32	8.21
	LC08_L1TP_188032_20180125_20180206_01_T1	25/1/18	9.34	188	32	1.10
	LC08_L1TP_188032_20171224_20180103_01_T1	24/12/17	9.34	188	32	0.86
	LC08_L1TP_188032_20170818_20170826_01_T1	8/8/17	9.34	188	32	0.17
	LC08_L1TP_188032_20170412_20180527_01_T1	12/4/17	9.34	188	32	5.32
	LC08_L1TP_188032_20170223_20170301_01_T1	23/2/17	9.34	188	32	29.05
25,26, 27,28	LC08_L1TP_189034_20180929_20181009_01_T1	29/9/18	9:41	189	34	1.50
	LC08_L1TP_189034_20180812_20180815_01_T1	12/8/18	9:41	189	34	6.32
	LC08_L1TP_189034_20180727_20180731_01_T1	27/7/18	9:41	189	34	4.69
	LC08_L1TP_189034_20180609_20180615_01_T1	9/6/18	9:41	189	34	5.33
	LC08_L1TP_189034_20180524_20180605_01_T1	24/5/18	9:41	189	34	3.62
	LC08_L1TP_189034_20180406_20180417_01_T1	6/4/18	9:41	189	34	0.54
	LC08_L1TP_189034_20171215_20171224_01_T1	15/12/17	9:41	189	34	2.97
	LC08_L1TP_189034_20171012_20171024_01_T1	12/10/17	9:41	189	34	5.61
	LC08_L1TP_189034_20170825_20180527_01_T1	25/8/17	9:41	189	34	0
	LC08_L1TP_189034_20170622_20170630_01_T1	22/6/17	9:41	189	34	3.21
	LC08_L1TP_189034_20170318_20170328_01_T1	18/3/17	9:41	189	34	0
12,13, 14,15	LC08_L1TP_197032_20181023_20181031_01_T1	23/10/18	10:30	197	32	2,22
	LC08_L1TP_196033_20180930_20181010_01_T1	30/9/18	10:24	196	33	1,46
	LC08_L1TP_197032_20180921_20180928_01_T1	21/9/18	10:30	197	32	1,16
	LC08_L1TP_196033_20180829_20180911_01_T1	29/8/18	10:24	196	33	5,45
	LC08_L1TP_197032_20180820_20180829_01_T1	20/8/18	10:30	197	32	0,33

	LC08_L1TP_197032_20180804_20180814_01_T1	4/8/18	10:30	197	32	9,79
	LC08_L1TP_196033_20180728_20180731_01_T1	28/7/18	10:24	196	33	7,18
	LC08_L1TP_197032_20180719_20180731_01_T1	19/7/18	10:30	197	32	0,91
	LC08_L1TP_196033_20180712_20180717_01_T1	12/7/18	10:24	196	33	1,99
	LC08_L1TP_197032_20180703_20180717_01_T1	3/7/18	10:30	197	32	5,07
	LC08_L1TP_197032_20180617_20180703_01_T1	17/6/18	10:30	197	32	15,65
	LC08_L1TP_197032_20180601_20180614_01_T1	1/6/18	10:30	197	32	4,68
	LC08_L1TP_197032_20180516_20180604_01_T1	16/5/18	10:30	197	32	15,06
	LC08_L1TP_197032_20180124_20180206_01_T1	24/1/18	10:30	197	32	1,48
	LC08_L1TP_196033_20180117_20180205_01_T1	17/1/18	10:24	196	33	0,82
	LC08_L1TP_196033_20180101_20180104_01_T1	1/1/18	10:24	196	33	4,8
	LC08_L1TP_197032_20171121_20171206_01_T1	21/11/17	10:24	196	33	3,73
	LC08_L1TP_196033_20171029_20171109_01_T1	29/10/17	10:30	197	32	11,37
	LC08_L1TP_197032_20171020_20171106_01_T1	20/10/17	10:24	196	33	17,55
	LC08_L1TP_196033_20171013_20171024_01_T1	13/10/17	10:30	197	32	3,32
	LC08_L1TP_197032_20171004_20171014_01_T1	4/10/17	10:24	196	33	9,81
	LC08_L1TP_196033_20170927_20171013_01_T1	27/9/17	10:30	197	32	2,71
	LC08_L1TP_196033_20170911_20170927_01_T1	11/9/17	10:30	197	32	0,88
	LC08_L1TP_197032_20170817_20170826_01_T1	17/8/17	10:24	196	33	0,05
	LC08_L1TP_197032_20170716_20170727_01_T1	16/7/17	10:24	196	33	9,07
29,30, 31,32, 33	LC08_L1TP_190029_20181022_20181031_01_T1	22/10/18	9:46	190	29	26,52
	LC08_L1TP_190029_20180819_20180829_01_T1	19/8/18	9:46	190	29	2,98
	LC08_L1TP_190029_20180718_20180731_01_T1	18/7/18	9:46	190	29	7,78
	LC08_L1TP_190029_20180531_20180614_01_T1	31/5/18	9:46	190	29	13,72
	LC08_L1TP_190029_20180429_20180502_01_T1	29/4/18	9:46	190	29	3,21
	LC08_L1TP_190029_20180328_20180405_01_T1	28/3/18	9:46	190	29	11,75
	LC08_L1TP_190029_20180123_20180206_01_T1	23/1/18	9:46	190	29	9,98
	LC08_L1TP_190029_20171222_20180103_01_T1	22/12/17	9:46	190	29	3,06
	LC08_L1TP_190029_20171120_20171206_01_T1	20/11/17	9:46	190	29	4,23
	LC08_L1TP_190029_20171104_20171109_01_T1	4/11/17	9:46	190	29	22,97
	LC08_L1TP_190029_20171019_20171025_01_T1	19/10/17	9:46	190	29	7,73
	LC08_L1TP_190029_20170816_20170825_01_T1	16/8/17	9:46	190	29	1,8
	LC08_L1TP_190029_20170731_20170811_01_T1	31/7/17	9:46	190	29	0,44
	LC08_L1TP_190029_20170613_20170628_01_T1	13/6/17	9:46	190	29	2,71

	LC08_L1TP_190029_20170528_20170615_01_T1	28/5/17	9:46	190	29	4,29
	LC08_L1TP_190029_20170410_20170414_01_T1	10/4/17	9:46	190	29	0,19
	LC08_L1TP_190029_20170325_20180523_01_T1	25/3/17	9:46	190	29	7,35
	LC08_L1TP_190029_20170309_20170317_01_T1	9/3/17	9:46	190	29	2,3
	LC08_L1TP_190029_20170120_20170311_01_T1	20/1/17	9:46	190	29	31,89
35,36	LC08_L1TP_187030_20180830_20180911_01_T1	30/8/18	9:27	187	30	4,33
	LC08_L1TP_187031_20180830_20180911_01_T1	30/8/18	9:28	187	31	1,69
	LC08_L1TP_187030_20180713_20180717_01_T1	13/7/18	9:27	187	30	25,21
	LC08_L1TP_187030_20180526_20180605_01_T1	26/5/18	9:27	187	30	15,92
	LC08_L1TP_187031_20180526_20180605_01_T1	26/5/18	9:28	187	31	0,28
	LC08_L1TP_187030_20180424_20180502_01_T1	24/4/18	9:27	187	30	18,56
	LC08_L1TP_187031_20180424_20180502_01_T1	24/4/18	9:28	187	31	3,07
	LC08_L1TP_187030_20180408_20180417_01_T1	8/4/18	9:27	187	30	4,37
	LC08_L1TP_187031_20180408_20180417_01_T1	8/4/18	9:28	187	31	0,27
	LC08_L1TP_187030_20180118_20180206_01_T1	18/1/18	9:27	187	30	10,37
	LC08_L1TP_187031_20180118_20180206_01_T1	18/1/18	9:28	187	31	1,43
	LC08_L1TP_187030_20170827_20170914_01_T1	27/8/17	9:27	187	30	3,6
	LC08_L1TP_187031_20170827_20170914_01_T1	27/8/17	9:28	187	31	6,85
	LC08_L1TP_187030_20170811_20170824_01_T1	11/8/17	9:27	187	30	0,16
	LC08_L1TP_187031_20170811_20170824_01_T1	11/8/17	9:28	187	31	2,63
	LC08_L1TP_187030_20170710_20170725_01_T1	10/7/17	9:27	187	30	0,17
	LC08_L1TP_187031_20170710_20170725_01_T1	10/7/17	9:28	187	31	0,36
	LC08_L1TP_187030_20170608_20170616_01_T1	8/6/17	9:27	187	30	36,01
	LC08_L1TP_187031_20170608_20170616_01_T1	8/6/17	9:28	187	31	0,52
	LC08_L1TP_187030_20170523_20170526_01_T1	23/5/17	9:27	187	30	30,46
	LC08_L1TP_187031_20170523_20170526_01_T1	23/5/17	9:28	187	31	7,41
	LC08_L1TP_187030_20170304_20170316_01_T1	4/3/17	9:27	187	30	8,83
	LC08_L1TP_187031_20170304_20170316_01_T1	4/3/17	9:28	187	31	0,75
	LC08_L1TP_187030_20170216_20170228_01_T1	16/2/17	9:27	187	30	0,98
	LC08_L1TP_187031_20170216_20170228_01_T1	16/2/17	9:28	187	31	2,02
34	LC08_L1TP_188030_20181227_20190129_01_T1	27/12/18	9:34	188	30	11,5
	LC08_L1TP_188030_20181109_20181116_01_T1	9/11/18	9:34	188	30	4,66
	LC08_L1TP_188030_20181008_20181029_01_T1	8/10/18	9:34	188	30	4,66
	LC08_L1TP_188030_20180922_20180928_01_T1	22/9/18	9:34	188	30	7

	LC08_L1TP_188030_20180906_20180912_01_T1	6/9/18	9:34	188	30	6,9
	LC08_L1TP_188030_20180821_20180829_01_T1	21/8/18	9:34	188	30	2,81
	LC08_L1TP_188030_20180720_20180731_01_T1	20/7/18	9:34	188	30	0,57
	LC08_L1TP_188030_20180704_20180717_01_T1	4/7/18	9:34	188	30	20,2
	LC08_L1TP_188030_20180602_20180615_01_T1	2/6/18	9:34	188	30	1,84
	LC08_L1TP_188030_20180125_20180206_01_T1	25/1/18	9:34	188	30	2,3
	LC08_L1TP_188030_20171224_20180103_01_T1	24/12/17	9:34	188	30	5,63
	LC08_L1TP_188030_20171021_20171106_01_T1	21/10/17	9:34	188	30	5,95
	LC08_L1TP_188030_20171005_20171014_01_T1	5/10/17	9:34	188	30	18,17
	LC08_L1TP_188030_20170818_20170826_01_T1	18/8/17	9:34	188	30	0,45
	LC08_L1TP_188030_20170802_20170812_01_T1	2/8/17	9:34	188	30	0,03
	LC08_L1TP_188030_20170717_20170727_01_T1	17/7/17	9:34	188	30	8,62
	LC08_L1TP_188030_20170530_20180527_01_T1	30/5/17	9:34	188	30	1,94
	LC08_L1TP_188030_20170514_20180527_01_T1	14/5/17	9:34	188	30	9,81
	LC08_L1TP_188030_20170412_20180527_01_T1	12/4/17	9:34	188	30	0,71
	LC08_L1TP_188030_20170327_20170414_01_T1	27/3/17	9:34	188	30	17,8
	LC08_L1TP_188030_20170311_20170317_01_T1	11/3/17	9:34	188	30	30,07
	LC08_L1TP_188030_20170122_20170311_01_T1	22/1/17	9:34	188	30	6,15
37	LC08_L1TP_185033_20180917_20180928_01_T1	17/9/18	9:16	185	33	1,29
	LC08_L1TP_185033_20180901_20180912_01_T1	1/9/18	9:16	185	33	1,56
	LC08_L1TP_185033_20180731_20180814_01_T1	31/7/18	9:16	185	33	4,6
	LC08_L1TP_185033_20180715_20180730_01_T1	15/7/18	9:16	185	33	0,65
	LC08_L1TP_185033_20180613_20180615_01_T1	13/6/18	9:16	185	33	3,6
	LC08_L1TP_185033_20180528_20180605_01_T1	28/5/18	9:16	185	33	13,16
	LC08_L1TP_185033_20180512_20180517_01_T1	12/5/18	9:16	185	33	5,64
	LC08_L1TP_185033_20180426_20180502_01_T1	26/4/18	9:16	185	33	14,84
	LC08_L1TP_185033_20180205_20180220_01_T1	5/2/18	9:16	185	33	1,16
	LC08_L1TP_185033_20171016_20171024_01_T1	16/10/17	9:16	185	33	0,05
	LC08_L1TP_185033_20170914_20170928_01_T1	14/9/17	9:16	185	33	0,06
	LC08_L1TP_185033_20170728_20170810_01_T1	28/7/17	9:16	185	33	3,29
	LC08_L1TP_185033_20170712_20170726_01_T1	12/7/17	9:16	185	33	1,14
	LC08_L1TP_185033_20170626_20180527_01_T1	26/6/17	9:16	185	33	1,54
	LC08_L1TP_185033_20170610_20180527_01_T1	10/6/17	9:16	185	33	7,04
	LC08_L1TP_185033_20170423_20170502_01_T1	23/4/17	9:16	185	33	4,12

	LC08_L1TP_185033_20170101_20170312_01_T1	1/1/17	9:16	185	33	1,94
38,39, 40	LC08_L1TP_183034_20181224_20190129_01_T1	24/12/18	9:04	183	34	1,82
	LC08_L1TP_183034_20181208_20181211_01_T1	8/12/18	9:04	183	34	1,52
	LC08_L1TP_183034_20181106_20181115_01_T1	6/11/18	9:04	183	34	6,35
	LC08_L1TP_183034_20180919_20180928_01_T1	19/9/18	9:04	183	34	2
	LC08_L1TP_183034_20180919_20180928_01_T1	3/9/18	9:04	183	34	0,02
	LC08_L1TP_183034_20180818_20180829_01_T1	18/8/18	9:04	183	34	1,9
	LC08_L1TP_183034_20180802_20180814_01_T1	2/8/18	9:0	183	34	10,41
	LC08_L1TP_183034_20180717_20180730_01_T1	17/7/18	9:04	183	34	0,16
	LC08_L1TP_183034_20180530_20180614_01_T1	30/5/18	9:04	183	34	6,55
	LC08_L1TP_183034_20180514_20180517_01_T1	14/5/18	9:04	183	34	1,27
	LC08_L1TP_183034_20180428_20180502_01_T1	28/4/18	9:04	183	34	0,09
	LC08_L1TP_183034_20180106_20180119_01_T1	6/1/18	9:04	183	34	1,63
	LC08_L1TP_183034_20171205_20171222_01_T1	5/12/17	9:04	183	34	5,74
	LC08_L1TP_183034_20170916_20170929_01_T1	16/9/17	9:04	183	34	0,02
	LC08_L1TP_183034_20170831_20170915_01_T1	31/8/17	9:04	183	34	2,68
	LC08_L1TP_183034_20170815_20170825_01_T1	15/8/17	9:04	183	34	5,23
	LC08_L1TP_183034_20170730_20170811_01_T1	30/7/17	9:04	183	34	0,04
	LC08_L1TP_183034_20170714_20170726_01_T1	14/7/17	9:04	183	34	1,9
	LC08_L1TP_183034_20170628_20170714_01_T1	28/6/17	9:04	183	34	2,94
	LC08_L1TP_183034_20170511_20170516_01_T1	11/5/17	9:04	183	34	1,24
	LC08_L1TP_183034_20170425_20170502_01_T1	25/4/17	9:04	183	34	2,5
	LC08_L1TP_183034_20170324_20180527_01_T1	24/3/17	9:04	183	34	0,21
	LC08_L1TP_183034_20170103_20170312_01_T1	3/1/17	9:04	183	34	1,83
41,42	LC08_L1TP_181036_20181124_20181210_01_T1	8/11/18	8:53	181	36	17,46
	LC08_L1TP_181036_20181007_20181029_01_T1	7/10/18	8:53	181	36	5,15
	LC08_L1TP_181036_20180921_20180928_01_T1	21/9/18	8:53	181	36	3,12
	LC08_L1TP_181036_20180905_20180912_01_T1	5/9/18	8:53	181	36	0,03
	LC08_L1TP_181036_20180820_20180829_01_T1	20/8/18	8:53	181	36	1,24
	LC08_L1TP_181036_20180719_20180731_01_T1	19/7/18	8:53	181	36	0,15
	LC08_L1TP_181036_20180703_20180717_01_T1	3/7/18	8:53	181	36	0,7
	LC08_L1TP_181036_20180601_20180614_01_T1	1/6/18	8:53	181	36	0,05
	LC08_L1TP_181036_20180516_20180604_01_T1	16/5/18	8:53	181	36	5,94
	LC08_L1TP_181036_20180430_20180502_01_T1	30/4/18	8:53	181	36	6,22

	LC08_L1TP_181036_20180414_20180501_01_T1	14/4/18	8:53	181	36	15,35
	LC08_L1TP_181036_20180225_20180308_01_T	25/2/18	8:53	181	36	42,38
	LC08_L1TP_181036_20180108_20180119_01_T1	8/1/18	8:53	181	36	2,55
	LC08_L1TP_181036_20171020_20171106_01_T1	20/10/17	8:53	181	36	5,75
	LC08_L1TP_181036_20171004_20171014_01_T1	4/10/17	8:53	181	36	1,28
	LC08_L1TP_181036_20170918_20180527_01_T1	18/9/17	8:53	181	36	0
	LC08_L1TP_181036_20170902_20170916_01_T1	2/9/17	8:53	181	36	0
	LC08_L1TP_181036_20170801_20170811_01_T1	1/8/17	8:53	181	36	0,78
	LC08_L1TP_181036_20170716_20170727_01_T1	16/7/17	8:53	181	36	2,43
43,44, 45	LC08_L1TP_180034_20181101_20181115_01_T1	1/11/18	8:46	180	34	0.07
	LC08_L1TP_180034_20181016_20181030_01_T1	16/10/18	8:46	180	34	0
	LC08_L1TP_180034_20180914_20180928_01_T1	14/9/18	8:46	180	34	5.57
	LC08_L1TP_180034_20180813_20180828_01_T1	13/8/18	8:46	180	34	3.31
	LC08_L1TP_180034_20180728_20180731_01_T1	28/7/18	8:46	180	34	2.09
	LC08_L1TP_180034_20180712_20180717_01_T1	12/7/18	8:46	180	34	0.31
	LC08_L1TP_180034_20180610_20180615_01_T1	10/6/18	8:46	180	34	1.52
	LC08_L1TP_180034_20180509_20180517_01_T1	9/5/18	8:46	180	34	11.93
	LC08_L1TP_180034_20180423_20180502_01_T1	23/4/18	8:46	180	34	5
	LC08_L1TP_180034_20180218_20180307_01_T1	18/2/18	8:46	180	34	0.65
	LC08_L1TP_180034_20180101_20180104_01_T1	1/1/18	8:46	180	34	1.19
	LC08_L1TP_180034_20171013_20171024_01_T1	13/10/17	8:46	180	34	0.04
	LC08_L1TP_180034_20170927_20171013_01_T1	27/9/17	8:46	180	34	2.01
	LC08_L1TP_180034_20170826_20170913_01_T1	26/8/17	8:46	180	34	0.02
	LC08_L1TP_180034_20170709_20170717_01_T1	9/7/17	8:46	180	34	0.05
	LC08_L1TP_180034_20170506_20170515_01_T1	6/5/17	8:46	180	34	10.42
	LC08_L1TP_180034_20170303_20170316_01_T1	3/3/17	8:46	180	34	9.52
	LC08_L1TP_180034_20170215_20170228_01_T1	15/2/17	8:46	180	34	25.38
46,47, 48	LC08_L1TP_178034_20181221_20181227_01_T1	21/12/18	8:33	178	34	17.22
	LC08_L1TP_178034_20181103_20181115_01_T1	3/11/18	8:33	178	34	0.07
	LC08_L1TP_178034_20180916_20180928_01_T1	16/9/18	8:33	178	34	0.07
	LC08_L1TP_178034_20180815_20180828_01_T1	15/8/18	8:33	178	34	0.04
	LC08_L1TP_178034_20180119_20180206_01_T1	19/1/18	8:33	178	34	8.56
	LC08_L1TP_178034_20171031_20171109_01_T1	31/10/17	8:33	178	34	4.76
	LC08_L1TP_178034_20170929_20171013_01_T1	29/9/17	8:33	178	34	15.51

	LC08_L1TP_178034_20170828_20170914_01_T1	28/8/17	8:33	178	34	0.15
	LC08_L1TP_178034_20170321_20170328_01_T1	21/3/17	8:33	178	34	21.56
	LC08_L1TP_178034_20170217_20170228_01_T1	17/2/17	8:33	178	34	1.69
49	LC08_L1TP_176036_20181105_20181115_01_T1	5/11/18	8:22	176	36	27.70
	LC08_L1TP_176036_20181004_20181010_01_T1	4/10/18	8:22	176	36	3.48
	LC08_L1TP_176036_20180918_20180928_01_T1	18/9/18	8:22	176	36	0.17
	LC08_L1TP_176036_20180326_20180404_01_T1	26/3/18	8:22	176	36	1.03
	LC08_L1TP_176036_20180206_20180221_01_T1	6/2/18	8:22	176	36	3.11
	LC08_L1TP_176036_20171017_20171024_01_T1	17/10/17	8:22	176	36	0.60
	LC08_L1TP_176036_20170915_20180526_01_T1	15/9/17	8:22	176	36	5.60
	LC08_L1TP_176036_20170830_20170914_01_T1	30/8/17	8:22	176	36	1.20
	LC08_L1TP_176036_20170729_20170811_01_T1	29/7/17	8:22	176	36	2.78
	LC08_L1TP_176036_20170510_20170516_01_T1	10/5/17	8:22	176	36	0.02
	LC08_L1TP_176036_20170424_20170502_01_T1	24/4/17	8:22	176	36	0.18
	LC08_L1TP_176036_20170307_20170317_01_T1	7/3/16	8:22	176	36	0.49
	LC08_L1TP_176036_20170118_20170311_01_T1	18/1/17	8:22	176	36	0.75
50	LC08_L1TP_176035_20181004_20181010_01_T1	4/10/18	8:21	176	35	0.18
	LC08_L1TP_176035_20180918_20180928_01_T1	18/9/18	8:21	176	35	1.71
	LC08_L1TP_176035_20180817_20180829_01_T1	17/8/18	8:21	176	35	5.32
	LC08_L1TP_176035_20180716_20180730_01_T1	16/7/18	8:21	176	35	2.62
	LC08_L1TP_176035_20180630_20180716_01_T1	30/6/18	8:21	176	35	6.85
	LC08_L1TP_176035_20180326_20180404_01_T1	26/3/18	8:21	176	35	2.19
	LC08_L1TP_176035_20180206_20180221_01_T1	6/2/18	8:21	176	35	1.04
	LC08_L1TP_176035_20171017_20171024_01_T1	17/10/17	8:21	176	35	0.25
	LC08_L1TP_176035_20170729_20170811_01_T1	29/7/17	8:21	176	35	0.77
	LC08_L1TP_176035_20170526_20170616_01_T1	26/5/17	8:21	176	35	3.31
	LC08_L1TP_176035_20170424_20170502_01_T1	24/4/17	8:21	176	35	0.78
	LC08_L1TP_176035_20170323_20170329_01_T1	23/3/17	8:21	176	35	4.96
	LC08_L1TP_176035_20170118_20170311_01_T1	18/1/17	8:21	176	35	0.87
51,52	LC08_L1TP_174036_20181107_20181116_01_T1	7/11/18	8:09	174	36	17.03
	LC08_L1TP_174036_20180702_20180716_01_T1	7/11/18	8:09	174	36	2.37
	LC08_L1TP_174036_20180515_20180604_01_T1	7/11/18	8:09	174	36	2.53
	LC08_L1TP_174036_20180413_20180417_01_T1	7/11/18	8:09	174	36	1.49
	LC08_L1TP_174036_20180224_20180308_01_T1	7/11/18	8:09	174	36	12.59

	LC08_L1TP_174036_20180107_20180119_01_T1	7/11/18	8:09	174	36	1.57
	LC08_L1TP_174036_20171019_20171025_01_T1	7/11/18	8:09	174	36	0.02
	LC08_L1TP_174036_20171003_20171014_01_T1	7/11/18	8:09	174	36	1.94
	LC08_L1TP_174036_20170901_20170915_01_T1	7/11/18	8:09	174	36	5.97
	LC08_L1TP_174036_20170731_20170811_01_T1	7/11/18	8:09	174	36	1.46
	LC08_L1TP_174036_20170528_20170615_01_T1	7/11/18	8:09	174	36	1.25
	LC08_L1TP_174036_20170512_20170525_01_T1	7/11/18	8:09	174	36	1.07
	LC08_L1TP_174036_20170325_20170329_01_T1	7/11/18	8:09	174	36	1.50
	LC08_L1TP_174036_20170221_20170301_01_T1	7/11/18	8:09	174	36	1.85
53	LC08_L1TP_174037_20181225_20190129_01_T1	25/12/18	8:10	174	37	29.85
	LC08_L1TP_174037_20181107_20181116_01_T1	7/11/18	8:10	174	37	16.73
	LC08_L1TP_174037_20180920_20180928_01_T1	20/9/18	8:10	174	37	1.10
	LC08_L1TP_174037_20180904_20180912_01_T1	4/9/18	8:10	174	37	0.88
	LC08_L1TP_174037_20180702_20180716_01_T1	2/7/18	8:10	174	37	0.91
	LC08_L1TP_174037_20180616_20180703_01_T1	16/6/18	8:10	174	37	0.02
	LC08_L1TP_174037_20180413_20180417_01_T1	13/4/18	8:10	174	37	0.23
	LC08_L1TP_174037_20180224_20180308_01_T1	24/2/18	8:10	174	37	7.47
	LC08_L1TP_174037_20180107_20180119_01_T1	7/1/18	8:10	174	37	2.47
	LC08_L1TP_174037_20171019_20171025_01_T1	19/10/17	8:10	174	37	0.06
	LC08_L1TP_174037_20170731_20170811_01_T1	31/7/17	8:10	174	37	0.84
	LC08_L1TP_174037_20170715_20170727_01_T1	15/7/17	8:10	174	37	0.29
	LC08_L1TP_174037_20170528_20170615_01_T1	28/5/17	8:10	174	37	0.51
	LC08_L1TP_174037_20170512_20170525_01_T1	12/5/17	8:10	174	37	0.25
	LC08_L1TP_174037_20170325_20170329_01_T1	25/3/17	8:10	174	37	2.85
	LC08_L1TP_174037_20170221_20170301_01_T1	21/2/17	8:10	174	37	1.31
	LC08_L1TP_174037_20170205_20170216_01_T1	5/2/17	8:10	174	37	1.80
	LC08_L1TP_174037_20170120_20170311_01_T1	20/1/17	8:10	174	37	13.20
54	LC08_L1TP_184038_20181012_20181030_01_T1	12/10/18	9:12	184	38	17,32
	LC08_L1TP_184038_20180910_20180913_01_T1	10/9/18	9:12	184	38	7,37
	LC08_L1TP_184038_20180809_20180815_01_T1	9/8/18	9:12	184	38	0
	LC08_L1TP_184038_20180708_20180717_01_T1	8/7/18	9:12	184	38	0,17
	LC08_L1TP_184038_20180622_20180703_01_T1	11/6/18	9:12	184	38	12,24
	LC08_L1TP_184038_20180606_20180615_01_T1	6/6/18	9:12	184	38	0,01
	LC08_L1TP_184038_20180505_20180517_01_T1	5/5/18	9:12	184	38	8,93

	LC08_L1TP_184038_20180419_20180501_01_T1	19/4/18	9:12	184	38	18,29
	LC08_L1TP_184038_20180403_20180417_01_T1	3/4/18	9:12	184	38	0,12
	LC08_L1TP_184038_20180318_20180403_01_T1	18/3/18	9:12	184	38	5,08
	LC08_L1TP_184038_20180214_20180222_01_T1	14/2/18	9:12	184	38	5,47
	LC08_L1TP_184038_20171212_20171223_01_T1	12/12/17	9:12	184	38	9,72
	LC08_L1TP_184038_20171126_20171206_01_T1	26/11/17	9:12	184	38	0,36
	LC08_L1TP_184038_20171110_20171121_01_T1	10/11/17	9:12	184	38	1,55
	LC08_L1TP_184038_20170923_20171013_01_T1	23/9/17	9:12	184	38	0,35
	LC08_L1TP_184038_20170907_20170926_01_T1	7/9/17	9:12	184	38	0,41
	LC08_L1TP_184038_20170822_20170911_01_T1	22/8/17	9:12	184	38	9,4
	LC08_L1TP_184038_20170806_20170813_01_T1	6/8/17	9:12	184	38	0,19
	LC08_L1TP_184038_20170721_20170728_01_T1	21/7/17	9:12	184	38	1,74
	LC08_L1TP_184038_20170705_20170716_01_T1	5/7/17	9:12	184	38	8,46
	LC08_L1TP_184038_20170619_20170629_01_T1	19/6/17	9:12	184	38	16,92
	LC08_L1TP_184038_20170518_20170525_01_T1	18/5/17	9:12	184	38	13,58
	LC08_L1TP_184038_20170416_20170501_01_T1	16/4/17	9:12	184	38	0,01
	LC08_L1TP_184038_20170315_20170328_01_T1	15/3/17	9:12	184	38	0,85

Figure 1, Appendix A: Percentage of successful and unsuccessful SGD identifications for all SGD springs that were identified at least once throughout 2017 and 2018.

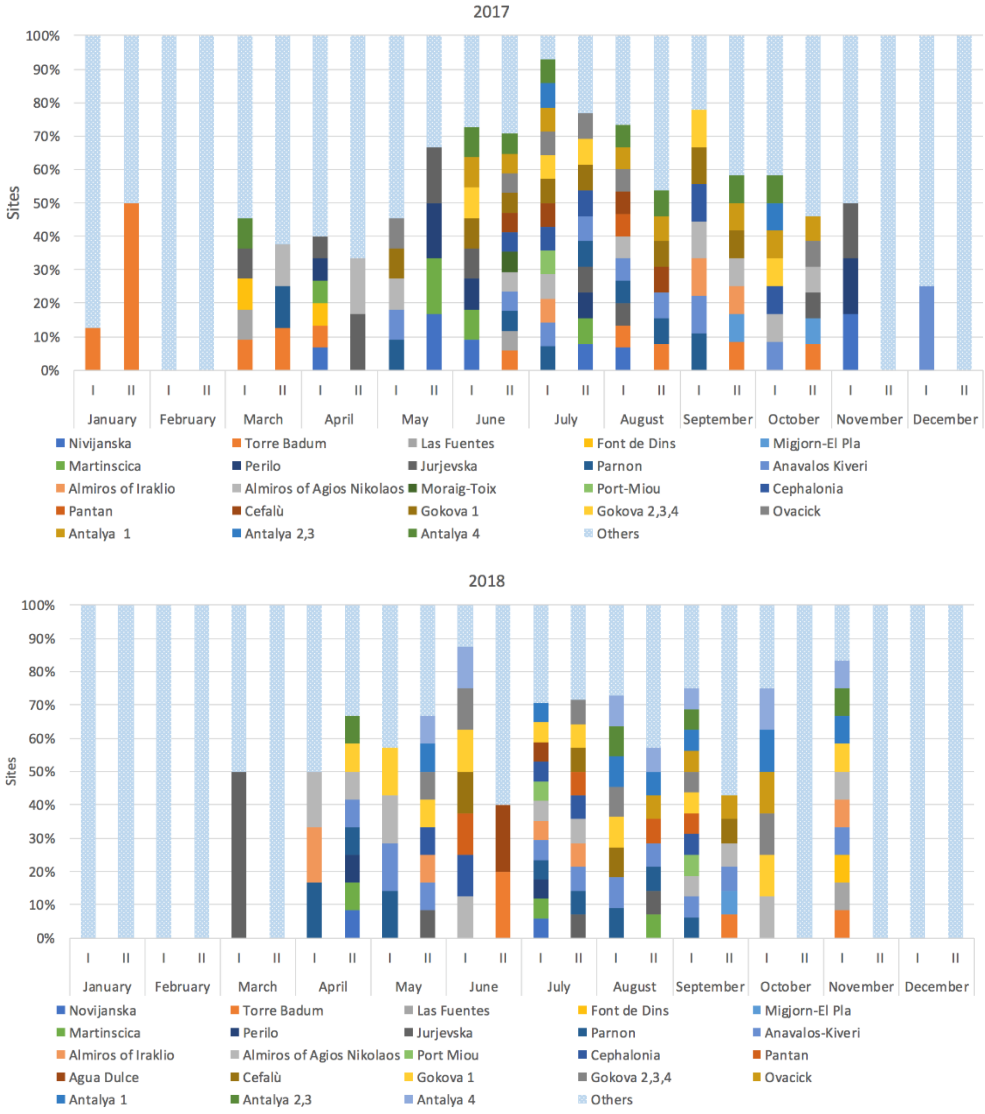

Figure 2, Appendix A: Percentage of SGD springs visualizations.

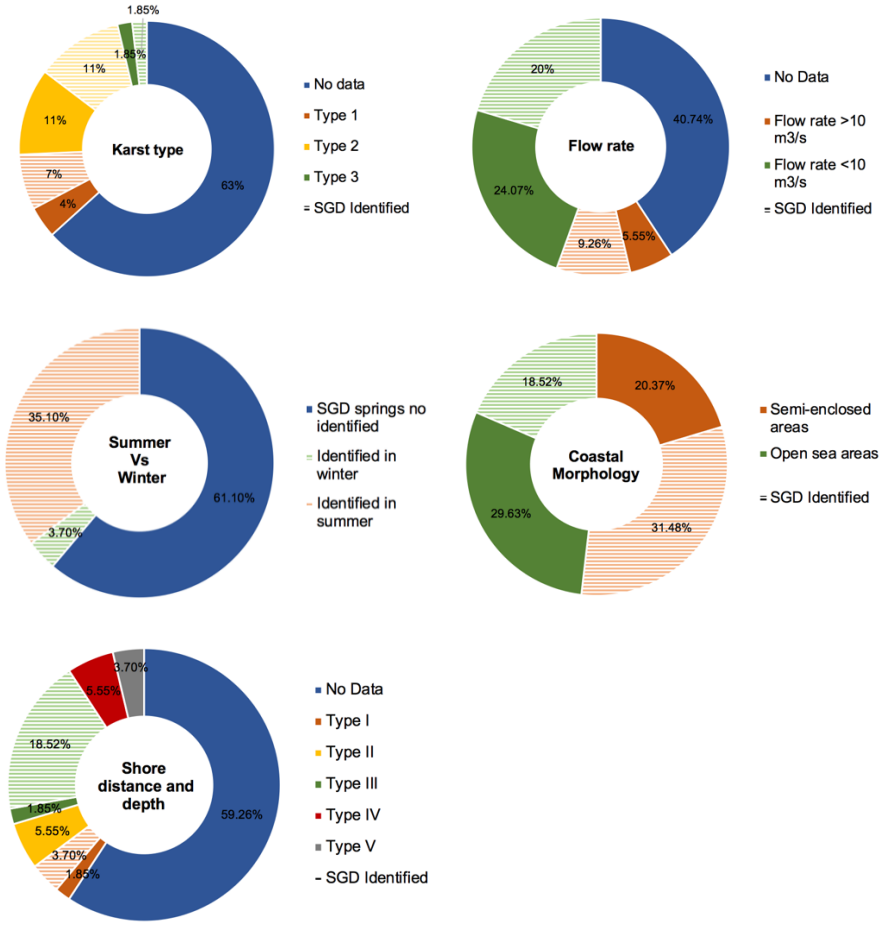

Figure 3, Appendix A: Thermal anomalies from streams and anthropogenic sources. A)Vandellós II nuclear power plant in Spain, B)Benicarló port in the north and Peñíscola port in the south, both in Spain, C)Small river in Croatia. © Google Earth 2021.

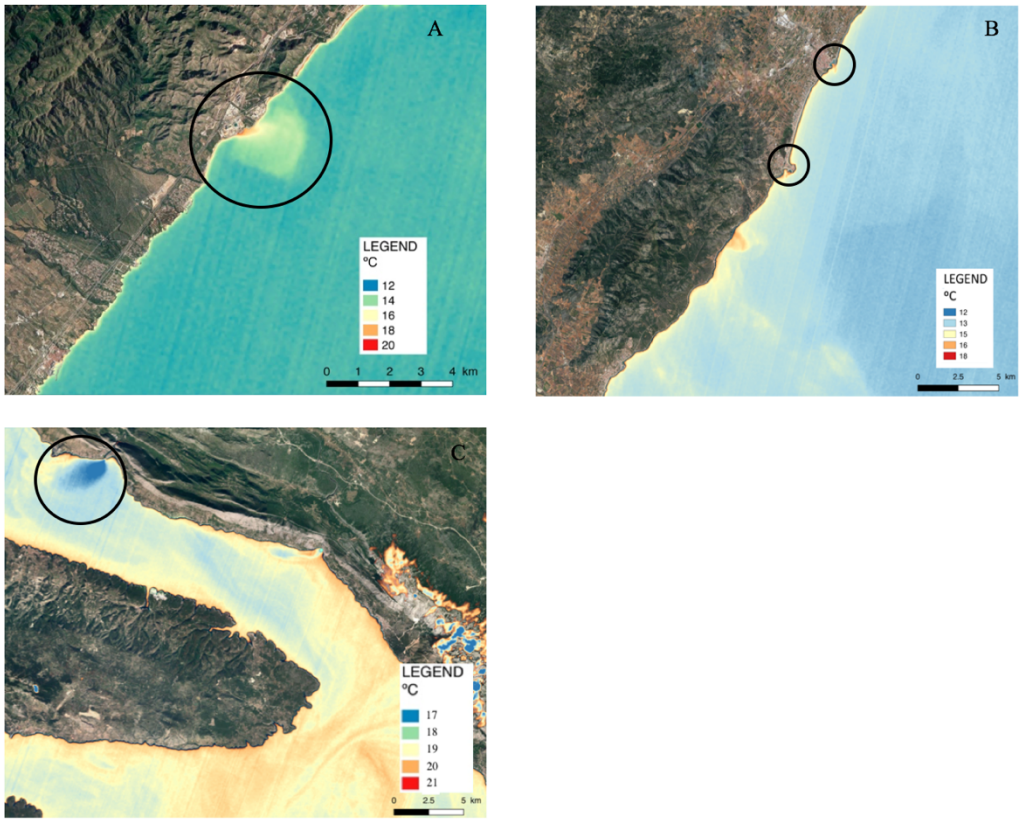

Figure 4, Appendix A: Conceptual framework of technical limitation factors that can limit the identification of SGD springs by using Landsat 8 TIRS images.

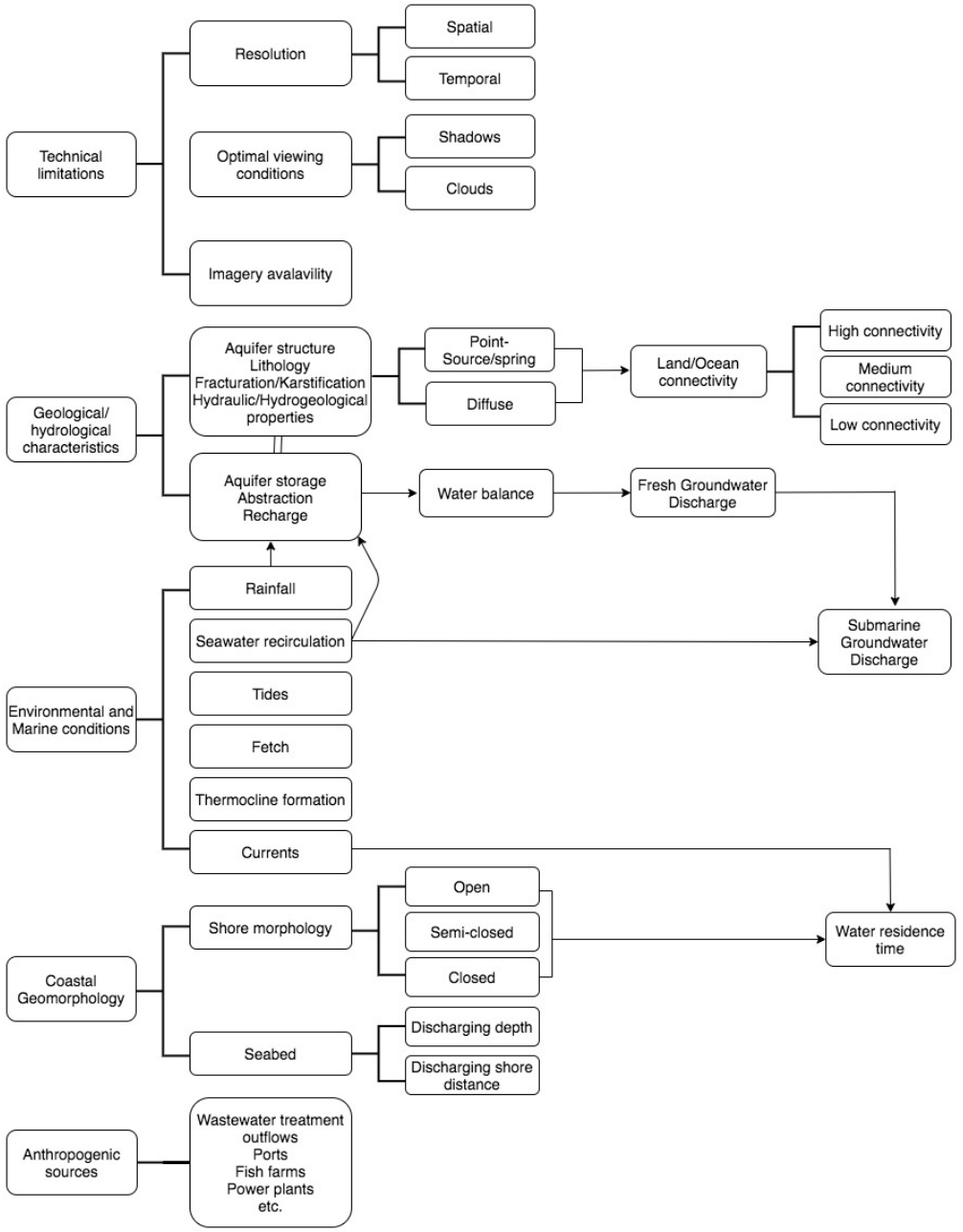

Appendix B. Supplementary information of Chapter 3

Figure 1, Appendix B: Temporal evolution of the ecologically impacted area by SGD in Aimakapä fishpond in Hawai.

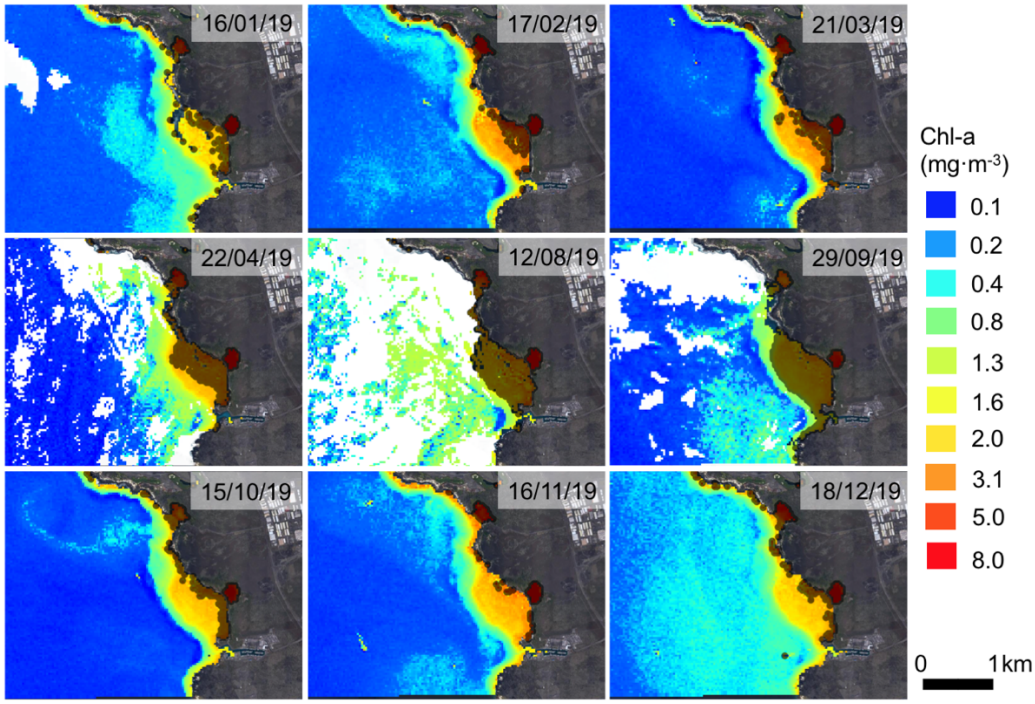

Figure 2, Appendix B: Temporal evolution of the ecologically impacted area by SGD in Bangdu Bay in Jeju Island.

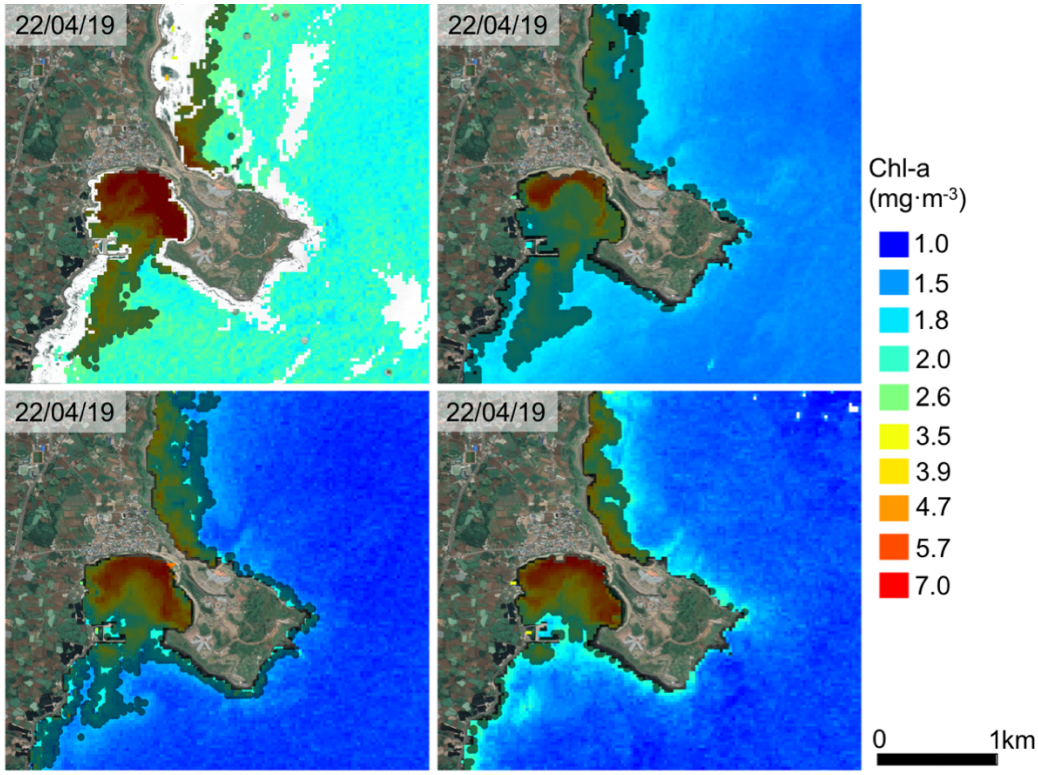

Figure 3, Appendix B: Temporal evolution of the ecologically impacted area by SGD in La Paz Bay in México.

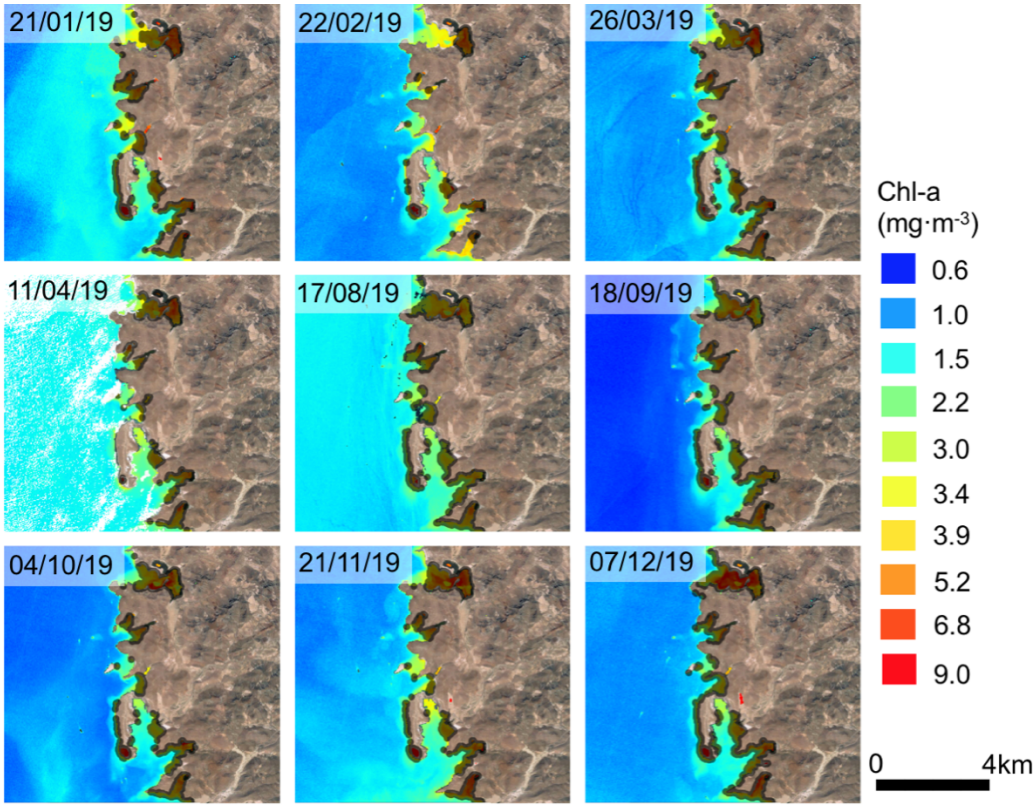

Figure 4, Appendix B: Temporal evolution of the ecologically impacted area by SGD in Serra d'Irta in the east of the Iberian Peninsula.

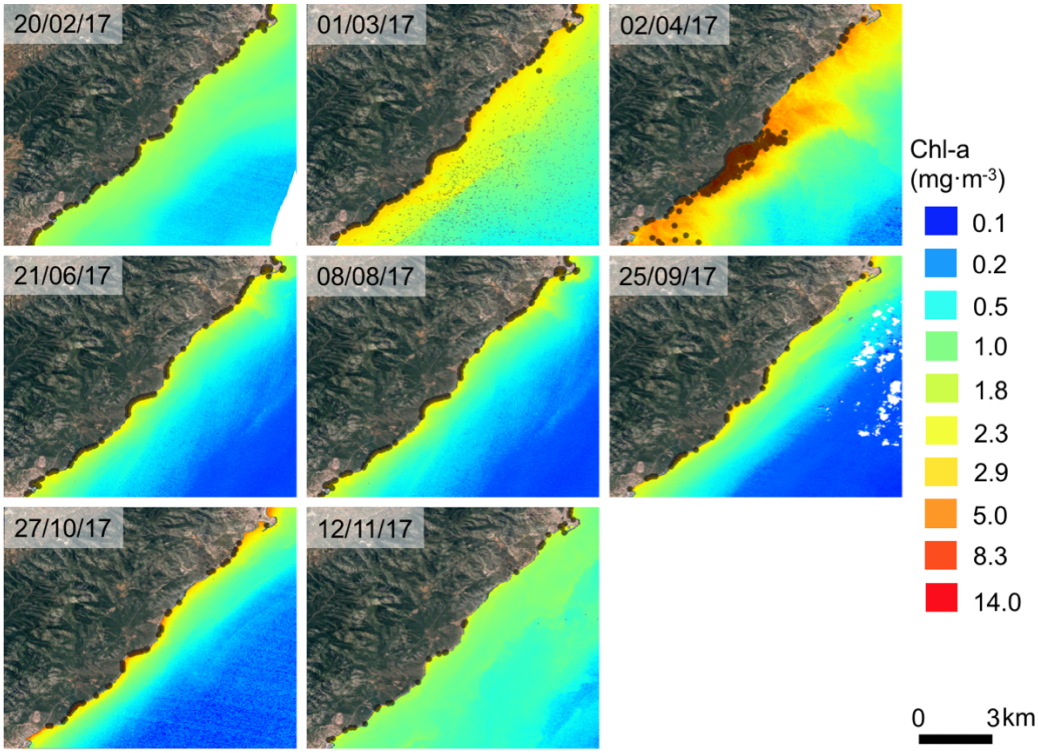

Appendix C. Supplementary information of Chapter 4

Figure 1, Appendix C: Evolution of Electrical conductivity (EC) *versus* cumulative time in infiltration water (Inf) and observation points (O, A2, and B2) of the sand and compost systems. The horizontal straight color bars represent the monitoring intervals of each sampling point.

SAND TREATMENT

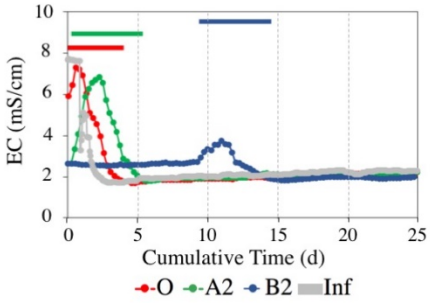

MONITORING POINT	MONITORING TIME (d)
Oblique-ST	0.5; 0.6; 0.7; 0.83; 0.95; 1; 1.52; 1.76; 1.90
A2-ST	1.79;2.55;2.76;3.54;4.71;5.53;6.67
B2-ST	6.97;9.69;11.91;13.94;16.60;18.77;20.69;23.66
Soil	0; 6; 8; 28; 61
Biofilm	0; 6; 8; 28; 61

COMPOST TREATMENT

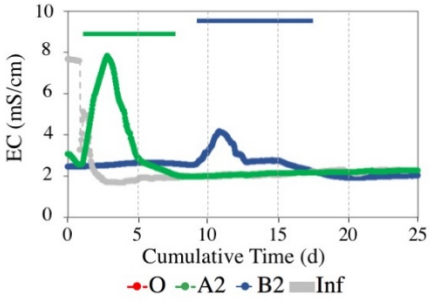

MONITORING POINT	MONITORING TIME (d)
Oblique-CT	0.52;0.61;0.70;0.85;0.96;1.01;1.52;1.80;1.91
A2-CT	1.82;2.56;2.74;3.52;4.73;5.54;6.68
B2-CT	6.98;9.72;11.93;13.95;16.61;18.78;20.70;23.67
Soil	0; 6; 8; 28; 61
Biofilm	0; 6; 8; 28; 61

Table 1, Appendix C: Concentration of bacterial density and EPS in the biotraps at different monitoring points.

		Bacterial density (cel x 10^7/cm^3)		**EPS (µg glucose-EPS/cm^3)**	
		SAND TREATMENT	**COMPOST TREATMENT**	**SAND TREATMENT**	**COMPOST TREATMENT**
O	Initial (0 d)	10.54	15.26	44.75	29.07
	Injection (6 d)	11.13	14.39	10.03	12.11
	After injection (61 d)	17.33	7.57	41.99	30.65
A2	Initial (0 d)	11.29	13.16	32.79	29.98
	Injection (8 d)	13.59	15.35	34.88	3.52
	After injection (61 d)	7.05	6.76	20.56	11.62
B2	Initial (0 d)	8.13	12.05	19.35	21.99
	Injection (28 d)	6.73	6.63	11.40	14.03
	After injection (61 d)	18.94	5.79	19.82	9.98

Validation performance of the method in biofilm, Appendix C

In order to validate the method for the biofilm, method limits of detection (MLODs) and method limits of quantification (MLOQs) were determined as the lowest compound concentration that yielded a signal-to-noise (S/N) ratio of 3 and 10, respectively. Analytical calibration curves were constructed according to the individual response range of each analyte. Accuracy was evaluated by the recovery rates of each standard spiked in the blank biofilm, determined in four replicate spiked extracts at two concentration levels; 5, and 100 ng/mL in standard solutions, and measured 3 times (n=9). Precision was expressed as percentage of relative standard deviation (RSD (%)), for each concentration level. The matrix effect (ME) was evaluated by comparing the slopes of the analytical calibration curves prepared in MeOH and in sample extracts (matrix-matched calibration standards).

Calibration range

Calibration curves at ten different concentrations (1, 3, 5, 10, 30, 50, 100, 300, 500, and 700 ng/mL) were built, both in pure MeOH and in the matrix extract (matrix-matched standards solutions) to evaluate the potential ME. Correlation coefficients (r^2) of analytical calibration curves were $r^2 > 0.99$ in both MeOH and in the matrix-matched standards, indicating good linearity for all compounds. There were significant differences between the signals in methanol and in the matrix, so matrix matched calibration curves were prepared for all the analysis.

Accuracy

The recovery rates ranged between 73.2 % and 138% (without taking into account 4HB, that presented bad recovery values at the high concentration level). The lowest recovery value was obtained for 4HB and the highest for DHMB. The complete list of recovery values is listed in the end of this section in tables S.2.

Sensitivity

The MLOD and MLOQ obtained are listed in Tables S.3, along with the determination coefficient for each compound. The MLODs for biofilm ranged between 0.18 and 0.87 ng/g dw and the MLOQs ranged between 0.60 and 2.89 ng/g dw, showing that the method presents good sensitivity.

Precision

Four replicates of spiked samples at two concentrations (5 ng/mL and 100 ng/mL) were analyzed. The RSD values are listed in table S.4. They ranged between 0.32 and 22.25, showing good precision values in the intra-day analysis.

Table 2, Appendix C: Recoveries obtained in the biofilm for each compound in different replicates and concentrations. (1), (2), (3), (4) are the number of replicates.

	BP3	**BP1**	**BP4(-)**	**4HB**	**4DHB**	**DHMB**	**AVO**
5 ng/g dw (1)	129.4	93.6	113.2	64.2	81.6	125.2	116.0
5 ng/g dw (2)	103.0	81.6	115.8	114.0	88.2	131.2	95.2
5 ng/g dw (3)	124.0	73.2	104.4	103.8	92.4	128.6	109.4
5 ng/g dw (4)	107.2	119.2	72.5	105.6	97.2	127.2	90.4
100 ng/g dw (1)	86.4	96.3	73.4	4.6	122.9	122.1	107.6
100 ng/g dw (2)	79.6	99.3	104.2	5.4	113.8	138.0	84.4
100 ng/g dw (3)	86.5	79.5	94.0	4.9	94.3	117.0	85.6
100 ng/g dw (4)	88.0	94.2	65.2	4.9	116.4	122.0	85.2

Table 3, Appendix C: Limits of detection and quantification of the method and coefficient of determination for each compound analyzed in the method. MLOD: limit of detection of the method; MLOQ: limit of quantification of the method; r2: coefficient of determination.

	BP3	BP1	BP4(-)	4HB	4DHB	DHMB	AVO
MLOD (ng/g dw)	0.18	0.83	0.85	0.80	0.35	0.87	0.57
MLOQ (ng/g dw)	0.60	2.75	2.83	2.67	1.15	2.89	1.89
r2	0.99958	0.99115	0.99167	0.99842	0.99024	0.99581	

Table 4, Appendix C: Relative standard deviations among replicates of each spiking level in the different compounds. RSD: Relative standard deviation.

	RSD intra 5 ng/g	RSD intra 100 ng/g
BP3	12.78	3.76
BP1	20.03	8.80
BP4 (-)	19.93	18.02
4HB	22.25	0.32
4DHB	6.62	12.31
DHMB	2.52	9.14
AVO	11.96	11.28

Hydrol. Earth Syst. Sci., 25, 4789–4805, 2021
https://doi.org/10.5194/hess-25-4789-2021

Hydrology and Earth System Sciences
Open Access
EGU

Applicability of Landsat 8 thermal infrared sensor for identifying submarine groundwater discharge springs in the Mediterranean Sea basin

Sònia Jou-Claus[1,2], **Albert Folch**[1,2], **and Jordi Garcia-Orellana**[3,4]

[1]Department of Civil and Environmental Engineering, Universitat Politècnica de Catalunya, Jordi Girona 1–3, 08034 Barcelona, Spain
[2]Associated Unit: Hydrogeology Group (UPC-CSIC), Barcelona, Spain
[3]Institut de Ciència i Tecnologia Ambientals – ICTA, Universitat Autònoma de Barcelona, 08193 Bellaterra, Spain
[4]Departament de Física, Universitat Autònoma de Barcelona, 08193 Bellaterra, Spain

Correspondence: Sònia Jou-Claus (soniajouclaus@gmail.com)

Received: 3 November 2020 – Discussion started: 16 December 2020
Revised: 3 June 2021 – Accepted: 4 August 2021 – Published: 2 September 2021

Abstract. Submarine groundwater discharge (SGD) has received increasing attention over the past 2 decades as a source of nutrients, trace elements and ocean pollutants that may alter coastal biogeochemical cycles. Assessing SGD flows and their impact on coastal marine environments is a difficult task, since it is not easy to identify and measure these water flows discharging into the sea. The aim of this study is to demonstrate the significant usefulness of the freely available thermal infrared (TIR) imagery of the Landsat 8 thermal infrared sensor (TIRS) as an exploratory tool for identifying SGD springs worldwide, from local to regional scales, for long-term analysis. The use of satellite thermal data as a technique for identifying SGD springs in seawater is based on the identification of thermally anomalous plumes obtained from the thermal contrasts between groundwater and sea surface water. In this study, we use the TIR remote sensing (TIR-RS) imagery provided by Landsat 8 at a regional scale and discuss the principle limiting factors of using this technique in SGD studies. The study was developed in karstic coastal aquifers in the Mediterranean Sea basin during different seasons and under diverse meteorological conditions. Although this study demonstrates that freely available satellite TIR remote sensing is a useful method for identifying coastal springs in karst aquifers both locally and regionally, the limiting factors include technical limitations, geological and hydrogeological characteristics, environmental and marine conditions and coastal geomorphology.

1 Introduction

Submarine groundwater discharge (SGD) is an important component of the hydrological cycle and has been commonly defined as any flow of water across the continental margin in the ocean–aquifer interface, regardless of fluid composition or driving force, with spatial scale lengths of meters to kilometers (Burnett and Dulaiova, 2003; Moore, 2010; Taniguchi et al., 2019). This definition includes meteoric fresh groundwater resulting from inland recharge, but also seawater circulated through the sediments of coastal aquifers (Burnett and Dulaiova, 2003). Both water flows mix in coastal aquifers, where biogeochemical reactions may occur when this groundwater interacts with the geological matrix (Moore, 1999; Moosdorf et al., 2021; Rocha et al., 2021; Ruiz-González et al., 2021). This dynamic mixing zone influences the transfer of chemical compounds such as nutrients, trace metals and other contaminants to coastal waters (Alorda-Kleinglass et al., 2019; Boehm et al., 2004; Rodellas et al., 2015; Trezzi et al., 2016). SGD-derived inputs from chemical compounds can highly impact coastal ecosystems by influencing productivity, biomass, species composition and sonification (Andrisoa et al., 2019; Garcés et al., 2011; Garcia-Orellana et al., 2016; Krest et al., 2000). According to Garcia-Orellana et al. (2021), groundwater discharge pathways of SGD can be grouped into the following five different SGD pathways according to the characteristics of the processes: (1) terrestrial groundwater dis-

charge, (2) density-driven seawater circulation, (3) seasonal exchange of seawater, (4) shoreface circulation of seawater and (5) centimeter-scale porewater exchange (PEX). The discharge of fresh groundwater (pathway 1) and, to a lesser extent, density-driven seawater circulation (pathway 2) is the only mechanism that represents a net source of freshwater, usually mixed with seawater, to the coastal ocean. The SGD discharge process related to this fresher fraction of SGD occurs mainly through three different ways, namely coastal onshore springs, which discharge on the coastline via surface sinkholes (Garcia-Solsona et al., 2010; Mejías et al., 2012), submarine springs, where the discharge occurs via deep sinkholes (Bakalowicz, 2015; Fleury et al., 2007), and diffuse discharge, a type of discharge which is not concentrated and occurs throughout sediments (Rodellas et al., 2014).

Identifying and mapping groundwater discharge areas is challenging, despite the number of traditional methods available for locating the main groundwater discharge locations and quantifying their flow rates. These methods include simple procedures such as deploying traditional local knowledge, conducting visual observations, monitoring changes in vegetation, as well as in water temperature and salinity, and using seepage meters or radioactive isotope tracers (Garcia-Orellana et al., 2021; Mejías et al., 2012; Rosenberry et al., 2020; Schubert et al., 2014). Apart from these methods, several authors have suggested thermal infrared remote sensing (TIR-RS) as an alternative methodology for identifying potential SGD spring sites, since it enables the screening and study of inaccessible zones and/or areas with a scarcity of hydrogeological information (Wilson and Rocha, 2012). Temperature has been used successfully to study SGD by comparing the relatively constant temperature of groundwater with that of surface seawaters, which fluctuates seasonally (Dale and Miller, 2007). In general, groundwater maintains a relatively constant temperature between depths of 5 and 100 m, approximately 1–2 °C higher than the mean annual air temperature (Anderson, 2005). The detection of SGD springs via TIR-RS is possible in any environment where there is thermal contrast between the discharging fluid and the receiving surface water body (Kelly et al., 2013). TIR images have the potential to identify the location of major SGD springs, and to study their spatial and temporal variability, by exploring the temperature difference between coastal seawater and brackish groundwater discharges at different times.

There are two types of platforms for obtaining thermal infrared information, i.e., airborne TIR-RS (airplane, helicopter and drone) and satellite TIR-RS (Modis, Aster and Landsat). Airborne TIR has been used for different applications; for example, Shaban et al. (2005) and Akawwi et al. (2008) conducted aerial TIR surveys along the Mediterranean Sea and Dead Sea coastlines to identify potential SGD sites. Kelly et al. (2013) used TIRS images from localized point source SGD to demonstrate that groundwater plume areas are linearly and highly correlated to in situ groundwater fluxes. Airborne TIR-RS has also been applied in combination with other methods, not only for qualitative SGD recognition, but also for quantifying groundwater flows from freshwater springs (Danielescu et al., 2009; Mejías et al., 2012). In the coastal carbonate aquifer of El Maestrazgo (Iberian Peninsula), a combination of complementary techniques was used to locate submarine springs via airborne high-resolution thermal infrared, radon measurements and physical–chemical anomalies and to quantify the groundwater discharge by direct quantification with flowmeters and Ra isotopes (Mejías et al., 2012). Tamborski et al. (2015) combined airborne TIR overflights with coastal radionuclide surveys to investigate the significance of SGD along the northern shore of Long Island (New York, USA) to provide quantitative evidence for TIR-RS as a tool to remotely identify and measure SGD. Finally, Danilescu et al. (2009) assessed total freshwater discharge in two small nutrient-sensitive estuaries in Prince Edward Island (Canada), using a combination of TIR images, direct discharge measurements and numerical simulations.

Compared to airplane, helicopter and drone platforms, satellite TIR-RS has some characteristics that limit its use for coastal water observation. The temporal resolution is fixed and varies depending on the satellite, with a minimum daily revisit frequency and a maximum frequency of every 16 d for a specific area. Furthermore, the spatial resolution, which varies between 30 and 1000 m, is lower than the airborne resolution. This results in the fact that small thermal anomalies, induced by small flows of SGD, are likely not to be detected. Additionally, satellite TIR-RS images are affected by atmospheric conditions (i.e., clouds and shadows). However, satellite TIR-RS imagery has the great advantage of being free of charge (Landsat), easily accessible, globally available, multi-temporal and covering a regional scale instantaneously. These advantages turn satellite TIR-based approaches into a viable and promising option for detecting SGD worldwide.

There are several satellite missions capable of measuring sea surface temperatures (SST) with a moderate spatial resolution and acquisition, namely the Advanced Spaceborne Thermal Emission and Reflection Radiometer (ASTER) and the Landsat satellite, among others, which provide an appropriate spatial and temporal resolution for large-scale SGD monitoring. For those sensors suitable for SGD research, Landsat is the one with the longest TIR data provision (from 1982 until today and already planned to go beyond 2030; Wulder et al., 2019) and is the one most widely applied for the purposes of SGD research (Wilson and Rocha, 2012, among others).

The use of satellite imagery in SGD studies has evolved in parallel with the launch of new sensors that feature spatial resolution improvements over previous sensors. However, the application of satellite TIR images is neither extensive nor widespread compared to airborne TIR images. Several SGD studies used Landsat 7 to locate groundwater discharge areas (e.g., Wang et al., 2008), to detect known but previously unmapped SGD locations (Varma et al., 2010), to

determine the spatial extent and scale of SGD-derived temperature anomalies (Wilson and Rocha, 2012) and to infer SGD temporal variation using long-term thermal anomaly size variations (Mallast et al., 2014). More recent studies used data obtained by the Landsat 8 thermal infrared sensor (TIRS) to identify and characterize SGD sites using the sensor's technical improvements. For example, McCaul et al. (2016) proposed a multi-approach methodology for understanding submarine and intertidal groundwater discharge patterns. Xing et al. (2016) evaluated the ability of satellite remote sensing methods (Landsat 7 and 8) to detect thermal anomalies related to SGD as a possible index of the presence of offshore low-salinity groundwater storage at local scale. To the best of our knowledge, there is no study that thoroughly compares SGD locations with satellite-data-derived thermal anomalies over large spatial scales in order to assess the suitability of satellite TIR-RS data for conducting SGD research.

The aim of this work is to study the usefulness of satellite TIR images at different sites, covering a large scale and in different seasons to assess whether Landsat 8 TIR-RS can be used as an exploratory tool for identifying SGD springs worldwide, from local to regional scales, for long-term analysis. The second aim is to discuss the influencing factors to be considered in the identification of SGD at the local and regional level.

The study was carried out on the coastal karstic aquifers of the Mediterranean Sea basin, where there are many local studies that describe the discharge processes thanks to the significant connectivity between this coastal aquifer type and the sea (e.g., Bakalowicz, 2005; Barberá and Andreo, 2015; Worthington, 1999). In this hydrogeological context, SGD takes place mainly through submarine or aerial springs (point source). Although the groundwater discharge from submarine springs represents a negligible fraction of the global SGD (Luijendijk et al., 2020), in some areas, such as the Mediterranean Sea, this fraction can be locally important, strongly influencing marine ecosystems and serving as a freshwater resource for the population (Rodellas et al., 2015; Alorda-Kleinglass et al., 2021). To validate the temporal effectiveness of this technique, Landsat 8 images from 2017 and 2018 on the coasts of the Mediterranean Sea basin were used to locate SGD springs previously described in the scientific literature, showing in which period of the year these SGD springs are observable via satellite. In addition, we will hypothesize and discuss those factors that may condition the identification of SGD springs in order that future studies might take them into account when using satellite remote sensing TIR techniques.

2 Methods

2.1 Study area

The Mediterranean basin has been selected for this study because it is one of the areas of the world where numerous SGD studies have been carried out and where dozens of coastal springs have been described dating back to ancient times in countries such as Spain, France, Italy, Croatia, Greece, Turkey, Syria, Lebanon and Libya (Fig. 1). In this study, we focus on a set of 54 springs mentioned in the scientific peer review literature published in English (Basterretxea et al., 2010; Bakalowicz, 2018; Fleury et al., 2007; Mejías et al., 2012; Garcia-Solsona et al., 2010) where groundwater discharge is known to occur, and where there is a description of the hydrogeological context of each spring (Supplement 1). The number of springs included in the study represents at least 88 % of the submarine karst springs described in the English peer review literature concerning the Mediterranean basin.

The SGD contribution to the Mediterranean ranges from 3 to 50×10^{11} m^3 yr^{-1}, where fresh groundwater inputs represent 1 %–25 % of the total SGD inputs (Rodellas et al., 2015). SGD has been described and studied in several locations along the Mediterranean coast (e.g., Bakalowicz, 2015; Mejías et al., 2012; Tulipano et al., 2005; Bejannin et al., 2017). The Mediterranean basin is characterized by 46 % of its coastline being formed by karstic aquifers (Bakalowicz, 2015; Fleury et al., 2007; Trezzi et al., 2016). Its narrow continental shelves prevent large tidal amplification along the coast; tidal amplitude is usually less than 0.2 m (Werner et al., 2013). The Mediterranean climate is seasonal, characterized by windy, mild, wet winters and by relatively calm, warm and dry summers. Strong local winds, such as the cold and dry tramontane, mistral and bora from the north and the hot and dry sirocco from the south, are typical of the region. These strong regional and seasonal wind regimes provide a substantial amount of vertical mixing in the seawater column. In general, the main rainfall season is during fall and spring, with an average annual precipitation of 500 mm yr^{-1} (Andreo and Carrasco, 1993). The sea temperature is approximately between 26–30 and 14–19 °C in the summer and winter, respectively.

The available information for each of the 54 studied springs (Supplement 1) shows that the mean flow rates range between 0.009 and 50 m^3 s^{-1}, the distances from the shore range from the coastline to 1 km offshore and that discharge depths vary between 7 m a.s.l. (above sea level) and 150 m b.s.l. (below sea level). In accordance with these characteristics, we might classify the studied springs into five groups. The first group of springs discharge inland near the seashore and reach the sea through small streams; these karstic springs are located between 300 and 500 m inland and at elevations of 2, 3 and 15 m a.s.l. for Patan in Croatia, Almyros of Heraklion, Crete, in Greece and Maro in

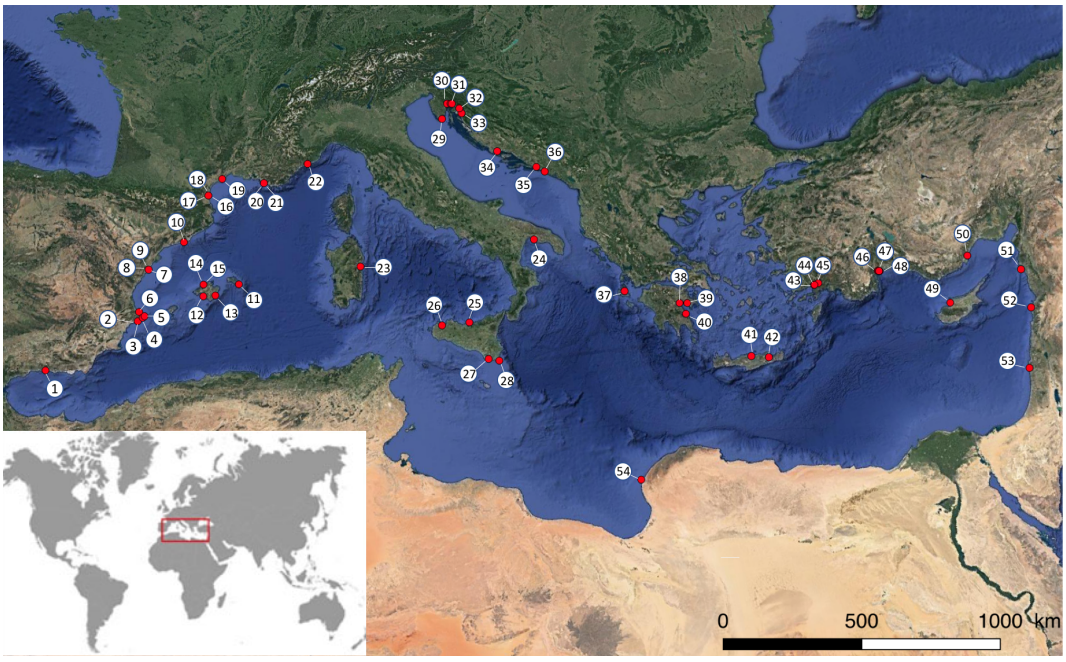

Figure 1. Location of the 54 SGD springs used for this study. The SGD springs shown in the figure are described in Bakalowicz (2018), Basterretxea et al. (2010), Fleury et al. (2007), Garcia-Solsona et al. (2010) and Mejías et al. (2012). © Google Earth 2021.

Spain, respectively. The second group of springs discharges in coastal lagoons at a distance of 100 m from the sea shore and a depth of 4 m b.s.l. (Font Dame and Font Estramar in Salses-Leucate lagoon in France) and at an unknown shore distance and 30 m b.s.l. (Vise in Thau lagoon, respectively). The third group of springs is located between 0 and 10 m from the shoreline and in shallow sea waters of between 0 and 7 m b.s.l. (Torre Badum, Las Fuentes and Font de Dins in Spain, Ain Zayana in Libya, Agios Nikolaos, Kefalonia and Anavalos Kiveri in Greece, and Ovacık and Gökova in Turkey). The fourth group of springs is also located close to the shoreline but at a water column depth of 12 m b.s.l. The two springs of this group are Moraig in Spain and Port Miou and Bestouan in France. The fifth and last group consists of Mortola in Italy and Chekka in Lebanon, in which discharges occurs offshore between 100 m and 1 km and with a water column depth of between 35 and 150 m b.s.l.

The type of coastal karst aquifer studied has been defined using the same classification as in Tulipano et al. (2005) for Mediterranean coastal karst aquifers. The first type has systems with poorly developed, but highly fractured, karstification. This karst type included three different subsystems in which (1) faults dissect the aquifer, such as in the Gökova (four springs; Bayari and Kurttaş, 2002) and Ovacık spring, where the faults are located in the underlying beds that extend towards the sea (Elhatip, 2003), (2) groundwater flows along the zones of cracks, fractures and karst hollows, such as in the Donnalucata spring (Povinec et al., 2006), and (3) groundwater flows through stratification joints, such as in the Mortola spring (Fleury et al., 2007). The second type has systems with well-developed karstification connected to the sea (e.g., Moraig, Port Miou, Bestouan, Almyros of Heraklion, Almyros of Agios Nikolaos, Kefalonia, Ain Zayana and Chekka). The last type of defined karst system is a well-developed karstification but with low connectivity with the sea. This group is represented by only two springs, i.e., Kiveri Anavalos in Greece and Vise in France.

2.2 Landsat 8 TIRS data acquisition

To determine the optimal time period for SGD detection using remote sensing, the SST of a series of images covering all seasons was compared. The TIRS instrument of Landsat 8 is a thermal imager with two thermal infrared bands centered at 10.8 and 12.0 µm and a ground sampling distance (GSD) of 100 m. However, all thermal images are resampled using a cubic convolution to 30 m (Roy et al., 2014). To carry out this study, only the thermal band 10 TIRS 1 (10.6–11.2 µm) of the 11 Landsat 8 bands was used to study the SGD sites. The other Landsat 8 thermal band, 11 TIRS 2 (11.50–12.51 µm), was not used because the data collected in this band had some large calibration uncertainties (US Geological Survey, 2014).

A total of 27 path and row combinations were analyzed with the Landsat 8 TIR images of the Mediterranean coast between January 2017 and December 2018 to cover all 54 known SGD sites. To that end, a total of 1296 images (two images per month for the 2 years of study) were acquired from the US Geological Survey (USGS), with cloud coverage between 0 % and 90 % in each image. A manual

inspection of all images resulted in finer selection of 413 images with cloud-free conditions above the areas of interest (Supplement 2). The finer selection of cloud-free images was used for subsequent steps.

2.3 Deriving SST values from Landsat 8 TIRS data

Data processing included the conversion of digital numbers to SST, including an atmospheric correction of each image following the methodology presented by Chander et al. (2009). Image processing began with radiometric correction, which was performed by converting the digital number (DN) to sensor spectral radiance through band-specific rescaling gain and bias factors according to Eq. (1).

$$L_\lambda = G_{\text{rescale}} \cdot Q_{\text{cal}} + B_{\text{rescale}}, \quad (1)$$

where L_λ is the sensor spectral radiance ($\mathrm{W\,m^{-2}\,sr^{-1}\,\mu m^{-1}}$), G_{rescale} is the band-specific rescaling gain factor ($\mathrm{W\,m^{-2}\,sr^{-1}\,\mu m^{-1}\,DN^{-1}}$), Q_{cal} is the quantized and calibrated standard product pixel values (DN) and B_{rescale} is the band-specific rescaling bias factor ($\mathrm{W\,m^{-2}\,sr^{-1}\,\mu m^{-1}}$).

The next step was an atmospheric correction to remove the atmospheric component of the recorded thermal signal which strongly depends on atmospheric conditions (aerosol content, humidity, temperature, etc.) at a specific recording time and place. To atmospherically correct images at sensor spectral radiance, it was necessary to transform them into surface radiance of an ideal blackbody, considering the scene-specific up- and downwelling radiance and transmission values and the emissivity of the water surface, according to Eq. (2) (Barsi et al., 2003).

$$L_t = \frac{L_\lambda - L_{\text{U}} - \tau \cdot (1-\varepsilon) \cdot L_{\text{D}}}{\tau \cdot \varepsilon}, \quad (2)$$

where L_t is the radiance of an ideal blackbody ($\mathrm{W\,m^{-2}\,sr^{-1}\,\mu m^{-1}}$), L_λ is the sensor spectral radiance ($\mathrm{W\,m^{-2}\,sr^{-1}\,\mu m^{-1}}$), L_{U} is the upwelling radiance ($\mathrm{W\,m^{-2}\,sr^{-1}\,\mu m^{-1}}$), L_{D} is the downwelling radiance ($\mathrm{W\,m^{-2}\,sr^{-1}\,\mu m^{-1}}$), ε is the emissivity of the surface (–), and τ is the atmospheric transmission (–).

A web-based atmospheric correction tool (Atmospheric Correction Parameter Calculator) developed by Barsi et al. (2003), based on MODTRAN, was used to obtain values for atmospheric transmissivity and the upwelling and downwelling radiances of the atmosphere. The emissivity of water in the Landsat 8 TIR bands ranges from 0.98 (band 11) to 0.99 (band 10), and in this study, we assume a constant emissivity of 0.99 (Wen-Yao et al., 1987).

Finally, to obtain the sea surface temperature (SST), the corrected radiances were introduced into Eq. (3).

$$T = \frac{K_2}{\ln\left(\frac{K_1}{L_t} + 1\right)}, \quad (3)$$

where T is the effective sensor brightness temperature (K), L_t is the radiance of an ideal blackbody ($\mathrm{W\,m^{-2}\,sr^{-1}\,\mu m^{-1}}$), K_1 is prelaunch calibration constant 1 ($\mathrm{W\,m^{-2}\,sr^{-1}\,\mu m^{-1}}$), and K_2 is prelaunch calibration constant 2 (K).

The resulting atmospherically corrected SST data represent temperature with an error of less than 1.3 K for the temperature range 270–330 K. This temperature represents the skin temperature of the water (< 1 mm of the upper most water layer), which differs from the bulk temperature below it by about 0.1 K due to sensible heat fluxes, evaporative heat loss and longwave radiation (Donlon et al., 2002; Wloczyk et al., 2006).

2.4 Site inter-comparison between a single image and multiple images

Temperature maps of coastal waters were created from temperature data to assess the significance of the SST anomalies. The identification of SGD spring sites was based on the assumption that temperatures of discharging groundwater may be different than seawater and less variable than seawater temperatures throughout the year. SGD spring sites were analyzed using two different procedures. First, single images were used to identify SGD springs by means of the water temperature anomalies. As a second step of the single image approach, the change between images along the study period was also evaluated. This qualitative analysis allows us to observe variations in the morphology and temperature range of the known discharge plume between images. As a second approach, called multiple imaging, SGD spring sites were detected by evaluating the pixel-by-pixel standard deviation (SD) across all image sets. Lower values of SD were used as indicators for groundwater discharge using a sea surface temperature (SST) data series. This statistical parameter has been previously applied in semi-arid areas to study groundwater and surface water interactions and identify spring discharge into lakes or enclosed seas (Mallast et al., 2014; Tcherepanov et al., 2005). It was assumed that groundwater tends to be less variable than surface water, which varies seasonally and daily. The applied multi-temporal thermal remote sensing approach was based on a variable number of Landsat 8 TIRS images. The images used to calculate the standard deviation varied between 5 and 17 images, depending on the number of images without clouds available for each studied site. The resulting thermal maps were combined with satellite imagery from Google Earth (only the land part) using GIS (geographic information system; QGIS Las Palmas) to show the location the SGD springs at the identified sites.

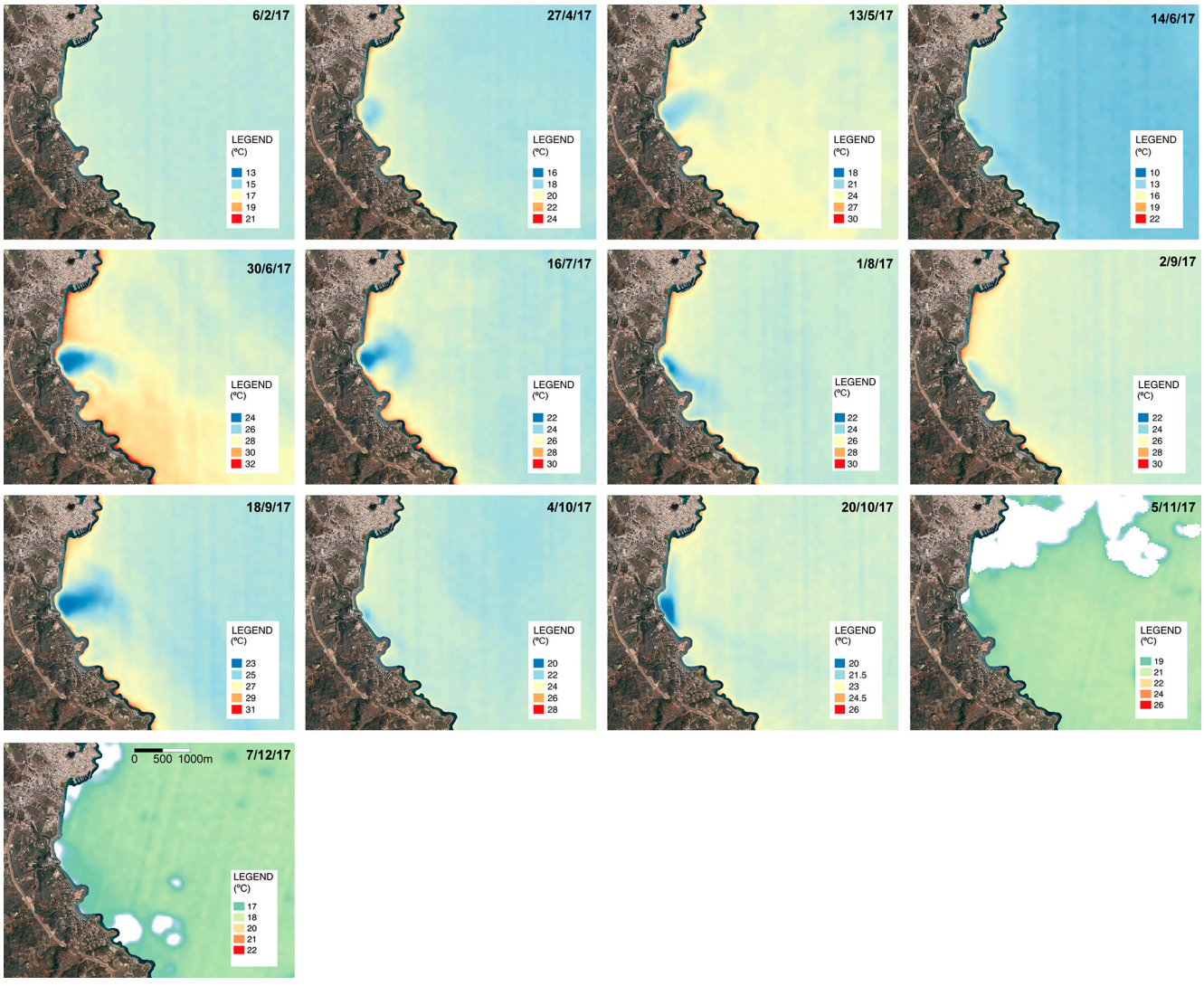

Figure 2. SST images (degrees Celsius) obtained via band 10 of Landsat 8 OLI/TIRS of the region of Almyros of Agios Nikolaos (Crete, Greece) throughout 2017. Of the 23 images analyzed, the presence of an SGD spring was clearly visible in nine images that represent a 37 % ratio of success. In January, March and November 2017, it was not possible to obtain an SST image due to the presence of clouds. © Google Earth 2021.

3 Results and discussion

3.1 Overall identifications

As an example of the Landsat 8 TIR images analyzed in the Mediterranean Sea basin, the thermal images of the Almyros SGD spring in Agios Nikolaos (Crete, Greece) throughout the year 2017 are shown in Fig. 2. In general, a thermal anomaly plume is observed in several of the 23 images (one of the July images is missing) occurring near and perpendicular to the coastline, reflecting the continuous discharge of groundwater. Since a satellite image provides the sea surface temperature (SST) of the first millimeter of seawater (Donlon et al., 2002; Wloczyk et al., 2006), the thermal contrast due to SGD can be observed as the fresh groundwater flows over seawater due to its lower density (i.e., lower salinity; Wilson and Rocha, 2012). The images series of Almyros Agios Nikolaos (Fig. 2) show how thermal contrast caused by the groundwater discharge cannot be observed throughout the whole year. The thermal contrast is more identifiable from the second half of April until the end of October, but the best thermal plume observations were from June to October (Fig. 2). Conversely, this spring cannot be identified from November to March. The groundwater discharge was not identified in February and December, due to the absence of thermal contrast, and in the other months (January, March and November) because clouds made identification difficult. Thus, the overall percentage of time for optimal SGD spring identification was 37 % in 2017.

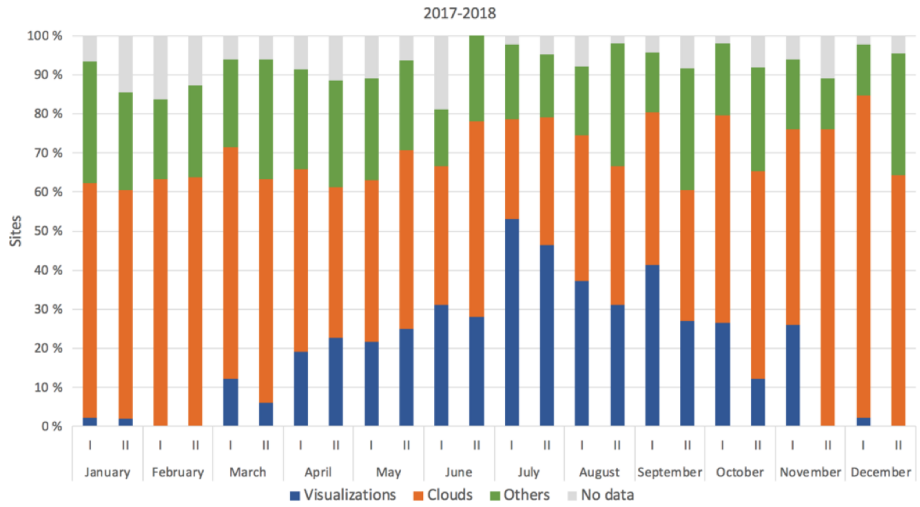

Figure 3. Percentage of successful and unsuccessful SGD identifications for all SGD springs that were identified at least once (23 springs representing 44 %) throughout the year 2017 and during the year 2018 (based on the selection of 720 images) are shown individually in the Supplement 3. The x axis shows the months of the year. Roman numerals (I and II) represent the two satellite passes per month that cover every area. No image available is represented in gray, while the presence of clouds is in orange and blue for successful SGD identifications. Those for which the images were not covered by clouds, and where SGD springs were not identified, are shown in the figure as "others" in green.

If the same approach is applied for the total of 54 SGD springs studied, only 23 springs were identified in individual images, representing a 44 % success rate for the technique over the entire study period (2017 and 2018). The success percentage for identifying the 23 SGD springs, according to the period of the year, is shown in Supplement 3. The highest success percentage for SGD identification was during the summer, specifically from June to September (Fig. 3), which corresponds to an average of 21 % of the images analyzed. Conversely, the SGD springs were not identified in the remaining 79 % of the images. The winter period, from December to February (Fig. 3), had the lowest percentage of SGD spring identifications.

3.2 Influencing factors to consider in the identification of SGD springs

The analysis of the images of the Mediterranean coast obtained by Landsat 8 TIRS during 2017 and 2018 was successful for several studied springs but did not identify SGD springs in all the images analyzed. Thus, identifying SGD springs using Landsat 8 TIRS presents some limitations, as the success rate was slightly less than 50 %. The following potential limitations were previously reported in the literature in some local studied areas: only information for the first millimeters of seawater is available (Donlon et al., 2002; Wloczyk et al., 2006), spatial resolution (Wilson and Rocha, 2012), period of the year (Bayari and Kurttaş, 2002; Wilson and Rocha, 2012; Xing et al., 2016), the results are highly dependent on atmospheric temperature, seawater currents, wind speed and direction, sea surface effects (Kelly et al., 2013) and cloud cover, and the need for specialist knowledge to convert the data into accessible (visualized) information (McCaul et al., 2016).

Given the abovementioned limitations, we propose a conceptual framework of factors representing technical limitations in order to assess those issues that should be considered when applying TIR-RS to the study of SGD. These technical limitation factors can be grouped as follows: (1) technical limitations, (2) geological and hydrogeological characteristics, (3) environmental and marine conditions, (4) coastal geomorphology, and (5) anthropogenic sources (Fig. 4).

3.2.1 Technical limitation factors

Some of the main limitations of the technique are related to the temporality of obtaining images, the spatial resolution, the availability of images in the desired period and the atmospheric conditions during the image capture. Each satellite has an image acquisition spatial and temporal resolution, and therefore, the results are subject to these pre-established conditions. For Landsat 8 TIRS, the temporal resolution is 2 weeks, and the spatial resolution is 100 m resampled to 30 m, so a smaller thermal anomaly plume than this produced by an SGD spring will not be identified. For example, in the 20 m wide semi-enclosed cove of Alcaufar (Menorca; western Mediterranean), there are several described springs (García-Solsona et al., 2010) that were not identified by satellite due to the small dimensions of the cove (García-Solsona et al., 2010). The availability of satellite images depends, in some cases, on technical problems that the satellite experiences during image collection, which implies that there are

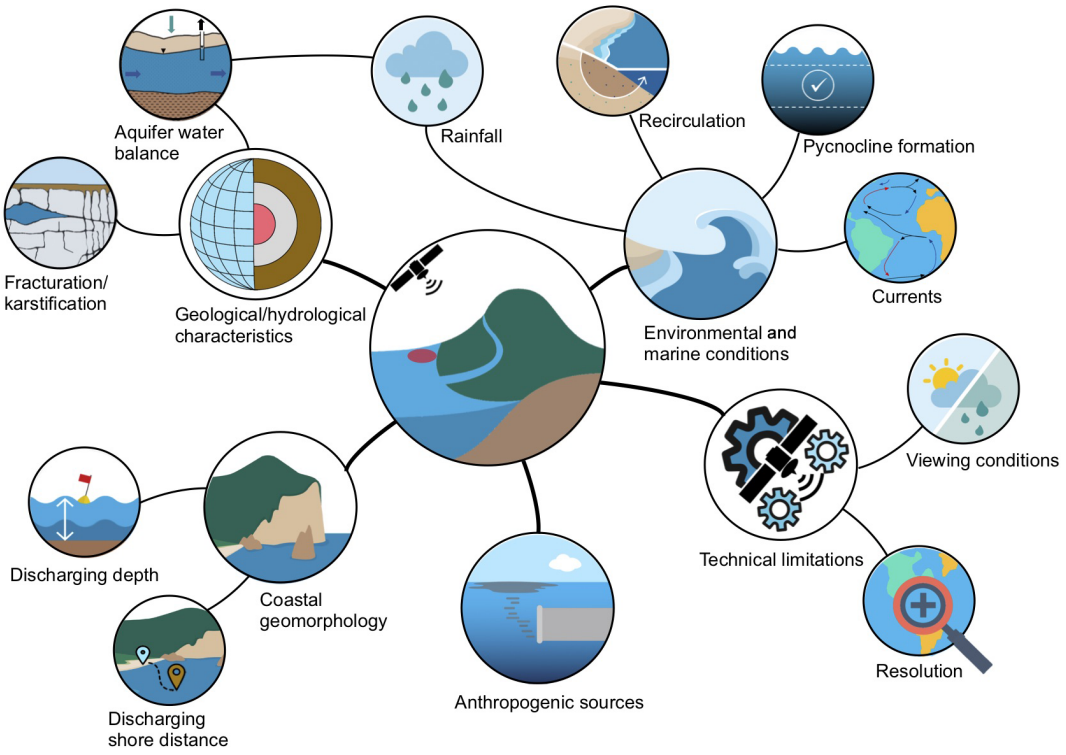

Figure 4. Conceptual framework of technical limitation factors that can limit the identification of SGD springs by using Landsat 8 TIRS images.

annual series of images with some missing images. In the example used in Fig. 2, where the Almyros of Agios Nikolaos (Greece) SGD spring is identified, only 23 of the 24 images that should have been produced during 2017 were obtained. The striping noise that can be seen in the images (Fig. 2), and which affect TIR bands especially, is another technical limitation. Sometimes the difference is so large that it would hinder a proper SGD detection (Gerace and Montanaro, 2017).

Other important limitations related to the technique include the atmospheric conditions at the time of the image capture. Clouds and clouds shadows change radiometric information leaving the sea surface and prevent a correct analysis of the images. For the Mediterranean Sea basin, of 80 % of the images in which SGD springs were not identified, 60 % were due to the high presence of clouds. Thus, clouds are the main factor limiting the identification of SGD springs. The presence of clouds is higher in winter than in summer; therefore, warmer months are much better for identifying SGD springs in the Mediterranean Sea. However, in at least 20 % of the cloudless images, it was not possible to observe and locate SGD springs described in the literature. Therefore, a detailed analysis of the cloudless imagery is necessary to confirm the optimal conditions for locating SGD springs in the area of interest (Anderson, 2005).

3.2.2 Geology and hydrogeology limitation factors

The characteristics of coastal aquifers and the different driving forces that allow groundwater discharge into the sea are other factors that can limit the identification of SGD springs. According to Garcia-Orellana et al. (2021), SGD is the combination of fresh terrestrial groundwater discharge driven by hydraulic gradient between land and sea and saline groundwater discharge from the seawater recirculation through the coastal and continental margin. Thus, the thermal signal of both types of groundwater will define the intensity and shape of the plume that can be observed in the sea.

For coastal aquifer SGD springs, geological factors such as the lithology (e.g., type of rock, degree of karstification, presence of faults and/or fractures, etc.) determine the hydraulic properties that greatly influence the groundwater flow that discharges into the sea (Brunner et al., 2007; Edet et al., 1998). Another aspect to consider is the connectivity of the aquifer with the sea. Coastal aquifers may be totally or partially hydraulically connected to the sea, depending on several factors such as the geological structure of the aquifer and the seabed, as well as the hydraulic properties of both onshore and offshore geological formations. In addition, the amount of SGD depends on the aquifer water budget, which produces variations in groundwater discharge flow. The main factors that influence this budget are the natural variations in

recharge at different temporal scales (rainfall events, seasonality and inter-annual changes) and the abstraction of groundwater, which can reduce the discharge of the fresh groundwater component of the SGD or even induce seawater intrusion into the coastal aquifer. Unfortunately, these factors are linked since, in most cases, when recharge is low, abstractions tend to be higher.

In the presented research, from the 54 karstic SGD studied springs, information on the type of coastal karst aquifer is only available for 37 % of the springs (Supplement 4). From those, the first karst-type system, characterized by poorly developed but highly fractured karstification, represents 11 % of the springs, and 7 % of the total were successfully identified. The second type of karst system, characterized by well-developed karstification connected to the sea, represents 22 % of the springs, and half of those were identified (11 % of the total). Finally, the third karst type system, with well-developed karstification but low connectivity with the sea, represents only 4 % of the springs, and half of those were identified (1.8 % of the total). Therefore, the best geological and hydrogeological settings for identifying SGD springs are karst systems with well-developed karstification and that are well-connected to the sea, as well as those systems with poorly developed but highly fractured karstification. This is because these systems have high transmissivities that can induce high local SGD rates, making it easy to detect their thermal plumes. However, it depends on the recharge area and its rate.

Conversely, low groundwater discharge water volumes may limit the identification of thermal anomalies because they could attenuate the thermal anomaly produced by the SGD. Therefore, low discharge water volumes are unlikely to be identified using this technique. Of the 54 karstic SGD studied springs, the flow rate information was only available for 59 % of the springs (Supplement 4). Springs with a flow rate lower than $10\,m^3\,s^{-1}$ represent 40 % of the springs. From those, only 50 % were identified. The springs with a flow rate higher than $10\,m^3\,s^{-1}$ represent 15 % of the springs, and from those, 60 % were identified. This indicates that, apart from flow rate, other factors affect the failure to identify these SGD springs on the coastline.

Inter-annual and annual changes, such as humid–dry periods, overexploitation and extreme events such as strong rainfall storms, etc., can also modify SGD flows. Thus, the research period in which the images were collected is also important because seasonal variations (Lee et al., 2016) can lead to SGD thermal plume variations, not only due to the temperature difference between groundwater and seawater (Lee et al., 2016) but also the annual SGD flow rate variations (Michael et al., 2005) that allow their identification.

Regarding hydrogeological conditions in the Mediterranean Sea basin, it was expected that the best seasons for identifying SGD springs using satellite TIR-RS would be spring and autumn, when rainfall is higher, and therefore, a higher discharge flow rate is expected. However, results showed that late spring and summer were the best seasons for identifying SGD springs, indicating that other factors influence the identification of SGD springs using this technique.

3.2.3 Environmental and marine conditions

Other aspects that could affect the thermal contrast between the groundwater plume and seawater include environmental and marine conditions. Both factors can make the identification of SGD difficult because they cause seawater mixing with the discharging groundwater, reducing the thermal contrast between them and modifying the sea surface temperature. The main environmental condition that can affect SGD identification is the action of wind, which can mix the first millimeters of the sea surface water, limiting the identification of SGD springs using remote sensing techniques. Similarly, marine conditions can affect SGD identification if they reduce the thermal contrast between the groundwater plume and the seawater. These marine conditions are basically reduced to the coastal water hydrodynamic conditions that can be affected by processes such as the influence of tides or coastal currents, the formation of a pycnocline in surface seawater or the fetch due to wind action. Tides, coastal currents and fetch generate seawater movement and mix groundwater with seawater, causing a thermal contrast attenuation. Similarly, the presence of a pycnocline can result in less vertical mixing of the water column. In subtropical areas with cold winters and hot summers, such as the Mediterranean Sea, coastal waters often develop a pycnocline during the summer months, as high temperatures increase the evaporation of seawater, generating an increase in salinity and therefore water density. This effect causes cold, fresh groundwater to flow over salty and dense seawater, generating an SGD layer on the sea surface.

The temperature of the Mediterranean Sea oscillates seasonally between 26–30 °C in summer and 14–19 °C in winter, while the groundwater temperature remains relatively constant over time, implying a greater contrast between summer and winter. However, SGD spring visualizations in cloud-free images decrease significantly in winter months compared to warmer months (Fig. 4). In total, 35 % of the springs were identified in summer, and only 4 % were identified in winter (Supplement 4). Consequently, the number of SGD spring visualizations is much higher in summer than in winter. In the winter months, wind, water column mixing, currents, etc., are more intense and reduce the thermal contrast. Therefore, environmental and marine conditions during the winter months are unfavorable for the identification of coastal springs.

For this reason, areas where the influence of various marine factors such as tides, coastal currents or fetch is small are ideal for identifying SGD springs because such factors induce mixing attenuating the thermal contrast needed to identify SGD springs. Similarly, in subtropical areas such as the Mediterranean Sea, it is easier to identify SGD springs be-

cause coastal waters often develop a pycnocline during the summer months, resulting in less vertical mixing of the water column and, therefore, better identification of SGD springs. Therefore, in the Mediterranean basin, environmental and marine conditions in summer months are much more favorable for the identification of coastal springs than in winter months.

3.2.4 Coastal morphology limitation factors

Another aspect that influences SGD thermal plume visualization is the coastal morphology; depending on its characteristics, the seawater residence time in the study zone may allow the formation of a thermal plume. In semi-enclosed areas, such as bays or coves, where the residence time of discharging water in the sea is in the range of 1 to several days (Tamborski et al., 2020), the formation of thermal plumes from SGD can easily be detected by satellite, in comparison with open-sea areas, where the seawater residence time is shorter (less than 1 d), due to the effect of marine or weather factors such as waves, coastal currents or fetch. Groundwater discharge can occur below sea level, either at shallow (< 10 m) or at greater depths, right on the shoreline or a few meters from it (Zektser et al., 2006). The morphology of the coastal seabed combined with the geological characteristics of the aquifer (e.g., karstification degree and coastal hydraulic gradient) determine both the depth and offshore distance of the groundwater discharge. These two characteristics are very significant, since the location of the SGD spring on the coast is critical for the correct identification of the thermal contrast between groundwater and seawater using satellite thermal images. While groundwater discharges produced at coastal level or several meters inland usually generate thermal contrasts that are easily detectable by satellite (Mejías et al., 2012), submarine springs located several meters deep often represent a challenge for satellite detection. This is because, when groundwater discharges below sea level, it rises to the sea surface, generating a buoyant thermal layer of several millimeters due to its lower density that arises from its temperature and salinity characteristics. Therefore, a greater discharge depth requires more time to reach the sea surface, adapting the SGD's thermal signal at the sea surface to the surrounding water temperature. Thus, marine factors may have a greater influence in balancing the seawater and groundwater temperatures, preventing the recognition of thermal anomalies on the sea surface, as stated by Mallast et al. (2013).

However, the time required for groundwater to reach the sea surface depends not only on the depth of the discharge below sea level but also on hydrogeological factors, such as the discharge flow. Thus, SGD springs characterized by shallow depths and large flow rates will favor the detection of SGD-induced thermal plumes on the sea surface, while deep areas with small flows may be undetectable. Intermediate situations, such as shallow areas with small flows or deep areas with large flows, may be detected, depending on the relative importance of the environmental and/or marine limiting factors.

For studied springs in the Mediterranean Sea basin, 52 % of the springs were located in semi-enclosed coastal areas (Supplement 4). Of these, 31 % of the studied springs were identified (Port Miou and Bestouan in France; Kefalonia, Anavalos Kiveri and Almyros of Agios Nikolaos in Greece; Martinšćica, Perilo, Novijanska, Jurjevska and Patan in Croatia; Gökova (three springs), Ovacık and Antalya (three springs) in Turkey). These results show that, when discharge occurs in semi-enclosed areas where the seawater residence time is large, the springs can be identified until late autumn, even though the flow of groundwater is relatively small ($0.75\ m^3\ s^{-1}$ was reported for the Ovacık spring in Turkey). Therefore, the success in identifying SGD springs in semi-enclosed areas also is higher throughout the year.

Of the 54 SGD studied springs, the distance and depth information are available for 41 % of the springs (Supplement 4). The first group of springs, which discharge near the seashore and reach the sea through small streams, represents 6 % of the springs (Patan in Croatia, Almyros of Heraklion in Greece and Maro in Spain), and from those, 66 % were identified (Patan and Almyros of Heraklion). The second group of springs, which represent 6 % (Font Dame, Font Estramar and Vise) and are characterized by discharge in coastal lagoons, was not identified. The third group of springs, which discharge close to the shoreline and in shallow water, represents 20 % of the springs (Torre Badum, Las Fuentes, Font de Dins in Spain, Ain Zayana in Libya, Agios Nikolaos, Kefalonia and Anavalos Kiveri in Greece, and Ovacık (3 springs) and Gökova in Turkey), and we were able to identify 91 % (all of them except the Ain Zayana spring). No springs were identified from the fourth group, which represents 6 % of the springs (Moraig in Spain and Port Miou and Bestouan in France) and is characterized by discharge close to the shoreline but at a water column depth of 12 m b.s.l. None of the springs in the fifth group (Mortola in Italy and Chekka in Lebanon), which represent 4 % of the springs and are characterized by discharge offshore with a water column depth between 35 and 150 m b.s.l., were identified.

From the analysis of the images obtained by Landsat 8 TIRS, and considering the hydrogeological data of the various coastal springs, we conclude that groundwater discharges that occur at significant depths (> 12 m b.s.l.) are unlikely to be identified by this technique, probably because the thermal anomaly generated between groundwater and seawater does not reach the sea surface. This is the probable reason for the failure to identify the springs of Vise in France, Mortola in Italy and Chekka in Lebanon. For the Vise spring, which discharges at 30 m b.s.l., the hydrogeological information indicates that it is a mixture of karstic water, thermal water and seawater (Aquilina et al., 2002); most likely, the discharging groundwater does not produce enough thermal contrast to be detected with a satellite sensor. On the

other hand, SGD springs located in very shallow areas, such as the Salses-Leucate lagoon, which has an average maximum depth of 2 m b.s.l. (Bejannin et al., 2017), and where there are two well-known springs (Font Dame and Font Estramar), were not identified. A possible reason is that these types of shallow coastal lagoons are highly influenced by atmospheric temperature, since the small water column has little capacity to buffer temperature fluctuations (Lee et al., 2016). However, Anavalos Kiveri and Torre Badum, identified during winter months, are shallow (0 to 10 m b.s.l.) SGD springs. Therefore, although initially these types of springs should be easily detectable by satellite, atmospheric factors can greatly influence the formation of the thermal contrast needed to identify them.

The shore distance at which groundwater discharge occurs is another factor that affects the identification of groundwater discharge in coastal areas. SGD springs discharging further than 500 m from the seashore were not recognized, such as the Mortola spring with a distance of 800 m. This may be related to the fact that, as the distance to the coast increases, the depth of the water column increases, and the travel time of the fresher groundwater also increases, allowing a complete temperature equilibrium. Furthermore, these zones are more affected by ocean currents that increase water mixing, attenuating the thermal signal.

In some cases, there is not one single factor affecting SGD spring identification but rather a combination of several factors (flow rate, season, coastal morphology, etc.) which makes it difficult to explain why an SGD spring was not identified.

3.2.5 Thermal anomalies from streams and anthropogenic sources

When looking for coastal thermal anomalies by using satellite TIR images, some anomalies can be detected that are not necessarily related to SGD. These anomalies can be from natural sources, such as rivers or streams, or civilian facilities such as ports, thermal power plants, fish farms or wastewater treatment plants. These thermal anomalies may misidentify or mask some SGD springs when discharge occurs in shallow areas with high seawater residence times.

For example, natural water sources, such as small rivers or streams, also produce a thermal signal at sea. As SGD, they may have a different temperature than seawater. This is the case for the small river near Split in Croatia (Supplement 5), which produces a thermal anomaly that could be misinterpreted as an SGD spring. Furthermore, when SGD and rivers discharge at the same location, the thermal signal of SGD will be masked and/or modified by surface water discharge. In the case of civil facilities, the most common facilities that could be confused with SGD springs would be the discharges from wastewater treatment plants as they usually discharge water with a different thermal signal than the sea. For example, in the Hyperion Treatment Plant (HTP) and the Orange County Sanitation District (OCSD) wastewater diversion events in Southern California, where treated water discharge takes place at depth, it is possible to detect its thermal effect on the coastal waters (DiGiacomo et al., 2004) with SST differences of at least 0.5 °C identifiable with TIR-RS (Gierach et al., 2017). Other examples of civilian facilities that can generate thermal signals and induce non-identification or masking of SGD springs are power plants or ports. In the case of the Mediterranean Sea basin, it was observed that facilities located along NE of the Iberian Peninsula, such as the Vandellós II Nuclear Power Plant, the Port of Barcelona and the Port of Benicarló, showed thermal anomalies similar to those produced by the SGD springs (Supplement 5). These outflows can also mask and modify the SGD thermal signal of the plume when both outflows take place at the same location, such as the case of Peñíscola in Spain, where the SGD discharge takes place at the same location as the port (Supplement 5).

3.3 Application of the multi-temporal SST series method

In some studied areas, there may be low thermal contrast that can prevent the identification of SGD springs. In these cases, it is possible to deepen the analysis of the images by using the multi-temporal SST series proposed by Mallast et al. (2014) in the Dead Sea, which minimizes the effect of the previously indicated limiting factors. Unlike single images, the multi-temporal SST series method allows several images and, thus, several points in time to be integrated, accentuating the small thermal anomalies for easy identification. An example of the usefulness of the multi-temporal SST series method is in the Serra d'Irta (eastern Iberian Peninsula; Mejías et al., 2012; Garcia-Solsona et al., 2010; Trezzi et al., 2016). At this site, Mejías et al. (2012) identified four large thermal anomalies (Torre Badum, Punta del Pebret and Les Fonts springs), by using airborne thermal remote sensing, that were not identified using Landsat 7. Using single images with Landsat 8 TIRS, only the Torre Badum spring was identified when compared with the four thermal anomalies identified by aerial thermal infrared images in 2012. The multi-temporal SST series method, which integrates 10 cloud-free images from 2017 to 2018, enables the identification of Torre Badum and Les Fonts, two of the four springs identified in 2012 by Mejías et al. (2012; Fig. 5).

Although the multi-temporal SST series method is better for identifying SGD springs because the thermal contrast is enhanced, this method did not enable SGD spring identification in other places where the single-image method did not identify them. Furthermore, with multi-temporal SST series, the temporal morphological information, such as the shape and size of the discharge plume, is lost (Mallast et al., 2013). Conversely, single images allow the identification of morphological variations in the discharge plume and the temperature variations along that plume. Therefore, if the study ob-

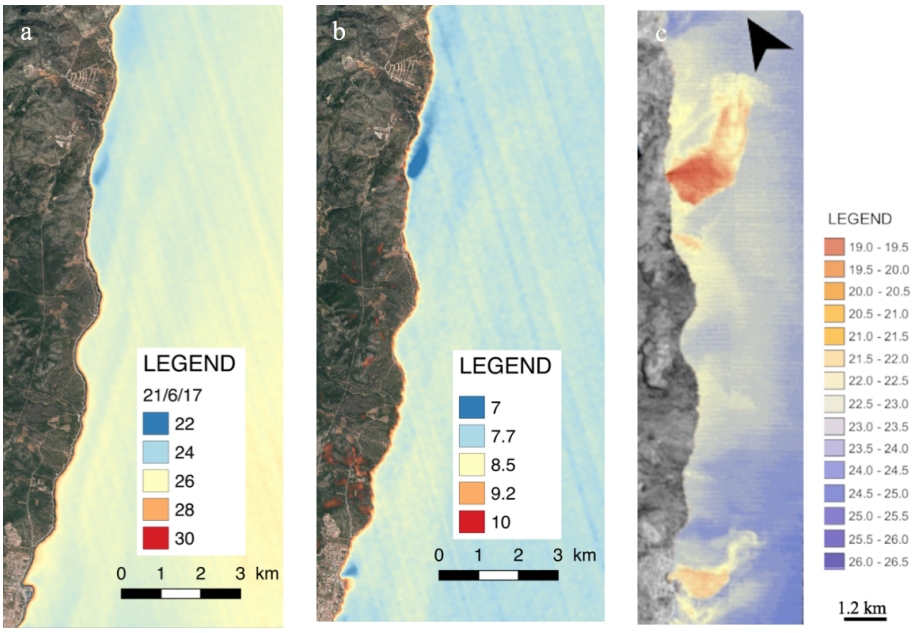

Figure 5. **(a)** Serra d'Irta single image map using an image taken on 21 June 2017. One spring in the middle of the Torre Badum spring was identified. **(b)** Serra d'Irta standard deviation (SD) map using 10 cloud-free images acquired between 2017 and 2018. In total, two springs in Serra d'Irta, in the south of the Les Fonts beach at the Alcossebre spring and in the middle at the Torre Badum spring, were identified. **(c)** Image modified from Mejías et al. (2012), where SGD springs were identified using aerial thermal infrared images. © Google Earth 2021.

jective is to identify SGD springs, the multi-temporal SST series method is the best option, but if the objective is to study the SGD plume variation, single images are better.

3.4 Identification of new SGD springs: challenges and recommendations for future SGD studies

One of the main objectives of this study is to demonstrate the great usefulness of satellite TIR imagery at local and regional scales, identifying SGD springs not previously described in the scientific literature. An example of this usefulness is the identification of 21 SGD springs undescribed in the bibliography along the Croatian coast using single images (Fig. 6). This demonstrates that the analysis of single images obtained from Landsat 8 TIRS allows the identification of new SGD springs. Therefore, this economical technique is very useful in inaccessible areas (Gumma and Pavelic, 2013; Edet et al., 1998). For this reason, in the design of SGD studies at both local and regional levels, it is recommended that the coastal water temperatures for thermal anomalies first be screened using the presented satellite-based TIR-RS approach, as this will help narrow the sampling surveys. Although the study of the thermal images during a single year should be sufficient to identify potential coastal springs, it is highly advisable to analyze thermal images over several years, since there may be one or several factors (technical, marine, environmental, hydrogeological, etc.) that may alter the SGD thermal signal.

Although this study focused on the discharge of groundwater from springs located in karst aquifers, the study of satellite TIR-RS images could be extrapolated to other types of aquifers where the discharge is more diffused and where the proportion of meteoric water is lower. To identify thermal plumes, water discharging into the sea, whether of meteoric origin or marine circulation, must have acquired sufficient thermal contrast in the coastal aquifer before discharge. This thermal contrast can also occur in places where coastal aquifers are volcanic rocks or fractured granites and even in sedimentary formations. However, in each case, the specific geological context (aquifer matrix, hydraulic parameter distribution, etc.) should be considered in the analysis.

Several studies have shown the possibility of quantifying SGD through the study of thermal plumes obtained by aircraft (Tamborski et al., 2015; Danielescu et al., 2009; Mejías et al.,2012). By determining the thermal plume area, which is often directly related to the discharge volume, SGD may be quantitatively identified. However, there are several factors that can alter the thermal plume shape that could result in error. Furthermore, because the TIR-RS image only allows us to observe less than 1 mm of the sea surface, and thus prevents a determination of the volume beneath the thermal plume, the required information is missing. Moreover, quantification by means of images represents a major challenge because satellite images (e.g., Landsat 8 TIRS) can only be obtained once every 16 d, and many factors can alter the shape of the plume independent of the actual discharge. Therefore, unless the discharge occurs in locations where the environmental and marine conditions are well known, quan-

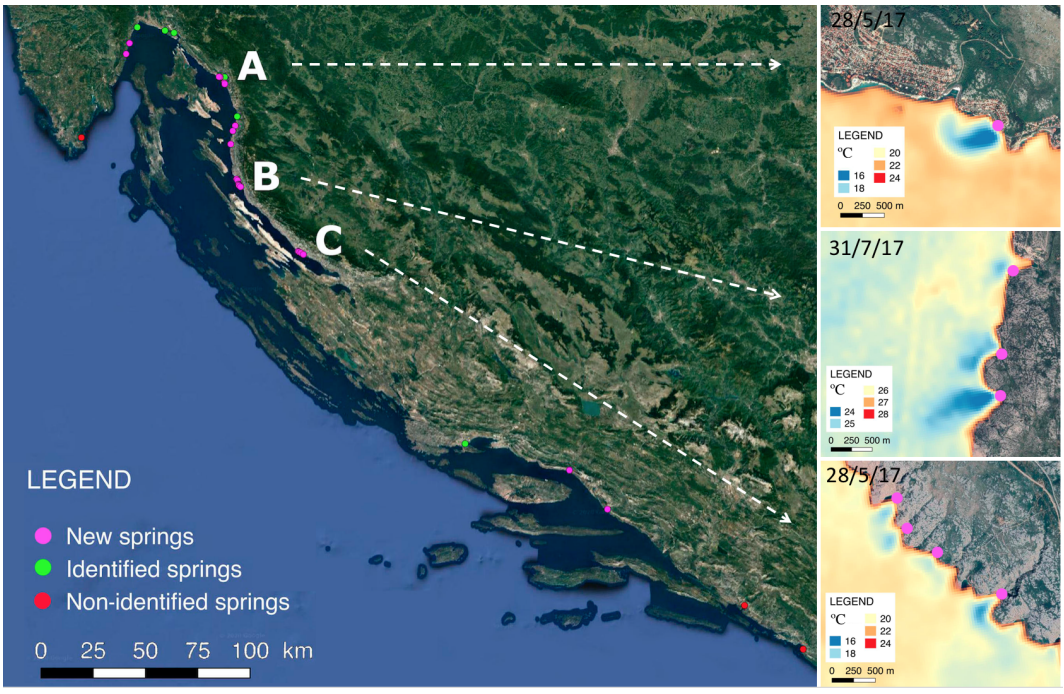

Figure 6. Springs reported in the literature (described SGD spring) vs. a new SGD spring identified with Landsat 8 TIRS. New SGD springs, not reported in the literature, are represented in pink. Springs reported in the literature are represented in green and white. © Google Earth 2021.

tification by satellite images represents a major challenge that should be further investigated.

Although this study focused regionally on the Mediterranean Sea basin, it can be extrapolated to other parts of the world and in places where the SGD has sufficient thermal contrast when discharging into the sea. This technique has been successfully used in regional areas such as Ireland (Wilson and Rocha, 2012; McCaul et al., 2016) or Laizhou Bay in China (Xing et al., 2016). However, in areas where the thermal contrast between the sea and the aquifer is low and/or temperature does not fluctuate during the year, such as in tropical zones, the use of satellite images represents a challenge that must be explored in detail. Furthermore, it is important to perform an initial study to attempt to identify the previously described main factors that can limit SGD spring identification in the study area, to try to control/avoid these effects.

4 Conclusions

This study demonstrates that satellite remote sensing is a useful tool for the identification of coastal SGD springs in karst aquifers, both locally and regionally, by performing an initial screening of the coastal water temperature images to identify possible thermal anomalies that can help narrow SGD study sampling surveys. However, this study highlights the following limiting factors that should be considered: (1) technical limitations, (2) geological/hydrogeological characteristics, (3) environmental and marine conditions and (4) coastal geomorphology.

In the karstic coastal aquifer of the Mediterranean Sea basin, the highest success percentage of SGD visualizations was during June, July, August and September. The main factor limiting the identification of SGD springs was clouds, which are far more abundant in winter months. The best geological and hydrogeological settings for identifying SGD springs were karst systems with well-developed karstification that are well-connected to the sea and those systems with poorly developed, but highly fractured, karstification. Environmental and marine conditions (such as pycnocline formation, light winds, etc.) in the summer months were much more favorable for the identification of coastal springs than in the winter months. Semi-enclosed areas, where the seawater residence time is large, favor the identification of SGD springs throughout the year. Groundwater discharges that occurred at a depth of more than 12 m b.s.l. or in very shallow waters were not identified. Also, SGD springs that discharged further than 500 m from the seashore were not recognized.

Multi-temporal SST series are better for identifying SGD springs in coastal zones, but the information for changes in the discharge plume changes is lost, while single images are more suited to studying the morphological variations in the discharge plume and temperature variations along the plume.

Although this study focused regionally on the Mediterranean Sea basin, it can be extrapolated to other parts of the world and other aquifer types in places where the SGD has sufficient thermal contrast when discharging into the sea and where the specific geological contexts (e.g., aquifer matrix and hydraulic parameters distribution) are considered. Long time series are better for identifying SGD spring areas, since there may be one or several factors (technical, marine, environmental, hydrogeological, etc.) that can alter the SGD's thermal signal. It is recommended to first screen the coastal water temperature images obtained by satellite to identify possible thermal anomalies that will help narrow the sampling surveys. This technique allows the identification and quantification of SGD springs in zones without hydrogeological information.

Data availability. All data are available from the corresponding author upon request.

Supplement. The supplement related to this article is available online at: https://doi.org/10.5194/hess-25-4789-2021-supplement.

Author contributions. SJC, AF and JGO contributed to design and implementation of the research, to the analysis of the results and to the writing of the paper.

Competing interests. The authors declare that they have no conflict of interest.

Disclaimer. Publisher's note: Copernicus Publications remains neutral with regard to jurisdictional claims in published maps and institutional affiliations.

Acknowledgements. The authors want to acknowledge Francisco Carreño Conde, from the Universidad Rey Juan Carlos, for the initial discussions on the topic and Ulf Mallast, from the Helmholtz Centre for Environmental Research – UFZ, for the review of the paper. Albert Folch is a Serra Húnter Fellow.

Financial support. This work was partly funded by the Spanish Government (grant nos. PID2019-110212RB-C22 and PID2019-110311RB-C21) the "Maria de Maeztu" program for Units of Excellence (grant no. CEX2019-000940-M) of the Spanish Government and the project TerraMar (grant no. ACA210/18/00007) of the Catalan Water Agency. The authors want to thank the support of the Generalitat de Catalunya to GHS (grant no. 2017 SGR 1485) and MERS (grant no. 2018 SGR-1588) for additional funding.

Review statement. This paper was edited by Marnik Vanclooster and reviewed by Alice Alonso and one anonymous referee.

References

Akawwi, E., Al-Zouabi, A., Kakish, M., Koehn, F., and Sauter, M.: Using thermal infrared imagery (TIR) for illustrating the submarine groundwater discharge into the eastern shoreline of the Dead Sea-Jordan, Am. J. Environ. Sci., 4, 693–700, https://doi.org/10.3844/ajessp.2008.693.700, 2008.

Alorda-Kleinglass, A., Garcia-Orellana, J., Rodellas, V., Cerdà-Domènech, M., Tovar-Sánchez, A., Diego-Feliu, M., Trezzi, G., Sánchez-Quilez, D., Sanchez-Vidal, A., and Canals, M.: Remobilization of dissolved metals from a coastal mine tailing deposit driven by groundwater discharge and porewater exchange, Sci. Total Environ., 688, 1359–1372, https://doi.org/10.1016/j.scitotenv.2019.06.224, 2019.

Alorda-Kleinglass, A., Ruiz-Mallén, I., Diego-Feliu, M., Rodellas, V. Bruach-Menchén, J. M., and Garcia-Orellana, J.: The social implications of Submarine Groundwater Discharge from an Ecosystem Services perspective: A systematic review, Earth Sci. Rev., 103742, https://doi.org/10.1016/j.earscirev.2021.103742, in press, 2021.

Anderson, M. P.: Heat as a ground water tracer, Ground Water, 43, 951–968, https://doi.org/10.1111/j.1745-6584.2005.00052.x, 2005.

Andreo, B. and Carrasco, F.: Estudio hidrogeológico del entorno de la Cueva de Nerja, in: Geología de la Cueva de Nerja, edited by: Carrasco, F., Trabajos sobre la Cueva de Nerja nº 3, Geología de la Cueva de Nerja, Patronato de la Cueva de Nerja, Málaga, 163–187, 1993.

Andrisoa, A., Stieglitz, T. C., Rodellas, V., and Raimbault, P.: Primary production in coastal lagoons supported by groundwater discharge and porewater fluxes inferred from nitrogen and carbon isotope signatures, Mar. Chem., 210, 48–60, https://doi.org/10.1016/j.marchem.2019.03.003, 2019.

Aquilina, L., Ladouche, B., Doerfliger, N., Seidel, J. L., Dupuy, C., and Le Strat, P.: Origin, evolution and residence-time of saline thermal fluids (Balaruc springs, S-France): Implications for large-scale fluid transfer across the continental shelf, Chem. Geol., 192, 1–21, 2002.

Bakalowicz, M.: Karst groundwater: A challenge for new resources, Hydrogeol. J., 13, 148–160, https://doi.org/10.1007/s10040-004-0402-9, 2005.

Bakalowicz, M.: Karst and karst groundwater resources in the Mediterranean, Environ. Earth Sci., 74, 5–14, https://doi.org/10.1007/s12665-015-4239-4, 2015.

Bakalowicz, M.: Coastal Karst groundwater in the mediterranean: A resource to be preferably exploited onshore, not from Karst Submarine springs, Geoscience, 8, 258, https://doi.org/10.3390/geosciences8070258, 2018.

Barberá, J. A. and Andreo, B.: Hydrogeological processes in a fluviokarstic area inferred from the analysis of natural hydrogeochemical tracers. The case study of eastern Serranía de Ronda (S Spain), J. Hydrol., 523, 500–514, https://doi.org/10.1016/j.jhydrol.2015.01.080, 2015.

Barsi, J. A., Barker, J. L., and Schott, J. R.: An Atmospheric Correction Parameter Calculator for a Single Thermal Band Earth-

Sensing Instrument, Int. Geosci. Remote Sens. Symp., 5, 3014–3016, https://doi.org/10.1109/igarss.2003.1294665, 2003.

Basterretxea, G., Tovar-Sanchez, A., Beck, A. J., Masqué, P., Bokuniewicz, H. J., Coffey, R., Duarte, C. M., Garcia-Orellana, J., Garcia-Solsona, E., Martinez-Ribes, L., and Vaquer-Sunyer, R.: Submarine groundwater discharge to the coastal environment of a Mediterranean island (Majorca, Spain): Ecosystem and biogeochemical significance, Ecosystems, 13, 629–643, https://doi.org/10.1007/s10021-010-9334-5, 2010.

Bayari, C. S. and Kurttaş, T.: Coastal and submarine karstic discharges in the Gökova Bay, SW Turkey, Q. J. Eng. Geol. Hydrogeol., 35, 381–390, https://doi.org/10.1144/1470-9236/01034, 2002.

Bejannin, S., van Beek, P., Stieglitz, T., Souhaut, M., and Tamborski, J.: Combining airborne thermal infrared images and radium isotopes to study submarine groundwater discharge along the French Mediterranean coastline, J. Hydrol.: Reg. Stud., 13, 72–90, https://doi.org/10.1016/j.ejrh.2017.08.001, 2017.

Boehm, A. B., Shellenbarger, G. G., and Paytan, A.: Groundwater discharge: Potential association with fecal indicator bacteria in the surf zone, Environ. Sci. Technol., 38, 3558–3566, https://doi.org/10.1021/es035385a, 2004.

Brunner, P., Hendricks Franssen, H. J., Kgotlhang, L., Bauer-Gottwein, P., and Kinzelbach, W.: How can remote sensing contribute in groundwater modeling?, Hydrogeol. J., 15, 5–18, https://doi.org/10.1007/s10040-006-0127-z, 2007.

Burnett, W. C. and Dulaiova, H.: Estimating the dynamics of groundwater input into the coastal zone via continuous radon-222 measurements, J. Environ. Radioact., 69, 21–35, https://doi.org/10.1016/S0265-931X(03)00084-5, 2003.

Chander, G., Markham, B. L., and Helder, D. L.: Summary of current radiometric calibration coefficients for Landsat MSS, TM, ETM+, and EO-1 ALI sensors, Remote Sens. Environ., 113, 893–903, https://doi.org/10.1016/j.rse.2009.01.007, 2009.

Dale, R. K. and Miller, D. C.: Spatial and temporal patterns of salinity and temperature at an intertidal groundwater seep, Estuar. Coast. Shelf Sci., 72, 283–298, https://doi.org/10.1016/j.ecss.2006.10.024, 2007.

Danielescu, S., MacQuarrie, K., and Faux, R.: The integration of thermal infrared imaging, discharge measurements and numerical simulation to quantify the relative contributions of freshwater inflows to small estuaries in Atlantic Canadae, Hydrol. Process., 23, 2847–2859, 2009.

DiGiacomo, P. M., Washburn, L., Holt, B., and Jones, B. H.: Coastal pollution hazards in southern California observed by SAR imagery: Stormwater plumes, wastewater plumes, and natural hydrocarbon seeps, Mar. Pollut. Bull., 49, 1013–1024, https://doi.org/10.1016/j.marpolbul.2004.07.016, 2004.

Donlon, C. J., Minnett, P. J., Gentemann, C., Nightingale, T. J., Barton, I. J., Ward, B., and Murray, M. J.: Toward Improved Validation of Satellite Sea Surface Skin Temperature Measurements for Climate Research, J. Climate, 15, 353–369, https://doi.org/10.1175/1520-0442(2002)015<0353:TIVOSS>2.0.CO;2, 2002.

Edet, A. E., Okereke, C. S., Teme, S. C., and Esu, E. O.: Application of remote-sensing data to groundwater exploration: A case study of the Cross River State, southeastern Nigeria, Hydrogeol. J., 6, 394–404, https://doi.org/10.1007/s100400050162, 1998.

Elhatip, H.: The use of hydrochemical techniques to estimate the discharge of Ovac1k submarine springs on the Mediterranean coast of Turkey, Environ. Geol., 43, 714–719, https://doi.org/10.1007/s00254-002-0668-y, 2003.

Fleury, P., Bakalowicz, M., and de Marsily, G.: Submarine springs and coastal karst aquifers: A review, J. Hydrol., 339, 79–92, https://doi.org/10.1016/j.jhydrol.2007.03.009, 2007.

Garcés, E., Basterretxea, G., and Tovar-Sánchez, A.: Changes in microbial communities in response to submarine groundwater input, Mar. Ecol. Prog. Ser., 438, 47–58, https://doi.org/10.3354/meps09311, 2011.

Garcia-Orellana, J., López-Castillo, E., Casacuberta, N., Rodellas, V., Masqué, P., Carmona-Catot, G., Vilarrasa, M., and García-Berthou, E.: Influence of submarine groundwater discharge on ^{210}Po and ^{210}Pb bioaccumulation in fish tissues, J. Environ. Radioact., 155–156, 46–54, https://doi.org/10.1016/j.jenvrad.2016.02.005, 2016.

Garcia-Orellana, J., Rodellas, V., Tamborski, J., Diego-Feliu, M., van Beek, P., Weinstein, Y., Charette, M., Alorda-Kleinglass, A., Michael, H. A., Stieglitz, T., and Scholten, J.: Radium isotopes as submarine groundwater discharge (SGD) tracers: Review and recommendations, Earth-Sci. Rev., 220, 103681, https://doi.org/10.1016/j.earscirev.2021.103681, 2021.

Garcia-Solsona, E., Garcia-Orellana, J., Masqué, P., Garcés, E., Radakovitch, O., Mayer, A., Estradé, S., and Basterretxea, G.: An assessment of karstic submarine groundwater and associated nutrient discharge to a Mediterranean coastal area (Balearic Islands, Spain) using radium isotopes, Biogeochemistry, 97, 211–229, https://doi.org/10.1007/s10533-009-9368-y, 2010.

Gerace, A. and Montanaro, M.: Remote Sensing of Environment Derivation and validation of the stray light correction algorithm for the thermal infrared sensor onboard Landsat 8, Remote Sens. Environ., 191, 246–257, https://doi.org/10.1016/j.rse.2017.01.029, 2017.

Gierach, M. M., Holt, B., Trinh, R., Jack Pan, B., and Rains, C.: Satellite detection of wastewater diversion plumes in Southern California, Estuar. Coast. Shelf Sci., 186, 171–182, https://doi.org/10.1016/j.ecss.2016.10.012, 2017.

Gumma, M. K. and Pavelic, P.: Mapping of groundwater potential zones across Ghana using remote sensing, geographic information systems, and spatial modeling, Environ. Monit. Assess., 185, 3561–3579, https://doi.org/10.1007/s10661-012-2810-y, 2013.

Kelly, J. L., Glenn, C. R., and Lucey, P. G.: High-resolution aerial infrared mapping of groundwater discharge to the coastal ocean, Limnol. Oceanogr. Meth., 11, 262–277, https://doi.org/10.4319/lom.2013.11.262, 2013.

Krest, J. M., Moore, W. S., Gardner, L. R., and Morris, J. T.: Marsh nutrient export supplied by groundwater discharge: Evidence from radium measurements, Global Biogeochem. Cy., 14, 167–176, https://doi.org/10.1029/1999GB001197, 2000.

Lee, E., Kang, K. M., Hyun, S. P., Lee, K. Y., Yoon, H., Kim, S. H., Kim, Y., Xu, Z., Kim, D. J., Koh, D. C., and Ha, K.: Submarine groundwater discharge revealed by aerial thermal infrared imagery: a case study on Jeju Island, Korea, Hydrol. Process., 30, 3494–3506, https://doi.org/10.1002/hyp.10868, 2016.

Luijendijk, E., Gleeson, T., and Moosdorf, N.: Fresh groundwater discharge insignificant for the world's oceans but important for coastal ecosystems, Nat. Commun., 11, 1260, https://doi.org/10.1038/s41467-020-15064-8, 2020.

Mallast, U., Siebert, C., Wagner, B., Sauter, M., Gloaguen, R., Geyer, S., and Merz, R.: Localisation and temporal variability of groundwater discharge into the Dead Sea using thermal satellite data, Environ. Earth Sci., 69, 587–603, https://doi.org/10.1007/s12665-013-2371-6, 2013.

Mallast, U., Gloaguen, R., Friesen, J., Rödiger, T., Geyer, S., Merz, R., and Siebert, C.: How to identify groundwater-caused thermal anomalies in lakes based on multi-temporal satellite data in semi-arid regions, Hydrol. Earth Syst. Sci., 18, 2773–2787, https://doi.org/10.5194/hess-18-2773-2014, 2014.

McCaul, M., Barland, J., Cleary, J., Cahalane, C., McCarthy, T., and Diamond, D.: Combining remote temperature sensing with in-situ sensing to track marine/freshwater mixing dynamics, Sensors, 16, 1402, https://doi.org/10.3390/s16091402, 2016.

Mejías, M., Ballesteros, B. J., Antón-Pacheco, C., Domínguez, J. A., Garcia-Orellana, J., Garcia-Solsona, E., and Masqué, P.: Methodological study of submarine groundwater discharge from a karstic aquifer in the Western Mediterranean Sea, J. Hydrol., 464–465, 27–40, https://doi.org/10.1016/j.jhydrol.2012.06.020, 2012.

Michael, H. A., Mulligan, A. E., and Harvey, C. F.: Seasonal oscillations in water exchange between aquifers and the coastal ocean, Nature, 436, 1145–1148, https://doi.org/10.1038/nature03935, 2005.

Moore, W. S.: The subterranean estuary: A reaction zone of ground water and sea water, Mar. Chem., 65, 111–125, https://doi.org/10.1016/S0304-4203(99)00014-6, 1999.

Moore, W. S.: The Effect of Submarine Groundwater Discharge on the Ocean, Annu. Rev. Mar. Sci., 2, 59–88, https://doi.org/10.1146/annurev-marine-120308-081019, 2010.

Moosdorf, N., Böttcher, M. E., Adyasari, D., Erkul, E., Gilfedder, B. S., Greskowiak, J., Jenner, A.-K., Kotwicki, L., Massmann, G., Müller-Petke, M., Oehler, T., Post, V., Prien, R., Scholten, J., Siemon, B., Ehlert von Ahn, C. M., Walther, M., Waska, H., Wunderlich, T., and Mallast, U.: A State-Of-The-Art Perspective on the Characterization of Subterranean Estuaries at the Regional Scale, Front. Earth Sci., 9, 95, https://doi.org/10.3389/feart.2021.601293, 2021.

Povinec, P. P., Aggarwal, P. K., Aureli, A., Burnett, W. C., Kontar, E. A., Kulkarni, K. M., Moore, W. S., Rajar, R., Taniguchi, M., Comanducci, J. F., Cusimano, G., Dulaiova, H., Gatto, L., Groening, M., Hauser, S., Levy-Palomo, I., Oregioni, B., Ozorovich, Y. R., Privitera, A. M. G., and Schiavo, M. A.: Characterisation of submarine groundwater discharge offshore south-eastern Sicily, J. Environ. Radioact., 89, 81–101, https://doi.org/10.1016/j.jenvrad.2006.03.008, 2006.

Rocha, C., Robinson, C. E., Santos, I. R., Waska, H., Michael, H. A., and Bokuniewicz, H. J.: A place for subterranean estuaries in the coastal zone, Estuar. Coast. Shelf Sci., 250, 107167, https://doi.org/10.1016/j.ecss.2021.107167, 2021.

Rodellas, V., Garcia-Orellana, J., Tovar-Sánchez, A., Basterretxea, G., López-Garcia, J. M., Sánchez-Quiles, D., Garcia-Solsona, E., and Masqué, P.: Submarine groundwater discharge as a source of nutrients and trace metals in a Mediterranean bay (Palma Beach, Balearic Islands), Mar. Chem., 160, 56–66, https://doi.org/10.1016/j.marchem.2014.01.007, 2014.

Rodellas, V., Garcia-Orellana, J., Masqué, P., Feldman, M., Weinstein, Y., and Boyle, E. A.: Submarine groundwater discharge as a major source of nutrients to the Mediterranean Sea, P. Natl. Acad. Sci. USA, 112, 3926–3930, https://doi.org/10.1073/pnas.1419049112, 2015.

Rosenberry, D. O., Duque, C., and Lee, D. R.: History and evolution of seepage meters for quantifying flow between groundwater and surface water: Part 1 – Freshwater settings, Earth-Sci. Rev., 204, 103167, https://doi.org/10.1016/j.earscirev.2020.103167, 2020.

Roy, D. P., Wulder, M. A., Loveland, T. R., C.E., W., Allen, R. G., Anderson, M. C., Helder, D., Irons, J. R., Johnson, D. M., Kennedy, R., Scambos, T. A., Schaaf, C. B., Schott, J. R., Sheng, Y., Vermote, E. F., Belward, A. S., Bindschadler, R., Cohen, W. B., Gao, F., Hipple, J. D., Hostert, P., Huntington, J., Justice, C. O., Kilic, A., Kovalskyy, V., Lee, Z. P., Lymburner, L., Masek, J. G., McCorkel, J., Shuai, Y., Trezza, R., Vogelmann, J., Wynne, R. H., and Zhu, Z.: Landsat-8: Science and product vision for terrestrial global change research, Remote Sens. Environ., 145, 154–172, https://doi.org/10.1016/j.rse.2014.02.001, 2014.

Ruiz-González, C., Rodellas, V., and Garcia-Orellana, J.: The microbial dimension of submarine groundwater discharge: current challenges and future directions, FEMS Microbiol. Rev., fuab010, 1–25, https://doi.org/10.1093/femsre/fuab010, 2021.

Schubert, M., Scholten, J., Schmidt, A., Comanducci, J. F., Pham, M. K., Mallast, U., and Knoeller, K.: Submarine groundwater discharge at a single spot location: Evaluation of different detection approaches, Water, 6, 584–601, https://doi.org/10.3390/w6030584, 2014.

Shaban, A., Khawlie, M., Abdallah, C., and Faour, G.: Geologic controls of submarine groundwater discharge: Application of remote sensing to north Lebanon, Environ. Geol., 47, 512–522, https://doi.org/10.1007/s00254-004-1172-3, 2005.

Tamborski, J., van Beek, P., Conan, P., Pujo-Pay, M., Odobel, C., Ghiglione, J. F., Seidel, J. L., Arfib, B., Diego-Feliu, M., Garcia-Orellana, J., Szafran, A., and Souhaut, M.: Submarine karstic springs as a source of nutrients and bioactive trace metals for the oligotrophic Northwest Mediterranean Sea, Sci. Total Environ., 732, 1–14, https://doi.org/10.1016/j.scitotenv.2020.139106, 2020.

Tamborski, J. J., Rogers, A. D., Bokuniewicz, H. J., Cochran, J. K., and Young, C. R.: Identification and quantification of diffuse fresh submarine groundwater discharge via airborne thermal infrared remote sensing, Remote Sens. Environ., 171, 202–217, https://doi.org/10.1016/j.rse.2015.10.010, 2015.

Taniguchi, M., Dulai, H., Burnett, K. M., Santos, I. R., Sugimoto, R., Stieglitz, T., Kim, G., Moosdorf, N., and Burnett, W. C.: Submarine Groundwater Discharge: Updates on Its Measurement Techniques, Geophysical Drivers, Magnitudes, and Effects, Front. Environ. Sci., 7, 1–26, https://doi.org/10.3389/fenvs.2019.00141, 2019.

Tcherepanov, E. N., Zlotnik, V. A., and Henebry, G. M.: Using Landsat thermal imagery and GIS for identification of groundwater discharge into shallow groundwater-dominated lakes, Int. J. Remote Sens., 26, 3649–3661, https://doi.org/10.1080/01431160500177315, 2005.

Trezzi, G., Garcia-Orellana, J., Rodellas, V., Santos-Echeandia, J., Tovar-Sánchez, A., Garcia-Solsona, E., and Maqué, P.: Submarine groundwater discharge: a significant source of dissolved trace metals to the North Western Mediterranean Sea. Marine Chemistry, Mar. Chem., 186, 90–100, https://doi.org/10.1016/j.marchem.2016.08.004, 2016.

Trezzi, G., Garcia-Orellana, J., Rodellas, V., Masqué, P., Garcia-Solsona, E., and Andersson, P. S.: Assessing the role of submarine groundwater discharge as a source of Sr to the Mediterranean Sea, Geochim. Cosmochim. Ac., 200, 42–54, https://doi.org/10.1016/j.gca.2016.12.005, 2017.

Tulipano, L., Panagopoulus, A., and Fidelibus, M. D.: Cost Action 621 "Groundwater management of coastal karstic aquifers", Final Report, EU Publications Office (OPOCE), 366, 2005.

U.S. Geological Survey: Landsat 8 (L8) Operational Land Imager (OLI) and Thermal Infrared Sensor (TIRS): Calibration Notices, available at: https://www.usgs.gov/core-science-systems/nli/landsat/landsat-8-oli-and-tirs-calibration-notices (last access: 15 February 2019), 2014.

Varma, S., Turner, J., and Underschultz, J.: Estimation of submarine groundwater discharge into Geographe Bay, Bunbury, Western Australia, J. Geochem. Explor., 106, 197–210, https://doi.org/10.1016/j.gexplo.2010.02.003, 2010.

Wang, L. T., McKenna, T. E., and Deliberty, T. L.: Locating Ground-Water Discharge Areas In Rehoboth And Indian River Bays And Indian River, Delaware Using Landsat 7 Imagery, available at: http://udspace.udel.edu/handle/19716/3174 (last access: 20 October 2020), 2008.

Wen-Yao, L., Field, R. T., Gantt, R. G., and Klemas, V.: Measurement of the Surface Emissivity, Remote Sens. Environ., 5, 97–109, https://doi.org/10.1016/0034-4257(87)90009-5, 1987.

Werner, A. D., Bakker, M., Post, V. E. A., Vandenbohede, A., Lu, C., Ataie-Ashtiani, B., Simmons, C. T., and Barry, D. A.: Seawater intrusion processes, investigation and management: Recent advances and future challenges, Adv. Water Resour., 51, 3–26, https://doi.org/10.1016/j.advwatres.2012.03.004, 2013.

Wilson, J. and Rocha, C.: Regional scale assessment of Submarine Groundwater Discharge in Ireland combining medium resolution satellite imagery and geochemical tracing techniques, Remote Sens. Environ., 119, 21–34, https://doi.org/10.1016/j.rse.2011.11.018, 2012.

Wloczyk, C., Richter, R., Borg, E., and Nueberts, W.: Sea and lake surface temperature retrieval from Landsat thermal data in Northern Germany, Int. J. Remote Sens., 27, 2489–2502, https://doi.org/10.1080/01431160500300206, 2006.

Worthington, S. R. H.: A comprehensive strategy for understanding flow in carbonate aquifers, Karst Model., 5, 30–37, 1999.

Wulder, M. A., Loveland, T. R., Roy, D. P., Crawford, C. J., Masek, J. G., Woodcock, C. E., Allen, R. G., Anderson, M. C., Belward, A. S., Cohen, W. B., Dwyer, J., Erb, A., Gao, F., Griffiths, P., Helder, D., Hermosilla, T., Hipple, J. D., Hostert, P., Hughes, M. J., Huntington, J., Johnson, D. M., Kennedy, R., Kilic, A., Li, Z., Lymburner, L., McCorkel, J., Pahlevan, N., Scambos, T. A., Schaaf, C., Schott, J. R., Sheng, Y., Storey, J., Vermote, E., Vogelmann, J., White, J. C., Wynne, R. H., and Zhu, Z.: Current status of Landsat program, science, and applications, Remote Sens. Environ., 225, 127–147, https://doi.org/10.1016/j.rse.2019.02.015, 2019.

Xing, Q., Braga, F., Tosi, L., Lou, M., Zaggia, L., Teatini, P., Gao, X., Yu, L., Wen, X., and Shi, P.: Detection of Low Salinity Groundwater Seeping into the Eastern Laizhou Bay (China) with the Aid of Landsat Thermal Data, J. Coast. Res., 74, 149–156, https://doi.org/10.2112/si74-014.1, 2016.

Zektser, I. S., Everett, L. G., and Dzhamalov, R. G.: Submarine Groundwater, CRC Press, Boca Raton, USA, 2006.

Science of the Total Environment 694 (2019) 133634

Contents lists available at ScienceDirect

Science of the Total Environment

journal homepage: www.elsevier.com/locate/scitotenv

How does water-reliant industry affect groundwater systems in coastal Kenya?

Nuria Ferrer [a,b,*], Albert Folch [a,b], Mike Lane [c], Daniel Olago [d], Jacob Katuva [e], Patrick Thomson [e], Sonia Jou [a,b], Rob Hope [e], Emilio Custodio [a,b]

[a] Department of Civil and Environmental Engineering (DECA), Universitat Politècnica de Catalunya (UPC), Jordi Girona 1-3, 08034 Barcelona, Spain
[b] Associated Unit: Hydrogeology Group (UPC-CSIC), Spain
[c] Rural Focus Ltd., Kenya
[d] Department of Geology, University of Nairobi, Kenya
[e] Smith School of Enterprise and the Environment, University of Oxford, United Kingdom

HIGHLIGHTS

- New water-reliant industries are becoming established on the East African coast.
- New methodology used to estimate abstraction in areas with uncertain or no abstraction data.
- Even after severe droughts, recharge recovers from current abstraction rates.
- The shallow aquifer that local communities rely on is less resilient to drought than the deep aquifer.
- Aquifer storage recovers the year after drought but groundwater quality does not.

GRAPHICAL ABSTRACT

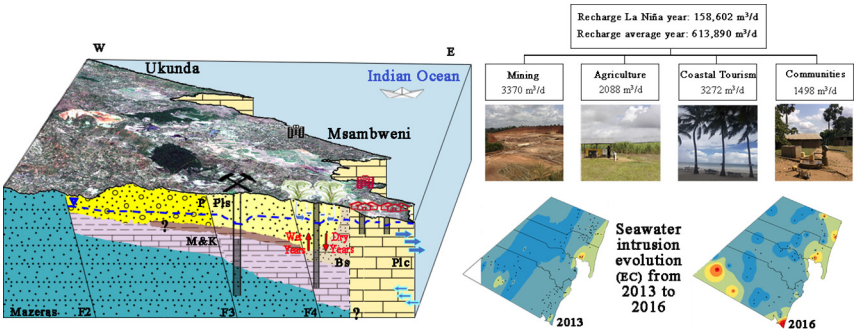

ARTICLE INFO

Article history:
Received 1 April 2019
Received in revised form 3 July 2019
Accepted 26 July 2019
Available online 03 August 2019

Editor: José Virgílio Cruz

Keywords:
Aquifer
Development
Coastal Kenya
Sustainability
Climate change

ABSTRACT

The industrialization process taking place in Africa has led to an overall increase in groundwater abstraction in most countries in the continent. However, the lack of hydrogeological data, as in many developing countries, makes it difficult to properly manage groundwater systems. This study presents a real case study in which a combination of different hydrogeological tools together with different sources of information allow the assessment of how increased competition for water may be affecting groundwater systems by analysing the sustainability of new abstraction regimes under different real climatic condition (before, during and after La Niña 2016). The area where this approach has been applied is Kwale County (in Coastal Kenya) in a hydrogeological context representative of an important part of the east coast of the continent, where new mining and agriculture activities co-exist with tourism and local communities. The results show that the lack of aquifer systems data can be overcome, at least partly, by integrating different sources of information. Most of the time, water-reliant users collect specific hydrogeological information that can contribute to defining the overall hydrogeological system, since their own main purpose is to exploit the aquifer with the maximum productivity. Therefore, local community water usage, together with different stakeholder's knowledge and good corporate water management act as a catalyst for providing critical data, and allows the generation of credible models for future groundwater management and resource allocation. Furthermore, complementary but simple information sources such as in situ interviews, Google Earth, Trip Advisor and easy-to use analytical methods that can be applied in the African context as

* Corresponding author at: Department of Civil and Environmental Engineering (DECA), Universitat Politècnica de Catalunya (UPC), Jordi Girona 1-3, 08034 Barcelona, Spain.
E-mail address: nuria.fr.ramos@gmail.com (N. Ferrer).

https://doi.org/10.1016/j.scitotenv.2019.133634

in many developing countries, and enables groundwater abstraction to be estimated and the sustainability of the aquifer system to be defined, allowing potential future risks to be assessed.

1. Introduction

The exploitation of groundwater generates different types of negative externalities (Giannoccaro et al., 2017): (i) reduced availability of the resource for other current or future uses; (ii) increase in extraction costs; (iii) possible risk of water quality degradation; and (iv) damage to groundwater dependent ecosystems. If the exploitation of groundwater occurs close to the coastline, other negative externalities and costs are generated: (i) reduced groundwater supply due to enhanced corrosion and well failure; (ii) health problems, (iii) negative effects on agriculture, since crop, land quality and cropping area potentially decline (SASMIE, 2017).

Anticipated increases in abstraction must be considered together with the expected increase in droughts in dry periods and precipitation in wet periods (Solomon and Qin, 2013; Stocker et al., 2013). Climate change will affect hydrogeological system dynamics and their water resources quality (Mas-Pla and Menció, 2018). For example, aquifer recharge reduction caused by climate change is an important factor in aquifer salinization (Oiro and Comte, 2019). The increased abstraction is poorly compatible with the sustainable use of coastal aquifers where there is a high population density and where tourism is concentrated (Dhar and Datta, 2009; Mantoglou, 2003; Okello et al., 2015), since the use of coastal groundwater is compromised by salinization (Michael et al., 2017). Many coastal aquifers in the world are currently experiencing intensive saltwater intrusion (SWI) caused by both natural and man-induced processes (Custodio, 2010; De Filippis et al., 2016a, 2016b; SASMIE, 2017; Werner et al., 2013).

In the last couple of decades many African countries have seen unprecedented economic growth rates, and this has drawn the region into the global limelight (World Bank, 2013). This growth has led to an increase in groundwater abstraction in most African countries (Adelana and MacDonald, 2008). The drilling of new deep boreholes with higher abstraction rates than traditional dug wells or shallow borehole handpumps has increased in many areas to meet the water demands of these new economic activities (Comte et al., 2016).

The high socio-economic and ecological importance of groundwater and the fact that groundwater is an important strategic resource are recognised throughout developing countries. A study by Pavelic et al. (2012) emphasizes that data on groundwater systems throughout Sub-Saharan Africa SSA are sparse, so the current state of knowledge creates a barrier to sustainable groundwater development. In order to define realistic local management policy it is essential to understand groundwater use and users. One of the major challenges to proper governance is lack of scientific and general (social, economic, environmental among others) knowledge about aquifers. Without an adequate general understanding of aquifers, actors may not properly identify the source of aquifer pollution or depletion and may be prone to blaming each other for mismanagement (IGRAC, 2019). Thus, in the absence of coordinated efforts to manage aquifers, it is unlikely that any advanced understanding will be achieved. This paradox is the crux of the groundwater governance challenge and perhaps explains why effective groundwater governance regimes are still elusive today.

Therefore, key aquifers need urgent characterization to change the current situation, in which development proceeds with insufficient aquifer knowledge (Olago, 2018). One of the main challenges when studying these aspects in developing countries is the lack of information, especially with respect to abstraction data and the location of abstraction well fields, in order to determine the possible future impacts at the local and/or regional scale on groundwater systems. To the knowledge of authors, there are no studies that determine the effects of new abstractions in relation to current economic growth in Africa.

Hence the aim of this study is to present a real case study in which a combination of different hydrogeological tools together with different sources of information allow the assessment of how increased competition for water may be affecting groundwater systems by analysing the sustainability of new abstraction regimes under different real climatic conditions. The coastal area of Kwale (Kenya coast) has been selected as a unique case due to: 1) local communities co-exist with tourist activity in the coast and new water-reliant industries established since 2012, representative of what is happening in many areas of the continent; and 2) this area presents a hydrogeological context representative of an important part of the East coast of the continent. Furthermore, aquifer sustainability has been assessed during a drought period caused by the 2016 La Niña event and during the following recovery period after the significant rains of 2017.

The approach presented looks to avoid repeating the errors made in many areas worldwide, such as in the Mediterranean basin, where some coastal aquifers were salinized decades ago by tourism, industrial and agricultural groundwater abstraction and where local economies suffered the consequences, costs and expense of developing the new water sources that were required (SASMIE, 2017). In this regard, some final remarks are made considering the socio-economical and institutional situation in many parts of the Africa continent.

2. Methods

2.1. Application area

The 660 km^2 study site is located in Kwale County, on Kenya's southern coast, around 50 km south of Mombasa; it had a 2013 population of around 730,000 (Commission on Revenue Allocation, 2013). The majority (82%) of Kwale's inhabitants live in rural areas in small and scattered communities. The coastal areas host urban communities, including Ukunda, Msambweni and Diani. Most of the local economy is based on small-scale agriculture.

Protected wells and boreholes are accessed by more than a fifth of the county's populace and 43% of households use an improved drinking water source (Foster and Hope, 2016). There are around 300 handpumps providing drinking water to local communities, schools and healthcare centres scattered across the study area. These handpumps are used daily by the population to fill buckets for different purposes, such as drinking and domestic water uses. The coastal strip has a long established coastal tourism industry at Diani. Most of the hotels are located in the coastal area in the north of the study area. Furthermore, the Ukunda area has many private homes that have their own shallow well or borehole. In the last two decades, the acquisition of small parcels of land has increased in this area to build bungalows/maisonettes for which the source of water for construction and supply is often groundwater.

Since 2012, two new, major economic activities have been established in Kwale County, increasing the pace of environmental, economic and social change in the area. One is the country's largest mining operation: the Kwale Mineral Sands Project, operated by Base Titanium Ltd. (Base). The other is irrigated sugarcane by the Kwale International Sugarcane Company Limited (KISCOL). Water demand for both companies is met by a combination of surface and groundwater.

The Special Mining Lease operated by Base Titanium cover 1661 ha. The Project resource comprises two dunes that contain economically

viable concentrations of heavy minerals. These two areas are separated by the Mkurumudzi River (Fig. 1). Mine construction was completed at the end of 2013 and the first bulk shipment of mineral departed from Mombasa in February 2014. Projected 2019 production is up to 450,000 t of ilmenite; 93,000 t of rutile (14% of the world's rutile output); and 37,000 t of zircon. The total mineral resource on 30th June 2018 was estimated to be 134 million t.

Currently KISCOL's sugarcane fields occupy a total area of 5500 ha, of which 4100 ha has been put to cultivation of sugarcane since 2008; 800 ha are currently under sub-surface drip irrigation (www.kwale-group.com). The fields are located in the Kinondo, Milalani/Shirazi and Nikaphu areas, the last one being located south of the study area (Fig. 1). The factory has the capacity to crush 3000 t of cane per day and it is projected to produce 3500 t/day of sugar at full capacity, self-generating 18 MW of electricity in a bagasse-fired power plant, and producing around 50,000 L/day of ethanol (http://www.kwale-group.com). The planned area for irrigated (not rain-fed) sugar at KISCOL is 3000 ha, to be achieved when all dams and the bulk water system (BWS) is completed in the coming years.

The study area is divided into 4 zones (Fig.1) that represent the areas where each economic activity takes place. Zone 1 covers the area where the sugar fields irrigated with groundwater from in-situ boreholes are located; Zone 2 includes the mine and its well field; Zone 3 is the area where the sugar fields are irrigated with surface water from the Mtawa River but not from boreholes; and Zone 4 includes the area where most of the hotels are located.

2.1.1. Climate

The area experiences a bimodal rainfall pattern: 1) "long rains" generally fall from April to June (AMJ), and "short rains" occur between October and December (OND) (CWSB, 2013). The driest months on the coast are those from January to March (JFM). The precipitation range is between 900 and 1500 mm/year and the average temperature is about 26.5 °C (County Government of Kwale, 2013). In recent years, from 2012 to 2017, the average rainfall was 1145 mm/year. Rainfall in 2013 (1286 mm) and 2017 (1265 mm) were close to the average whilst 2014 (1604 mm) and 2015 (1345 mm) were well above, and 2012 (711 mm) and 2016 (636 mm) were both well below the average. From May 2016 to early 2017, the study area experienced unusually dry conditions. Local weather data (Kwale Agricultural Department Station KMD 9439001 in Kwale) suggest that this period represents one of the most extreme droughts since 1974 in this area (Ferrer et al., 2019).

2.1.2. Hydrogeology

The region is physiographically divided into three units, from inland to the coast: the Coast Range (Shimba Hills) in the west, with elevations ranging from 366 to 454 m a.s.l (above mean sea level); the Foot Plateau from 60 to 137 m a.s.l., and the Coastal Plain, generally below 50 m a.s.l. (Fig. 2).

The conceptual model of the groundwater system has been defined in detail in Ferrer et al. (2019). This aquifer system comprises two hydrogeological systems: a shallow aquifer composed of young geological materials, including silicate sands (Pliocene Fm.) and carbonates, corals and sands (Pleistocene Fm.), and a deep aquifer composed of older materials, mainly sandstones (Jurassic and Triassic) which crop out in the western part of the area in the Shimba Hills range. The shallow aquifer thickness is 25 m thick and the deep aquifer is around 350 m thick (ISGEAG, 2019). The hydrochemical facies and the water isotopic composition indicate that there is hydraulic connectivity across the materials that comprise the shallow aquifer. The same data show that the Mazeras sandstones in the Shimba Hills are hydraulically connected with the deep aquifer.

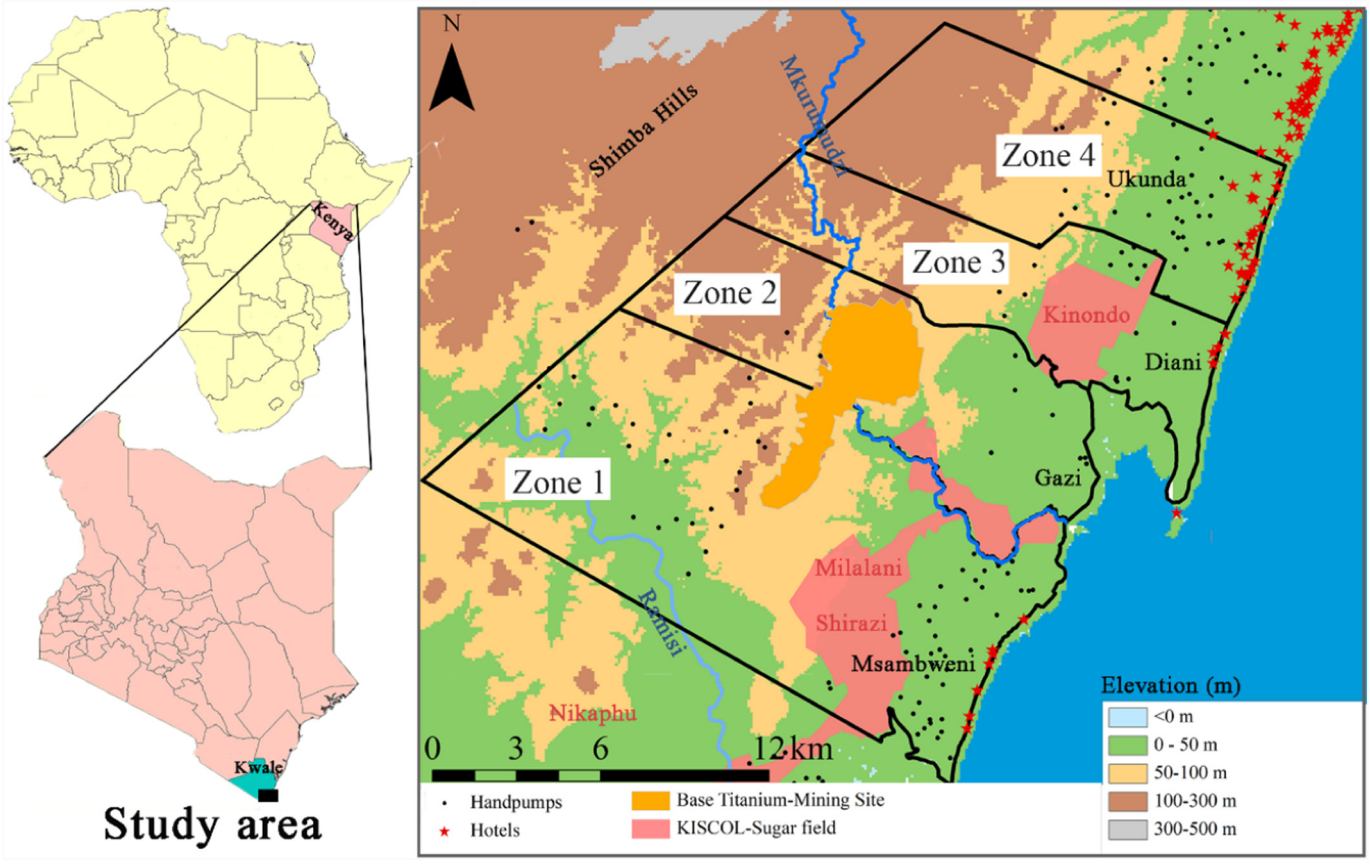

Fig. 1. Location of the study area, which is divided into four zones according to the different economic activities present: 1) includes the larger part of KISCOL's Milalani fields and a part of the mine; 2) includes Base Titanium mining facilities; 3) includes KISCOL's Kinondo fields; and 4) includes the major proportion of hotels and private plots.

The Kilindini sands and coral limestone form the major part of the shallow aquifer in the study area. The deep aquifer acts as a confined unit due to the presence of a very low permeability aquitard emplaced between the young and old materials. This confined aquifer is disrupted across the area by two in-filled palaeochannels perpendicular to the coast (in Zones 1 and 3) that enhance the connectivity between the shallow and deep aquifer in each of these zones. These palaeochannels are filled with sedimentary and re-worked fluvio-deltaic materials.

The shallow aquifer is directly recharged by local rain through the ground surface and the deep aquifer is recharged laterally from the Shimba Hills where it outcrops. The discharge of both aquifer systems is at the littoral zone of the Indian Ocean (Fig. 2). Equipotential lines of the shallow aquifer show that the groundwater flow direction is from the Shimba Hills to the Indian Ocean (Fig. 2). The potentiometric map and the hydrochemistry indicate that the Ramisi (Zone 1) and Mkurumudzi (Zone 2) Rivers are gaining streams, receiving water from the aquifer, at least in their upper parts (Ferrer et al., 2019).

2.2. Estimation of the water budget with lack of data

2.2.1. Recharge estimation

In order to assess the sustainability of the aquifer system during the 2016 La Niña drought and the recovery period in 2017, the total recharge to the aquifers of the study area needs to be known, as it is the main input to the system (Ferrer et al., 2019). The recharge was calculated following the methodology presented in Ferrer et al. (2019), based on the soil water balance for the period 2010–2017. As the resolution of the geological map is not the optimal to obtain proper recharge estimation, the soil and terrain database for Kenya (KENSOTER) was used as the principal data source to define the soil properties for the study area. The information of the soil map has been correlated with the geological map and validated with several field samples in different locations across the study area.

In that study, groundwater recharge was calculated for each land cover type and each soil type, following the process presented in the supplementary material. Rainfall data and meteorological parameters were obtained from three different stations for the period 2010–2015. At the end of 2015, 11 manual rain gauge stations were established across the study area. These new data improved the accuracy of recharge estimation. During 2016–2017, temperature data were obtained from the Trans-African HydroMeteorological Observatory (TAHMO) stations (www.tahmo.org) (Fig. 3).

2.2.2. Current and future abstraction estimation

One of the main challenges when studying this type of area is the lack of information, especially abstraction data and the location of production boreholes. Depending on the abstraction data available in a specified area, different methodologies can be applied. The abstraction data accuracy will depend on the information source used.

In the study area, it proved very helpful to integrate information from the Water Resources Authority (WRA) and from groundwater users in the area (particularly the mining and sugar companies). The abstraction permits for each economic activity were obtained from the Water Resources Authority (WRA). The WRA data comprised the permitted daily well/borehole abstraction volumes for individual consumers and companies, such as Base, KISCOL, the hotels in the South Coast, and community boreholes. However, not all the abstraction data from the different water users have the same accuracy.

Base Titanium provided daily abstraction data from the end of 2013 to 2017. These actual abstraction estimates are very accurate.

Unlike Base Titanium, KISCOL's actual abstraction rates were not available. However, the company report that they control drip irrigation by means of soil humidity sensors to conserve water. Therefore, KISCOL's estimated monthly abstraction is based on soil evaporation deficit (ETD). The ETD is the difference between potential evapotranspiration and actual evapotranspiration under natural conditions, which gives the minimum amount of irrigation water required to maintain

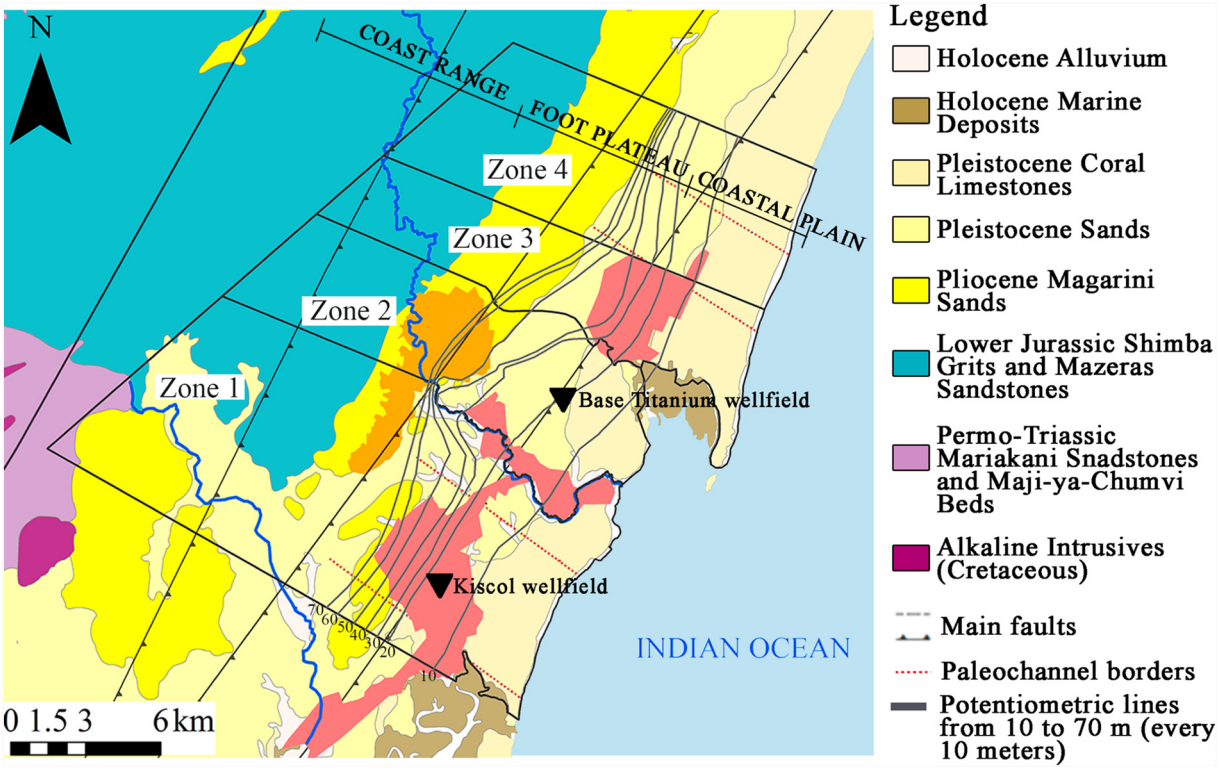

Fig. 2. Geological map with the main faults and the two palaeochannels (red dotted lines) shown. Potentiometric contours measured in the March 2016 field survey. The triangles indicate the locations of the wellfields developed by Base Titanium and KISCOL (Milalani area). (For interpretation of the references to colour in this figure legend, the reader is referred to the web version of this article.)

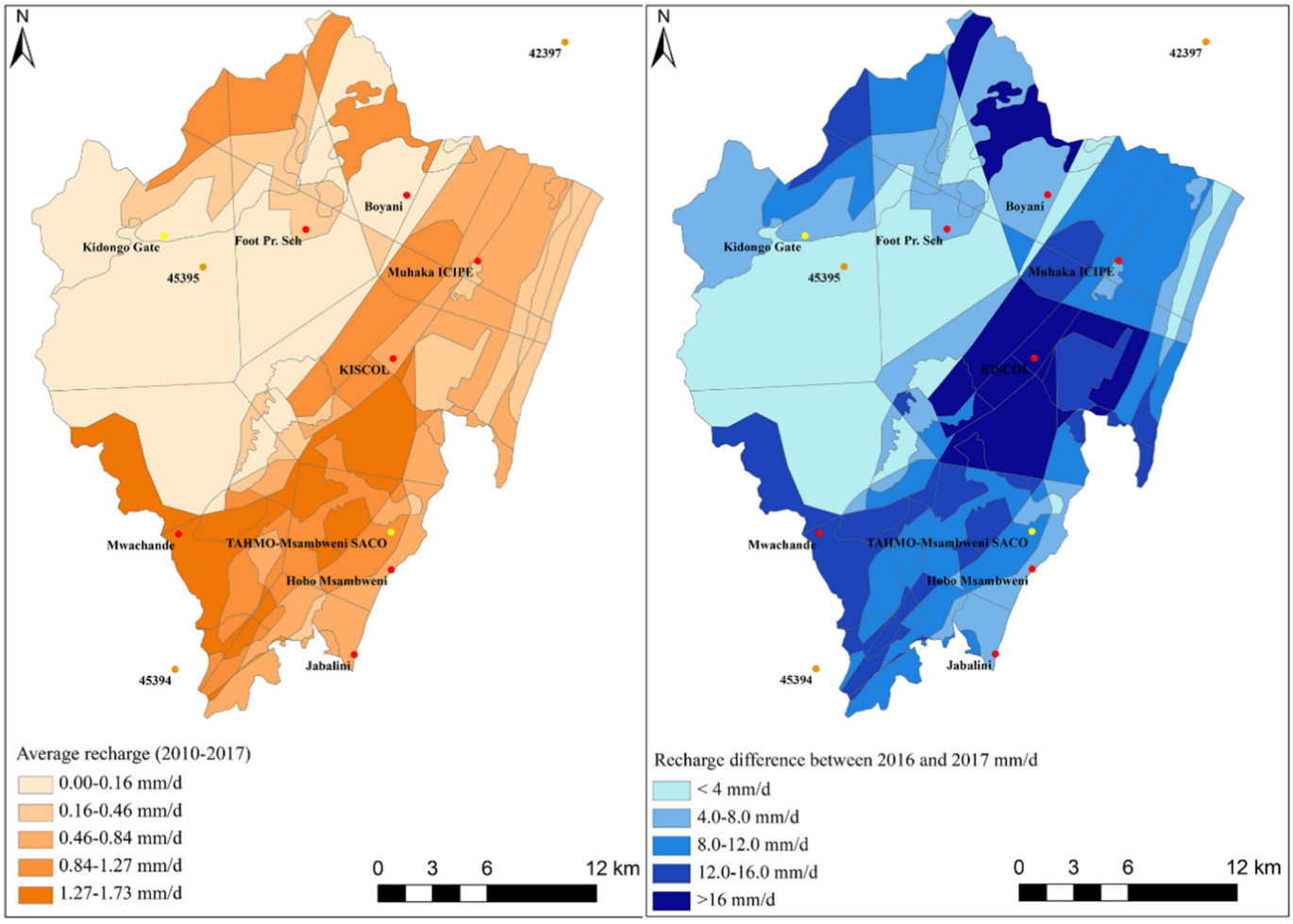

Fig. 3. (Left) Average recharge from 2010 to 2017 in mm/d. (Right) Recharge difference between La Niña (2016) and a normal climatic year (2017). The coloured dots are the meteorological stations used to calculate the net recharge. (For interpretation of the references to colour in this figure legend, the reader is referred to the web version of this article.)

the soil moisture that allows the crop to get the water it needs. Multiplying the ETD by the KISCOL irrigation area, the minimum crop water requirement (MCWR) is obtained.

Observed groundwater abstraction was available for only one hotel located at the coast in Zone 4. Therefore, a complementary estimate of hotel abstractions using other data sources was made. Hotel locations, both those with and without WRA permit data, were obtained from Google Earth. The number of rooms for each hotel and the hotels' class were collected from the TripAdvisor webpage. Total groundwater volume consumed by hotels was estimated using the consumptions specified in the Practice Manual for Water Supply Services in Kenya (2005) for each type of hotel, assuming a water use of 600 L/day per bed for high class hotels and 300 L/day per bed for medium class. For 35% of the hotels identified from Google Earth, interviews with hotel managers validated consumption data. The Kenya National Bureau of Statistics (KNBS) provided bed occupancy data for the South Coast 2015 to 2017. Despite hotel abstraction data not having the same degree of accuracy as Base Titanium data, using this methodology it is possible to estimate the order of magnitude of hotel abstraction.

The average abstraction of the community handpumps was obtained from Water point Data Transmitters (WDTs), which provide reliable real-time data on handpump usage (Thomson et al., 2012). Using a low cost integrated circuit (IC) based accelerometer, the WDT automatically monitors the number of strokes made in operating a handpump and then transmits this information to a computer over the GSM network. Volumetric abstraction was calculated from the accelerometer data for the period 2014–2015. These data provide information on hourly pump use.

The abstraction of the water-reliant industries will increase in the near future; Base Titanium planned to drill more boreholes within the same wellfield, thus increasing the total groundwater abstracted. In the absence of any better estimates, we arbitrarily assumed a 20% increase in groundwater abstraction for irrigated sugar. The Draft Kwale Water Master Plan has assumed a 1% growth per year in water demand for the tourism sector over the next 20 years. In order to supply more water to the population, the Water Supply Master Plan (2018) for Mombasa and other towns within the Coast Province (CWSB, 2016) has proposed developing the Msambweni wellfield to meet future demand for the middle and south coast zones. This is the considered future scenario for groundwater abstraction.

2.2.3. Groundwater levels and quality data

Groundwater levels and quality data, such as field physicochemical parameters (pH, temperature, electrical conductivity …), are easy and cheap to obtain in countries with lack of data. Therefore, it is relevant to create a monitoring network managed by local people with low cost in order to obtain hydrogeological data for a specified period to evaluate changes under different climatic conditions.

In order to assess the possible effects of the water-reliant industries on the groundwater system, hydrochemical field data obtained during the La Niña event in 2016 from Ferrer et al. (2019) were used.

In order to study the aquifer recovery after the La Niña event in the study area, the groundwater level and electrical conductivity (EC) of 23 points were measured in Magarini sands, Kilindini sands and the Pleistocene corals every two weeks, with a groundwater level range from 4 m bgl to 27 m bgl (below ground level) after the La Niña event (April 2017), until December 2017. These points are part of a monitoring network in which groundwater levels and physicochemical parameters were measured every two weeks. Fortnightly groundwater levels of 35 piezometers measured by Base Titanium in its monitoring network (2012–2017) have also been used to study the aquifer response as well as the potential interaction between the shallow and the deep aquifer during the study period.

To represent EC evolution in the study area, this information was mapped for each of the seven field surveys using ArcGis 10.0 software, and the hydrogeochemical analysis tool QUIMET (Velasco et al., 2014). To represent the spatial distribution of the variables, the Inverse Distance Weighting (IDW) method was used, which is a deterministic method that allows multivariate interpolation from a set of known scattered points. The EC data were obtained from different wells measured during the field surveys carried out in the study area in September 2013, March 2014, June 2014, March–May 2015, and September 2015. The physiochemical parameters measured in situ were temperature, pH and EC_{25} (electric conductivity at 25 °C) by means of a Hanna Instruments meter.

In order to understand the geochemical processes occurring in the area affected by seawater intrusion (SWI), a geochemical modelling exercise was carried out to understand the long-term evolution in this geological context and the potential impacts of SWI dynamics. Given the composition of the Pleistocene corals, different geochemical models considering several conceptual hydrogeological models were generated to understand which reactions are taking place, to what extent, under which conditions, and how water quality and aquifer mineralogy could change due to SWI.

PHREEQC software was used to simulate the mixing between fresh groundwater located inland in the Pleistocene formation with EC < 1000 μS/cm and one sample from the saline water upwelling on the beach (Diani), which is 83% seawater according to chloride concentration (Table 1. Supplementary material). A total of 20 mixed waters were simulated.

3. Results

This section presents all the results analysed in order to determine the sustainability of the groundwater system. First of all, the recharge from 2010 to 2017 and its change is assessed, since it is the main water input of the system and key to understanding the water budget. Secondly, abstraction for each groundwater use is estimated and used as outputs from the groundwater system. In the third component, the groundwater level evolution is analysed as the main indicator of storage changes in the system, showing the relationship between system inputs and outputs. To evaluate the system in the coastal zone, where groundwater quality plays an important role in the sustainability of the system, the evolution of electrical conductivity (as a proxy for salinity) is analysed. Finally, the results of the geochemical models, which are needed to understand the geochemical processes occurring in the area affected by seawater intrusion, are also presented.

Table 1
Rainfall and temperature data from different meteorological stations used to calculate groundwater recharge. The location of each station is shown in Fig. 3.

Rainfall & temperature 2010–2015	Rainfall from manual rain gauge station 2016–2017	Temperature 2016–2017
SWAT N° 45395	Boyani station Footprints Kidongo gate KISCOL Muhaka ICIPE Mwachande	TAHMO Kidongo gate
SWAT N° 45394	KISCOL Muhaka	TAHMO Msambweni SACO
SWAT N° 42397	Hobo Msambweni Jabalini KISCOL Mwachande	TAHMO Msambweni SACO

3.1. Recharge

Total recharge volume was calculated for an area of 660 km^2. This area is bigger than the four study Zones (Fig. 1), covering the recharge area of the shallow and deep aquifers from the sea to the Shimba Hills (Ferrer et al., 2019). While the shallow aquifer is recharged directly from the surface, the underlying deep aquifer is recharged from the Shimba Hills. To estimate recharge across the study area, 123 soil water balances were calculated (Fig. 3).

The spatial distribution of recharge follows the rainfall spatial pattern. Higher recharge occurs near the coast and decreases inland, west of Shimba Hills. However, in the eastern Shimba Hills (around 450 m a.s.l., see Fig. 1) recharge is higher. The highest average recharge volume for the period 2010–2017 occurred in areas underlain by ferralic arenosols, which have low usable soil water reserves (UR). Some areas overlying the shallow aquifer in the Kilindini and Magarini sands also have this type of soil. On the contrary, lower average recharge occurs in areas with high UR ferric acrisols. These soils are mainly located on the Mazeras sandstone, in the Shimba Hills.

The total recharge during La Niña in 2016 was $58 \cdot 10^6$ m^3/year, 74% less compared to 2017 ($224 \cdot 10^6$ m^3/year). A comparison of recharge during La Niña with previous years (Table 2) shows that there is minimal correlation between total annual rainfall and total annual recharge. This is because the rainfall intensity and distribution through the year influences net recharge, rather than the total annual volume of rainfall. High rainfall peaks produced by intense but short storms are more effective in driving recharge than lower, more continuous rainfall. An intense rainfall event (>100 mm) on a saturated catchment leads to intense and significant recharge. This is consistent with other studies on the phenomenon (Taylor et al., 2012; Taylor and Jasechko, 2015). The recharge volume represents 7% of the annual rainfall in the driest years, but up to 23% in 2017.

3.2. Groundwater use by water-reliant industry

In this sub-section we present a detailed description of each water-reliant user in the area and its abstraction rate estimate.

3.2.1. Base Titanium Ltd

The mining company constructed and commissioned an 8.4 10^6 m^3 water supply dam on the Mkurumudzi River to meet most of its water requirements for mining. This supply is backed up by a wellfield comprising four, 95–105 m deep boreholes. At the end of 2013, both surface and groundwater were abstracted to start the mine. The average

Table 2
Annual precipitation in mm/year obtained from the different meteorological stations located in the study area (Table 1) and the annual recharge volume in 10^6 m^3/year.

Year	Precipitation (mm/year)	Recharge (10^6 m^3/year)
2010	1022	71
2011	1406	160
2012	987	50
2013	1154	86
2014	1715	156
2015	1757	169
2016	867	58
2017	1442	224

groundwater abstraction for a "normal climate year" such as 2014 and 2015 was 1449 and 1806 m^3/day, respectively. However, during the 2016 La Niña event, this abstraction increased by around 66% to 4272 m^3/day on average (Table 3). After the La Niña event, the daily average abstraction fell by around 26% (3370 m^3/d) in 2017, compared to 2016 (Fig. 4). It should be pointed out that Base Titanium recycles a considerable proportion of process water: in 2016, it recycled >70% of the total daily water use. It improved in 2017, recycling around 78%.

The mine site is located on the Pliocene formation but the Base wellfield is on the Kilindini sands (Pleistocene) east of the mine (Fig. 2). These production wells are screened in the deep aquifer, to ensure that groundwater is pumped only from the Jurassic and Triassic formations. This was a deliberate design philosophy to reduce as much as possible adverse effects to the shallow aquifer that local communities use for water supply.

Adjacent to each operational borehole a shallow and deep monitoring piezometer measures the groundwater level fluctuations under baseline conditions and due to subsequent abstraction. Under natural conditions before abstraction started in 2013, the deep groundwater levels were higher than the shallow groundwater levels as the piezometric control area of the confined deep aquifer is at a higher elevation, in the Shimba Hills. Once abstraction started at the end of 2013, the shallow piezometric trend shows a limited effect from pumping from the deep aquifer, maintaining the hydraulic relationship between the shallow and deep aquifer, except sporadically due to occasionally higher abstraction rates, as in April 2014 (Fig. 4). However, during the dry year of 2016 (the La Niña event), some deep boreholes had a piezometric level below the shallow aquifer groundwater level.

Since 2013, Base Titanium has also monitored the groundwater quality in its production boreholes and some shallow and deep community wells spread around the mine. The hydrochemical composition of the pumped water from 2013 to the present (data not shown, Base Titanium monitoring network) indicates that there is no significant change in groundwater quality in the groundwater pumped from the deep aquifer, even during the La Niña event. The EC values measured in the inland deep community wells monitored by Base Titanium have been <1500 μS/cm from 2012 until the present.

3.2.2. KISCOL sugar fields

KISCOL uses different water sources to meet sugarcane water demand. Its water demand depends on the crop water requirements of the sugar plant. As expected, the minimum crop water requirement (MCWR) is higher during the driest months, with an average of 40,784 m^3/day from January to March and 28,349 m^3/day for the wet period (April to June).

Groundwater is obtained from up to 17 boreholes, 60–100 m deep, drilled in and spread across the sugar fields. According to WRA, KISCOL has been allocated a total of 10,535 m^3/day from 12 production boreholes. However, information available indicates that only eight boreholes are currently operational, so actual groundwater abstraction is probably lower than the WRA allocation. These eight boreholes are operational (since mid-2015), and are located in the Milalani fields (Zone 1, Fig. 1). The Kinondo fields are irrigated by surface water (Zone 3, Fig. 1) as the borehole pumps are not connected to power lines and electrical generators have been vandalized. Pumped groundwater is stored in one-day storage lagoons, together with water coming from the dams, which is the other water source for sugar irrigation. Groundwater acts as a strategic water reserve; volumes used are small compared with water from dams. According to current WRA rules, the maximum volume that may be pumped is 60% of the well test discharge rate over a ten-hour pumping day. It means that the mean estimated abstraction rate for the eight KISCOL boreholes is 2088 m^3/day (Table 3). This value is in accordance with the KISCOL test yields for these eight boreholes and it is in the same range as other unpublished data from KISCOL.

KISCOL wells are multi-screened, taking water from multiple water-bearing zones in the shallow and deep aquifer units. This well design increases the yield but produces a mix of groundwater from aquifer levels, as shown by the isotopic and hydrochemical composition (Ferrer et al., 2019). Therefore, this screen configuration may facilitate the entrance of contaminated water from the shallow aquifer towards the deep one, contrary to the Base Titanium boreholes which are only screened in the deep aquifer.

Water quality was measured within KISCOL's Milalani plantation in a monitored borehole at different depths in the June 2016 field survey (Ferrer et al., 2019). The most significant result was the measured nitrate concentration in this borehole: 48 mg/L at 21 m bgl and 31 mg/L at 65 m bgl, as NO_3. Furthermore, a well located at Nikaphu, south of the study area, had 1.2 mg/L of ammonia, as NH_4, during the March 2016 field campaign. Taking into account that groundwater has an Eh of +239.4 mV and dissolved oxygen of 1.42 mg/L, the relatively high ammonia content indicates that the sample is not in chemical equilibrium. This shows a relatively fast recirculation of shallow groundwater around the pumping well. Currently, there are no nitrate polluted shallow wells around the KISCOL Mililani fields. Conversely, in the Kinondo fields (Zone 3), where sugar is irrigated only with surface water, there is only one point at the outflow from the end of the fields that is polluted by nitrates, at 73 mg/L NO_3 in June 2016.

3.2.3. Tourism

From the data obtained from Google Earth, 85% of the hotels located on the coast are located in Zones 3 and 4 on the Diani coast, with only a few situated on the Msambweni coast in Zones 1 and 2 (Fig. 1).

The highest tourism season is from October to March and the lowest from April to July. Hotel water use is closely associated with the number of tourists, so both intra- and inter-annual abstraction varies considerably (Fig. 5). Most hotels use water from private boreholes, from which large volumes of water are withdrawn using electrical and/or

Table 4
Hotel groundwater abstraction (m^3/d) based on different information sources.

Source	Kind of data	Number of points with available data	Abstraction (m^3/day)
WRA	WRA allocation permits	29	2760
Hotels	Answer direct from the Hotels	38	1809
Estimate	Google Earth + Trip Advisor + Manual for Water Supply Services	91	3272

Table 3
The allocated and the actual or estimated groundwater abstraction for each water user. Hotel groundwater use marked with (*) is based on Table 4.

Period	Recharge (m^3/d)	Groundwater abstraction (m^3/d)				
		Base titanium	KISCOL	Hotels	Handpumps	Community boreholes
Dry year: La Niña 2016	158,602	Current: 4272 Allocated: 5280	Current: 2088 Allocated: 2528	3272*	450	991
Recovery/average year: 2017	613,890	Current: 3370 Allocated: 5280				
Future abstraction		8800	9504	3926	540	11,500

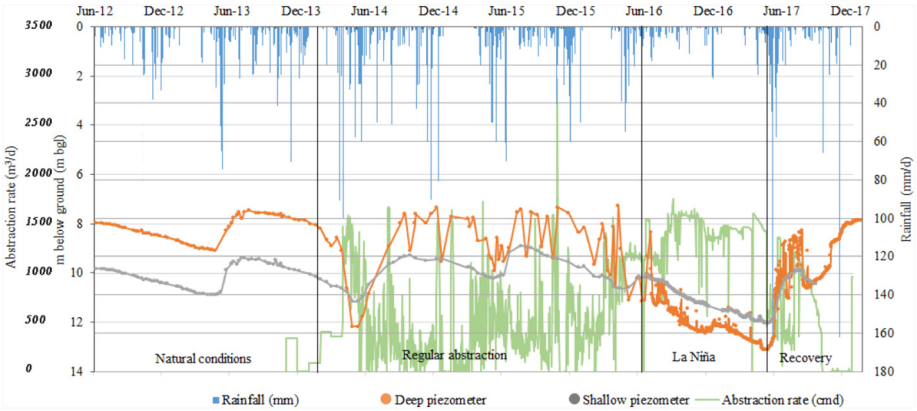

Fig. 4. Comparison between shallow and deep groundwater levels of piezometers located near a production borehole recorded by Base Titanium. Black vertical lines indicate the hydraulic relationship between the shallow and the deep aquifer under different conditions: 1) "Natural conditions" refers to groundwater levels when the wellfield was not intensively pumped before October 2013; 2) "regular abstraction" shows the shallow and deep groundwater levels once the deep aquifer exploitation started; 3) "La Niña" shows the groundwater levels during the drought period caused by the La Niña event in 2016/2017 and 4) "Recovery" refers to the recovery of the aquifer hydraulic relationship after the rains of April 2017. Rainfall volume data is from Kwale Agricultural Department station (Kenya Meteorological Department) (mm/d). The green line shows Base Titanium groundwater abstraction as m^3/d. (For interpretation of the references to colour in this figure legend, the reader is referred to the web version of this article.)

diesel driven pumps. The groundwater abstraction points that support this economic activity are located near the coast, mainly exploiting the shallow aquifer located in the Pleistocene corals formation (Fig. 1). Using both Google Earth and Trip Advisor it was possible to identify 109 hotels and obtain the number of rooms for 91 hotels. Personal interviews with hotel managers improved the understanding of water use and water source for each hotel. Around 40% of the hotels were unwilling to answer the questions and the remaining 60% of hotels at least revealed the water source. Of the 60% of the hotels that answered, 72% are only supplied by private boreholes while the remaining 28% supplement groundwater with municipal piped water from the Tiwi aquifer, located 6–12 km north of Ukunda and covering an area of approximately 30 km^2.

We estimated hotel groundwater abstraction according to the different type of data source (WRA allocations and hotel interviews). We also estimated hotel groundwater abstraction using the number of rooms and the hotel class type.

The total number of beds available on the south coast has decreased around 40% from 2015 to 2017, since some hotels closed during this period. However, the percentage of beds occupied has increased, maintaining an occupancy rate of around a million bed-nights/year for the period 2015–2017. The Draft Kwale Water Master Plan assumed a 1%/year growth in water demand for the tourism sector over the next 20 years.

Hotel groundwater use varies through an order of magnitude across the months of the year, based on bed occupancy (Fig. 5). Water consumption is lower during the wet season, since it coincides with the months with lowest tourism activity. However, the water consumption in the rest of the year is significant. It is worth emphasizing that the highest bed occupancy rate and thus the highest water consumption occur from October to December, just before the dry season.

3.2.4. Community abstraction

Groundwater abstraction from commercial activities takes place alongside the traditional dispersed 300 functional handpump-equipped shallow wells and boreholes, and 22 community boreholes (some with solar pumps installed by Base Titanium), that provide drinking water to communities and institutions. The WRA allocation for 22 community boreholes within the study area is 991 m^3/day (Table 3). There are also some open wells operated with buckets within the study area for which no abstraction data exist; however, anticipated abstraction rates are much lower than in handpump-equipped boreholes.

Weekly data obtained from the transmitters (WDT) from the 300 handpumps during 2014 and 2015 gave a mean daily abstraction of approximately 1.5 m^3/day per pump. Water pumped from community handpumps also depends on rainfall (Thomson et al., 2019). Abstraction varied from 0.71 m^3/day per pump in the wet season to 2.05 m^3/day per pump in the dry season, with monthly variation shown in Fig. 6. They operate under different dynamics, according to the economic activities in the area. The monthly average volume pumped is lower than the annual average abstractions from May to December. This shows that communities use other water sources during wet periods, such as rainwater collection (Thomson et al., 2019).

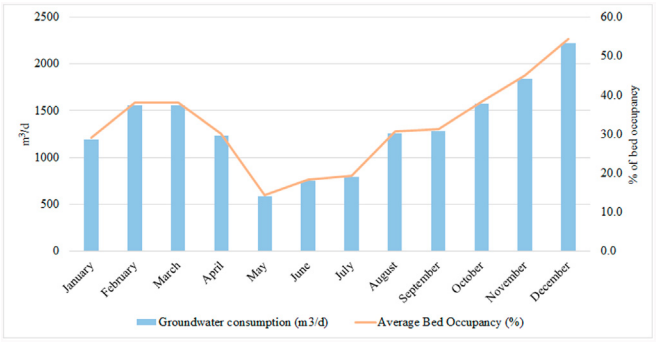

Fig. 5. Groundwater consumed in (m^3/d) each month based on the average bed occupancy from 2015 to 2017 obtained from the Kenya National Bureau of Statistics (KNBS).

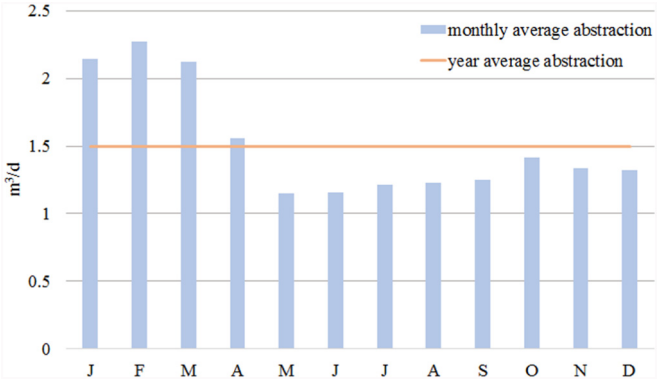

Fig. 6. Monthly average abstraction variation for handpumps during 2014 and 2015

3.3. Groundwater level evolution

In order to determine the sustainability of the groundwater system under different abstraction regimes, it is important not only to consider how abstraction could affect aquifers during a drought, but also how the systems recover after such climatic events. Therefore, the present study goes beyond that of Ferrer et al. (2019), as it focuses on the recovery of groundwater levels during 2017 after La Niña event and especially on shallow aquifer recovery. The shallow aquifer is the source of water for most communities in the study area.

During the La Niña event, there was a groundwater level decline in 86% of the measured shallow wells. In the remaining shallow wells, the groundwater levels were nearly constant. However, levels in 95% of the shallow wells affected by La Niña drawdown recovered after the first rainy season (AMJ) in 2017 (Table 2S Supplementary material). In this regard, the first rainy season (AMJ) is more effective in the recovery of the groundwater system than the short rains (OND).

Regarding groundwater level recovery after the La Niña event in the deep aquifer, there are only data from Zone 2 (from the Base Titanium monitoring network). Fig. 4 shows the effects of recharge and abstraction on deep piezometer water levels; this shows that groundwater levels recovered after the first rainfall event in April 2017, to values close to those observed in previous wet years.

3.4. Groundwater quality on the coastal strip

Sea water intrusion (SWI) in aquifers occurs naturally in coastal areas around the world (Custodio, 2010; SASMIE, 2017). The position of the seawater/fresh water-mixing zone is influenced by groundwater discharge into the sea and aquifer thickness, as well as aquifer hydraulic conductivity. The natural discharge rate could be affected by groundwater abstraction, reducing diffuse discharge into the sea. In order to study short-term salinity changes, we carried out a spatial analysis of groundwater EC (electrical conductivity) between 2013 between 2016.

The evolution of EC since 2013 (Fig. 7) shows that salinity increased, mainly in 2016. This illustrates the relationship between EC increase and decreasing rainfall, since the total rainfall during 2016 (when the La Niña event occurred), was 49% less compared to the 2014 total (Table 2). The highest EC values in June 2016 correspond to the wells located in Zones 3 and 4 (except for a point in Zone 1), with an EC mean value of 2814 μS/cm and a maximum of 3793 μS/cm (Table 3, Supplementary material). Looking at the EC variation across 2016–2017 for the wells located near the coast, around 88% of the sampled sites show an EC increase across the period. The wells that do not show any EC increase are mainly located inland in Zone 4, and in some wells in the Magarini sands in Zone 1 (Table 2, Supplementary material).

We compared hydrogeochemical modelling results with the samples from wells/boreholes affected by SWI in the shallow aquifer to understand the importance of the SWI change. Field samples contain between 0% and 30% of seawater (Fig. 8a), except for the sample taken from a beach upwelling, which had 83% seawater. The conceptual model that gives results closest to the observed field samples is the mixing of fresh and saline water, both in equilibrium with calcite (i.e. Fig. 8a).

Looking at the delta ion evolution for calcite (total quantity of precipitated/dissolved calcite mineral) in this conceptual model, during mixing between fresh groundwater and saline water (Fig. 8b) the increase in salinity tends to dissolve calcite, with 30–40% maximum dissolution in a water mixture containing 50% of seawater.

4. Discussion

4.1. Current situation

The total groundwater abstraction represented 6% of the recharge during La Niña and 1.3% of recharge during a normal climatic year,

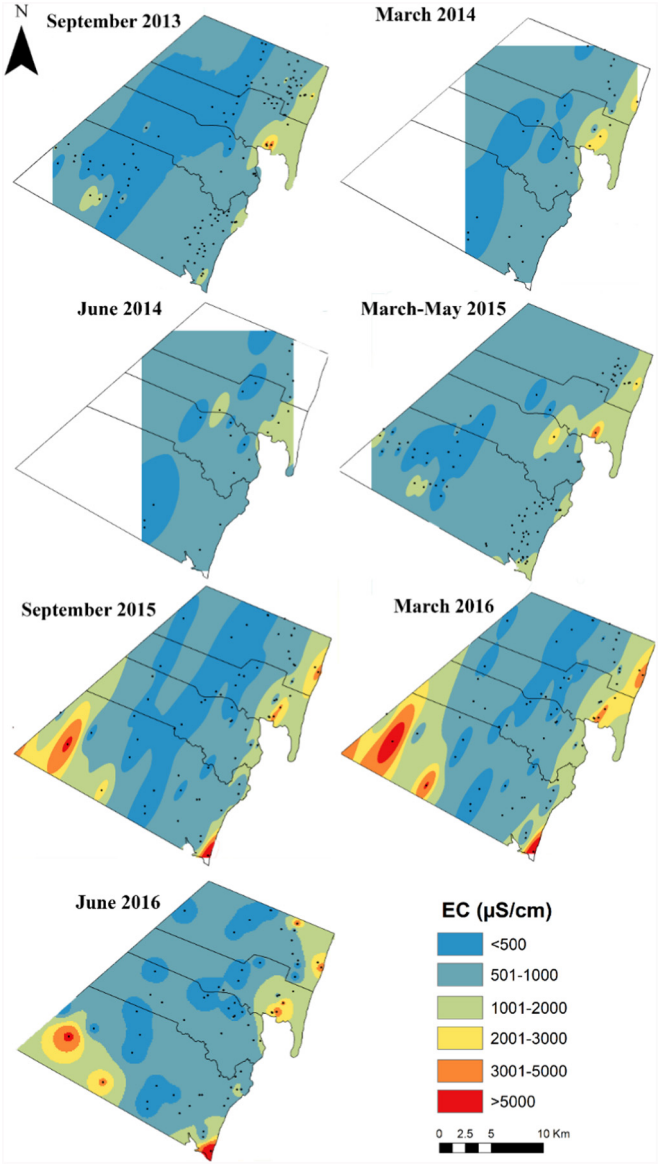

Fig. 7. EC spatial distribution along time after the different field surveys from 2013 to 2016. The inland white areas mean that no data is available. The high EC values located inland in from September 2015 to June 2016 correspond to a saline geological formation, the Maji ya Chumvi beds (Caswell, 1953).

such as 2017. The recharge volume is an important component of the aquifer system dynamics, responsible for groundwater level variation in both the shallow and deep aquifers.

Not all water users exploit the same aquifers layers. The community wells, handpumps and hotels mainly abstract groundwater from the shallow aquifer. The recharge areas of this aquifer unit are those exhibiting more volume variation between drought and a normal climatic year (i.e. 2017) (Fig. 3). The shallow aquifer unit is less resilient to climate variation than the deep one. This explains why some wells located in the Kilindini and Magarini sands became dry during the La Niña drought. The aquifer system exhibited swift recovery after the first normal rainy season in 2017. This allowed the system to return to the average groundwater budget and to face the next drought period.

One consequence of wells becoming dry is the increase in walking distance to collect water. As reported during fieldwork in June 2016, during the La Niña event, some communities stated that they had to walk longer distances to collect water because the nearest borehole or well was dry. Among other impacts, Demie et al. (2016) found that spending more time searching for water had a negative impact on

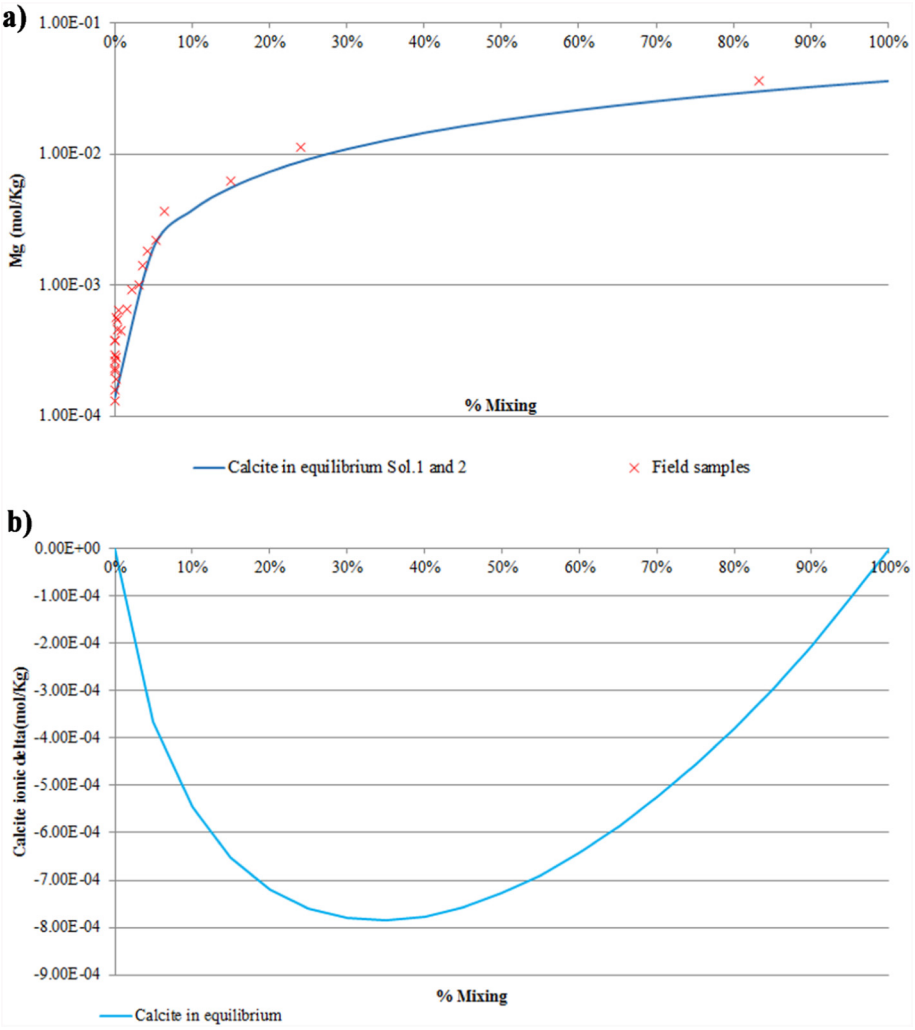

Fig. 8. a) Mg vs. percentage of mixing. The red crosses represent sampled waters near the coast. The X-axis shows the percentage of mixing from 0% to 100% of fresh water in the coast samples and the upwelling. The light blue line represents the best-fitting conceptual model (water solutions in equilibrium with calcite). b) Calcite ion delta (change) vs. percentage of mixing of the model in equilibrium with calcite. The Y-axis represents the calcite saturation index and the X-axis shows percent mixing. (For interpretation of the references to colour in this figure legend, the reader is referred to the web version of this article.)

girls and women, since this forces them to stop investing time in their education and other important activities. Furthermore, the reduction in groundwater availability leads to an increase in the price of the water sold to local residents. The Gro for Good research team found that during the drought event of 2016/2017, some areas having very limited access to drinking water suffered a peak in the price of vended water, with charges ranging from 20 to 50 Ksh per 20 L reported west of the Shimba Hills. Such costs are an order of magnitude higher than the usual price for vended water, which is 2 to 3 Ksh per 20 L. This price increase has a huge impact on families is an area where the average household income is about 330 Ksh/day, about the cost of 2.5 kg of rice. This price increase will either result in households having reduced funds for other needs because of the drought, or reducing their water use, or a combination of both. This may cause adverse health impacts from compromised hygiene behaviour.

Unlike communities and hotels, Base exploits the deep aquifer and KISCOL both aquifer units. The fact that the recharge variation is less in the Shimba Hills than in the lowland means that the deep aquifer is more resilient to drought events. This favours groundwater abstraction by these users, since they can continue to exploit the deep aquifer during periods of drought without impacting the shallow aquifer exploited by the communities and hotels lasting at least as long as the last La Niña event.

Focusing on mining, the abstraction rate depends on rainfall patterns, increasing during the dry period in 2016, and reducing during wet years, such as in 2017. The influence of abstraction on the shallow aquifer is insignificant up to the present, according to observation piezometer water level data in the shallow and deep aquifer in the Base wellfield. This is due to the presence of an aquitard between the two aquifers. Groundwater abstraction only significantly affected the piezometric level of the deep aquifer system during the 2016 drought. This groundwater level decline could be due to the combination of abstraction from the deep aquifer and the reduced recharge during the drought in the Shimba Hills (Fig. 4). Unlike in other areas, like Italy, Tunisia, Mediterranean Spain and the Canary Islands (La Vigna et al., 2013; Maliki et al., 2000; SASMIE, 2017), where intensive exploitation permanently affects the relationships between aquifer units, after La Niña event the hydraulic relationship between the shallow and deep aquifer recovered following the rains in April 2017, showing that the impact on the deep aquifer in 2016 was attributed to reduced recharge.

Like Base, KISCOL water use changes over time, as their principal use is for irrigation: less water is consumed during the wet season and more during the dry season and droughts. At present, current KISCOL abstraction has a dual effect on groundwater quality, as the potential pollutants related to fertilizers used in the sugarcane fields are present in the deep pumping wells but do not spread beyond the sugar fields due to the

recharge of irrigation return flow (Fig. 9). The presence of NO_3 concentration (31 mg/L) at 65 m depth in a KISCOL control piezometer located in Milalani (in the southern fields), demonstrates the aquifer unit's connection through the well due to the long screened sections. The northern fields (Kinondo), which are irrigated with surface water, shows how the pollutants may move following groundwater flow, as a well located down flow of the fields is one of the few in the area with elevated nitrate (Ferrer et al., 2019).

The relationship between the shallow and deep aquifer at the coast itself is unknown. Furthermore, as there are no data for the deep aquifer in the area between the coast on the one hand and the sugar fields and the mine on the other, it is not possible to determine the effects of sugarcane irrigation and mining abstraction on saline intrusion in the deep aquifer. However, none of the deep boreholes sampled during this study (up to 100 m depth, from the Base Titanium monitoring network) shows SWI influence. Moreover, it is unknown how water abstraction from boreholes located within or near the palaeochannel could increase the SWI, mainly around the Msambweni area, in Zone 1 (Fig.1).

In the coastal areas with major tourism concentrations, recent years' data seem to show a local salinization effect in the shallow aquifer due to the higher abstraction induced by tourism and associated activities. However, a longer period of observation is needed to determine the saline water intrusion dynamics in order to consider rainfall fluctuations and to differentiate between seasonal effects (still unclear but possible) and long-term trends. As the zone with most of the hotels is also the area with the highest population density, it is not possible to differentiate between saline intrusion caused by the hotel sector itself and that caused by wells and boreholes serving private dwellings or used by local communities.

EC in most measured shallow wells remained high after the drought period, even after the important rains of early 2017, indicating that groundwater quality in the coastal zone did not fully recover (Table 2, supplementary material). This behaviour is in agreement with many other well-studied areas (Custodio, 2002; SASMIE, 2017), which show that salinity takes much longer than groundwater level to change and to recover once the aquifer is salinized.

4.2. Future situation

Total groundwater abstraction is expected to increase by a factor of four over the current rate (see Table 3). This level of abstraction would represent 22% of the total recharge occurring during the La Niña event. Currently, the existing water-reliant industries are exploiting the aquifer without significantly affecting groundwater levels. However, the possible local effect of pumping wells on the aquifer system and the consequences of future increased groundwater abstraction during long drought periods should be evaluated. The number of dry shallow wells could increase in the future due to more frequent and longer droughts, but also due to augmented abstraction.

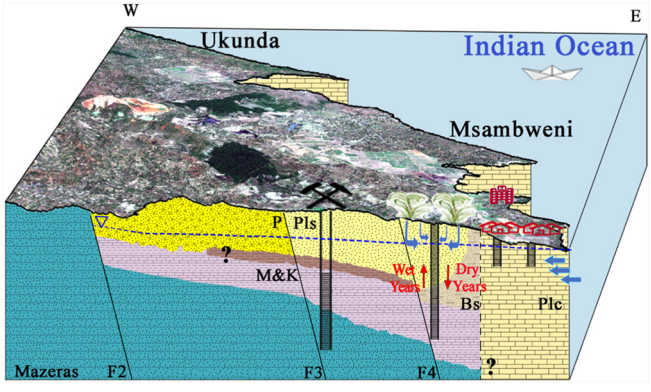

Fig. 9. Schematic hydrogeological conceptual model (not to scale) of the aquifer system with the main economic activities in the area and the location in the geology of the abstraction boreholes for each activity. The question marks indicate the unknown extension of the clay layer (in brown) acting as an intercalated aquitard that reduces the connectivity between the Mazeras Fm and Pleistocene corals and sands, and the discharge of the deep aquifer. Mazeras (Mazeras Fm), M&K (Mtomkuu and Kambe Fm), P (Magarini sands), Pls (Kilindini sands), Bs (Bioclastic sands with clay lenses), Plc (Pleistocene corals). F2 to F4 indicate the main faults in the study area. (For interpretation of the references to colour in this figure legend, the reader is referred to the web version of this article.)

Considering the groundwater level difference between aquifer units during La Niña in the 14 m-thick aquitard (the minimum aquitard thickness reported by Base) and the estimated vertical hydraulic conductivity, Darcy's Law shows that the vertical water downward displacement through the aquitard is of the order of 2 m/year, penetrating much less than the aquitard thickness in one year. Consequently, pollution from the upper aquifer level cannot reach the deep aquifer except due to poor well construction. However, in a future scenario with a four-fold increase in groundwater abstraction rate and/or longer droughts, a longer and possibly permanent shift in the difference in piezometric levels between the aquifer units may occur, produced by induced larger vertical gradients across the aquitard, increasing the risk of contamination from vertical drainage through the aquitard.

A future increase in groundwater abstraction by the sugar company during a drought period may affect both the shallow and the deep aquifer, as those wells are screened in both aquifers (for maximum borehole yield). A potential reduction in groundwater level in the shallow aquifer in Zone 1 may affect the Ramisi River-aquifer relationship in that area. A fall in the shallow aquifer level would decrease aquifer discharge to the river and at some point could induce river water infiltration into the aquifer. The infiltration of naturally saline water from the Ramisi River could affect the groundwater quality in shallow wells adjacent to the river by increasing its salinity, thus limiting their use. The maximum EC upstream in the Ramisi River was 5594 μS/cm (Ferrer et al., 2019). In extreme cases, the EC could limit the use of groundwater from the shallow aquifer. This does not only apply to domestic uses but also to sugar irrigation, as the threshold EC for sugarcane is 1700 μS/cm (FAO, 2018), if some of abstraction wells were located close to the river. In order to prevent this occurring, KISCOL might consider irrigating the south sugar fields with surface water from dams located in the Mkurumudzi catchment. Furthermore, it is expected that in periods when the groundwater level in the deep aquifer stays lower than in the shallow aquifer, pollution of the deep aquifer can be induced in the wells, as has occurred in other areas (Menció et al., 2011) and is a common occurrence in coastal areas.

SWI is an important issue in coastal aquifers, and has already been observed in Kwale County (Oiro and Comte, 2019). A reduction in groundwater flow would lead to a penetration of the saltwater wedge inland, increasing the percentage of saline water in shallow wells already affected by SWI and affecting new areas. The significance of SWI is that only 2 to 3% of seawater mixed with fresh water is enough to make the resulting water useless for most purposes.

The calculation of the freshwater-saltwater mixing zone is a complex task, but an approximation can be obtained assuming a sharp freshwater-saline water interface and comparing the results with the final equilibrium state. The steady state penetration of the sea water wedge in the case of an homogeneous aquifer can be easily calculated from aquifer thickness and hydraulic conductivity for a given groundwater flow discharging at the coast (see Section 13, (Custodio and Bruggeman, 1986; Custodio and Llamas, 1976). We calculated seawater wedge growth from the coastline for the shallow aquifer, under the future increased abstraction scenario with the same net recharge as during the La Niña event (data in Supplementary material). Increasing groundwater abstraction from 9535 m^3/d to 34,270 m^3/d will move the steady state saline water wedge from 232 m inland up to 280 m in the final equilibrium state. This advance of the saline wedge could affect hotel groundwater supply and community handpumps located near the coast.

We also calculated the saline wedge depth for different distances from the coast and for the different geologies near the coast, i.e. the Pleistocene corals and Kilindini sands (data in Supplementary material). The results show that even during the future abstraction scenario during a drought year like the 2016 La Niña, the saline wedge will not affect the Kilindini sands. Under the future scenario, the saline wedge in the Kilindini sands (around six kilometres inland from the coast) would be around 400 m deep, so the shallow aquifer would not be affected. Only the coral limestone formation is affected by SWI in the present and future scenarios. The saline wedge depth in the coral formation ranges from two meters deep at one meter inland from the coastline, to 100 m deep at the geological contact between the corals and the Kilindini sands, located around four kilometres inland.

The future consequences of borehole salinization would be an increasingly salty taste and at some point unsuitability of the water for human consumption and agriculture. This would increase costs, due to corrosion of domestic appliances, hotel facilities, pipes, and pumps, besides the cost of providing drinking water by other means, and the early abandonment of wells and associated facilities. Furthermore, as shown by Foster et al. (2018), handpump failure risks are higher and lifespans are shorter when groundwater is more saline and the static water level is deeper.

The increase in salinity, as observed in 2016, and the dynamics of the SWI will tend to increase calcite dissolution (Fig. 8b). The related increase in karstification would have a number of potential long-term effects: 1) induced hydraulic conductivity rise will hasten further aquifer salinization and 2) would increase the creation of sinkholes already observed in parts of the coral limestone during fieldwork. New sinkholes may be caused when caverns or channels in the coral limestone collapse due to groundwater overexploitation (Alfarrah et al., 2017; Jakemann et al., 2016; Khanlari et al., 2012). Occurrences of land subsidence in limestone have been globally reported, such as in Spain (Molina et al., 2009), India (Sahu and Sikdar, 2011), Mexico (Ortiz-Zamora and Ortega-Guerrero, 2010) and the United States (Holzer and Galloway, 2005). This has implications for the stability of buildings and other structures constructed on the limestone.

Despite the uncertainty of the impacts caused by the future abstraction scenario and longer forecast drought periods (Stocker et al., 2013), aquifer management decisions regarding the potential impacts on the aquifer system and the linked communities and economic activities are needed. Private sector and public participation in water resources management should be enhanced through decentralised management approaches. In this way, stakeholders, including the Water Resources Authority, private water users and communities in the study area, should carry out decision-making. Water infrastructure and technologies should be fit-for-purpose in application and scale, and the pro-poor focus should be underpinned by appropriately focused management regimes (Olago, 2018).

This decision-making must focus on managing the aquifer system in a sustainable way in order to protect the communities. These are the most vulnerable stakeholders, since they rely on the less resilient aquifer for water supply. Therefore, alternative, secure water resources must be developed to supply vulnerable communities before community wells become dry or salinize. One potential solution could be to supply the communities from deep boreholes, since this aquifer unit is more resilient in the face of adverse climate events. Base Titanium is already working together with Kwale County government to install community water sources into the deep aquifer to provide water security to communities, with a number of Base-drilled boreholes originally with handpumps installed planned to be converted to solar or mains-powered pumps. Other possible actions to ensure community well sustainability would comprise taking measures to protect the main recharge areas as is being done by the Kenya Wildlife Service supported by Base Titanium together with conservation organisations in the Shimba Hills National Reserve – the Water Tower for the Mkurumudzi catchment; managing land use to ensure high infiltration rates; promoting managed artificial recharge; and conjunctive water use. A common conjunctive management strategy is the recharge and storage of surface water in aquifers when it is available in excess of demand, for withdrawal later when surface supplies are reduced, as during drought (Foster and van Steenbergen, 2011). Furthermore, private companies should strive to manage their groundwater resources sustainably, minimising the impact on community well water quality and availability. For example, Base Titanium adopts recycling and conjunctive use, combining surface and groundwater during drought periods as a management strategy.

This study uses easy-to-apply calculations to illustrate the possible future risks of increased abstraction under climate stress to an aquifer system in Kwale County. At present, under 'normal' climatic conditions, we have observed no adverse consequences in the aquifer system since major abstraction started in 2012. However, the study underlines the importance of evaluating all risks to any aquifer system prior to major groundwater abstraction.

5. Conclusions and final remarks

Water-reliant growth in Africa needs to manage multiple risks for sustainable management of strategic groundwater resources. Securing new investors in rural areas where poverty is high and environmental regulation is weak may focus on the former at the cost of the latter. Lack of historical data such as water level, abstraction and quality data is typically the norm and challenge objective decision-making in the face of urgent development priorities. Government and enterprises may find environmental sustainability of secondary importance to advancing economic production, creating local jobs and new sources of taxation. This may translate into unknown risks to local, vulnerable populations and future generations who rely on shallow groundwater for water supply. Droughts compound this risk, with multiple and competing bulk water users abstracting from the same aquifer system without any shared understanding of impacts, including short and long-term damage from saline intrusion in coastal aquifers. As in most aquifers, water quality does not recover in all wells after wet season recharge, and significant amounts of data are needed to evaluate future aquifer response. Furthermore, in areas of the continent with lower precipitation and consequently lower recharge, a lower level of abstraction could be harmful to aquifers. Future risk should therefore be predicted under different abstraction future scenarios, before major abstraction takes place.

While gambling with groundwater may be common in Africa and globally, this study shows that groundwater resources can be significant and resilient to unpredictable but recurrent drought events. Given over half a billion dollars in capital investment in the two water-reliant industries in Kwale, in addition to tourism and related investment, understanding investor risk and liability from groundwater sustainability would seem prudent, if not a legal obligation, before major abstraction starts. Government leadership is essential to manage the aquifer as a system for all, including environmental services, rather than for the powerful few. Without technical, material and political support, water resource management agencies face stark choices in Africa, as limited staff and capacity are unable to ensure that adequate monitoring systems exist to guide regulations that manage water resources in the public interest. Governance failure can promote market failure, by mismanaging groundwater, by design or by accident. Furthermore, the expected impact of climate change across the continent, with variable consequences for water resources availability, could even worsen the situation.

However, this is not inevitable and this study shows how one of the main problems, the lack of aquifer systems data, can be overcome at least partially by integrating different sources of information. Most of the time, water-reliant users present specific hydrogeological information that can contribute to define the overall hydrogeological system, since their own main purpose is exploiting the aquifer with the maximum productivity. Therefore, local community water usage, together

with different stakeholders knowledge and good corporate water management as a catalyst for providing critical data use, allows us to develop credible models for future groundwater management and resource allocation. Furthermore, complementary but simple information sources such as in-situ interviews, Google Earth, Trip Advisor, easy-to-apply analytical methods, etc., that can be achieved in the African context as in many developing countries, enables groundwater abstraction to be estimated and the sustainability of the aquifer system to be defined, allowing potential future risks to be assessed as has been shown by this study.

Declaration of interests

The authors declare that they have no known competing financial interests or personal relationships that could have appeared to influence the work reported in this paper.

Acknowledgements

The authors gratefully acknowledge the collaboration and key data shared by Base Titanium Ltd., and the support of Kenya's Water Resource Authority, the Kwale Country Government, Kwale International Sugar Company Ltd., and Rural Focus Ltd. This research was funded by the UK Government via NERC, ESRC and DFID as part of the Gro for GooD project (UPGro Consortium Grant: NE/M008894/1).

Appendix A. Supplementary data

Supplementary data to this article can be found online at https://doi.org/10.1016/j.scitotenv.2019.133634.

References

Adelana, S.M.A., MacDonald, A.M., 2008. Groundwater research issues in Africa. IAH Sel. Pap. Hydrogeol. 13, 1–7.
Alfarrah, N., Berhane, G., Hweesh, A., Walraevens, K., 2017. Sinkholes due to groundwater withdrawal in Tazerbo wellfield, SE Libya.
Caswell, P.V., 1953. Geology of the Mombasa-Kwale Area. Geological Survey of Kenya.
Commission on Revenue Allocation, 2013. Kenya Ctry. Fact Sheets. Second ed. Comm. Revenue Alloc, Nairobi.
Comte, J.C., Cassidy, R., Obando, J., Robins, N., Ibrahim, K., Melchioly, S., Mjemah, I., Shauri, H., Bourhane, A., Mohamed, I., Noe, C., Mwega, B., Makokha, M., Join, J.L., Banton, O., Davies, J., 2016. Challenges in groundwater resource management in coastal aquifers of East Africa: investigations and lessons learnt in the Comoros Islands, Kenya and Tanzania. J. Hydrol. Reg. Stud. 5, 179–199.
Custodio, E., 2002. Low Llobregat aquifers: intensive development, salinization, contamination and management. In: Sabater, S., Ginebreda, A., Barceló, D. (Eds.), The Story of a Polluted Mediterranean River. The Handbook of Environmental Chemistry, pp. 27–50.
Custodio, E., 2010. Coastal aquifers of Europe: an overview. Hydrogeol. J. 18, 269–280.
Custodio, E., Bruggeman, G., 1986. Groundwater problems in coastal areas. Studies and Reports in Hydrology. UNESCO, pp. 1–596.
Custodio, E., Llamas, M., 1976. Hidrología Subterránea. Omega, Barcelona.
CWSB, 2013. Coastal Water Services Board- Strategic Plan (2013–2017) [WWW Document]. URL. www.cwsb.go.ke.
CWSB, 2016. Services Coast Water Board [WWW Document]. https://www.cwsb.go.ke/, Accessed date: 20 August 2011.
De Filippis, G., Foglia, L., Giudici, M., Mehl, S., Margiotta, S., Negri, S.L., 2016a. Seawater intrusion in karstic, coastal aquifers: current challenges and future scenarios in the Taranto area (southern Italy). Sci. Total Environ. 573, 1340–1351.
De Filippis, G., Giudici, M., Margiotta, S., Negri, S., 2016b. Conceptualization and characterization of a coastal multi-layered aquifer system in the Taranto Gulf (southern Italy). Environ. Earth Sci. 75, 686.
Demie, G., Bekele, M., Seyoum, B., 2016. Water accessibility impact on girl and women's participation in education and other development activities: the case of Wuchale and Jidda Woreda. Ethiopia. Env. Syst Res 5, (11).
Dhar, A., Datta, B., 2009. Saltwater intrusion management of coastal aquifers. I: linked simulation-optimization. J. Hydrol. Eng. 14, 1263–1272.
FAO, 2018. Food and Agriculture Organization of the United Nations (FAO). [WWW Document]. URL. www.fao.org.
Ferrer, N., Folch, A., Lane, M., Olago, D., Odida, J., Custodio, E., 2019. Groundwater hydrodynamics of an eastern Africa coastal aquifer, including La Niña 2016–17 drought. Sci. Total Environ. 661, 575–597.
Foster, T., Hope, R., 2016. A multi-decadal and social-ecological systems analysis of community waterpoint payment behaviours in rural Kenya. J. Rural. Stud. 47, 85–96.
Foster, S., van Steenbergen, F., 2011. Conjunctive groundwater use: a 'lost opportunity' for water management in the developing world? Hydrogeol. J. 19, 959–962.
Foster, T., Willetts, J., Lane, M., Thomson, P., Katuva, J., Hope, R., 2018. Risk factors associated with rural water supply failure: a 30-year retrospective study of handpumps on the south coast of Kenya. Sci. Total Environ. 626, 156–164.
Giannoccaro, G., Scardigno, A., Prosperi, M., 2017. Economic analysis of the long-term effects of groundwater salinity: bringing the farmer's perspectives into policy. J. Integr. Environ. Sci. 14, 59–72.
Holzer, T.L., Galloway, D.L., 2005. Impacts of land subsidence caused by withdrawal of underground fl uids in the United States. Eng. Geol. 16, 87–99.
IGRAC, 2019. Groundwater governance|IGRAC [WWW document]. https://www.un-igrac.org/areas-expertise/groundwater-governance, Accessed date: 29 January 2019.
ISGEAG, 2019. Improving Sustainable Groundwater Exploration with Amended Geophysics.
Jakemann, A., Randall, O., Huntt, J., Andrewwross, J.-D., 2016. Integrated Groundwater Management Concepts. Approaches and Challenges.
Khanlari, G., Heidari, M., Momeni, A.A., Ahmadi, M., Taleb Beydokhti, A., 2012. The effect of groundwater overexploitation on land subsidence and sinkhole occurrences, western Iran. Q. J. Eng. Geol. Hydrogeol. 45, 447–456.
La Vigna, F., Mazza, R., Capelli, G., 2013. Detecting the flow relationships between deep and shallow aquifers in an exploited groundwater system, using long-term monitoring data and quantitative hydrogeology: The Acque Albule basin case (Rome, Italy). Hydrol. Process. 27, 3159–3173.
Maliki, M.A., Krimissa, M., Michelot, J.-L., Zouari, K., 2000. Relationship between shallow and deep aquifers in the Sfax basin (Tunisia), Comptes Rendus de l'Academie des Sciences Series IIA Earth and Planetary Science.
Mantoglou, A., 2003. Pumping management of coastal aquifers using analytical models of saltwater intrusion. Water Resour. Res. 39, 1–12.
Mas-Pla, J., Menció, A., 2018. Groundwater nitrate pollution and climate change: learnings from a water balance-based analysis of several aquifers in a western Mediterranean region (Catalonia). Environ. Sci. Pollut. Res. 1–19.
Menció, A., Mas-Pla, J., Otero, N., Soler, A., 2011. Nitrate as a tracer of groundwater flow in a fractured multilayered aquifer. Hydrol. Sci. J. 56, 108–122.
Michael, H.A., Post, V.E.A., Wilson, A.M., Werner, A.D., 2017. Science, society, and the coastal groundwater squeeze. Water Resour. Res. 53, 2610–2617.
Molina, J.L., García Aróstegui, J.L., Benavente, J., Varela, C., de la Hera, A., López Geta, J.A., 2009. Aquifers overexploitation in SE Spain: a proposal for the integrated analysis of water management. Water Resour. Manag. 23, 2737–2760.
Oiro, S., Comte, J.C., 2019. Drivers, patterns and velocity of saltwater intrusion in a stressed aquifer of the East African coast: joint analysis of groundwater and geophysical data in southern Kenya. J. African Earth Sci. 149, 334–347.
Okello, C., Tomasello, B., Greggio, N., Wambiji, N., Antonellini, M., 2015. Impact of population growth and climate change on the freshwater resources of Lamu Island, Kenya. Water (Switzerland) 7, 1264–1290.
Olago, D.O., 2018. Constraints and Solutions for Groundwater Development, Supply and Governance in Urban Areas in Kenya.
Ortiz-Zamora, D., Ortega-Guerrero, A., 2010. Evolution of long-term land subsidence near Mexico City: review, field investigations, and predictive simulations. Water Resour. Res. 46, 1–15.
Pavelic, P., Giordano, M., Keraita, B., Ramesh, V., Rao, T., 2012. Groundwater availability and use in sub-Saharan Africa: A review of 15 countries Colombo, Sri Lanka.
Sahu, P., Sikdar, P.K., 2011. Threat of land subsidence in and around Kolkata City and East Kolkata Wetlands, West Bengal, India. J. Earth Syst. Sci. 120, 435–446.
SASMIE, 2017. Salinización de las aguas subterráneas en los acuíferos costeros mediterráneos e insulares españoles [Groundwater salinization in Mediterranean and island coastal aquifers in Spain].
Solomon, S., Qin, D., 2013. Climate change 2007 the physical science basis the. J. Chem. Inf. Model. 42, 17–19.
Stocker, T.F., Qin, D., Plattner, G.-K., Tignor, M.M.B., Allen, S.K., Boschung, J., Nauels, A., Xia, Y., Bex, V., Midgley, P.M., 2013. Climate Change 2013. The Physical Science Basis Working Group I Contribution to the Fifth Assessment Report of the Intergovernmental Panel on Climate Change.
Taylor, R.G., Jasechko, S., 2015. Intensive rainfall recharges tropical groundwaters. Environ. Res. Lett. 10, 124015.
Taylor, R.G., Todd, M.C., Kongola, L., Maurice, L., Nahozya, E., Sanga, H., MacDonald, A.M., 2012. Evidence of the dependence of groundwater resources on extreme rainfall in East Africa. Nat. Clim. Chang. 3, 374–378.
Thomson, P., Hope, R., Foster, T., 2012. GSM-enabled remote monitoring of rural handpumps: a proof-of-concept study. J. Hydroinf. 14, 829–839.
Thomson, P., Bradley, D., Katilu, A., Katuva, J., Lanzoni, M., Koehler, J., Hope, R., 2019. Rainfall and groundwater use in rural Kenya. Sci. Total Environ. 649, 722–730.
Velasco, V., Tubau, I., Vázquez-Suñé, E., Gogu, R., Gaitanaru, D., Alcaraz, M., Serrano-Juan, A., Fernàndez-Garcia, D., Garrido, T., Fraile, J., Sanchez-Vila, X., 2014. GIS - based hydrogeochemical analysis tools (QUIMET). Comput. Geosci. 70.
Werner, A.D., Bakker, M., Post, V.E.A., Vandenbohede, A., Lu, C., Ataie-Ashtiani, B., Simmons, C.T., Barry, D.A., 2013. Seawater intrusion processes, investigation and management: recent advances and future challenges. Adv. Water Resour. 51, 3–26.
World Bank, 2013. An Analysis of Issues Shaping Africa's Economic Future. Africa's Pulse. TheWorld Bank, Washington, DC.